Functional Magnetic Resonance Imaging in Patients with Kidney Failure: Optimising Imaging Biomarkers

Alastair J Rankin

BSc (Med Sci), MBChB, MRCP(UK)

August 2022

Thesis in journal format

Submitted for the Degree of Doctor of Philosophy (PhD)

to

University of Glasgow

From

The Institute of Cardiovascular and Medical Sciences

College of Medical, Veterinary and Life Sciences

University of Glasgow

Supervisors

Professor Patrick B Mark

Professor Colin Berry

Abstract

Introduction: The prevalence of kidney failure is increasing globally. Patients with kidney failure experience a vastly increased risk of cardiovascular disease and premature death, which is incompletely offset with current kidney replacement therapies. The development of reliable biomarkers in kidney failure could allow novel therapeutics to be more readily trialled in patients with kidney failure due to enhanced patient selection, reduced participant burden and reduced trial duration and cost. The present thesis utilises 6 distinct studies to examine imaging biomarkers applied to 2 sub-populations of patients with kidney failure. Firstly, I explore several imaging techniques assessing the excess cardiovascular risk observed in patients on dialysis (studies 1-4). Secondly, I examine the utility of renal MRI to investigate kidney transplant dysfunction (studies 5, 6).

Methods and Results:

1. **Global longitudinal strain on cardiovascular MRI.** In a retrospective study of 215 participants with kidney failure, left ventricular global longitudinal strain on cardiovascular MRI associated with all-cause mortality, independent of baseline clinical variables and future renal transplantation.
2. **Effect of haemodialysis on native T1 mapping.** In a prospective study of 26 patients undergoing regular haemodialysis, acute changes in cardiac volumes and myocardial composition were detectable on 3T cardiovascular MRI following a single session of haemodialysis with fluid removal.
3. **Radial-VIBE MRI for the detection of vascular calcification.** In a prospective study of 96 individuals with kidney failure (24 haemodialysis, 72 transplant), a radial-VIBE sequence on MRI was subjectively able to detect thoracic aortic calcification. However, significant bias existed with respect to quantification of calcification volume, with MRI over-estimating volume when minimal calcification was present and under-estimating it at greater volumes. Improvements in radial-VIBE image quality are necessary, and until then CT should remain the primary modality for assessing vascular calcification in clinical practice.
4. **Myocardial extracellular volume by contrast enhanced CT.** In a prospective study of 23 participants on regular haemodialysis there was no correlation between extracellular volume on CT and myocardial native T1 (a surrogate for myocardial fibrosis).

5. **Different regions of interest for the analysis of multiparametric renal MRI.** In a pooled study consisting of 40 participants (10 healthy volunteers, 10 patients with left ventricular systolic dysfunction and 20 renal transplant recipients) comparing different regions of interest (ROI) for the analysis of renal MRI, it was found that manually drawn ROIs delineating the cortex or in a representative area of cortex could be used interchangeably, with acceptable inter-observer reproducibility.
6. **Multiparametric renal MRI for the investigation of renal transplant dysfunction.** In a study of 28 participants (20 with complete data) that was stopped prematurely due to the COVID-19 pandemic, there was no correlation between any renal MRI variable and the percentage of renal cortex containing fibrosis.

Conclusion: There is a clear clinical need for the development and validation of reliable biomarkers for patients with kidney failure. However, the results of the present thesis suggest that, in their present form, neither functional MRI for the identification of cardiovascular disease in patients undergoing dialysis, nor renal MRI in patients with transplant dysfunction, are ready for implementation into clinical trial research protocols or clinical practice.

Contents

List of Tables

List of Figures

Awards

- Chief Scientist Office (CSO) Clinical Academic Training Fellowship CAF/18/02 - July 2018- December 2020. £144,252

- Named ‘day-to-day’ supervisor on Medical Research Scotland Vacation Scholarship (VAC-1514-2019) June 2019.

- Runner-up for the 2022 Gerald M Pohost Award. The Pohost Award is awarded to that manuscript deemed by the JCMR Editorial Board to be the best manuscript published for the prior year. (for the paper see Chapter 5 - Cardiovascular magnetic resonance for the detection of descending thoracic aorta calcification in patients with end-stage renal disease. *J Cardiovasc Magn Reson* (2021).)

Other publications arising from this thesis

- Morrow AJ, Sykes R, McIntosh A, Kamdar A, Bagot C, Bayes HK, Blyth KG, Briscoe M, Bulluck H, Carrick D, Church C, Corcoran D, Findlay I, Gibson VB, Gillespie L, Grieve D, Barrientos PH, Ho A, Lang NN, Lennie V, Lowe DJ, Macfarlane PW, Mark PB, Mayne KJ, McConnachie A, McGeoch R, McGinley C, McKee C, Nordin S, Payne A, **Rankin AJ**, Robertson KE, Roditi G, Ryan N, Sattar N, Allwood-Speirs S, Stobo S, Touyz RM, Veldtman G, Watkins S, Weeden S, Weir RA, Welsh P, Wereski R, CISCO-19 Consortium, Mangion K & Berry C. A multisystem, cardio-renal investigation of post-COVID-19 illness. Nat Med. 2022. 28, 1303-1313.

- Mark PB, Mangion K, **Rankin AJ**, Rutherford E, Lang NN, Petrie MC, Stoumpos S, Patel RK. Left ventricular dysfunction with preserved ejection fraction: the most common left ventricular disorder in chronic kidney disease patients. *Clin Kidney J*. 2022. Online ahead of print. https://doi.org/10.1093/ckj/sfac146

- **Rankin AJ**, Mayne K, Allwood-Speirs S, Hall Barrientos P, Roditi G, Gillis KA, Mark PB. Will advances in functional renal magnetic resonance imaging translate to the nephrology clinic? *Nephrology (Carlton)*. 2022. 27(3);223-230.

- **Rankin AJ**, Mark PB. Cardiac Screening prior to renal transplantation – good intentions, rather than good evidence, dictate practice. *Kidney Int*. 2021. 99 (2); 306-308.

- Lees JS, **Rankin AJ**, Gillis KA, Zhu LY, Mangion K, Rutherford E, Roditis GH, Witham MD, Chantler D, Panarelli Maurizio, Jardine AG, Mark PB. The ViKTORIES trial: a randomised, double-blind, placebo-controlled trial of vitamin K supplementation to improve vascular health in kidney transplant recipients. *Am J Transplant*. 2021. 21(10):3356-3368

- Stoumpos S, **Rankin AJ**, Hall Barrientos P, Mangion K, McGregor EM, Thomson PC, Stevenson K, Welsh P, Kasthuri R, Kingsmore DB, Roditi G, Mark PB.

Interrogating the haemodynamic effects of haemodialysis arteriovenous fistula on cardiac structure and function. *Sci Rep. 2021.* **11(1):**18102.

Scientific presentations and abstracts

- ‘Myocardial changes on 3T Cardiovascular Magnetic Resonance Imaging in response to haemodialysis with fluid removal’. UK Kidney Week, October 2021, virtual congress. Moderated poster presentation.

- ‘A randomised, double-blind, placebo-controlled trial of vitamin K supplementation to improve vascular health in kidney transplant recipients’. British Transplant Society, Belfast, March 2020. Moderated poster presentation.

- ‘A novel magnetic resonance sequences that accurately detects aortic calcification in patients with end-stage kidney disease’. 1) Scottish Renal Association Annual meeting, Dumfries, UK, October 2019 (oral presentation). 2) American Society of Nephrology, November 2019, Washington DC, USA (poster presentation).

- ‘Global Longitudinal Strain on cardiac MRI is supervisor to conventional cardiac parameters at predicting mortality in patients with end-stage kidney disease’. 1) Scottish Renal Association Annual meeting, Dumfries, UK, October 2019 (oral presentation). 2) American Society of Nephrology, November 2019, Washington DC, USA (poster presentation) 3) CKJ online journal club April 2021(oral presentation).

- ‘Evaluation of transplant renal vascular disease by 4D flow’. 3rd International symposium on renal imaging, Nottingham, October 2019 (oral presentation)

- ‘Relationship between aortic distensibility, coronary artery calcification and left ventricular mass in renal transplant recipients: assessments from a clinical trial’. 1) 56th annual ERA-EDTA conference, Budapest, June 2019 (poster presentation). 2) UK Kidney week (joint meeting of Renal Association and British Renal Society), Brighton, UK, June 2019 (Poster presentation).

- ‘Association between dietary components and vascular stiffness: assessments from renal transplant recipients participating in a clinical trial’. UK Kidney week (joint

meeting of Renal Association and British Renal Society) June 2019, Brighton, UK (Poster presentation)

- ‘Multi-parametric magnetic resonance imaging in acute renal allograft transplantation’. 1) American Society of Nephrology Conference, San Diego, USA. October 2018 (poster presentation). 2) 3rd International symposium on renal imaging, Nottingham, October 2019 (oral presentation).

Acknowledgements

Completion of this research fulfils a major personal and academic life goal for me. I am very grateful for the support and guidance I have received along the way. Firstly, to Professor Patrick Mark for his resolute support, wise counsel, patience, and endless good humour. From the very beginning it was clear to me that you genuinely cared about my progress and had my best interests in mind. You supported me through several difficult academic decisions at the start of this period of research, and under lesser supervisors, I suspect my PhD aspirations would have failed several times over in the first year. Thank you to Professor Colin Berry for his expertise and guidance throughout my research. Your support and wisdom have been vital to allow a nephrology trainee to safely foray into the realms of cardiovascular imaging research. I owe a million thank yous to the renal research imaging group, in particular Dr Jennifer Lees and Dr Keith Gillis, without whose abundant academic, moral, statistical and computer coding support I would not have enjoyed this research as much as I did, and to Dr Elaine Rutherford, Dr Sokratis Stoumpos, Dr Mark Findlay and Dr Rajan Patel for their guidance, especially at the beginning of my research period. I am also very grateful to Dr Emily McQuarrie, for the patience and time she gave me while nurturing my research interest at a very early stage in my career. A special thanks to Dr Kenneth Mangion for mentoring me in cardiovascular MRI analysis and fielding my many, many questions.

I am very grateful to the staff at the Glasgow Clinical Research facility, in particular the research nurses (Deborah McGlynn, Nicola Thomson, Kirsty Forsyth, Rowan MacDougall and Barbara McLaren), clinical support (Christina Love and Christine McAllister) and the project assistant (Andrew Tiftickjian). I am indebted to the physics support that I received from Dr Sarah Allwood-Spiers, Dr Pauline-Hall Barrientos and Dr Aleksandra Radjenovic. A special thanks to the radiographers of The Glasgow Research Imaging Facility (especially, Rosie Woodward, Tracey Hopkins, Evonne McLennan, and Laura Dymock), your patience, guidance, expertise and cups of tea greatly enhanced my research experience.

To Michael McBride, my best friend of 22 years. You massively enriched my life and I will forever miss you, but it is only fair to point out that your contribution to this thesis was a diabolical distraction that I could have done without out. I still love you though. May you rest in peace.

To my family (Emma, Lucas and Oliver) for the unwavering support, patience and joy you provide me with. Lucas was born during my first year of research, while much of this thesis was written overnight with Oliver (a 10kg 6-month-old baby) in a papoose. To my parents, for everything that you do, but specific to this thesis, for nurturing my academic interest from a young age and for the many hours of additional childcare you provided to let me write this thesis.

I am very grateful to the funders of this research (The Chief Scientist Office (Scotland) and Kidney Research UK), for recognising the unmet research needs that face patients living with chronic kidney disease. My final acknowledgement is to the participants of these studies and the wider populations that they represent. It is to them and for them that we do research. I am incredibly grateful for the time each participant contributed to these research studies and I hope that these results may in some way contribute to improving patient care in the future.

P.S. To COVID, your wrath on the world goes well beyond inconveniencing my PhD. However, while this crime is small in comparison to your global devastation, I hate you very specifically and personally for your impact on my research. This is in conjunction with the much greater grief I harbour for the disaster you have wrought more generally.

Author's declaration

The work presented in this thesis was conducted by me unless explicitly stated otherwise. The contribution of other researchers is detailed in each chapter under the title 'Author contributions', with key contributions summarised below. This thesis, including all statistical analysis and presentation of results, has been prepared by myself and is a record of work performed by myself. It has not previously been submitted for a higher degree.

I acknowledge support from Dr Kenneth Mangion for performing duplicate analysis of cardiovascular magnetic resonance imaging (MRI) parameters in a random selection of participants. I acknowledge support from Mr Luke Zhu for performing the primary analysis of the cardiovascular MRI scans for the retrospective study examining global longitudinal strain in patients with end-stage kidney disease. I performed the analyses for inter-observer reproducibility in addition to the primary data collection, statistical analysis, and presentation of results for this section. I acknowledge support from Mr Elbert Edy for performing duplicate qualitative assessment of the cardiovascular MRI scans for the chapter relating to the detection of vascular calcification using non-contrast MRI and duplicate analysis of the CT scans in the chapter examining myocardial extracellular volume quantification using contrast enhanced CT. Mr Elbert Edy also did the primary quantitative analysis and figures for the section on vascular calcification detection on MRI. I acknowledge support form Dr Stephen Rankin who performed duplicate analysis of the CT scans in the chapter examining myocardial extracellular volume quantification using contrast enhanced CT. I acknowledge support from Dr Keith Gillis, Dr Matthew Lee, Dr Sarah Allwood-Spiers and Mr Luke Zhu who analysed renal MRI for the study comparing inter-observer reproducibility of different regions of interest on multiparametric renal MRI.

Alastair Rankin

1st February 2022

Abbreviations

ADC	apparent diffusion coefficient
BNP	brain natriuretic peptide
CKD	chronic kidney disease
CM-CKD	cardiomyopathy of chronic kidney disease
CT	computed tomography
DBD	donation after brain-stem death
DCD	donation after circulatory death
DTI	diffusion tensor imaging
DWI	diffusion weighted imgaing
eGFR	estimated glomerular filtration rate
GLS	global longitudinal strain
KRT	kidney replacement therapy
LV	left ventricular
LV-GLS	left ventricular global longitudinal strain
LVEF	left ventricular ejection fraction
LVH	left ventricular hypertrophy
mm	millimetres
MRI	magnetic resonance imaging
ms	milliseconds
NT-proBNP	N-terminal pro-brain natriuretic peptide

ROI	region of interest
SD	standard deviation

Chapter 1 – Introduction

This thesis will outline the implications of kidney failure and the potential role that imaging biomarkers could play in the future management of patients with kidney failure. Across 6 distinct research studies (4 addressing cardiovascular imaging; 2 addressing functional renal MRI), this thesis examines specific aspects of proposed imaging biomarkers that are of relevance to patients with kidney failure.

1.1 Chronic Kidney Disease

Chronic kidney disease (CKD) is defined as "abnormalities of kidney structure or function, present for >3 months, with implications for health"[1]. The diagnosis is based on markers of kidney damage, which can be any one of: estimated or measured glomerular filtration rate < 60 ml/min per 1.73 m^2, urinary abnormalities (albuminuria, proteinuria, haematuria), structural abnormalities on imaging, abnormalities detected by histology, history of kidney transplantation or other electrolyte and tubular abnormalities. The staging of CKD is based on estimated glomerular filtration rate (eGFR), and sub-divided by degree of albuminuria (Figure 1.1)[1].

Figure 1.1 - Prognosis of chronic kidney disease (CKD) by glomerular filtration rate (GFR) and albuminuria.

The risk of death increases as GFR declines and albuminuria increases. (Kidney Disease Improving Global Outcomes (KDIGO) 2012; reproduced with permission[1].

Prognosis of CKD by GFR and albuminuria categories: KDIGO 2012

GFR categories (ml/min per 1.73 m²) Description and range				Persistent albuminuria categories Description and range		
				A1	A2	A3
				Normal to mildly increased	Moderately increased	Severely increased
				<30 mg/g <3 mg/mmol	30–300 mg/g 3–30 mg/mmol	>300 mg/g >30 mg/mmol
	G1	Normal or high	⩾90			
	G2	Mildly decreased	60–89			
	G3a	Mildly to moderately decreased	45–59			
	G3b	Moderately to severely decreased	30–44			
	G4	Severely decreased	15–29			
	G5	Kidney failure	<15			

Green: low risk (if no other markers of kidney disease, no CKD); yellow: moderately increased risk; orange: high risk; red, very high risk.

There are numerous formulae available to calculate eGFR, of which the CKD-EPI formula[2] utilises serum creatinine, standardised for age, sex and, race, to mathematically estimate glomerular filtration rate. However, newer formula, which utilise cystatin-C, instead of creatinine, and which remove the race adjustment, have been shown to improve accuracy, and are expected to enter clinical practice in the future[3–5].

1.2 Kidney failure

Kidney failure refers to individuals with an eGFR <15 ml/min/1.73m^2 or those requiring kidney replacement therapies (KRT) to maintain life[6].

1.2.1 Epidemiology of kidney failure

On a global scale, kidney failure represents a major health problem. In 2017, the global prevalence of CKD was 9.1% (697.5 million) accounting for 1.2 million deaths that year[7]. The global prevalence of CKD increased by 29.3% from 1990 to 2017, albeit the age-standardised prevalence of CKD did not increase suggesting that this represents the ageing global population, with age being a key determinant of CKD prevalence in a population. However, the age-standardised global incidence of dialysis and kidney transplantation did increase, by 10.7% and 12.8%, respectively[7].

In Scotland, there were 5,470 prevalent patients receiving KRT on 31st December 2020. Of these, 61% had a functioning kidney transplant, 35% were being treated with haemodialysis and 4% with peritoneal dialysis[8]. Between 2015-2019, the most common aetiology for renal failure was diabetes, followed by multisystem causes, then interstitial causes, then glomerulonephritis, then unknown[8].

1.2.2 Kidney replacement therapy

Several modalities of kidney replacement therapy are available. Many of these are continuous therapies (e.g. continuous veno-veno haemofiltraton; slow continuous ultrafiltration) that are mostly utilised in critical care settings[9]. With regards maintenance kidney replacement therapy for out-patients with chronic kidney failure, there are three broad categories: haemodialysis, peritoneal dialysis and transplantation. Within each category exists numerous sub-types and permutations, the detail of which goes beyond what is relevant to the present thesis. A brief overview of the main modalities is outlined below. Renal transplantation is the optimal form of kidney replacement therapy in patients without contraindications to it. In patients unable to receive a kidney transplant, there is no superiority of one form of dialysis over another, therefore the decision as to which type to start is dictated by patient preference, resource availability and physician opinion[10].

1.2.2.1 Haemodialysis

In the UK, the majority of patients undergoing maintenance haemodialysis attend a renal dialysis unit thrice weekly on a Monday, Wednesday, Friday or a Tuesday, Thursday,

Saturday. Standard treatment length is 4 hours per dialysis session. A minority of in-centre haemodialysis patients undergo extended hours nocturnal dialysis. This is largely initiated due to patient preference (e.g. to accommodate work commitments, childcare) but is also associated with improved cardiovascular phenotypes, fluid balance and biochemical parameters[11,12]. A separate minority of maintenance haemodialysis patients perform their treatment at home. This often involves more frequent treatments (e.g. six times per week) of varying length and allows more flexibility in lifestyle and has similar associated health benefits as extended hours nocturnal dialysis affords[13]. The goal of maintenance dialysis is to use regular intermittent treatments to control biochemical and volume-related complications of kidney failure in order to preserve life and allow the possibility of health.

Haemodialysis requires blood to be drawn from the patient at consistent and sustainable flow rates of 200-350 ml/minute and, as such, requires suitable vascular access to achieve this. Haemodialysis access options comprise of native arterio-venous fistulae, synthetic arterio-venous grafts or large bore tunnelled central venous catheters. Choice of vascular access should be individualised for each patient depending on their preference, anatomy, co-morbidities, and future transplant potential, but with fistulae being the preference where all other factors are equal[14]. The patient's blood is then drawn into the dialysis machine where small and middle molecule clearance is achieved across a semi-permeable membrane using diffusion, with or without additional convective forces (in the case of haemo-diafiltration[15]). Counter-current dialysate fluid of pre-determined solute composition maintains concentration gradients so that blood returning to the patient has biochemical properties closer to that expected in the healthy population. However, while a patient's creatinine, urea, potassium, phosphate, bicarbonate, and other measurable blood indices will improve following dialysis, the correction rarely results in normalisation of results. Even where it does so, the indices would be expected to then become increasingly abnormal over the following hours to days until their next dialysis session. Volume management is achieved by ultrafiltration, which utilises pressure gradients between the blood flow and the dialysate flow within the dialysis machine in order to remove a pre-specified rate of fluid. This can be performed contemporaneously as dialysis and the volume of fluid to be removed is clinician-lead based on a patient's weight and fluid assessment.

1.2.2.2 Peritoneal Dialysis

Peritoneal dialysis utilises the patient's peritoneal membrane as the dialysis membrane[16]. Fluid is instilled into the patient's abdomen via an indwelling peritoneal catheter. Passive

diffusion of waste molecules then occurs to allow elimination of potassium, creatinine, urea and other small molecules when the peritoneal fluid is later drained out. Ultrafiltration is achieved depending on the osmotic qualities of the infused dialysis fluid, with higher strength glucose solutions (or icodextrin, a high molecular weight glucose polymer) drawing excess water from the intravascular space into the peritoneal space to allow a greater volume of fluid to be drained off at the end of a treatment session than was originally infused. The process is then repeated multiple times a day to achieve sufficient dialysis and fluid clearance. Continuous ambulatory peritoneal dialysis refers to a dialysis regime whereby the patient manually fills, and then later drains, fluid in/out of the peritoneal cavity 3-5 times per day. However, the majority of patients on peritoneal dialysis now perform automated peritoneal dialysis[8], where they connect themselves to a machine at night-time, which then cycles fluid in and out of the peritoneal space at programmable intervals to achieve the majority of dialysis overnight, followed by a final fill of fluid that remains in the abdomen providing ongoing dialysis and ultrafiltration during the day. This fluid is then drained off that evening when the patient connects back onto their automated peritoneal dialysis machine.

1.2.2.3 Kidney transplantation

Kidney transplantation is associated with improved survival and quality of life when compared to remaining on dialysis[17], and is therefore the optimal form of kidney replacement therapy in patients where no contraindications exist. The major contraindications to kidney transplantation include: unacceptable peri-operative risk, contraindications to immunosuppression (including active uncontrolled or recurrent infections and active cancer), anatomical barriers (diseased or unsuitable vasculature; lack of space in abdomen due to organomegaly or obesity) or any other factor that would prevent the individual from gaining significant improvement in quality or quantity of life by transplantation[18]. In addition, there is a significant population of patients who are suitable to receive a kidney transplant but have long delays on the transplant waiting list due to immunological barriers reducing the likelihood of receiving an immunologically acceptable kidney offer. Transplants can be from a live donor, which may be genetically related or not, or from a deceased donor (which can be donation after circulatory death (DCD) or donation after brain-stem death (DBD)). In the majority of cases, a single kidney in transplanted but where the donor is paediatric both kidneys may be transplanted "*en bloc*". Kidney transplants can also be performed as a simultaneous pancreas-kidney dual transplant in patients with diabetes who fulfil specific criteria[19]. Clinical outcomes vary with the type of transplant received with the best graft

survival seen in living donor kidneys, followed by DBD, then DCD. As a result, there are national campaigns to maximise living donor kidney transplants, including as part of the national kidney sharing scheme, which aims to improve transplant outcomes in potential recipients who have a willing, but immunologically incompatible, living donor[20]. Extended criteria donors are donors who are: over the age of 60 years, or are over 50 years old with a history of hypertension, death by intracranial haemorrhage or a baseline serum creatinine over 133 μmol/l[21]. Transplanted kidneys from extended criteria donors are known to yield outcomes superior than those achieved by staying on dialysis but inferior to transplantation with a standard criteria kidney, with graft survival rates at 5 years approximately 20% lower than standard criteria donor transplants[21].

Regardless of what type of kidney transplant is received, graft survival is still finite, with a median overall graft survival of 11.7 years and 19.2 years for deceased donor and living donor transplants, respectively[22]. The causes of graft failure are varied but the most prevalent is chronic fibrosis resulting from low grade inflammation and rejection[23–25]. Once a transplant kidney function deteriorates until the point it is no longer able to support health, the patient must undergo a further transplant (which is commonly performed but requires planning and carries a greater immunological risk with regards rejection), start dialysis or be managed conservatively.

1.2.2.4 Conservative Care

Conservative care is an approach to CKD management that is employed in patients who either do not wish kidney replacement therapy or in whom the medical team do not believe it to be an appropriate treatment for them. It refers to active supportive management of CKD that looks to prioritize symptom control. Conservative care is an essential part of any CKD service and it is increasingly being utilised due to the aging population and the increasingly recognised burdens of dialysis in comorbid patient populations[26].

1.2.2.5 Future kidney replacement therapies

Major advances in kidney replacement therapy are expected in the next 20 years. These range from the gradual to the radical. Gradual changes in the field of dialysis are expected to include increased usage of extended hours and home-based haemodialysis, improved vascular access creation and maintenance[27,28] and the potential for improved therapeutics once several ongoing clinical trials report[29–32]. There is also the possibility of radical ‘blue-sky’ therapies being realised, with notable advances in the development of wearable dialysis machines and

biologically enhanced renal assist devices, which utilise cultured renal tubule cells to improve fluid and biochemical homeostasis[33,34].

With regards transplantation, similar advances are anticipated. These are likely to include an increased utilisation of live donor kidney transplants, increased utilisation of potential deceased donor kidneys (e.g. through utilisation of normothermic perfusion[35], virally infected kidneys[36], optimisation of immunosuppressive therapy, especially in highly sensitized individuals[37]), as well as improved biomarker utilisation for the identification of acute rejection[38]. More radical changes in the field of transplantation may be achieved in the next few decades, which might include genetically-altered xenotransplantation[39].

While we optimistically await these major advances, it is not clear if they will be sufficient to off-set the impending health burden that is expected as the global prevalence of patients requiring kidney replacement therapy continues to rise rapidly[33].

1.2.3 Complications of kidney failure

The complications of CKD are multisystem and increase in severity as the degree of CKD increases, such that individuals with kidney failure requiring replacement therapy are at greatest risk. Consequently, as CKD progresses, the frequency and severity of complications becomes more prevalent[40]. Ultimately, without replacement therapy, kidney failure is fatal. However, while kidney replacement therapies are effective at preventing death from kidney failure, these therapies are less effective at preventing the amassing complications that result from prolonged existence with incomplete replacement of renal functions (in the case of dialysis or post-transplant CKD) or complications resulting directly from the therapies (e.g. dialysis access complications; opportunistic infections and malignancies resulting from immunosuppression post-transplantation).

1.2.3.1 Cardiovascular disease

Patients with CKD are at a greatly increased risk of cardiovascular disease[41]. This risk increases with severity of CKD[42], such that patients with CKD stage 5 are 3-4 times more likely to experience a cardiovascular event than age-standardized patients without CKD[43]. In patients with kidney failure requiring dialysis, the prevalence of cardiovascular disease is

approaching 70%[44] and cardiovascular disease remains the single most common cause of death accounting for between 25-40% of all deaths[45–47]. CKD populations have a high prevalence of traditional cardiovascular risk factors, such as hypertension, dyslipidaemia, diabetes, smoking and old age, and these factors remain predictive of cardiovascular risk[48] However, risk prediction models using only traditional cardiovascular risk factors under-estimate the risk in CKD populations[43,49], and adding an assessment of kidney function to these models improves prediction[43,50]. A number of CKD-specific risk factors, such as proteinuria, bone mineral disease and intradialytic hypotension, have been identified and contribute to the excess cardiovascular mortality[51,52].

CKD results in a unique cardiovascular phenotype: with relatively fewer deaths due to atherosclerotic processes but more due to sudden cardiac death and heart failure[44–47,53]. The pathophysiological basis for this phenotype is believed to be a combination of 2 processes. Firstly, Cardiomyopathy of Chronic Kidney Disease (CM-CKD), which is also called 'uraemic cardiomyopathy', refers to a specific pattern of myocardial fibrosis that is found in patients with CKD. It has been shown to be a strong predictor of cardiovascular mortality[54–56]. Secondly, arterial disease has been consistently demonstrated to associate with poor outcome in CKD[57,58]. CKD drives pathological changes to arterial function with 2 interlinked processes. The blood vessels stiffen (which we have shown associates with premature cardiovascular disease in kidney failure)[59,60] and exhibit accelerated calcification[51,61]. There are currently no available treatments, beyond transplantation, that have been consistently shown to reduce mortality from cardiovascular disease in patients with kidney failure.

1.2.3.2 Hypertension

Hypertension is common in CKD and occurs early in the disease course. Between 60-88% patients with CKD not requiring replacement therapy have hypertension[48,62,63]. In patients requiring dialysis, one study found that 86% had hypertension of whom only 30% were deemed to be adequately controlled[64]. In non-dialysis CKD, hypertension increases the risk of cardiovascular events, but this association is less clear in patients requiring dialysis where a U-shape relationship is evident, with the most extreme risk observed in individuals with low systolic blood pressure pre-dialysis[48,65]. The optimal blood pressure target for patients with kidney failure requiring replacement is not known[66–68].

1.2.3.3 Dyslipidaemia

The prevalence of hyperlipidaemia increases as the severity of CKD increases[69]. However, the beneficial effect of statins reduces as the severity of CKD increases, such that patients on haemodialysis gain less benefit from statin therapy than other patient groups[70,71].

1.2.3.4 Anaemia

Over 75% of patients with kidney failure have anaemia[72], of which the aetiology is multifactorial[73]. Erythropoietin stimulating agents and intravenous iron form the mainstay of anaemia management in patients with kidney failure[74]. Excessive doses of erythropoietin stimulating agents have been shown to be harmful, such that guidelines recommend avoiding over-correction of anaemia[74], while, in contrast, high dose intravenous iron resulting in supra-physiological iron stores has been shown to reduce cardiovascular events in patients on dialysis[75].

1.2.3.5 Metabolic disorders and CKD-related bone and mineral disease

The primary function of the kidney is to maintain homeostasis. In kidney failure, metabolic complications, including acidosis, hyperkalaemia, nutritional deficiency, altered glucose regulation and abnormal salt and water handling are common[76]. In addition, there is likely to be accumulation of unmeasured molecules that are usually excreted by the kidney, with unquantified effects on all organ systems. The specific syndrome of CKD-related bone and mineral disease encompasses a range of biochemical and skeletal abnormalities due to hyperphosphataemia, active vitamin D deficiency and secondary hyperparathyroidism that occur a consequence of kidney failure[77]. Secondary effects of the resulting metabolic milieu are far-reaching and difficult to quantify but likely impact on vascular calcification, left ventricular hypertrophy, platelet and coagulation function, myopathy, neuropathy, and skin function, amongst other body systems.

1.2.3.6 Malignancy

The risk of cancer is elevated in patients with kidney failure. In renal transplant recipients the risk is at least twice that of the general population and is a recognised, explainable consequence of the immunosuppressive therapy necessary to maintain transplant function[78]. In patients on dialysis the risk of multiple different cancers is also increased compared to the general population[79,80]. The causative role of kidney failure in the development of these cancers is unclear and it may be that starting dialysis denotes survivor bias, but regardless if

the relationship is causal or not, the association is consistently reported with implications for clinical management of patients on dialysis.

1.2.3.7 Cognitive impairment

Cognitive impairment is more prevalent within CKD populations than non-CKD populations[81]. The aetiology is multifactorial with suggested hypothesis including vascular injury and direct effect of uraemic toxins[81]. In a dialysis population, changes in cerebral blood flow during dialysis are evident and correspond with intradialytic cognitive dysfunction. In those who continued dialysis, these changes were associated with progressive cognitive decline which improved in those who underwent transplant[82].

1.2.3.8 Multimorbidity

CKD is associated, almost ubiquitously, with multimorbidity due to the inevitable complications it produces and the high prevalence of CKD resulting from another disease (e.g. diabetes). Increasing levels of multimorbidity in CKD is associated with increasing mortality[83], and in comparison to patients with multimorbidity but without CKD, those with CKD have 2-3 times higher risk of hospitalisation[84].

1.2.3.9 Mortality

There is a graded association between the severity of CKD and increasing risk of death, with CKD stage 5 yielding an adjusted hazard ratio for death of 5.9[42]. The risk is greatest in patients requiring dialysis[85], such that the 5 year adjusted life expectancy of 50% is worse than many solid organ cancers including colorectal and breast cancer[86].

1.2.3.10 Complications specific to kidney replacement therapy.

Patients requiring dialysis have the greatest risk of the aforementioned complications. In addition, there are specific complications relating to their dialysis modality. These include dialysis access complications (thrombosis, dysfunction, infection)[87], increased risk of blood borne viruses[88], and intradialytic end-organ hypo-perfusion, which can occur with[89] and without[90] systemic hypotension. For patients on peritoneal dialysis, there are similar risks of access failure and infection, including bacterial peritonitis, as well as the small risk of encapsulating peritoneal sclerosis[16].

Transplant recipients have greatly improved cardiovascular and metabolic risk profiles compared to those on dialysis but remain at a greater increased risk of death and cardiovascular disease compared to the age-matched general population[91]. They are also vulnerable to transplant-related complications such as the risks of immunosuppression pre-

disposing to severe and opportunistic infections, as well as an increased risk of diabetes and cancer[92].

1.3 Biomarkers and their use in medicine

A biomarker is a "defined characteristic that is measured as an indicator of normal biological processes, pathogenic processes, or responses to an exposure or intervention, including therapeutic interventions[93]." Biomarkers can be molecular, histological, radiographic, or physiologic characteristics that can be used in 7 broad settings: susceptibility/risk, diagnostic, monitoring, prognostic, predictive, pharmacodynamic/response and safety[93]. Biomarkers are ubiquitous in modern clinical practice, and there are whole fields of medical research aimed at identifying and honing novel biomarkers. The properties of an ideal biomarker vary depending on its intended application, often balancing sensitivity, specificity, cost, availability, responsiveness and biological plausibility depending on how it will be used.

1.4 Why are biomarkers important for patients with kidney failure?

There is no cure for kidney failure and, as outlined above, all kidney replacement therapies bring a risk of complications and reduced life expectancy. Despite this, nephrology lies far behind other medical specialties with regards the number of completed clinical trials, with ten times fewer nephrology trials published over a 40-year period compared to cardiology[94]. Without clinical trials, any progress in the management of kidney failure will be slow and unproven. There are multiple reasons for scarcity of trials in nephrology including an over-reliance on registry data, low prevalence of primary renal disease (e.g. glomerulonephritis) making recruitment challenging, high prevalence of secondary renal disease (e.g. diabetic nephropathy, ischaemic nephropathy) resulting in heterogenous cohorts, and repeated negative trial results[70,95,96] driving disengagement of funders, researchers and participants. As a result, the standard of care never improves.

The identification of reliable biomarkers relevant to CKD would allow incorporation into clinical trial design and overcome many of these problems. For instance, imaging biomarkers could be used to identify participants who stand most to benefit from a proposed treatment and therefore allow smaller sample sizes to be used due to the expected greater magnitude of

effect. This approach already been successfully applied in the field of nephrology[97], albeit there can be negative consequences to this strategy, including increased resources required for participant screening and limiting the generalisability of trial results. Alternatively, validated biomarkers could be used as surrogate outcome measures to allow novel therapeutics to be trialled more readily, with shorter follow-up durations and reduced cost, so that only promising treatments would go on to the more expensive and burdensome hard outcome clinical trials.

A reliable cardiovascular biomarker for patients with kidney failure is urgently needed to improve our understanding of pathophysiology, diagnosis and management of the excessive cardiovascular risk associated with kidney failure. CM-CKD, or 'uraemic cardiomyopathy', is challenging to study for a number of reasons. Myocardial biopsy is ethically difficult to justify due to procedural risks and potential sampling errors[98,99]. Animal models of uraemia exist but are not representative of human disease due to the relatively shorter duration of CKD and difficulties in replicating dialysis in animals. Therefore, non-invasive techniques to detect CM-CKD are required in order to allow diagnosis and prognostication, and for the identification of targets for new therapies.

1.5 Cardiovascular biomarkers in kidney failure

The most commonly used soluble cardiac biomarkers in routine clinical practice are derivatives of cardiac troponins and brain-natriuretic peptides. Cardiac troponin levels are often elevated in people with CKD, but this reflects the increased cardiovascular risk in this population, rather than the reduced renal excretion of the biomarker[100]. For the assessment of acute myocardial infarction, dynamic changes in troponin remain highly sensitive in people with CKD[100]. Beyond the assessment of myocardial infarction, high sensitivity troponin, as well as NT-pro-BNP and novel biomarkers sST2 and GDF-15[101] have been shown to associate with incident heart failure[102], cardiovascular mortality and all-cause mortality[103]. For the diagnosis of heart failure, BNP and NT-proBNP can be used in persons with CKD not on dialysis with similar accuracy to non-CKD controls, albeit higher threshold values are required[104]. In people on dialysis, BNP and NT-proBNP have prognostic value but limited role in the diagnosis of heart failure[100,105]. With regards identification of myocardial fibrosis, both Troponin and BNP have been shown to correlate with CKD-specific changes on CMR[106] but are not specific for this

finding.

The electrocardiograph (ECG) also has utility in the diagnosis and prognosis of cardiovascular disease in kidney failure. For instance, in one dialysis cohort, evidence of left ventricular hypertrophy by voltage criteria independently predicted cardiovascular mortality[107]. However, it is well recognised that ECG findings can vary significantly throughout a single dialysis session. In this study, the voltages increased throughout dialysis, while other studies have repeatedly reported QRS prolongation, T-wave inversion and QT prolongation occurring during dialysis[108,109]. It is plausible that the changes occur due to altered cell membrane potentials due to changing water and electrolyte contents of the myocardial interstitium.

Echocardiography is widely available and well-established clinical tool that allows assessment of cardiac structure and function. However, there are specific challenges to using echocardiography in patients with kidney failure[110]. Up to 70% of patients requiring regular dialysis will have left ventricular hypertrophy on echocardiography, however the prognostic significance of this finding is uncertain [110,111]. Furthermore, estimation of ventricular volumes by echo is inherently dependent on patient volume status and can yield inconsistent results in patients with kidney failure who are prone to volume overload[112,113]. While some more specialised echocardiographic techniques, in particular speckle-tracking echocardiography and integrated backscatter analysis, have shown promising results for the identification of myocardial fibrosis in CKD [114], cardiovascular MRI remains the gold-standard technique[115].

1.6 Cardiovascular MRI as a biomarker in kidney failure

Cardiovascular magnetic resonance imaging (MRI) is established as the reference method for imaging CM-CKD[114]. Cardiovascular MRI has been shown to be superior to echocardiography for accurate definition of cardiac dimensions in kidney failure[113]. Gadolinium-enhanced MRI can identify diffuse myocardial fibrosis in patients on dialysis[116], and associates with poor survival[117]. However, after initial success with gadolinium-based techniques, the discovery of an association between nephrogenic sclerosing fibrosis and gadolinium contrast media ended any further research with these agents[118,119]. The need for an alternative marker of CM-CKD is urgent and has been further intensified by recent doubts cast on the validity of isolated left ventricular hypertrophy (LVH) (admittedly diagnosed primarily by echocardiography), as a

marker for cardiovascular outcomes in CKD patients[111]. There are numerous cardiovascular imaging techniques that are emerging as potential biomarkers CM-CKD, including global longitudinal strain (GLS), native T1 mapping, native T2 mapping, novel sequences for the identification of vascular calcification and contrast-enhanced CT to allow quantification of myocardial extracellular volume.

1.6.1 Global longitudinal strain

Myocardial strain measures the percentage of muscle deformation during the cardiac cycle as an alternative approach to assessing cardiac function compared to volumetric methods such as left ventricular ejection fraction (LVEF)[120]. Strain can be assessed in 3 planes - longitudinal, circumferential and radial – in both the left and right ventricles (Figure 1.2). In patients with kidney failure, GLS is of theoretical advantage as a more sensitive indicator of myocardial stiffening due to fibrosis. Indeed, studies assessing GLS by echocardiography in patients with CKD have been shown it to be a strong independent predictor of cardiovascular and all-cause mortality[121–123]. However, GLS measured using cardiovascular MRI has not been assessed in this population.

Figure 1.2 – Representative images of global longitudinal strain.

Representative image showing endocardial and epicardial contours on the left ventricle from a 4 chamber long axis cine (left atrial and right ventricular endocardial contours also shown) (A); the resultant strain curve showing the percentage of global longitudinal deformation for each phase throughout the cardiac cycle (B); and a "bull's-eye" plot showing the peak longitudinal strain within each segment of the myocardium as defined by the American Heart Association (AHA) model (C) [124]

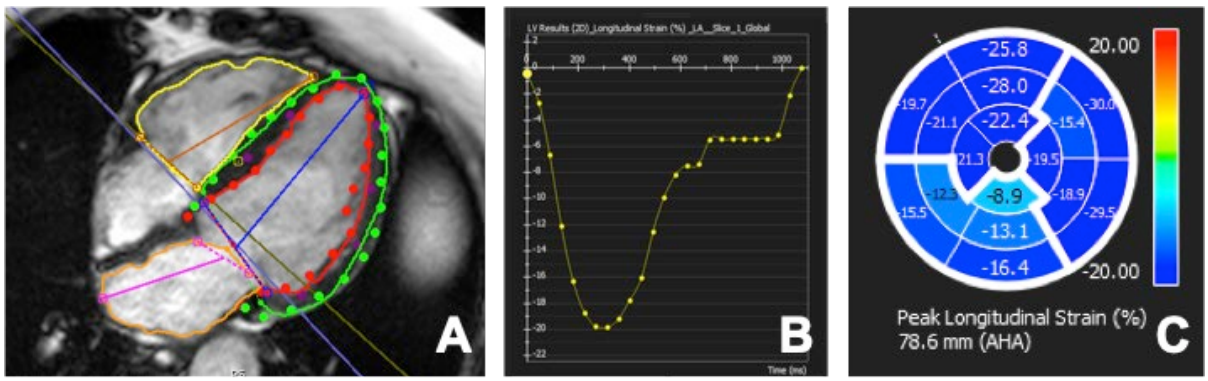

1.6.2 Myocardial native T1 and T2 mapping

Myocardial fibrosis is the pathological hallmark of the cardiomyopathy of chronic kidney disease but is difficult to image without the use of gadolinium-based contrast agents. However, native T1 mapping, which is a non-contrast MRI sequence that represents the constant for the longitudinal relaxation time (ms) of the myocardium to reflect changes in extra- and intracellular compartments is a promising biomarker for quantifying fibrosis (Figure 1.3). In non-CKD populations, native T1 mapping has been shown to correlate well with histological fibrosis[125,126]. The concern in CKD populations is that tissue oedema, rather than fibrosis, may confound the result[127,128] and further studies are needed to clarify this. Native T2 mapping, which assesses the transverse relaxation time constant (ms) and is sensitive to changes in proton (i.e. water) binding to macromolecules may be a useful biomarker of tissue oedema and could be used to complement T1 mapping, with specific relevance in kidney failure populations[106].

Figure 1.3 – Representative images of native T1 mapping (A) and native T2 mapping (B) of a mid-ventricular short-axis image of the heart on 3T MRI.

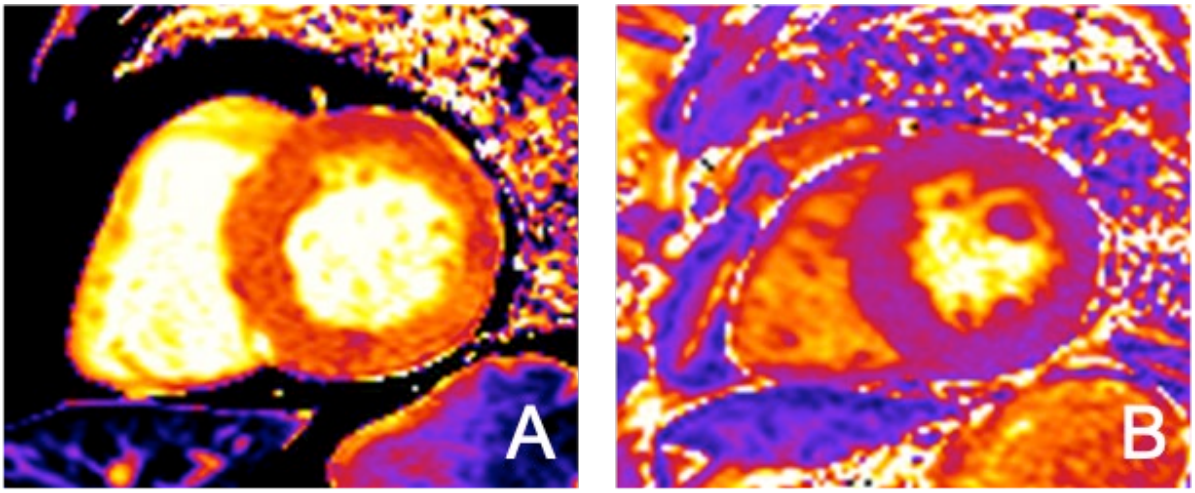

1.6.3 Radial-VIBE MRI for the detection of vascular calcification

The severity of vascular calcification associates with the severity of CKD and portends a poor outcome[58,129]. Several therapeutic agents are currently being trialled to treat vascular calcification in CKD, of which magnesium supplementation and sodium thiosulphate appear most promising[130]. Computed tomography (CT) is the gold standard non-invasive technique for assessing vascular calcification but is limited by the requirement of exposure to ionising radiation. Conventional spin-echo MRI sequences cannot identify vascular calcification as the low proton density within the calcification appears hypointense and indiscernible from the dark arterial lumen. Radial volumetric-interpolated breath-hold examination (radial-VIBE) is a novel non-contrast, free-breathing gradient-echo MRI sequence which may allow the identification and quantification of vascular calcification on MRI (Figure 1.4). This would be of particular value where serial scanning was required, especially in research settings, due to the lack of ionising radiation, or in patients undergoing magnetic resonance angiography or cardiovascular MRI where additional information on vascular calcification would be useful and easily attainable.

Figure 1.4 - Representative images of vascular calcification (red arrows) on CT (A) and MRI Radial-VIBE (B). Both images are sagittal slices of the thoracic aorta on 3T MRI.

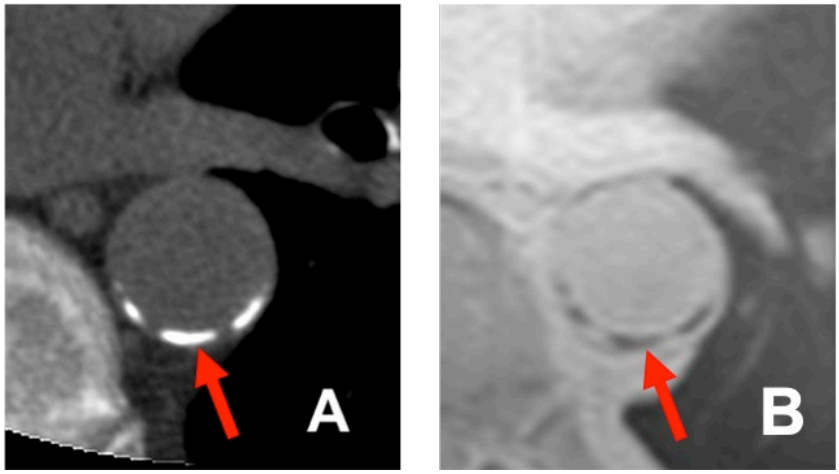

1.6.4 Myocardial extracellular volume

Myocardial extracellular volume measured using gadolinium-based contrast agent-enhanced MRI is the gold standard method for non-invasively quantifying diffuse myocardial fibrosis[131,132] but is relatively contraindicated in patients with kidney failure due to the risk of nephrogenic systemic fibrosis. An alternative approach using iodinated contrast-enhanced CT has been shown to reliably measure ECV, with close affinity to MRI, in patients with amyloid[133] and aortic stenosis[134] (Figure 1.5). If applicable to patients with kidney failure, this technique could be crucial for non-invasively identifying myocardial fibrosis, the key histological change in the cardiomyopathy of CKD, to improve the diagnosis and potential treatments of cardiovascular disease in kidney failure.

Figure 1.5 - Representative images of contrast-enhanced cardiac computed tomography. Panels show pre-contrast (A), post-contrast (B) and 5 minute delayed post-contrast (C) images. Regions of interest (ROI) were manually drawn in the inter-ventricular septum and the left ventricular blood pool on the post-contrast images (B). The ROIs were copied to the corresponding locations on the pre-contrast and the delayed post-contrast images (A, C). Myocardial extracellular volume on CT (ECV-CT) was calculated by the formula: ECV-CT = (1 – haematocrit) x (change in HU_{tissue}/change in HU_{blood}), where HU refers to the signal intensity in hounsfield units in the septum (HU_{tissue}) and blood pool (HU_{blood}).

1.7 Renal MRI as a biomarker in kidney failure

Functional renal MRI is a burgeoning area of research with potential to improve our understanding and diagnosis of renal disease. While previous studies exploring MRI to describe purely anatomical features, such as cortico-medullary differentiation, were found to be of limited clinical value[135,136], modern MRI sequences utilize a variety of parameters to draw inferences as to renal microstructure, perfusion, and diffusion and therefore have potential to offer comprehensive characterization of renal disease[137–140]. However, functional renal MRI is still a relatively new technique and further research is required to expand our understanding of its prognostic ability, histological correlations, and how to best combine different MRI sequences to aid translation into clinical practice[141].

Renal transplantation is the optimal treatment for patients with renal failure. Despite advances in our understanding of the immune system and development of drugs to prolong transplant function, the period of time for which a transplant functions remains finite, with 13% failing before 5 years and 26% failing before 10 years[142]. The most common reason for transplants to fail is the development of chronic immune-mediated rejection and other causes of irreversible fibrosis[23–25]. Incident transplant dysfunction is most commonly detected due to

a rise in serum creatinine with or without the emergence of proteinuria. These markers of acute transplant dysfunction are non-specific and usually herald further investigations into the individual causes, but ultimately, a biopsy of the transplant kidney is often required for definitive diagnosis[143,144]. Biopsy of renal transplants include the risks of bleeding (which can be severe), infection (with seeding from urinary tract to bloodstream), loss of transplant function, non-diagnostic results and discomfort for patients[145,146]. Furthermore, a standard renal biopsy samples <1% of renal cortex tissue and is therefore prone to sampling error, which may mis-inform clinical practice (e.g. if an area of focal scarring is biopsied). If a treatment is instigated on the basis of a biopsy result, it can be necessary to repeat the biopsy to assess treatment response, thus doubling the risk exposure for patients. Accordingly, a non-invasive biomarker of renal transplant pathology is needed. Several studies have shown that specific MRI sequences can detect parenchymal fibrosis in renal transplant recipients[147–150], albeit the ability of MRI to distinguish the aetiology of transplant dysfunction remains to be proven[141]. If validated, functional renal MRI could improve the management of renal transplant recipients by reducing risk exposure and increasing diagnostic accuracy[151].

1.7.1 Renal Native T1

The native T1 time (ms), which represents the constant for longitudinal re-magnetisation of protons following a pulsed MRI signal, can be applied to the renal parenchyma much as it is the myocardium (Figure 1.6). Renal T1 mapping will be affected by fibrosis, oedema and inflammation, with lower signal in tissues with increasing water content. Accordingly, T1 values (ms) can inform as to the microstructure of the renal parenchyma, with increasing T1 values seen in the presence of fibrosis[138]. In patients with CKD, cortical and medullary T1 values are significantly higher compared to healthy controls[137,152].

Figure 1.6 - Representative image of native T1 mapping of a transplant kidney.

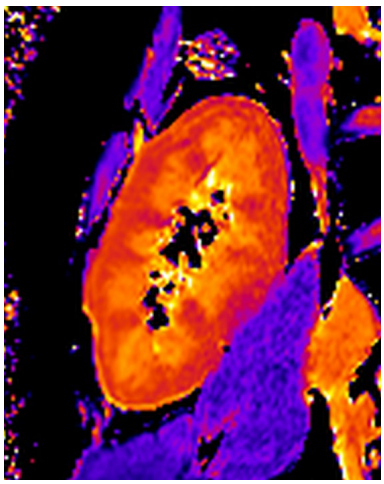

1.7.1 Diffusion Weighted Imaging

Diffusion weighted imaging (DWI) assesses the diffusibility of water within an individual voxel, which can be quantified by the apparent diffusion coefficient (ADC) (mm^2/s) (Figure 1.7). ADC values are reduced in patients with CKD compared to controls[153,154]. In renal transplant recipients, ADC differs between transplant patients and healthy controls[155,156], and has been shown to correlate with renal function[157,158].

Figure 1.7 - Representative image of diffusion weighted imaging (DWI) of a transplant kidney.

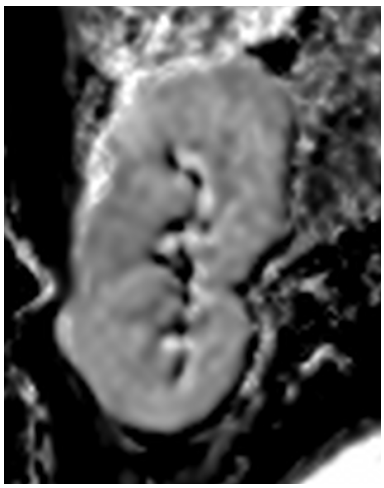

1.7.2 Diffusion Tensor Imaging

Diffusion tensor imaging (DTI), measures molecular motility of water molecules in a similar way to DWI but with additional assessment of directionality in order to produce a fractional anisotropy map (Figure 1.8). DTI is thought to be a measurement of organ 'stiffness'[159] and can therefore infer information regarding renal transplant scarring and fibrosis. In one study of 40 renal transplant recipients, DTI displayed a high accuracy for discriminating good from poor renal function[158]. The combination of DWI and DTI has been studied and was found to be able to detect delayed graft function in 33 renal transplant recipients and correlated closely with fibrosis[160].

Figure 1.8 - Representative image of diffusion tensor imaging (DTI) of a transplant kidney.

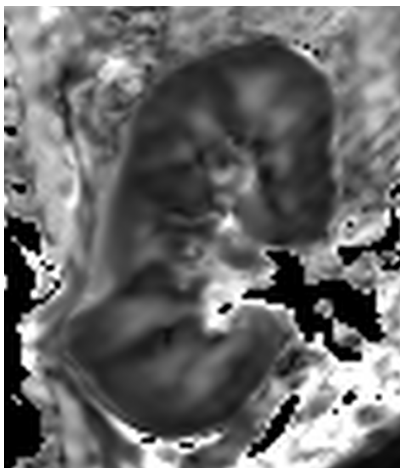

1.7.1 Blood oxygen level dependent Imaging

Blood oxygen dependent imaging (BOLD) utilises the magnetic properties of deoxyhaemoglobin to quantify intra-renal tissue oxygen bioavailability (Figure 1.9). Deoxyhaemoglobin results in an increase in R2* signal on MRI. R2* (s^{-1}) is 1/T2* where T2* is the observed, rather than the natural (i.e. T2), transverse time constant (ms). BOLD on renal MRI is highly reproducible[161,162] and has been shown to differentiate patients with chronic kidney disease from controls with normal renal function[154,155]. In transplant populations, BOLD has been shown to differentiate acute rejection from normal functioning transplants and those with acute tubular necrosis[156,163–165].

Figure 1.9 – Representative image of blood oxygen level dependent (BOLD) imaging of a transplant kidney.

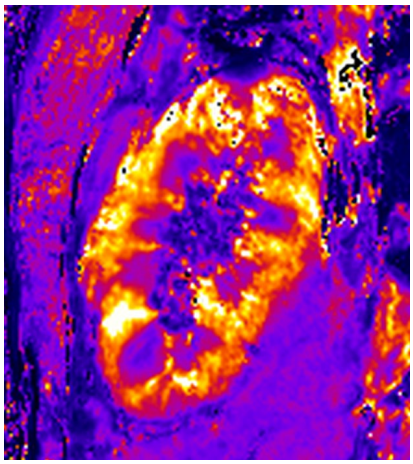

1.7.2 Arterial-spin labelling

Arterial spin labelling (ASL) MRI is a non-invasive method of measuring renal perfusion (ml/100g/min) using magnetised blood as endogenous contrast (Figure 1.10). ASL has been shown to be reproducible and extensively studied in healthy volunteers and patients with CKD[152,166–170]. Furthermore, ASL has been studied in renal transplant populations[171–174], and has been shown to differentiate good/moderate transplant function from poor transplant function[172].

Figure 1.10 - Representative image of arterial-spin labelling (ASL) imaging of a transplant kidney.

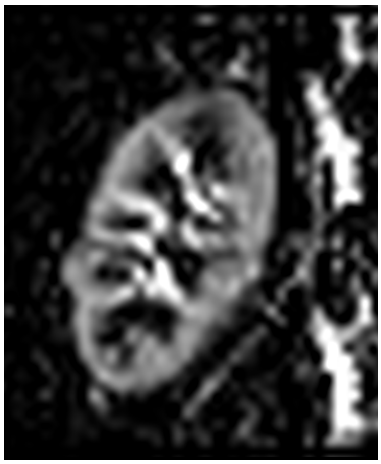

1.7.3 Multiparametric renal MRI protocols

While each of the individual MRI sequences discussed above have a potential clinical utility, the greatest benefit of renal MRI is likely to be a multiparametric approach, where a number of sequences are employed in a single imaging session. Given the likely complex relationship between the MRI signals and renal pathology, it is possible that deriving a composite 'fingerprint' from all sequences will be the optimal method of characterizing renal disease from imaging findings. This multiparametric approach is being increasingly adopted in CKD[137] and transplant research studies[147,149,150] but further clinical and histo-pathological correlation is required.

Chapter 2 – Methods and research questions

2.1 Justification for thesis in journal format

The distinct research studies included in this thesis are linked by the over-arching theme of functional MRI in patients with kidney failure. Accordingly, compilation of separate scientific publications into one thesis is justified. Furthermore, the majority of research in this thesis has already been published and so reproduction without correct acknowledgement would risk copyright infringement.

A prospective declaration stating the intention to use the cardiovascular studies as a whole is archived in The Chief Scientist Office (Scotland) clinical academic fellowship website (available at https://www.cso.scot.nhs.uk/outputs/cso-funded-research/caf/) and in the prospectively registered entry on clinicaltrials.gov (ClinicalTrials.gov Identifier: NCT03704701; https://clinicaltrials.gov/ct2/show/NCT03704701).

The addition of the functional renal MRI studies to this thesis was a logical scientific progression given the similarities in MRI techniques and patient populations, but was not formally added to this thesis plan until it was certain that the cardiovascular studies would be achievable, thus fulfilling my commitment with respect my funded fellowship (CAF/18/02).

All research included in this thesis was undertaken while registered as post-graduate research student at the University of Glasgow.

Patients with kidney failure are dependent on kidney replacement therapies to maintain life. All forms of kidney replacement therapy bring risk of complications. For those on dialysis, the incumbent cardiovascular risk is the primary driver of excess mortality for which there is no effective treatment (aside from kidney transplantation). Accordingly, we chose to study the cardiovascular phenotype of patients on dialysis in the hope to better understand, prognosticate and diagnose cardiovascular disease in kidney failure. For those patients with kidney failure who are fortunate enough to receive a kidney transplant, the finite life span of that transplant is a major concern. Existing strategies to investigate transplant dysfunction

rely heavily on invasive kidney biopsy. We chose to translate our experience in cardiovascular MRI, to see if we could use functional renal MRI to non-invasively assess kidney transplant dysfunction, with the hope that in the future it may be possible to more readily, reliably, and non-invasively investigate patients with declining transplant function.

2.2 Research questions

This thesis addresses the following research questions:

Cardiovascular imaging in patients with kidney failure on dialysis:

1) Is left-ventricular global longitudinal strain (LV-GLS), as measured on cardiovascular MRI, a predictor of all-cause mortality in patients on dialysis? (Chapter 3)

2) Is native T1 mapping on cardiovascular MRI affected by altering fluid status with ultrafiltration on dialysis, and therefore can it be used as a non-invasive measure of myocardial fibrosis in kidney failure? (Chapter 4)

3) Can vascular calcification be measured using a new MRI technique (radial-VIBE) with close affinity to the gold-standard CT techniques? (Chapter 5)

4) Can contrast-enhanced CT be used as a novel approach for identifying myocardial fibrosis with correlation between extra-cellular volume on CT (ECV-CT) and native T1 mapping measured on cardiovascular MRI? (Chapter 6)

Renal MRI in patients with kidney failure who have a kidney transplant:

5) What is the inter-observer reproducibility of different regions of interest used in renal MRI analysis? (Chapter 7)

6) Do functional renal MRI sequences correlate with histological markers of fibrosis and inflammation in kidney transplant recipients with transplant dysfunction? (Chapter 8)

2.3 Materials and methods

A separate scientific manuscript is included addressing each of the aforementioned research questions. Detailed description of the methods, including statistical analysis plan, for each study is included in each manuscript.

The data reported in Chapter 3 was retrospectively collated and re-analysed from previous research studies. The prospective studies described in Chapters 4 (n=26) and 6 (n=23) utilised the same participant cohort. These participants were recruited by me during the research period for this thesis. Data from the 26 participants in Chapter 4 were combined with another study cohort for the analysis described in Chapter 5. Chapter 7 utilised participant data from previously performed research studies within our centre. The participants reported in Chapter 8 were recruited by me as part of the work for this thesis.

2.4 Confirmation from publisher to reproduce published manuscripts

Four published manuscripts are included in their entirety in this thesis. All 4 manuscripts were distributed Open Access under Creative Commons CC BY license which permits "unrestricted use, distribution, and reproduction in any medium, provided the original work is properly cited" (https://creativecommons.org/licenses/). Two additional draft manuscripts have been included which describe provisional results and have not been submitted for publication in their current form and are therefore not subject to copyright restrictions.

Chapter 3 - Global longitudinal strain by feature-tracking cardiovascular magnetic resonance imaging predicts mortality in patients with end-stage kidney disease. *Clin Kidney J* (2021)

3.1 Manuscript

Alastair J Rankin, Luke Zhu, Kenneth Mangion, Elaine Rutherford, Keith A Gillis, Jennifer S Lees, Rosie Woodward, Rajan K Patel, Colin Berry, Giles Roditi, Patrick B Mark, Global longitudinal strain by feature-tracking cardiovascular magnetic resonance imaging predicts mortality in patients with end-stage kidney disease, *Clinical Kidney Journal*, Volume 14, Issue 10, October 2021, Pages 2187-2196, https://doi.org/10.1093/ckj/sfab020

Abstract

Background: Patients with end-stage kidney disease (ESKD) are at increased risk premature death, with cardiovascular disease being the predominant mode of death. We hypothesized that left ventricular global longitudinal strain (LV-GLS) measured by feature tracking cardiovascular magnetic resonance imaging (CMR) would be associated with all-cause mortality in patients with ESKD.

Methods: A pooled analysis of CMR studies in patients with ESKD acquired within a single centre between 2002 and 2016 was carried out. CMR parameters including left ventricular ejection fraction (LVEF), LV mass index (LVMI), left atrial emptying fraction (LAEF) and LV-GLS were measured. We tested independent associations of CMR parameters with survival using a multivariable Cox model.

Results: Among 215 patients (mean age: 54 years, 62% male), mortality was 53% over 5.0 years median follow-up. The median LVEF was 64.7% (IQR 58.5, 70.0) and median LV-GLS was -15.3% (-17.24, -13.6). While 90% of patients had preserved LVEF (>50%), 58% of this group had abnormal LVGLS (>-16%). On multivariable Cox regression, age (HR: 1.04, 95%CI: 1.02-1.05), future-renal transplant (HR 0.29 95%CI: 0.17-0.47), LAEF (HR: 0.98, 95%CI: 0.96-1.00) and LV-GLS (HR: 1.08, 95%CI: 1.01-1.16) were independently associated with mortality.

Conclusions: In this cohort of patients with ESKD, LV-GLS on feature tracking CMR and LAEF were associated with all-cause mortality, independent of baseline clinical variables and future renal transplantation. This effect was present even when >90% of the cohort had normal left ventricular ejection fraction (LVEF). Using LV-GLS, instead of LVEF, to diagnose cardiac dysfunction in patients with ESKD could result in a major advance in our understanding of cardiovascular disease in ESKD.

Keywords: ESKD, cardiovascular, Survival analysis, chronic renal failure, magnetic resonance imaging, left ventricular hypertrophy

What is already known?

Left ventricular global longitudinal strain (LV-GLS) measures percentage muscle deformation during the cardiac cycle as a sensitive marker of myocardial function.
LV-GLS measured on echocardiography is known to associate with mortality in patients with end-stage kidney disease (ESKD). The association of LV-GLS on cardiovascular MRI and survival has not been studied in patients with ESKD.

What this study adds?

LV-GLS on cardiovascular MRI was associated with all-cause mortality, independent of baseline clinical variables and future renal transplantation.
This effect was present even when >90% of the cohort had normal left ventricular ejection fraction (LVEF).
The survival benefit of renal transplantation was evident even in the quartile of participants with the most severely impaired LV-GLS.

What impact will this have?

Using LV-GLS, instead of LVEF, to diagnose cardiac dysfunction in patients with ESKD could result in a major advance in our understanding of cardiovascular disease and prognosis in ESKD
LV-GLS in isolation is unlikely to be helpful when assessing an individual's suitability for renal transplantation.
Further studies exploring cardiovascular therapeutics in patients with ESKD who have impaired LV-GLS are warranted.

Introduction

Patients with chronic kidney disease (CKD) are at increased risk of death from all-causes compared to the general population [175]. The majority of this increased risk is due to cardiovascular disease [42]. While ischaemic heart disease is the most common form of cardiovascular disease in the general population, patients with CKD have relatively fewer atherosclerotic events but a disproportionate increase in the risk of sudden cardiac death and death from arrhythmogenic causes [47]. This risk increases with severity of CKD [42], such that patients with CKD stage 5 are 3-4 times more likely to experience a cardiovascular event than age-standardized patients without CKD [43]. This excess cardiovascular risk is intrinsically linked to cardiac structural and functional abnormalities, which start to develop early in CKD [176]. These include left ventricular hypertrophy (LVH), cardiac dysfunction and myocardial fibrosis, which together are sometimes referred to as a 'uraemic cardiomyopathy' [54–56]. The utility of cardiac magnetic resonance (CMR) imaging to detect these abnormalities has been an area of growing interest and CMR may prove to be a useful tool in the development of non-invasive novel biomarkers for future risk-stratification [114,115].

Left ventricular global longitudinal strain (LV-GLS) measures percentage muscle deformation during the cardiac cycle as a sensitive marker of myocardial function [120]. Feature tracking CMR is a non-contrast post-processing technique that derives LV-GLS by tracking endo- and epicardial borders through successive images from routinely acquired cine CMR sequences [120]. Normal values for LV-GLS measured by feature tracking CMR are approximately -20 +/- 4%[177–179]. LV-GLS has been shown to be a strong correlate of mortality and clinical outcomes in patients with myocardial infarction [180], and improvements in LV-GLS have been reported following renal transplantation [181]. In patients with CKD, utilizing echocardiography, GLS has been reported to predict clinical outcomes [121]. However, CMR is considered the gold standard imaging modality in end-stage kidney disease (ESKD), as fluctations in volume status with renal replacement therapy may have an undue influence on images obtained in a two-dimensional plane.[113]

We hypothesised that LV-GLS on feature tracking CMR has incremental prognostic utility over clinical and conventional imaging parameters for predicting all-cause mortality in patients with ESKD.

Materials and Methods

Participants

CMRs from research studies carried out in participants with ESKD within a regional renal and transplant centre between 2002 and 2016 were pooled. Patients for whom CMR images were available and who had consented for long term data follow-up were eligible for inclusion. All participants had CKD stage 5 (eGFR <15 ml/min/1.73m^2) and were receiving, or estimated to be within 6 months of requiring, renal replacement therapy. Further details of the cohorts are described elsewhere (ClinicallTrials.gov ID NCT01951404)[116,182,183]. Participants provided written informed consent and regional ethics committee approval was granted; the study was conducted in agreement with the Declaration of Helsinki.

Clinical data were manually collected via the West of Scotland Electronic Renal Patient Record database (Vitalpulse, Chelmsford, UK) by members of the team blinded to other aspects of the study. Baseline clinical variables included demographic characteristics and medical history. The primary outcome was all-cause mortality. The secondary outcome was cardiovascular mortality defined as death due to myocardial infarction, heart failure, sudden cardiac death, stroke and peripheral vascular disease [184].

CMR Image Acquisition

CMR acquisition was performed using 1.5 Tesla (T) (Sonata, Siemens Erlangen, Germany) and 3T MRI scanners (Magnetom Verio and Prisma, Siemens Erlangen, Germany). For patients on haemodialysis, the scans were performed 24 hours following the end of their dialysis session. Imaging protocols were similar in all studies and were as described previously [116,182,183]. In short, electrocardiograph-gating was used and the images were acquired in end-expiration. Following the acquisition of localiser images, balanced steady state free precession sequences were used to acquire left ventricular cines in three long axis planes, followed by a short axis stack from the apex to the atrio-ventricular ring. Additional details are available in supplementary materials S1.

Supplementary material table S1. Imaging acquisition parameters for 1.5T and 3T

	1.5T	3T
TR (ms)	47.1	41.4
TE (ms)	1.6	1.51
Flip angle (°)	60	40
Field of view (mm*mm)	340 x 340	340 x 272
Slice thickness (mm)	8	8
Slice gap (mm)	2	2
Voxel size (mm^3)	2.2 x 1.3 x 8.0	1.5 x 1.3 x 8.0
Phases (minimum)	15	25

CMR Image Analysis

All data analysis was carried out in a core lab, utilizing dedicated CMR software (cvi42 software (version 5.10, Circle Cardiovascular, Canada)). Routinely analysed CMR measures of left ventricular (LV) and right ventricular (RV) function were carried out according to current guidelines [185], with parameters of myocardial mass and ventricular volumes derived from the short-axis views and indexed to body surface area. Ventricular endocardial and epicardial contours were manually drawn at end-diastole. Left ventricular endocardial contours were drawn at end-systole, which was deemed to be the phase with the smallest blood pool cavity. Papillary muscles were excluded from myocardial mass and included in volumes. For the purposes of strain measurements, the manually drawn ventricular contours were propagated throughout the cardiac cycle using the software's machine-learning algorithms. Automated contours were individually checked and corrected, where necessary. Global left ventricular strain (circumferential, longitudinal, and radial) and global right ventricular strain (longitudinal and radial) were derived using the tissue tracking module to derive values of peak strain and strain graphs following the manufacturer's advised standard protocols (Figure 3.1). Atrial volumes were indexed to body surface area and derived from automated contours, with manual correction as needed. Left atrial emptying fraction (LAEF) was calculated as the percentage difference between maximal and minimal left atrial volume divided by maximal atrial volume. The primary observer (LYZ) performed all CMR analyses in a random order. A second independent observer (AJR) analysed a random sample of >10% of the cohort to assess inter-observer variability. Both observers were blinded to clinical outcomes.

Figure 3.1 – Representative images of global longitudinal strain on cardiovascular MRI

Representative images showing 2D global longitudinal strain derivation using Cvi42 software (version 5.10, Circle Cardiovascular, Canada). Panels show horizontal long axis view at diastole (A) and systole (B) and vertical long axis views at diastole (C) and systole (D) and the resultant curve displaying peak global longitudinal strain (%) by time (milliseconds) (E).

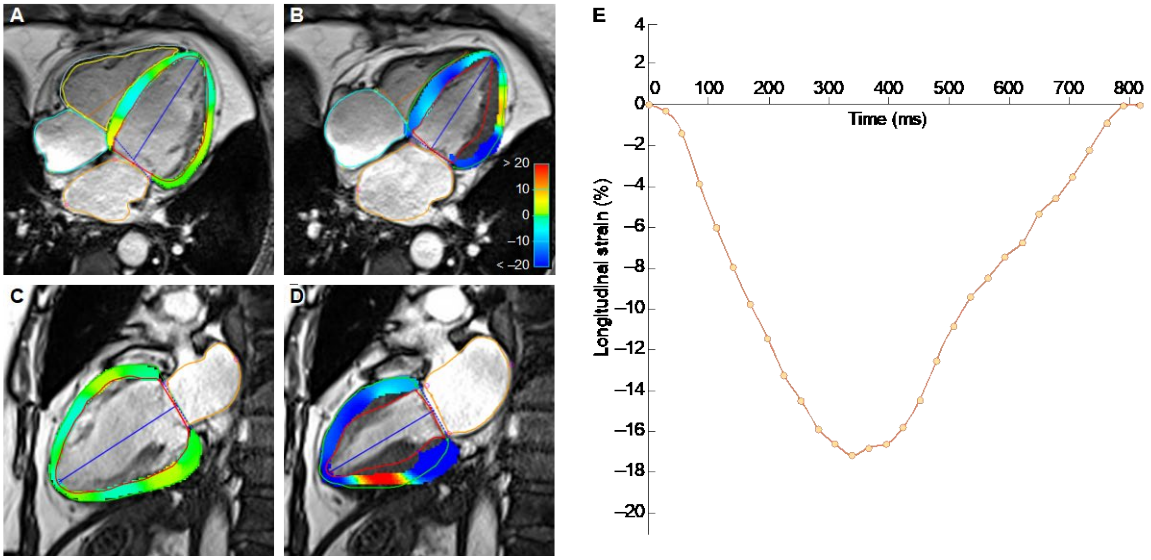

Statistical Analysis

Continuous data with a normal distribution are presented as mean ± standard deviation (SD), and median and interquartile range (IQR) for skewed data, with normality defined according to Shapiro-Wilk test. Exploratory analyses using independent Student's t-tests, Mann Whitney U test, and Pearson's Chi-squared test, as appropriate, were performed on baseline variables of clinical significance. Kruskal-Wallis test was used to compare LV-GLS by year of scan. Univariable Cox proportional hazards analysis was performed to identify CMR variables associated with outcome. Parameters that were significantly associated with outcome were then entered into a model including pre-specified baseline clinical variables of age, sex, diabetes, heart failure, and previous myocardial infarction. Future renal transplantation was added to the model as a time-dependant covariate. The proportional hazards assumption was tested for continuous variables using Schoenfeld's residuals and deemed satisfied when the p value was >0.05. A backwards stepwise regression model using Wald's statistic was performed with an exclusion threshold of $p > 0.1$. An assessment of

model fit was not performed due to the necessary inclusion of future renal transplantation as a time-dependent covariate. CMR variables of independent significance in the multivariable model were divided into quartiles and compared using Kaplan-Meier survival analysis and the log-rank test, including sub-group analyses based on future renal transplantation. Intra- and interobserver variability was assessed by the intra-class correlation (ICC) coefficient (two-way mixed effect, average measures). Receiver-operator curve analysis was used to identify an optimal prognostic threshold for LV-GLS. Statistical analysis was performed using SPSS (version 26, IBM Corp, New York).

Results

Participant characteristics

A total of 215 patients were included (144 of whom were being considered for renal transplant[116,183], and 71 incident dialysis patients without overt heart failure (33 from Rutherford et al [182] and 38 locally acquired baseline scans from a recent trial of allopurinol therapy in dialysis patients (ClinicallTrials.gov ID NCT01951404)). There was no difference in survival or LV-GLS by year of scan (log rank test p=0.99, and Kruskal Wallis test H=2.77, p=0.60, respectively).

In total, 133 (62%) were male and mean age was 54.0 ± 12.1 years (Table 3.1). The majority of participants were white (200; 93%), with 11 Asian, 3 black and 1 other. At the time of scanning, 181 (84%) patients were receiving renal replacement therapy, of whom 8 (4%) had a functioning renal transplant (median eGFR 10.5 (IQR 9.1 - 13.3) ml/min/1.73m^2). The remaining 34 (16%) patients had CKD stage 5 with median eGFR 10.4 (IQR 8.6 - 12.8) ml/min/1.73m^2. During a median follow-up of 5.0 years (range 1 day – 16.9 years), there were 115 deaths (53%). Specific cause of death was available for 96 (83%) patients and included 34 (35%) due to infection, 33 (34%) cardiovascular (22 cardiac, 9 peripheral vascular disease, 4 stroke), 13 (14%) cancer, 7 (7%) withdrawal of dialysis, and 9 (9%) other causes. Participants who survived were younger (51.6 +/- 11.7 versus 56.2 +/-12.2 years, p = 0.005), with similar sex distribution and body mass index (Table 3.1). Deceased patients were significantly more likely to have diabetes at baseline (37% vs 22%, p = 0.014), however history of cardiac disease including myocardial infarction and heart failure were similar (Table 3.1).

Table 3.1 – Baseline Demographics

	ALL N= 215	**Alive** *n = 100*	**Dead** *n = 115*	**P-value**
Age, years (mean (SD))	54 (+/- 12)	51.2 (+/- 11.7)	56.2 (+/- 12.2)	0.005
Gender, male (n (%))	133 (62%)	62 (62%)	71 (62%)	0.97
Body mass index (median, (IQR)), kg/m^2	25.6 (22.4-30.1	25.0 (22.2-29.2)	26.6 (22.4-31.6)	0.06
Diabetes Mellitus (n, (%))	65 (30%)	22 (22%)	43 (37%)	0.01
Previous myocardial infarction (n (%))	32 (15%)	14 (14%)	18 (16%)	0.73
Heart failure (n, (%))	2 (1%)	1 (1%)	1 (1%)	0.92
Primary Renal Diagnosis N, (%)				
Diabetes Mellitus	48 (22%)	15 (15%)	33 (27%)	
Glomerulonephritis	44 (20%)	25 (25%)	19 (17%)	
Hypertension / Renal vascular disease	18 (8%)	8 (8%)	10 (9%)	
Polycystic kidney disease	23 (11%)	13 (13%)	10 (9%)	
Pyelonephritis	19 (9%)	9 (9%)	10 (9%)	
Unknown	32 (15%)	18 (18%)	14 (12%)	
Other (defined)	31 (14%)	12 (12%)	19 (17%)	0.01
CKD status at time of CMR N, (%)				
Haemodialysis	136 (63%)	72 (72%)	64 (56%)	
Peritoneal dialysis	37 (17%)	8 (8%)	29 (25%)	
Functioning transplant	8 (4%)	5 (5%)	3 (3%)	
CKD stage 5 (pre-dialysis)	34 (16%)	15 (15%)	19 (17%)	
Previous renal transplant (non-functioning)	26 (12%)	15 (15%)	11 (10%)	0.04
RRT vintage at time of CMR (median, years (IQR))	1.7 (0.6-4.6)	2.1 (0.6-5.3)	1.3 (0.6-4.3)	0.37

Presented as: mean +/- standard deviation (SD), or median and interquartile range (IQR).

Abbreviations: CKD = chronic kidney disease; CMR = Cardiovascular magnetic resonance imaging; RRT = renal replacement therapy

Table 3.2 summarises the CMR results for the cohort. Seven patients had reduced left ventricular ejection fraction (LVEF) <40%, while a further 14 patients had mid-range ejection fraction between 40-49%, as defined by the 2016 European Society of Cardiology guidelines [186,187]. One hundred twelve patients with preserved LVEF >50% had abnormal LV-GLS when defined as >-16.0% [177]. Intra-and inter observer reproducibility were excellent for left atrial (LA), right atrial (RA) and LV parameters (ICC >0.92) and moderate for RV parameters (ICC 0.57-0.74) (Supplementary material table S2) [188].

CMR parameters and All-cause Mortality

On univariable analysis with each variable entered separately, LV-GLS, LV-GRS, RV-GLS, RV-GRS, minimum left atrial volume and LAEF were significantly associated with all-cause mortality (Table 3.3). A multivariable model was created of these variables combined with the pre-specified clinical variables of gender, age, diabetes, heart failure, previous MI and future renal transplant. Following backwards stepwise elimination, LV-GLS and LAEF were the only CMR parameters that remained independently associated with mortality, in combination with gender, age, and future renal transplantation (Table 3.3). All other variables were excluded.

Table 3.2 – Cardiovascular MRI characteristics

	ALL n=215		**Alive** n=100		**Dead** n=115		**p-value**
	Median	*IQR*	*Median*	*IQR*	*Median*	*IQR*	
LVMI (g/m²)	70.2	56.4, 84.8					
LV-EDVI (ml/m²)	82.7	67.3, 101.2					
LV-ESVI (ml/m²)	28.8	21.0, 39.3					
LVM/LV-EDV (g/ml)	0.83	0.71, 0.95					
LVEF (%)	64.7	58.5, 70.0					
LV-GLS (%)	-15.3	-17.24, -13.6					
LV-GRS (%)	24.9	21.1, 29.6					
LV-GCS (%)	-16.0	-17.8, -13.8					
RV-GLS (%)	-21.1	-21.1, -17.7	-22.1	-18.39, -20.7	-20.7	-23.3, -16.5	0.008
RV-GRS (%)	44.2	34.4, 56.0	48.7	36.0, 60.8,	42.8	33.1, 53.7	0.05
LAVI min (ml/ m²)	14.0	9.9, 20.6	13.1	8.8, 18.4	15.0	11.2, 23.1	0.002
LAVI max (ml/ m²)	33.6	26.1, 45.9					
LAEF (%)	57.5	50.1, 65.1	62.6	55.8, 67.6	54.3	47.1, 60.7	0.001
RAVI min (ml/ m²)	16.7	11.9, 22.8					
RAVI max (ml/ m²)	33.5	26.7, 43.0					
RAEF (%)	48.3	41.3, 58.3					

Presented as median and interquartile range (IQR). P-value refers to Mann-Whitney U test comparing baseline cardiovascular MRI parameters for alive versus dead. For simplicity, only those variables for which a statistically significant difference with a p value <0.05 are presented.

Abbreviations:

LVMI = left ventricular mass index

LV-EDVI = left ventricular end diastolic volume index

LV-ESVI = left ventricular end systolic volume index

LVM/LVEDV = ratio of left ventricular mass to left ventricular end diastolic volume

LVEF = left ventricular ejection fraction

LV-GLS = left ventricular global longitudinal strain

LV-GRS = left ventricular global radial strain

LV-GCS = left ventricular global circumferential strain

RV-GLS = right ventricular global longitudinal strain

RV-GRS = right ventricular global radial strain

LAVI min = minimum left atrial volume index

LAVI max = maximum left atrial volume index

LAEF = left atrial emptying fraction

RAVI min = minimum right atrial volume index

RAVI max = maximum right atrial volume index

RAEF = right atrial ejection fraction

Supplementary material table S2: Intra- and inter-observer reproducibility for cardiovascular MRI (CMR) parameters as assessed by the intraclass correlation coefficient (ICC) (two-way mixed effect, average measures).

CMR parameter	Intra-observer ICC	Inter-observer ICC
Myocardial mass (g)	0.99	0.99
LV end diastolic volume (ml)	0.99	0.99
LV end systolic volume (ml)	0.99	0.99
LV ejection fraction (%)	0.96	0.94
LV global longitudinal strain (%)	0.93	0.95
LV global circumferential strain (%)	0.99	0.96
LV global radial strain (%)	0.93	0.95
RV global longitudinal strain (%)	0.66	0.57
RV global radial strain (%)	0.68	0.71
minimum LA volume (ml)	0.99	0.99
maximum LA volume (ml)	0.99	0.99
minimum RA volume (ml)	0.99	0.98
maximum RA volume (ml)	0.98	0.98

Abbreviations:

LV = left ventricular

LA = left atrial

RA = right atrial

RV = right ventricular

Table 3.3 – Association between clinical and CMR parameters and all-cause mortality (Cox Proportional Hazards Model).

	Univariable			*Multivariable*		
	HR	CI	P-value	HR	CI	P-value
Sex (female)	1.14	0.79-1.67	0.48	1.43	0.95-2.17	0.09
Age	1.04	1.02-1.06	<0.001	1.04	1.02-1.05	<0.001
Diabetes	1.43	0.98-2.08	0.07			
Heart failure	0.83	0.11-5.78	0.83			
Previous myocardial infarction	1.23	0.75-2.04	0.41			
*Future renal transplant**	0.23	0.14-0.38	<0.001	0.29	0.17-0.47	<0.001
LVMI (g/m^2)	1.00	0.99-1.01	0.30			
LVEDVI (ml/m^2)	1.00	1.00-1.001	0.47			
LVESVI (ml/m^2)	1.01	1.00-1.02	0.11			
LVM/LVEDV (g/ml)	1.25	0.49-3.21	0.65			
LVEF (%)	0.99	0.97-1.01	0.18			
LVGLS (%)	1.10	1.03-1.16	0.003	1.08	1.01-1.16	0.03
LVGRS (%)	0.97	0.94-0.99	0.03			
LVGCS (%)	1.02	0.96-1.08	0.49			
RVGLS (%)	1.05	1.01-1.08	0.007			
RVGRS (%)	0.99	0.98-1.00	0.02			
LAVI min (ml)	1.03	1.01-1.04	0.002			
LAVI max (ml)	1.01	1.00-1.02	0.15			
LAEF (%)	0.97	0.95-0.99	0.001	0.98	0.96-1.00	0.03
RAVI min (ml)	1.01	1.00-1.03	0.13			
RAVI max (ml)	1.01	1.00-1.02	0.16			
RAEF (%)	1.00	0.99-1.02	0.75			

**time dependent covariate*

The multivariable model was created using pre-specified clinical variables including sex, age, diabetes mellitus, previous myocardial infarction, heart failure and future renal

transplantation, combined with CMR parameters that significantly associated with mortality on univariable analysis. Backwards stepwise elimination (Wald's) was used to select the optimal variables in the final model displayed here.

Abbreviations:
LVMI = left ventricular mass index
LV-EDVI = left ventricular end diastolic volume index
LV-ESVI = left ventricular end systolic volume index
LVM/LVEDV = ratio of left ventricular mass to left ventricular end diastolic volume
LVEF = left ventricular ejection fraction
LV-GLS = left ventricular global longitudinal strain
LV-GRS = left ventricular global radial strain
LV-GCS = left ventricular global circumferential strain
RV-GLS = right ventricular global longitudinal strain
RV-GRS = right ventricular global radial strain
LAVI min = minimum left atrial volume index
LAVI max = maximum left atrial volume index
LAEF = left atrial emptying fraction
RAVI min = minimum right atrial volume index
RAVI max = maximum right atrial volume index
RAEF = right atrial ejection fraction

Patients were divided into quartiles according to LV-GLS and LAEF. The quartiles for LV-GLS are as follows: first quartile < -17.24% (best), second quartile -17.25% to -15.28%, third quartile -15.29 to -13.62%, fourth quartile > -13.61% (worst). The quartiles for LAEF were: first quartile <50.12 % (worst), second quartile 50.13-57.30%, third quartile 57.31-64.94%, and fourth quartile >64.94% (best). Compared to the best quartile of LV-GLS, participants in the worst quartile had significantly poorer outcomes (p=0.03, Figure 3.2), with no difference between the other quartiles. Similarly, the first quartile of LAEF had significantly worse survival compared to participants in the 3rd and 4th quartiles of LAEF (Figure 3.2, p= 0.003 and 0.03).

Figure 3.2 – Kaplan-Meier Curves of All-Cause Mortality by quartiles of: A) peak left ventricular global longitudinal strain (LV-GLS) (%), B) left atrial emptying fraction (LAEF) (%).

Compared to the best quartile of LV-GLS, participants in the worst quartile had significantly poorer outcomes (log rank test p=0.03) with no difference between the other quartiles, For LAEF, the first quartile had significantly worse survival compared to participants in the 3rd and 4th quartiles (log rank test p= 0.003 and 0.03, respectively).

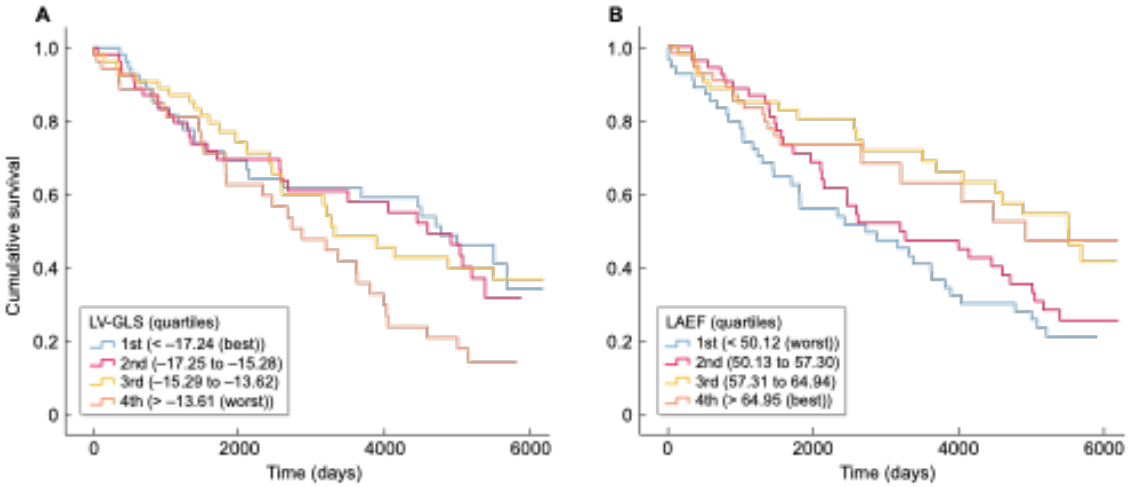

On receiver-operator curve (ROC) analysis, there was no single threshold of LV-GLS with meaningful prognostic value for all-cause mortality. When 1 -year mortality was examined, the area under the curve (AUC) for LV-GLS was 0.71 from which a LV-GLS cut-off of -14.1% would yield 77% sensitivity and 67% specificity. However, when 2-year mortality was examined the AUC fell to 0.52.

LV-GLS differed by sex within the cohort, with females having greater contractility than males (median GLS -16.17% (females) vs -14.52% (males); Mann-Whitney U test p<0.001). There was no difference in mortality by sex (log rank p=0.48). When only female patients were studied, LV-GLS was significantly associated with all-cause mortality (HR 1.21 (1.08-1.35, p=0.001) but the association was not detected when only male patients were studied (HR 1.08 (-.99-1.18, p=0.09)). There was no difference in LAEF by sex (Mann Whitney U test p=0.15).

CMR parameters and Cardiovascular mortality

With regards the secondary outcome of cardiovascular mortality, LV-GLS (HR 1.17 (95% CI: 1.00-1.25)) and LAEF (HR 0.949 (95% CI: 0.92-0.98)) were the only CMR parameters that significantly associated with outcome on univariable analysis. Following backwards elimination, LAEF was the only CMR parameter that remained significantly associated with cardiovascular mortality in the multivariable model containing age: HR 1.08 (95% CI: 1.04-1.12); diabetes: HR 2.30 (95% CI: 1.12-4.71); future renal transplant: HR 0.35 (95% CI: 0.13-0.95); LAEF: HR 0.96 (95% CI: 0.93-0.99).

CMR parameters and future Renal Transplantation

A total of 106 (49%) of patients received a renal transplant during the follow-up. Of these, 33 patients died. Patients who received a transplant had lower median LV-GLS than those who did not (-15.63% (-17.32 - -14.18) compared to -14.88% (-16.82- -13.08) p=0.04). There was no difference in LAEF between those who did and did not receive a future renal transplant (p=0.10). The survival benefit of renal transplantation was evident on Kaplan-Meier survival analysis across all quartiles of LV-GLS and LAEF (Figure 3.3 and Supplementary Material Figure S3).

Figure 3.3 – Kaplan-Meier curves of all-cause mortality comparing participants who did and did not receive a renal transplant during follow-up for each quartile of left ventricular global longitudinal strain (LV-GLS).

Survival benefit of renal transplantation was most marked in those in the best quartile of LV-GLS but was still significant in participants within the worst quartile of LV-GLS (log rank test $p<0.001$ for all groups).

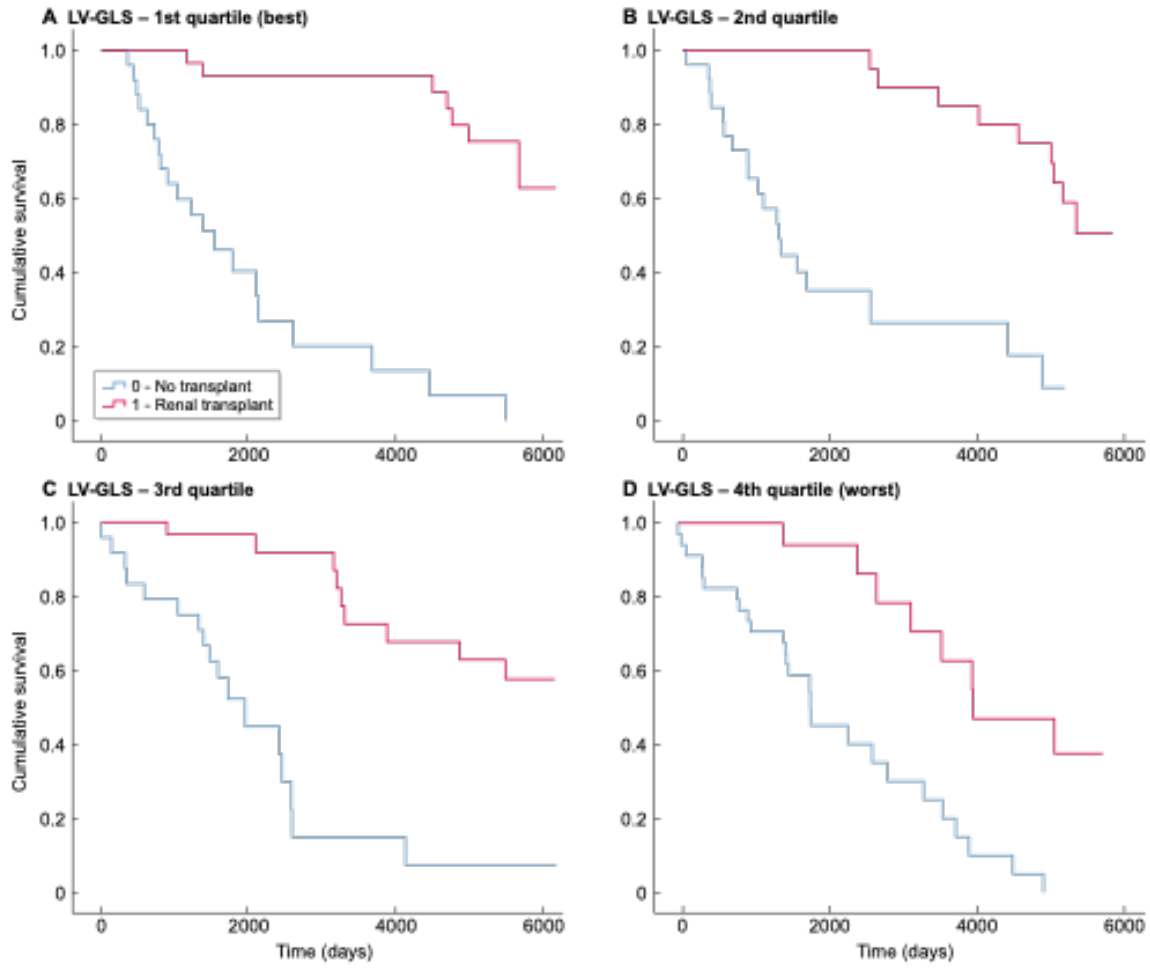

Supplementary Material S3 – Kaplan-Meier curves of all-cause mortality comparing participants who did and did not receive a renal transplant during follow-up for each quartile of left atrial emptying fraction (LAEF)). Survival benefit of renal transplantation was present, and of similar magnitude, across all quartiles of LAEF (log rank test p<0.001).

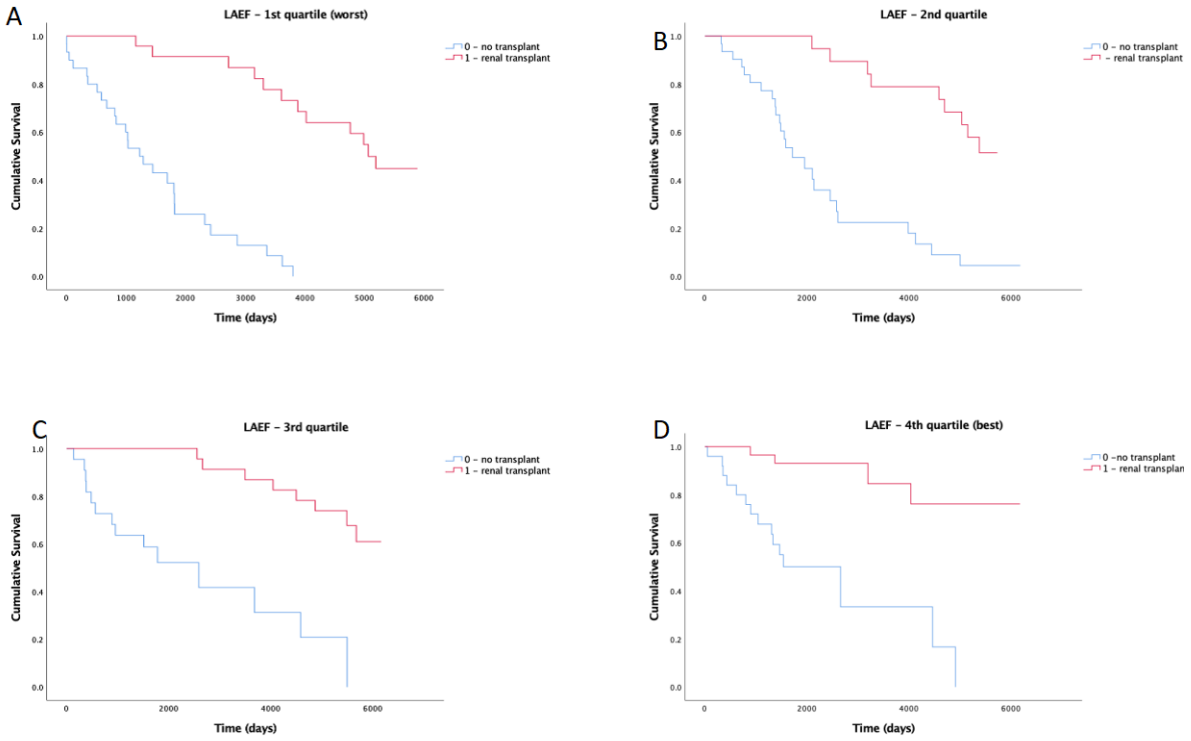

Discussion

This large, retrospective study of CMR in patients with ESKD found that LV-GLS by feature tracking CMR and LAEF have significant association with all-cause mortality, independent of baseline clinical variables and future renal transplantation. Importantly, these associations were present even when the majority of the cohort had normal cardiac function as defined by traditional parameters (i.e. LVEF).

Benefits of Using Feature Tracking CMR for Strain Analysis

CMR is the gold standard for the assessment of cardiac volumes and mass in patients with renal failure [113,115]. Although strain imaging by echocardiography is likely to be more accessible, it can be limited by poor availability of acoustic windows, image quality, expertise required and inter-operator variability. Fluid shifts associated with dialysis may further impair the accuracy and reliability of this measure. The ability to quantify LV-GLS accurately and quickly using CMR supports the superiority of CMR over echocardiography. Feature tracking is a technique that measures strain using routinely acquired steady state free procession (SSFP) sequences and obviates the need for acquisition of bespoke CMR strain sequences such as myocardial tagging. Feature tracking strain has been validated against myocardial tagging [189,190] with the additional advantage that it is able to generate this data in less than a quarter of the time needed by tagging. We believe feature tracking CMR is at the intersection of accuracy and ease of acquisition and have demonstrated its utility in this cohort.

Global Longitudinal Strain as a Predictor of Mortality and Cardiac Dysfunction

In patients with CKD, LV-GLS measured by echocardiography has consistently been shown to be an independent predictor of mortality. Associations have been demonstrated in patients with CKD stage 3B-5D [121], CKD stage 4-5D [191], and patients on dialysis [122]. LV-GLS has theoretical advantages over LVEF for the assessment of cardiac function in patients with CKD: reduced LVEF has been shown to occur late in the development of the uraemic cardiomyopathy [192], a finding that is supported by the high prevalence of heart failure with preserved ejection fraction in ESKD populations [193]. This is likely explained by the differential aspects of myocardial function that the 2 techniques measure. While LVEF

simply assesses the difference in volume at end diastole and systole, LV-GLS assesses the function of subendocardial fibres, which more directly correlates to the extent of interstitial myocardial fibrosis [122]. In our study, 112 (58%) of 194 patients with preserved LVEF (>50%) had abnormal LV-GLS when defined as >-16% (a threshold chosen based on the normal LV-GLS in healthy subjects being -20% +/-4% [177–179]). This may partly explain the extreme cardiovascular risk seen in ESKD populations, despite relatively low prevalence of heart failure. Accordingly, there would be an argument to investigate cardiovascular therapeutics, especially those with anti-fibrotic properties (such as mineralocorticoid receptor antagonists) in patients with ESKD who have impaired LV-GLS. Mineralocorticoid receptor antagonists have previously been studied in ESKD populations with no effect on LVMI but LV-GLS was not assessed [194,195]. Given the high prevalence of impaired LV-GLS in ESKD populations, and the expected high frequency of events, we believe these trials would be of significant interest. The difference in LV-GLS between men and women is well recognised [179]. Sex was accounted for in the multivariable model which found LV-GLS to independently associated with mortality, nevertheless our subgroup analysis suggests a greater prognostic ability of LV-GLS in women, compared to men, and this requires further study. The lack of association between LVEF and mortality in this cohort is likely explained by the low prevalence of reduced LVEF resulting in reduced statistical power. This is partly due to the entry criteria of the pooled studies which excluded patients with known severe left ventricular systolic dysfunction. On the contrary, the fact that LV-GLS associated with mortality, even when the vast majority of patients did not have heart failure, is striking. The lack of clear threshold of LV-GLS in predicting mortality on the ROC analysis suggests that LV-GLS alone is unlikely to be a useful prognostic tool, albeit there are numerous explanations for the lack of association including the observed influence of renal transplantation on survival and the long follow-up with high overall mortality.

Left Atrial Emptying Fraction as a Predictor of Mortality

LAEF was strongly correlated with mortality in our study on univariable and multivariable analyses. This was an unexpected finding and LAEF has not been extensively studied within this population. LAEF has been shown to associate with adverse cardiovascular events in the general population [196], elderly [197] and in patients with heart failure [198,199]. Furthermore, there is extensive evidence correlating left atrial volumes with mortality, including in patients on haemodialysis [183,200]. It is not clear if left atrial impairment is directly involved in the

pathophysiology of the excess mortality, or if it is a surrogate marker, perhaps for volume overload or left ventricular diastolic dysfunction [201,202].

CMR in the assessment of suitability for transplant

Renal transplantation, where appropriate, is the optimal treatment for patients with ESKD. However, transplants are a limited resource and have potential to cause some patients net harm due to the risks of surgery and long-term immunosuppression. Cardiovascular assessment (albeit to varying degrees) is standard practice in pre-transplant assessment and is recommended by international guidelines [203]. However, the evidence supporting this practice is scant and so it is becoming increasingly controversial [204]. We hypothesised that LV-GLS on CMR may be helpful for cardiovascular risk assessment when considering renal transplant suitability. LV-GLS significantly associated with mortality in the multivariable model, even when future renal transplantation was accounted for. However, the overwhelming survival benefit of renal transplantation was evident across all quartiles of LV-GLS (Figure 3.3), suggesting that there is no LV-GLS too poor (or too good) for a patient to reap survival benefit from a transplant, if not otherwise contraindicated. Regression of myocardial fibrosis following kidney transplant may account for part of this improved survival [56,205]. This retrospective observation will be heavily biased due to selection bias and immortal time bias, but as randomised controlled trials assessing this will never be ethically feasible, we feel the present data are sufficient to say that LV-GLS is unlikely to be helpful when assessing the majority of patients for transplant suitability. The utility of stress CMR protocol using GLS at peak stress has not been investigated and advances in free breathing cine acquisitions might make this feasible.

Limitations

This is a retrospective analysis of pooled studies, albeit at a single centre using consistent imaging protocols. The cohort combines patients scanned at both 1.5T and 3T. While the influence from field strength on LV-GLS is likely to be negligible [177], we accept there may be a small, unquantified difference in cine parameters between the acquisitions from different scanners. Inclusion from source studies was incomplete and unquantified for the studies published in 2006 [116] and 2010 [183] due to a combination of overlap in participants between the 2 studies and inability to retrieve some CMRs from archiving. The nature of the source

studies has resulted in a younger than expected mean age (54 +/- 12 years) within this cohort and an under-representation of older, prevalent dialysis patients. Further studies to confirm our findings in different populations of patients with ESKD are required. It was not possible to examine non-fatal cardiovascular outcomes as data from historic patients were insufficient to allow reliable examination of cardiovascular events. The source data for our primary outcome of all-cause mortality are robust, but the data on cause of death were incomplete resulting in reduced power to examine of our secondary outcome of cardiovascular mortality. Nevertheless, the weaker association between LV-GLS and cardiovascular mortality, as opposed to all-cause mortality, is surprising given the cardio-centric nature of LV-GLS and warrants further study. It is plausible that reduced functional myocardial reserve in ESKD would impair the ability to recover from other critical illness, such as severe infection, but we accept that any future interventional trials targeting LV-GLS as a surrogate marker would be expected to address cardiovascular mortality and events. Previous studies examining LV-GLS by echocardiography have found associations with all-cause mortality[121,191] and cardiovascular mortality [122,191] .

Conclusion

In this cohort of patients with ESKD, LV-GLS and LAEF were associated with all-cause mortality, independent of baseline clinical variables and future renal transplantation. Conversely, conventional imaging biomarkers, such as LVMI and LVEF, did not associate with mortality. Using LV-GLS, instead of LVEF, to diagnose cardiac dysfunction in patients with ESKD could result in a major advance in our understanding of cardiovascular disease in ESKD and may be a more relevant measure in this population. Despite this, the survival benefit of renal transplantation was evident across all quartiles of LV-GLS, suggesting that in the absence of other contraindications to renal transplant, LV-GLS is unlikely to be helpful when assessing patients' suitability for renal transplantation. Further studies are warranted to explore the potential role of LV-GLS as a sample enrichment tool and surrogate outcome measure in future clinical trials examining therapeutics to improve survival in patients with ESKD.

Acknowledgements

We wish to thank all participants who kindly volunteered their time for this study. We also thank the radiographers and physicists that work within the Clinical Research Imaging Facility in Glasgow. In addition, we are very grateful to the two external peer reviewers who reviewed this study on behalf of CKJ. Their considered and insightful comments allowed us to greatly improve this manuscript.

Conflict of interest Statement

The authors declare no competing interests relevant to the present study. Outside the present work: Keith Gillis reports speaker honoraria from Napp and consultancy fees from Vifor. Jennifer Lees reports speaker honoraria from Vifor-Fresenius, Astra Zeneca, Bristol Myers-Squibb and Pfizer. Patrick Mark reports speaker honoraria from Vifor-Fresenius, Astra Zeneca, Janssen, Napp, Novartis and Bristol Myers-Squibb, research grants from Boehringer Ingelheim and non-financial support from Pharmacosmos. The University of Glasgow holds research and consultancy agreements for work done by Colin Berry in the course of his employment with companies that have interests in cardiovascular disease. They include AstraZeneca, Abbott Vascular, Boehringer Ingelheim, HeartFlow, Novartis, Menarini, and Siemens Healthcare.

Authors' contributions

All authors have reviewed and contributed to this manuscript. PBM, AJR, ER, and KM conceived the idea for this study and designed the analysis plan. PBM, RP and ER recruited participants to the contributing studies. LYZ analysed the CMRs. AJR performed the data analysis and analysed a sample of CMRs. AJR and LYZ wrote the manuscript. KM, GR and CB advised on CMR analysis and critically reviewed the manuscript. RW led image acquisition. KG and JL assisted with data collection, analysis and critically reviewed the manuscript.

Funding

Dr Alastair Rankin is personally funded by a Clinical Academic Training Fellowship from The Chief Scientist Office (Scotland) (CAF/18/02). Dr Elaine Rutherford is supported by a Postdoctoral Clinical Lectureship from The Chief Scientist Office (Scotland) (PCL/03/18). Dr Jennifer Lees is personally funded by a Kidney Research UK Training Fellowship (TF_013_20161125) and a Postdoctoral Clinical Lectureship from The Chief Scientist Office (Scotland) (PCL/20/10). Luke Zhu was funded by a Medical Research Scotland Vacation Scholarship (Vac-1514-2019). Colin Berry and Jennifer Lees are funded by a British Heart Foundation Centre of Excellence Award (no. RE/18/6134217). The work was additionally funded by British Heart Foundation Clinical Research Training Fellowships to Kenneth Mangion, Rajan Patel and Patrick Mark.

Chapter 4 – Myocardial changes on 3T cardiovascular magnetic resonance imaging in response to haemodialysis with fluid removal. J Cardiovasc Magn Reson (2021).

4.1 Manuscript

Alastair J Rankin, Kenneth Mangion, Jennifer S Lees, Elaine Rutherford, Keith A Gillis, Elbert Edy, Laura Dymock, Thomas A Treibel, Aleksandra Radjenovic, Rajan K Patel, Colin Berry, Giles Roditi, Patrick B Mark. Myocardial changes on 3T cardiovascular magnetic resonance imaging in response to haemodialysis with fluid removal. *J Cardiovasc Magn Reson* **23,** 125 (2021). https://doi.org/10.1186/s12968-021-00822-4

Abstract

Background: Mapping of native myocardial T1 is a promising non-invasive, non-contrast imaging biomarker. Native myocardial T1 times are prolonged in patients requiring dialysis, but there are concerns that the dialysis process and fluctuating fluid status may confound results in this population. We aimed to assess the changes in cardiac parameters on 3T cardiovascular magnetic resonance imaging (CMR) before and after haemodialysis, with a specific focus on native T1 mapping.

Methods: This is a single centre, prospective observational study in which maintenance haemodialysis patients underwent CMR before and after dialysis (both scans within 24 hours). Weight measurement, bio-impedance body composition monitoring, haemodialysis details and fluid intake were recorded. CMR protocol included cine imaging and mapping native T1 and T2.

Results: Twenty-six participants (16 male, mean age 65 +/- 9 years) were included in the analysis. The median net ultrafiltration volume on dialysis was 2.3 L (IQR 1.8, 2.5), resulting in a median weight reduction at post-dialysis scan of 1.35 kg (IQR 1.0, 1.9), with a median reduction in over-hydration (as measured by bioimpedance) of 0.75 L (IQR 0.5, 1.4). Significant reductions were observed in LV end-diastolic volume (-25.4 ml, p=0.002), LV stroke volume (-13.3 ml, p=0.007), global T1 (21.3 ms, p=0.02), global T2 (-1.2 ms, p=0.02) following dialysis. There was no change in LV mass (p=0.35), LV ejection fraction (LVEF) (p=0.13) or global longitudinal strain (p=0.22). On linear regression there was no association between baseline over-hydration (as defined by bioimpedance) and global T1 or global T2 times, nor was there an association between the change in over-hydration and the change in these parameters.

Conclusions: Acute changes in cardiac volumes and myocardial native T1 times are detectable on 3T CMR following haemodialysis with fluid removal. The reduction in global T1 time suggests that the abnormal native T1 time observed in patients on haemodialysis is not entirely due to myocardial fibrosis.

Keywords: End-stage kidney disease, haemodialysis, cardiovascular, magnetic resonance imaging, left ventricular hypertrophy

Introduction

Patients with chronic kidney disease (CKD) are at a greatly increased risk of cardiovascular disease (CVD).[41] This risk increases with severity of CKD,[42] such that patients with CKD stage 5 are 3-4 times more likely to experience a cardiovascular event than age-standardized patients without CKD.[43] In patients with kidney disease requiring dialysis, CVD remains the single most common cause of death accounting for between 25-40% of all deaths.[45–47] CKD results in a unique cardiovascular phenotype; with relatively fewer deaths due to atherosclerotic processes and more due to sudden cardiac death and heart failure.[44–47,53] Cardiomyopathy of chronic kidney disease, often called 'uraemic cardiomyopathy', refers to a specific pattern of myocardial fibrosis, left ventricular hypertrophy and diastolic dysfunction, which is found in patients with CKD and forms the pathological basis for this unique CVD phenotype.[54–56]

Cardiac magnetic resonance imaging (CMR) is established as the reference method for imaging uraemic cardiomyopathy.[114] Previous studies using gadolinium-enhanced CMR demonstrated the presence of myocardial fibrosis in patients on dialysis,[116] and its association with poor survival.[117] However, the discovery of the association between the use of gadolinium based contrast media in patients with CKD and the development of the very rare disease nephrogenic systemic fibrosis curtailed further research using this technique.[118,119] There is a pressing need for an alternative marker of uraemic cardiomyopathy, further intensified by the observation that regression of left ventricular mass in isolation may not be robustly associated with improved cardiovascular outcomes in CKD patients.[111] Attempts to identify reliable imaging biomarkers in this population are hampered by the potential confounding influence of the dialysis process itself and fluctuating fluid status.

Native T1 mapping is a non-contrast technique that estimates myocardial longitudinal relaxation times (ms) and reflects changes in extra- and intra-cellular compartments. Myocardial T1 is commonly affected by changes in collagen (fibrosis), water (oedema), iron deposition (haemochromatosis, myocardial haemorrhage) and lipids (Fabry's disease) [206]. In addition, native T1 mapping has been shown to differentiate dialysis patients from both healthy[182] and co-morbid controls,[207] with excellent inter-observer reproducibility.[208,209] Outside of the CKD population, T1 mapping has been shown to correlate well with myocardial fibrosis in other disease states.[114,125,126] However, the major concern with using

native T1 mapping in dialysis patients is the potential confounding influence on the T1 signal of changing tissue oedema resulting from the large intra-dialytic fluid fluctuations that are typical of patients on intermittent haemodialysis [128]. A previous study using 1.5T CMR observed small, but detectable, differences in native T1 times immediately after haemodialysis [127]. In the present study we assess the myocardial changes on 3T CMR in response to haemodialysis with fluid removal, with a particular interest in native T1 mapping to inform its potential suitability as a surrogate outcome measure in future therapeutic trials. We also explored the potential bias of dialysis timing in relation to the clinical applicability of 3T CMR.

Materials and Methods

Participants

Participants were aged greater than 40 years and were established on regular, day-time hospital-based haemodialysis for at least 6 months. Participants were eligible for inclusion if they had a history of recurrent fluid overload (defined as requirement for ultrafiltration volumes of at least 1.5 litres mean fluid removal over the preceding 3 dialysis sessions) and without heart failure (defined as no previous clinical diagnosis of heart failure or with preserved left ventricular ejection fraction (LVEF) (>50%) on their most recent transthoracic echocardiogram). Participants had to be able to comply with study procedures, self-report an ability to lie flat for 1 hour and provide informed consent. Exclusion criteria included standard contra-indications to MRI and contraindications to iodine based radiological contrast (to facilitate a sub-study comparing CMR with a novel contrast CT technique) [210,211]. The study was prospectively registered at clinicaltrials.gov (NCT03704701). Favourable ethical opinion was granted by the West of Scotland Research Ethics Committee 1 (Ref: 18/WS/0138, 13th August 2018). All study procedures were carried out in accordance with local guidelines and regulations and with respect to the declaration of Helsinki.

Study Protocol

This single centre observational study consisted of 2 visits (Figure 4.1). Visit 1 occurred before a participant's routine dialysis session. Where possible, this occurred at the end of a participant's 'long', or two-day, gap, i.e., on a Monday for participants on a Monday,

Wednesday, Friday dialysis schedule. Participants on a morning dialysis schedule attended visit 1 the afternoon before dialysis. Between visits 1 and 2 participants were asked to consume food and drink as they normally would but to document what they had taken. Participants would then attend their routine haemodialysis session which was performed as per usual clinical practice. Details of the dialysis session were recorded including duration, ultrafiltration volume, settings and medications administered. Visit 2 occurred after dialysis. Participants on an afternoon dialysis schedule attended visit 2 the following morning. At each visit, weight measurement, bioimpedance body composition monitoring (using a Fresenius Body Composition Monitor, Fresenius Medical Care, Hong Kong as per manufacturer's instructions), blood tests and CMR were performed.

Figure 4.1 - Flow chart depicting study procedures

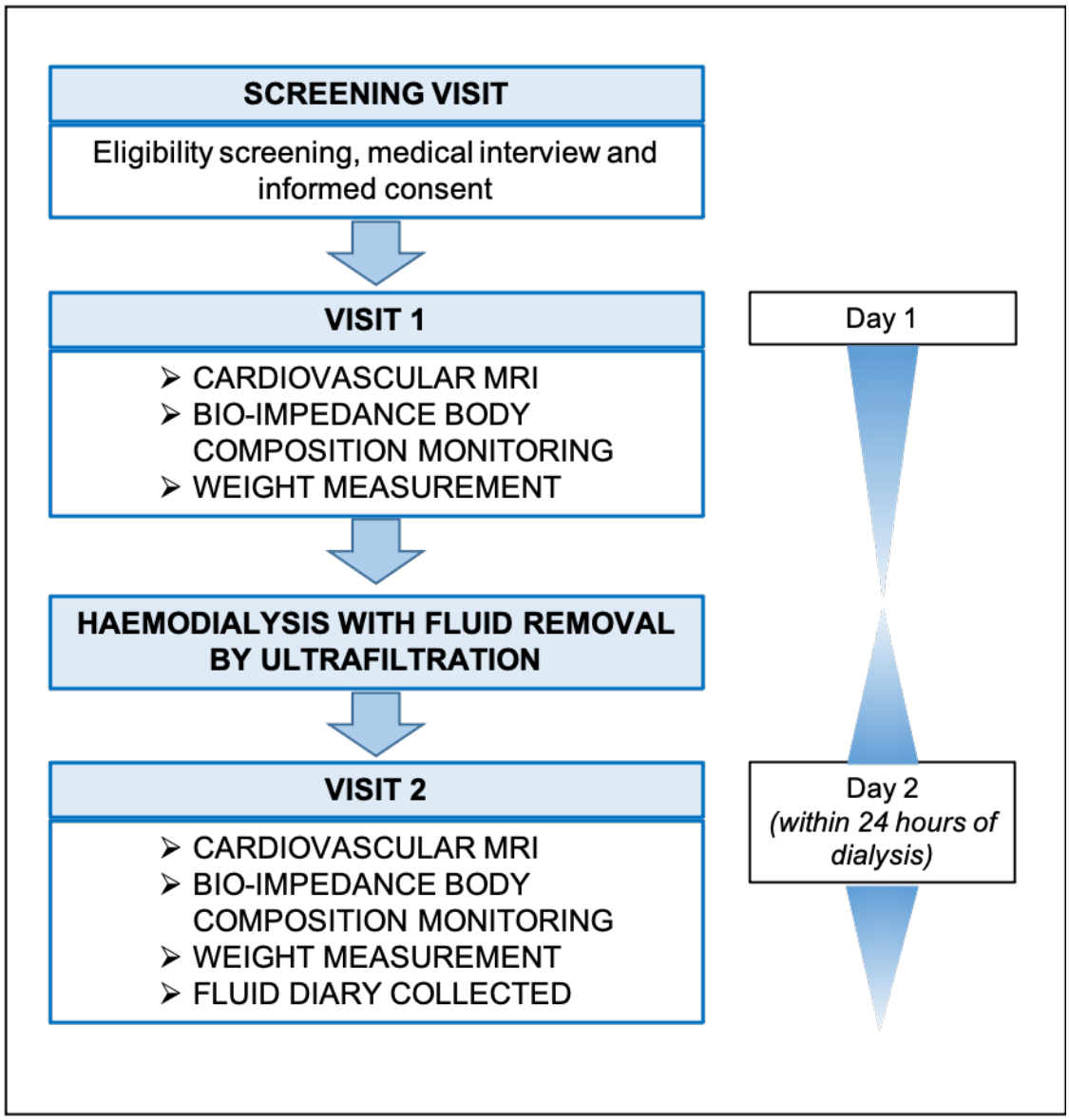

CMR Image Acquisition

CMR acquisition was performed at the Clinical Research Imaging Facility of the Queen Elizabeth University Hospital in Glasgow using a 3T MRI scanner (PRISMA, Siemens Healthineers, Erlangen, Germany) with an 18-channel surface coil placed anteriorly and a 32-channel spine coil placed posteriorly. Following the acquisition of localiser images, balanced steady state free precession sequences were used to acquire left ventricular cine imaging in three long axis planes, followed by a short axis stack from the apex to the atrio-ventricular ring, each with 25 phases. Images were obtained using retrospective electrocardiogram-gating at end-expiration. Where participants were unable to breath-hold or had cardiac arrhythmia, compressed sensing (CS cardiac Cine, Siemens, Erlangen, Germany) was used to allow real-time acquisition. Typical scan parameters were: field of view (FOV) 340 × 286 mm, slice thickness 7 mm with 3 mm gap in short axis stack, repetition time (TR) – 41.4 ms, echo time (TE) 1.51 ms, flip angle 50°, voxel size 1.33×1.33 x 7 mm.

For native T1 and T2 mapping, basal, mid and apical short axis views were acquired using SiemensMyoMaps sequences. For native T1, non-contrast, motion-corrected, optimized, modified Look-Locker inversion recovery sequences were used with the following typical parameters: FOV 340 x 272 mm, slice thickness 6.0 mm, voxel size: 1.9 x 1.9 x 6.0 mm, TR 272 ms, TE 1.12 ms, flip angle 35 degrees, minimum T1 100 ms, inversion-time increment 80 ms, bandwidth 1085 Hertz/pixel. For T2 mapping, three T2 weighted measurements were acquired followed by an automated exponential fit for each pixel after respiratory motion correction. The imaging used a T2-prepared single shot b-SSFP readout with T2 preparation times (TE) = 0, 25, and 55 ms with a recovery period of 3 heartbeats between measurements. Typical protocol parameters for T2 mapping were: FOV 360 x 270 mm, slice thickness 8 mm, matrix 192 x108, spatial resolution 1.9 x 2.5 mm, TR 207.39 ms, TE 1.32 ms, flip angle 12 degrees, bandwidth 1184 Hz/pixel.

CMR Image Analysis

All CMR scans were subject to a clinical report for clinical governance purposes. Research CMR analysis was performed utilizing dedicated CMR software (cvi42 software (version 5.10, Circle Cardiovascular, Canada)). Routinely reported CMR measures of left ventricular (LV) and right ventricular (RV) function were carried out according to current guidelines [185].

Parameters of myocardial mass and volumes were not indexed to body surface area to avoid confounding impact of weight changes falsely adjusting body surface area and is acceptable given the analysis of within-subject comparisons. Ventricular endocardial and epicardial contours were manually drawn at end-diastole (Figure 4.2). LV endocardial contours were drawn at end-systole, which was deemed to be the phase with the smallest blood pool cavity. Papillary muscles were excluded from myocardial mass and included in volumes. LV thickness was recorded as the maximum septal thickness measured perpendicular to the cavity on a short-axis mid-chamber view, at the approximate level of the mitral valve leaflet tips. Global LV strain (circumferential, longitudinal, and radial) and global RV strain (longitudinal and radial) were derived using the software's tissue tracking module to determine peak values for each parameter. Atrial volumes were manually drawn on 4-chamber horizontal long axis views at atrial systole and diastole (defined with respect to mitral valve closure) to report maximum and minimum right atrial volumes and atrial emptying fraction. For left atrial measurements, the vertical long axis views were additionally contoured to report biplanar derived values. For T1 and T2 measurements, scanner derived maps were used. Epi- and endocardial borders were manually drawn on each basal, mid and apical map. Areas of obvious artefact were excluded from regions of interest (ROI) and care was taken to include only myocardial tissue with a 10% epi- and endocardial offset applied. Global values were derived by averaging results from all three short axis slices. Septal values were reported as the mean of segments 2, 3, 8, 9 and 14 as per the American Heart Association's 16 segment model [124]. For blood pool T1 and T2, ROIs were drawn within the LV cavity on the mid-LV map, with care taken to avoid artefact and papillary muscles. Additional ROIs were manually drawn on a representative area of skeletal muscle, with the pectoralis major muscle used preferentially. A further ROI was drawn within a homogenous region within the right lobe of liver. The primary observer (AJR) batch analysed all CMRs in a random order and was blinded to participant identity and whether the scan was pre-or post-dialysis. A second independent observer (KM) analysed a random sample of >20% of the cohort to assess inter-observer variability. As a post-hoc experiment, a T1MES phantom [212], which is a commercially available agarose gel-based phantom that is certified for the standardisation of T1 mapping on MRI, was scanned on consecutive days at times that replicated the study schedule to assess inter-study T1 variability.

Figure 4.2 - Representative images on 3.0T cardiovascular MRI

Representative 3.0T CMR images of mid- left ventricle end-diastolic short axis stack cine (A. B), end-diastolic horizontal long axis cine (C, D), native T1 mapping (E, F) and native T2 mapping (G, H) acquired before and after dialysis. In this representative participant, global T1 and global T2 times reduced following 4 hours of haemodialysis with 2.3 litres ultrafiltration.

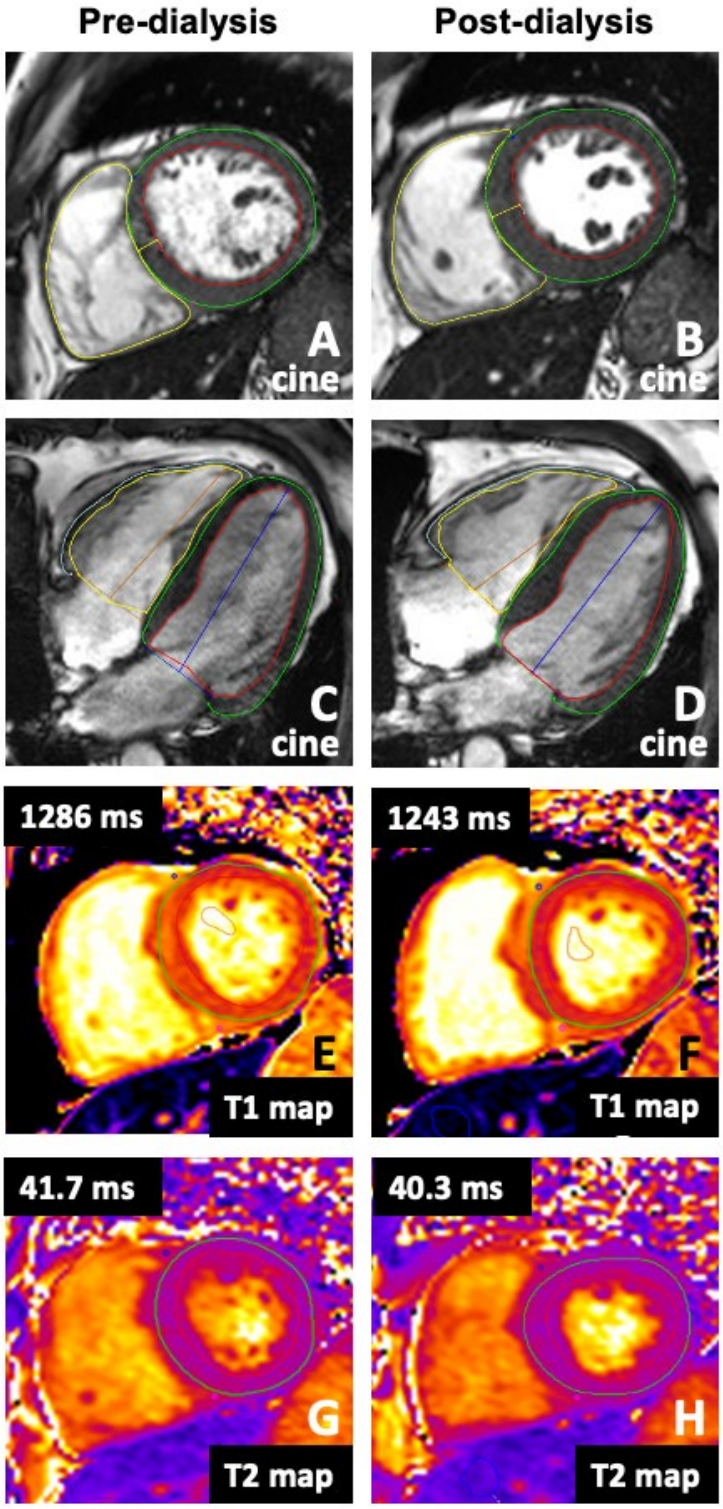

Statistical Analysis

Continuous data with a normal distribution are presented as mean ± standard deviation (SD), and median and interquartile range (IQR) for skewed data, with normality defined according to Shapiro-Wilk test. Pre and post dialysis CMR values were compared using paired t-tests and Wilcoxon singed rank tests accordingly. Linear regression and multiple regression were used to compare change in CMR parameters according to baseline variables. Repeated measures MANCOVA was used to account for covariates in the comparison of myocardial native T1 before and after dialysis. Intra- and interobserver variability was assessed by the intra-class correlation (ICC) coefficient (two-way mixed effect, average measures). Statistical analysis was performed, and figures created, using SPSS (version 27, IBM Corp, New York).

Sample Size

A prospective sample size calculation determined that a total of 9 participants would be required to detect a 2.5% difference in native T1 times with 80% power and alpha 0.05 based on previously published data [182,208]. A total of 22 participants would be sufficient to detect a 1.5% difference. A target of 30 participants was set to allow drop out and to facilitate a pre-specified sub-study (clinicaltrials.gov NCT03704701).

Results

Participant characteristics

Twenty-eight participants were recruited between 19th October 2018 and 9th March 2020. Recruitment was stopped early (target n=30) due to the COVID-19 pandemic. Two participants withdrew consent prior to any study procedures leaving 26 for analysis, of whom 16 (61.5%) were male, 22 (84.6%) were white and the mean age was 64.7 ± 9.4 years. Median duration of kidney replacement therapy at time of recruitment was 2.0 (1.3, 4.0) years. Multi-morbidity was prevalent in the cohort with a mean Charlson Comorbidity index of 6 (mean modified Charlson Comorbidity Index of 3) [213,214]. The median duration of haemodialysis treatment session was 4.0 hours (4.0, 5.0) with a mean blood flow of 265 (+/-32) ml/min. Eighteen (69.2%) participants followed an afternoon dialysis schedule and underwent dialysis median 2.5 (2.0, 2.8) hours after their first MRI, with repeat MRI at

median 15.3 (14.8, 16.7) hours after finishing dialysis. The remaining 8 (30.8%) participants followed a morning dialysis schedule and underwent dialysis at median 16 (14.7, 16.2) hours after their first MRI, with a repeat MRI 1.5 (1.2, 2.7) hours after completing dialysis. For 23 (88.5%) participants, visit 1 took place after their 'long gap' between dialysis sessions (i.e., pre-dialysis on a Monday for a patient on a Monday, Wednesday, Friday dialysis schedule). Additional baseline characteristics are detailed in supplementary material S4.1. In 6 participants, clinically significant incidental findings were detected, including 2 cancers requiring treatment (supplementary material S4.2).

Supplementary Material Table S4.1. Baseline characteristics. Values are displayed as count (percentage), mean +/- standard deviation or median (interquartile range), as appropriate.

Age, years	64.7 ± 9.4
Male	16 (62%)
Primary renal diagnosis - Diabetes - Glomerulonephritis - Polycystic - Tubulo-interstitial nephritis - Unknown - Other	 8 (31%) 6 (23%) 1 (4%) 2 (8%) 4 (15%) 5 (19%)
- Duration of renal replacement therapy, years	2.01 (1.34, 4.04)
Dialysis schedule - Morning - Afternoon	 18 (69%) 8 (31%)
Dialysis access - Catheter - Arterial venous fistula - Arterio-venous graft	 9 (5%) 12 (46%) 5 (19%)
Body mass index (kg/m2)	31.7 (27.2, 36.6)
Smoking - Previous - Current	 8 (31%) 1 (4%)
Hypertension	24 (92%)
Previous myocardial infarction	3 (12%)
Angina	5 (19%)
Stroke	7 (27%)

Supplementary Material Table S4.2: summary of clinically significant incidental findings. These findings were detected on the clinical radiology report which was issued by a consultant radiologist for each research scan. Participants were informed and appropriate follow-up arranged in each case.

N=26	
1	Renal cancer requiring nephrectomy
1	Metastatic bladder cancer
1	Aspiration pneumonia
1	Decompensated severe left ventricular systolic dysfunction
1	Pulmonary nodule requiring follow-up
1	Pleural plaques

Fluid status

All participants had a history of recurrent fluid overload with mean ultrafiltration volume of 2.2 L (+/- 0.4) from the preceding 3 dialysis sessions prior to recruitment. At visit 1 (pre-dialysis), 12 participants had demonstrable pitting oedema. 1 participant was unable to undergo bioimpedance monitoring for multifactorial reasons (body habitus, immobility, skin emollient). Of the remaining 25 participants, the median over-hydration was +0.35 L (-2.8, +3.5), with 10 participants measuring as volume deplete pre-dialysis. The median net ultrafiltration volume on dialysis was 2.3 L (1.8, 2.5) at a mean rate of 6 mL/kg/hour (+/- 1.74). Five participants experienced symptomatic intradialytic hypotension requiring adjustment of their dialysis prescription. Between visit 1 (pre-dialysis) and visit 2 (post-dialysis), the median estimated fluid intake was 0.85 L (0.6, 1.0). At visit 2 (post-dialysis), the median reduction in body weight was 1.35 kg (1.0, 1.9), with a median reduction in over-hydration of 0.75 L (0.5, 1.4). No participants gained weight between visit 1 and visit 2, albeit 2 participants' weight did not change. According to bioimpedance monitoring, 3 participants increased their over-hydration between visits (range 0.2-0.35 L).

CMR parameters pre- and post-dialysis

Table 4.1 shows the CMR results before and after dialysis. Notable findings include a significant reduction in LV end-diastolic volume, LV stroke volume, RV stroke volume, left atrial volumes, global circumferential strain, global native T1, septal native T1 and global T2 following dialysis. There was no change in LV mass, LV or RV ejection fraction or global longitudinal strain (Table 4.1). Figure 4.3 shows within-subject changes for LV mass, LVEF, left atrial maximum volume, global T1, septal T1 and global T2. The intra- and interobserver reproducibility for global t1 times was excellent with ICC of 0.989 and 0.949, respectively. Additional intra- and interobserver reproducibility results are included in supplementary material S4.3.

Table 4.1 - Cardiovascular Magnetic resonance (CMR) parameters pre- and post-dialysis.

Displayed as mean, standard deviation and paired t-test for variables with a normal distribution, and median, interquartile range and Wilcoxon signed rank test for those with a skewed distribution.

CMR parameter	Pre-dialysis	Post-dialysis	p-value
LV myocardial mass (g)	103.8 (78.8, 142.4)	97.5 (78.2, 136.0)	0.35
LV end diastolic volume (ml)	184.9 (159.1, 228.6)	159.5 (151.8, 220.1)	0.002
LV end systolic volume (ml)	87.9 (71.1, 112.6)	84.3 (68.6, 111.4)	0.81
LV stroke volume (ml)	102.9 (+/- 28.5)	89.6 (+/- 29.6)	0.007
LV ejection fraction (%)	53.6 (48.6, 59.5)	49.8 (46.2, 54.5)	0.13
LV global longitudinal strain (%)	-13.8 (+/- 3.3)	-13.1 (+/- 3.6)	0.22
LV global circumferential strain (%)	-16.3 (-19.5,-14.0)	-15.1 (-16.9, -13.4)	0.03
LV global radial strain (%)	22.2 (+/-6.7)	20.7 (+/- 7.1)	0.18
LV thickness (mm)	10.2 (8.4, 12.2)	10.6 (8.8, 12.3)	0.44
RV end diastolic volume (ml)	160.9 (133.4, 183.6)	136.4 (128.2, 171.1)	<0.001
RV end systolic volume (ml)	67.4 (56.2, 82.0)	61.9 (52.6, 75.2)	0.66
RV stroke volume (ml)	97.9 (+/- 29.6)	83.6 (+/- 25.9)	<0.001
RV ejection fraction (%)	56.9 (+/- 10.5)	53.8 (+/- 12.6)	0.05
RV global longitudinal strain (%)	-22.5 (+/-5.9)	-22.4 (+/- 6.8)	0.88
RV global radial strain (%)	48.3 (37.2, 66.7)	49.8 (40.0, 71.7)	0.77
Minimum LA volume (ml)	44.2 (28.1, 70.1)	39.8 (22.0, 70.4)	0.001
maximum LA volume (ml)	95.5 (74.8, 108.4)	86.4 (56.8, 100.9)	<0.001
minimum RA volume (ml)	30.4 (20.2, 43.6)	29.1 (22.0, 40.6)	0.95
maximum RA volume (ml)	59.5 (49.4, 77.4)	54.1 (45.3, 75.4)	0.09
Global native T1 (ms)	1282.9 (+/- 50.6)	1261.6 (+/- 49.4)	0.02
Septal native T1 (ms)	1312.6 (+/- 53.5)	1293.1 (+/- 46.5)	0.04
Blood pool native T1 (ms)	1956.7 (+/- 67.8)	1934.7 (+/- 72.9)	0.08
Skeletal muscle native T1 (ms)	1217.7 (+/- 64.8)	1209.8 (+/- 73.3)	0.60
Liver native T1 (ms)	685.9 (+/- 156.7)	678.6 (+/- 145.6)	0.45
Global T2 (ms)	42.2 (40.9, 44.8)	41.0 (39.9, 44.7)	0.02
Blood pool T2 (ms)	101.1 (+/- 20.9)	111.0 (+/- 24.5)	0.06
Skeletal muscle T2 (ms)	32.2 (+/- 2.1)	30.8 (+/- 3.0)	0.03
Liver T2 (ms)	21.6 (19.9, 23.5)	21.3 (20.1, 22.4)	0.81

The scanner-specific reference range for myocardial native global T1 in healthy subjects is mean (range) 1170.2 ms (1106.8 - 1233.5) and global T2 is mean 39.5 ms (34.7-44.3) (unpublished data, correspondence from Dr Kenneth Mangion and Dr Andrew Morrow)

Abbreviations: LV = left ventricular; RV = right ventricular; LA = left atrial; RA = right atrial.

Supplementary Material Table S4.3: Intra- and inter-observer reproducibility for cardiovascular MRI (CMR) parameters assessed by intraclass correlation coefficient (ICC) (two-way mixed effect, absolute agreement). Performed on a random sample of 11 participants representing >20% of total cohort.

CMR parameter	Intra-observer ICC	Inter-observer ICC
LV myocardial mass (g)	0.986	0.947
LV end diastolic volume (ml)	0.998	0.960
LV end systolic volume (ml)	0.975	0.934
LV stroke volume (ml)	0.968	-
LV ejection fraction (%)	0.870	0.863
LV global longitudinal strain (%)	0.969	0.903
LV global circumferential strain (%)	0.968	-
LV global radial strain (%)	0.956	-
LV thickness (mm)	0.887	-
RV end diastolic volume (ml)	0.983	-
RV end systolic volume (ml)	0.983	-
RV stroke volume (ml)	0.927	-
RV ejection fraction (%)	0.897	-
RV global longitudinal strain (%)	0.632	-
RV global radial strain (%)	0.608	-
minimum LA volume (ml)	0.927	-
maximum LA volume (ml)	0.995	-
minimum RA volume (ml)	0.981	-
maximum RA volume (ml)	0.987	-
Global native T1 (ms)	0.989	0.949
Septal native T1 (ms)	0.934	0.937
Blood pool native T1 (ms)	0.958	-
Skeletal muscle native T1 (ms)	0.694	-
Liver native T1 (ms)	0.989	-
Global T2 (ms)	0.962	0.953
Blood pool T2 (ms)	0.831	-
Skeletal muscle T2 (ms)	0.921	-
Liver T2 (ms)	0.978	-

Abbreviations:
LV = left ventricular
LA = left atrial
RA = right atrial
RV = right ventricular

Figure 4.3 - Within subject changes pre- and post- dialysis for left ventricular mass (A), left ventricular ejection fraction (B), left atrial maximum volume (C), global T1 times (D), septal T1 times (E), and global T2 times (F).

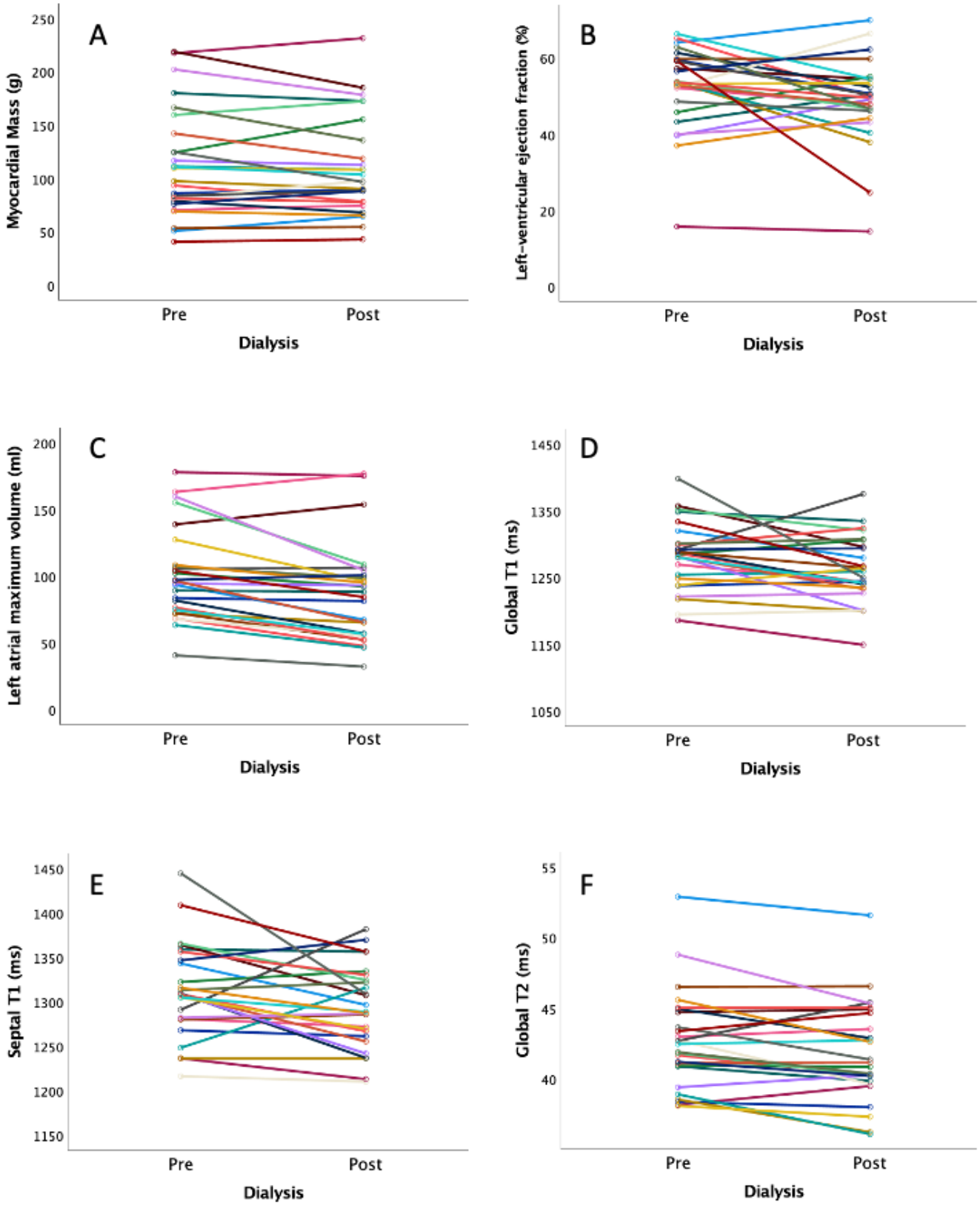

Change in native T1 and T2 by fluid status

On linear regression there was no relationship between baseline over-hydration and global T1, septal T1 or global T2 (Figure 4.4). There was also no relationship between the change in global T1, septal T1 or global T2 with ultrafiltration volume (p=0.88), change in over-hydration (p=0.87) or change in weight (p=0.95) (Figure 4.4). There was no difference in the mean change in global T1, septal T1 and global T2 in individuals who did versus did not achieve >0.5 L reduction in over-hydration (change in global T1: 11.3 (95% CI -30.2, 52.8), p=0.58; septal T1: 0.24 (95% CI -41.8, 42.3), p= 0.99; global T2: -0.65 (95% CI-2.1, 0.81), p=0.37) nor in those with or without >1.0 kg weight change (change in global T1: 6.3, (95% CI -39.4, 52.0) p=0.78; septal T1: 1.2 (95% CI -45.6, 48.1), p=0.95; global T2: 0.09, (95%CI -1.5, 1.7), p=0.91). Blood pool native T1 correlated with the degree of overhydration measured on bioimpedance at baseline (r^2 = 0.247, p=0.013) but there was no association between the change in blood pool T1 and the change in overhydration. There was also no correlation between the change in in myocardial native T1 time and the change in blood pool T1 (r=0.13, p=0.54), nor the change in haematocrit (r=-0.25, p=0.22). On repeated measures MANCOVA, when the change in blood pool T1 and the change in haematocrit were added as covariates to the comparison of myocardial native T1 time, there was no significant interaction between either covariate and the change in myocardial native T1. Both covariates had small, non-significant contributions to the observed effect (change in blood pool T1 (partial eta squared 0.06, p=0.72); change in haematocrit (partial eta squared 0.11, p=0.11), resulting in an adjusted p-value of 0.050 for the comparison of myocardial naïve T1 before and after dialysis. Additional determinants of blood T1 are examined in supplementary material S4.4.

Figure 4.4 - Scatter plots of global T1, septal T1 and global T2 according to baseline over-hydration (A, B, C, respectively), and the change in global T1, septal T1 and global T2 according to change in weight (D, E, F, respectively).

There was no significant association in any of the comparisons.

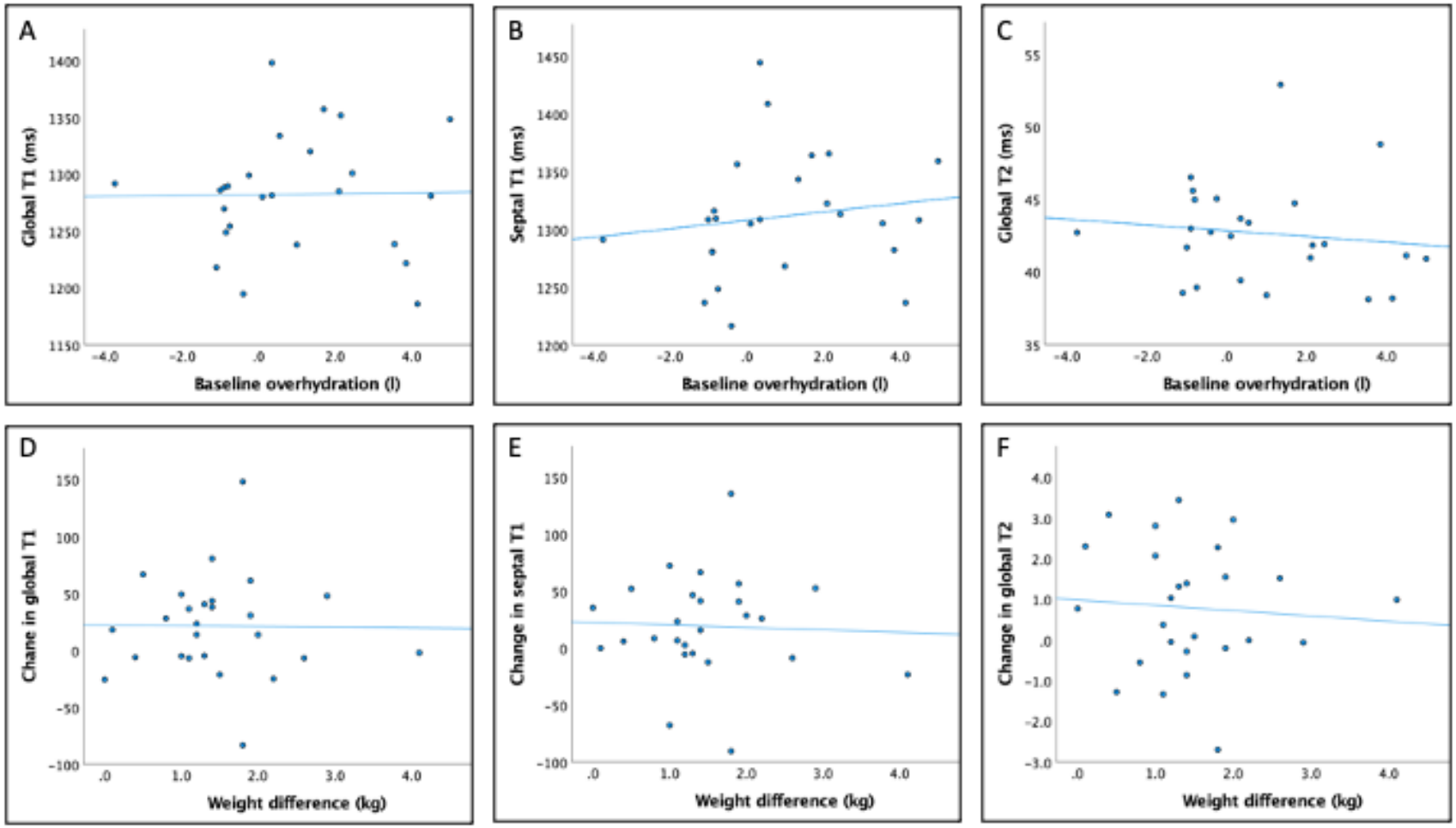

Supplementary Material Table S4.4: Determinants of blood pool T1

There was no significant difference in blood pool native T1 pre and post dialysis (Pre 1956.7 ms (+/- 67.8); Post 1934.7 (+/- 72.9); p=0.08). Blood pool native T1 correlated with the degree of overhydration measured on bioimpedance at baseline (r2 = 0.247, p=0.013) but there was no association between the change in blood pool T1 and the change in overhydration. There was no correlation between the change in blood pool T1 and the change in myocardial native T1 (r=0.13, p=0.54). Previous studies have suggested a high degree of correlation between blood pool native T1 and biochemical parameters (*S Rosmini, H Bulluck, A Abdel-Gadir et al, The Effect of Blood Composition on T1 Mapping, J Am Coll Cardiol Img. 2019. 12 (9);1888-1890)*. In the present study, there was no correlation between blood pool native t1 and the following parameters: haematocrit (p=0.84), haemoglobin (p=0.63), creatinine (p=0.69), iron (p=0.62), transferrin saturation (p=0.72), serum albumin (p=0.77), triglycerides (p=0.72), cholesterol (p=0.63), LDL (p=0.76) and HDL (p=0.73). The following table shows the mean change in blood parameters pre and post dialysis:

	Pre-dialysis	Post dialysis
Haemoglobin (g/L)	115 (15)	115 (14)
Haematocrit (L/L)	0.363 (0.046)	0.363 (0.045)
Sodium (mmol/L)	137 (4)	137 (2)
Potassium (mmol/L)	5.4 (0.9)	4.6 (0.7)
Urea (mmol/L)	21.1 (4.7)	10.5 (3.3)
Creatinine (umol/L)	815 (244)	507 (205)
Albumin (g/L)	35 (4)	34 (4)
Ferritin (ng/mL)	465 (346)	502 (358)
Iron (umol/L)	11 (6)	15 (10)
Transferrin (g/L)	1.9 (0.4)	1.9 (0.4)
Transferrin Saturation (%)	24 (12)	32 (22)
Triglycerides (mmol/L)	2.7 (2.3)	2.2 (2.1)
Cholesterol (mmol/L)	4.6 (1.5)	4.2 (0.9)

High density lipoprotein (mmol/L)	1.2 (0.5)	1.3 (0.4)
Low density lipoprotein (mmol/L)	2.1 (0.8)	2.0 (0.8)

Values displayed as mean (standard deviation)

Change in native T1 and T2 parameters by dialysis session

There was no association between the change in global T1, septal T1 or global T2 and the time from dialysis until repeat CMR (p=0.80, 0.55 and 0.77 respectively, when mean change in values was compared between morning and afternoon dialysis patients). Eighteen participants were on a morning dialysis schedule, whereas 8 were on an afternoon schedule and thus scanned at different times of day. The mean difference in myocardial native T1 pre/post dialysis was 24.7 ms in the morning group (n=8) and 19.8 ms in the afternoon group (n=18), with no significant difference between the groups (p=0.80). When the T1MES phantom was scanned on consecutive days the measured T1 was 1215.6 +/- 7.6 ms and 1214.6 +/- 13.4 ms, respectively. The same values for T2 were 80.8 +/- 0.9 ms and 80.2 +/- 1.9 ms. There was no difference in global T1, septal T1 or global T2 in those participants who experienced symptomatic intradialytic hypotension versus those who did not (p=0.87, 0.67 and 0.99, respectively). All but 1 participant were prescribed regular intravenous iron therapy. Excluding the 5 participants who received intravenous iron between visit 1 and visit 2 did not change the results (supplementary material S4.5).

Supplementary Material S4.5: Analyses exploring the potential influence of intravenous iron therapy. Excluding the 5 participants who received intravenous iron between visit 1 and visit 2 did not change results: a significant reduction in global T1 was still observed (mean 22.3ms, p=0.04).

The native T1 times for the 5 patients who received intravenous iron between scans is included in the table below:

Participant	Global native 1 pre-dialysis	Global native T1 post dialysis	Dose of intravenous iron sucrose received
1	1218.1	1200.1	150 mg
2	1289.6	1240.3	25 mg
3	1281.0	1233.1	100 mg
4	1221.7	1226.5	100 mg
5	1299.14	1324.1	50 mg

Change in LV ejection fraction

There was no overall change in LVEF following dialysis (Table 4.1). Six participants had abnormal LVEF pre-dialysis based on age and sex standardised reference ranges [187]. In 5 of these participants, LVEF improved following dialysis and fluid removal (range 3 to 9.5%). However, 11 participants with normal LVEF pre-dialysis, had abnormal LVEF post-dialysis. In one participant, a dramatic reduction in LVEF was clearly due to tachy-arrhythmia. In the remaining 10 participants, 4 had minor changes (<5% difference) that crossed the threshold for age and sex standardised normal values, while 6 had >5% reduction in LVEF but without obvious association between the change in LVEF and baseline hydration status (visit 1 bioimpedance hydration status ranging from -3.75 to + 2.45 L). On multivariable linear regression including baseline over-hydration, baseline LVEF, ultrafiltration volume, follow-up over-hydration, over-hydration change, weight change, time from visit 1 until dialysis and time from dialysis until repeat MRI, only baseline LVEF and the time from visit 1 until dialysis significantly associated with the change in LVEF following a backwards elimination approach (baseline LVEF: Beta 0.43, p=0.02; Time from MRI 1 until dialysis: Beta 0.38, p=0.04; adjusted r^2 for the model = 0.30). At lower baseline LVEF, repeat LVEF was more likely to increase, whereas those who had a longer gap between visit 1 MRI and dialysis were more likely to have a reduction in LVEF at visit 2 (Figure 4.5).

Figure 4.5 - Scatter plots of change in left ventricular ejection fraction (LVEF) (calculated by visit 2 post-dialysis LVEF (%) – visit 1 pre-dialysis LVEF (%)) by baseline LVEF (p=0.02) (A) and time from visit 1 MRI until dialysis (p=0.04) (B)

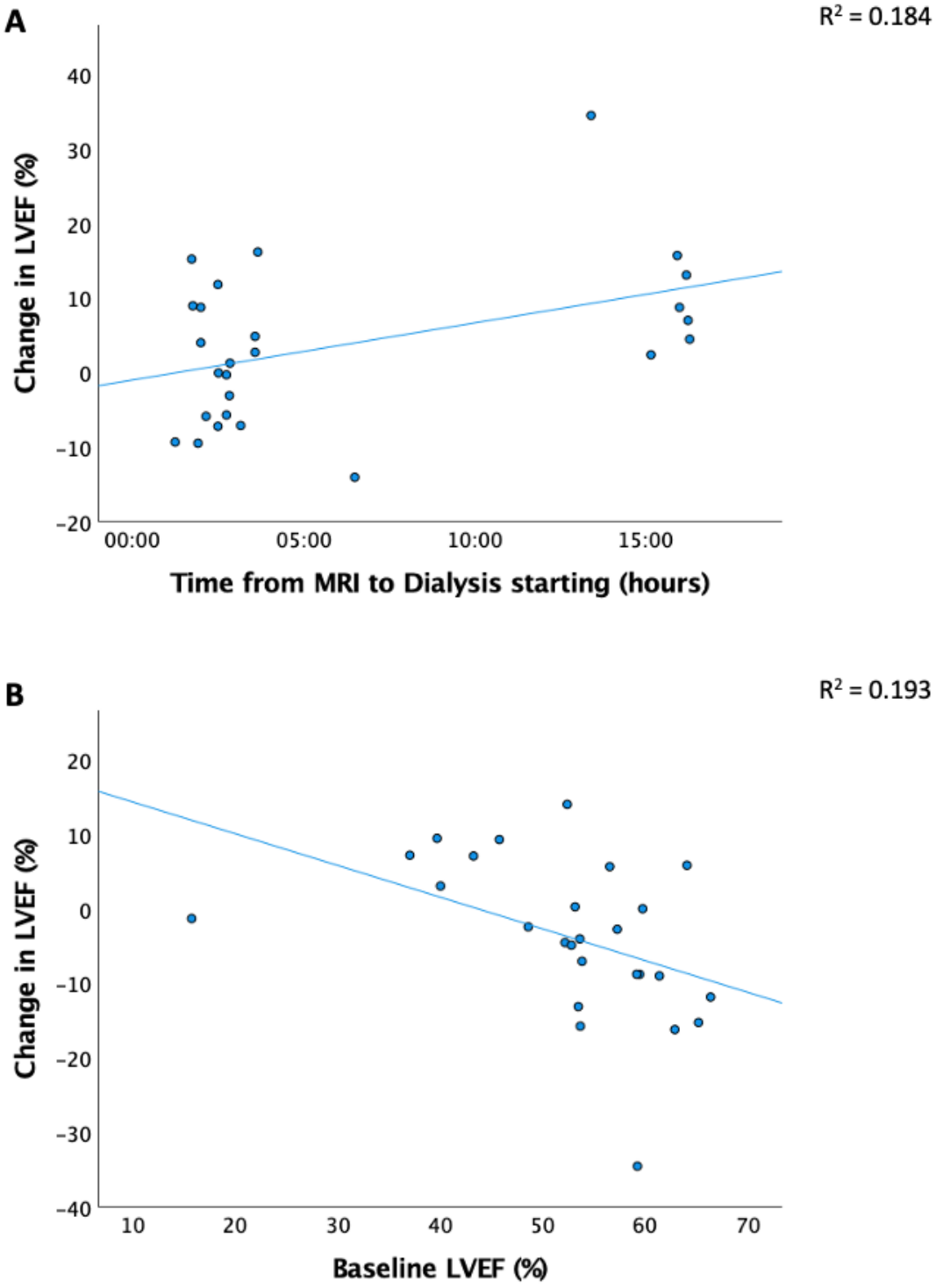

Discussion

This prospective study identified significant changes in cardiovascular parameters on 3T CMR in response to haemodialysis with fluid removal. Specifically, left and right ventricular end-diastolic volumes, stroke volumes, and atrial volumes reduced, as did global native T1, septal native T1 and global T2 times but not LV mass. There was no correlation between the change in these parameters and the change in fluid status measured by bodyweight or bioimpedance. The change in myocardial native T1 time was independent of changes in haematocrit and blood pool T1, suggesting that the observed difference is not explainable by reduced intravascular T1 time. Regardless of whether the change in native T1 time is due to fluid removal, or the dialysis process itself, the present results question the validity of native T1 mapping as a surrogate marker for myocardial fibrosis in patients on haemodialysis.

Native T1 mapping is an appealing potential biomarker for myocardial fibrosis, with proven superiority over volumes, function and late gadolinium enhancement in patients with non-ischaemic dilated cardiomyopathy [215,216], and encouraging data in patients with CKD [115,206,217]. However, there are conflicting results from previous studies exploring the influence of fluid status on native T1 mapping in patients with CKD. Native T1 times do not alter with varying end-diastolic volumes (an indicator of changing fluid status) in patients on dialysis [208]. Similarly, a study comparing 124 dialysis patients to 137 healthy controls found that the increased myocardial native T1 times observed in patients with CKD occurred independently of changes in T2 times, suggesting that fibrosis, rather than fluid, accounts for the differences in T1. However, these patients were scanned the day after dialysis when euvolaemia is most likely [218]. Furthermore, a study of 12 patients found no change in T1 values on 3T CMR immediately post dialysis [219]. These patients had relatively low ultrafiltration volumes (mean 1.1L) and the lack of effect could be explained by insufficient time to allow for fluid re-equilibration. In the MIDNIGHT study [12], which found significant improvements in native T1 time on 3T CMR with extended hours nocturnal haemodialysis, there was no association between native T1 time and fluid status on bio-impedance body composition monitoring. However, the change in T1 did occur in the presence of increased ultrafiltration volumes in the treatment group, and reduced

ultrafiltration volumes in the control group. In contrast, a study of 30 dialysis patients found a significant correlation (r=0.409) between fluid status and native T1 time on 1.5T CMR [128]. This result could be explained by reverse causality, with patients with more myocardial fibrosis being more prone to fluid overload. Kotecha *et al* found global native T1 times on 1.5T CMR reduced from 1085 ms pre-dialysis to 1072 ms post-dialysis in 25 dialysis patients undergoing a 3 hour dialysis session with mean 2.0 L ultrafiltration [127]. The present study confirms this result at 3.0T and supports the conclusion that the abnormal native T1 times observed in patients with CKD can be modulated by dialysis with fluid removal and therefore is not entirely due to fibrosis.

The minimal clinically significant change in native T1 time is difficult to define. Previous studies comparing native T1 times in patients on dialysis versus controls found a mean difference of 21 ms on 1.5T [182] and 185 ms on 3T [207]. In the present study, the mean global T1 times are greater than the scanner-specific healthy reference range by a mean of 112.7 ms pre-dialysis and 91.4 ms post dialysis (Table 4.1). The mean change in T1 time pre- and post-dialysis was 21.3 ms. In the MIDNIGHT trial [12], the intervention resulted in a mean reduction in native T1 time of 30.6 ms (from a mean baseline value of 1270ms). As another example, in non-CKD patients undergoing aortic valve replacement, native T1 times reduced by an average of 44.7 ms and were associated with improved prognosis [220]. So while the difference in global T1 observed by this study, and by Kotecha *et al* [127], is small, it is within the region of clinically significant difference. Similar magnitude of change has been observed in healthy volunteers and patients with coronary artery disease immediately post exercise, but in this setting native T1 times increased, rather than decreased [221]. In these patients with coronary artery disease, the magnitude of native T1 reactivity correlated with the severity of myocardial perfusion abnormality [221]. This suggests that any change in native T1 times following dialysis is unlikely to be due to dialysis-induced ischaemia (which would cause times to increase).

Native T1 mapping predicts outcome in patients with heart failure [222] and acute myocardial injury [223]. It also has proven diagnostic or prognostic benefit in a range of other conditions including amyloidosis, myocarditis, aortic stenosis, iron overload, and Fabry disease [114,131]. The present results question the on-going consideration of native T1 mapping as a surrogate for myocardial fibrosis in patients on haemodialysis.

Studies including myocardial biopsy data will be needed to answer this definitively but would be challenging to justify ethically and difficult to complete. There is an ongoing study correlating native T1 mapping with post-mortem histology in 9 participants (ClinicalTrials.gov Identifier: NCT03586518). For native T1 to proceed as a potential biomarker in CKD patients, it will require longitudinal studies with standardised timing of imaging in relation to dialysis therapy to establish if native T1 has a prognostic role in the CKD population, and if changes in native T1 times correspond with proportional changes in prognosis. If proven, the small changes in native T1 times following dialysis may be deemed negligible.

Global T2 times reduced following dialysis with fluid removal, in keeping with previous studies [127]. The native transverse relaxation time (T2) is sensitive to proton (water) binding to macromolecules and proton mobility. Native T2 reflects tissue water content and mobility to a greater extent than native longitudinal relaxation time (T1). Skeletal muscle T2 times also decreased suggesting that the observed myocardial change may be due to reduced total body water content, rather than a myocardial-specific process, but there was no change in hepatic or blood pool T2. The timing of radiofrequency pulse sequence used in T2-weighted images results in increasing signal intensity with increasing water content of tissues [224], and so it is physically plausible that the change in T2 time represents reduced tissue oedema. The lack of association between the change in T2 time and the change in fluid status is against this, but it still remains the most likely explanation.

There appears to be a complex relationship with regards to parameters of ventricular function and dialysis with fluid removal. A study using intradialytic CMR has previously shown that LVEF drops acutely during dialysis with incomplete recovery evident at 1 hour post dialysis [219]. This explains the present observation whereby the timing of dialysis and repeat CMR was a significant factor in predicting repeat LVEF (albeit with a very weak correlation), with those patients on a morning dialysis schedule (and therefore undergoing repeat CMR soon after dialysis) being more likely to have a reduction in repeat LVEF. Paradoxically, in the sub-group of patients with reduced LVEF, previous reports have suggested that dialysis with fluid removal can improve LVEF [127]. In the present study, 5 of the 6 patients with abnormal LVEF at visit 1 had an improvement on repeat LVEF measurement, presumably due to reduced

afterload. With regards to clinical practice, CMR scanning should be avoided immediately post-dialysis and serial scanning should be performed at same time in relation to dialysis schedule. Given the differential response in LVEF depending on baseline LVEF, it is conceivable that the wrong dialysis prescription could perpetuate a patient's cardiac dysfunction and is a reminder of the importance of the individualised medicine in dialysis prescribing. There is increasing interest in the role of LV global longitudinal strain as a potentially superior measure of cardiac function compared to LVEF, especially in patients with CKD [115,225].

This study addresses important questions in relation to 3T CMR to inform timing of clinical scanning in relation to dialysis and the potential bias of fluid overload in parametric mapping. The cohort is representative of the wider dialysis population with high prevalence of comorbidity and no changes to their prescribed dialysis session. The number of clinically relevant incidental findings that were identified is striking but is in keeping with previous reports [226]. Fluid assessment was comprehensive and CMR scans were performed utilising state-of-the-art hardware and software. However, there are several limitations. The sample was heterogeneous with regards to timing of scans in relation to dialysis, baseline LVEF (despite attempts to control this by excluding patients with known LV dysfunction) and baseline hydration status, with 10 participants measuring as volume deplete on bioimpedance monitoring at visit 1. We cannot discount a Type 2 error for the lack of correlation between myocardial native T1 and fluid removal. Further, there may have been a differential time-course between changes in fluid status and native T1. The impact of 1 litre fluid removal is likely to have differential effect on the myocardium if the starting state is volume overload, as opposed to volume depletion. Nevertheless, there was no apparent difference in change in native T1 times according to baseline hydration status. The study could have been improved by inclusion of a control group who underwent dialysis without fluid removal. Further work is warranted.

Conclusion

Acute changes in cardiac volumes and myocardial composition are detectable on 3T CMR following haemodialysis with fluid removal. Accordingly, the timing of clinical CMR scanning in relation to a patient's dialysis schedule is crucial, particularly if

serial scanning is required. Small, but significant, reductions in global myocardial T1 and T2 relaxation times were observed after dialysis suggesting that the abnormal native T1 signal in patients undergoing haemodialysis is not entirely due to fibrosis. The exact mechanism for the reduction in native T1 times is unclear. Despite the lack of association with the change in native T1 time and the change in fluid status, alterations in tissue oedema remain the most likely explanation, albeit removal of uraemic factors or the haemodynamic effects of dialysis itself may also contribute. Future studies examining the prognostic capabilities of native T1 in CKD populations are still warranted but will require careful standardisation of imaging schedules and awareness of the potential confounding effect of fluid status and the dialysis process.

Declarations

Ethics approval and consent to participate
All participants gave written consent prior to participation. Favourable ethical opinion was granted by the West of Scotland Research Ethics Committee 1 (Ref: 18/WS/0138, 13th August 2018).

Consent for publication

All participants gave written consent for their data and/or images to be published as part of a scientific report.

Availability of data and materials

Available via the corresponding author upon reasonable request.

Competing interests

The authors declare no competing interests relevant to the present study. Outside the present study: Patrick Mark reports speaker honoraria from Vifor-Fresenius, Astra Zeneca, Janssen, Napp, Novartis and Bristol Myers-Squibb, research grants from Boehringer Ingelheim and non-financial support from Pharmacosmos. Jennifer Lees reports speaker honoraria from Vifor-Fresenius, Astra Zeneca, Bristol Myers-Squibb

and Pfizer. Colin Berry is employed by the University of Glasgow which holds consultancy and research agreements with Abbott Vascular, AstraZeneca, Boehringer Ingelheim, Causeway Therapeutics, Coroventis, Genentech, GSK, HeartFlow, Menarini, and Siemens Healthcare.

Funding

Dr Alastair Rankin is personally funded by a Clinical Academic Training Fellowship from The Chief Scientist Office (Scotland) (CAF/18/02). Dr Elaine Rutherford is supported by a Postdoctoral Clinical Lectureship from The Chief Scientist Office (Scotland) (PCL/18/03). Dr Jennifer Lees is supported by a Postdoctoral Clinical Lectureship from The Chief Scientist Office (Scotland) (PCL/20/10). Thomas Treibel is currently supported by a BHF Intermediate fellowship (FS/19/35/34374). Colin Berry is funded by a British Heart Foundation Centre of Excellence Award (RE/18/6/34217).

Authors' contributions

All authors have reviewed and contributed to this manuscript. PBM, GR, AJR, ER and KM conceived the idea and analysis plan for this study. AJR recruited participants, performed study visits, analysed the CMRs, analysed the data and wrote the manuscript. KM, GR, TT and CB advised on CMR analysis and critically reviewed the manuscript. KM also analysed a sample of CMRs for inter-observer reproducibility. EE analysed data regarding the determinants of blood pool native T1. LD led image acquisition. KAG and JSL assisted with data collection, analysis and critically reviewed the manuscript. PBM, ER, RKP and AR advised on analysis plan and critically reviewed this manuscript.

Acknowledgements

We wish to thank all participants who kindly volunteered their time for this study. We also wish to thank Dr Andrew Morrow for providing the scanner-specific reference ranges for myocardial native T1 and T2 in healthy individuals.

Chapter 5 – Cardiovascular magnetic resonance for the detection of descending thoracic aorta calcification in patients with end-stage renal disease. J Cardiovasc Magn Reson (2021).

5.1 Manuscript

Elbert Edy*, Alastair J Rankin*, Jennifer S Lees, Pauline Hall Barrientos, Rosemary Woodward, Sokratis Stoumpos, Ioannis Koktzoglou, Robert R Edelman, Aleksandra Radjenovic, Patrick B Mark, Giles H Roditi. Cardiovascular magnetic resonance for the detection of descending thoracic aorta calcification in patients with end-stage renal disease. *J Cardiovasc Magn Reson* **23,** 85 (2021).
https://doi.org/10.1186/s12968-021-00769-6
**joint first authors*

Abstract

Background: Vascular calcification is an independent predictor of cardiovascular disease in patients with chronic kidney disease. Computed tomography (CT) is the gold-standard for detecting vascular calcification. Radial volumetric-interpolated breath-hold examination (radial-VIBE), a free-breathing gradient-echo magnetic resonance imaging (MRI) sequence, has advantages over CT as it is ionising radiation-free. However, its capability in detecting thoracic aortic calcification (TAC) has not been investigated. This study aims to compare radial-VIBE to CT for the detection of TAC in the descending aorta of patients with end-stage renal disease (ESRD) using semi-automated methods, and to investigate the association between TAC and coronary artery calcification (CAC).

Methods: Paired cardiac CT and radial-VIBE scans from ESRD patients participating in 2 prospective studies were obtained. Calcification volume was quantified using semi-automated methods in a 9 cm segment of the thoracic aorta. Correlation and agreement between TAC volume measured on MRI and CT were assessed with Spearman's correlation coefficient (ρ), linear regression, Bland-Altman plots and intraclass correlation coefficient (ICC). Association between CAC Agatston score and TAC volume determined by CT and MRI was measured with Spearman's correlation coefficient.

Results: Scans from 96 participants were analysed. Positive correlation was found between MRI and CT calcification volume (ρ = 0.61, 95% confidence interval (CI): 0.45-0.73). ICC for consistency was 0.537 (95% CI: 0.378-0.665). Bland-Altman plot revealed that compared to CT, MRI volumes were systematically higher at low calcification volume, and lower at high calcification volume. CT did not detect calcification in 41.7% of participants, while radial-VIBE detected signal which the semi-quantitative algorithm reported as calcification in all of those individuals. Instances of suboptimal radial-VIBE image quality were deemed to be the major contributors to the discrepancy. Correlations between CAC Agatston score and TAC volume measured by CT and MRI were ρ = 0.404 (95% CI: 0.214-0.565) and ρ = 0.211 (95% CI: 0.008-0.396), respectively.

Conclusion: Radial-VIBE can detect TAC with moderate positive association to CT, albeit with the presence of proportional bias. Quantification of vascular calcification by radial-VIBE remains an area for future research, but improvements in image quality are necessary. In the meantime, CT should remain the primary modality for assessing vascular calcification in clinical practice.

Keywords: Thoracic aortic calcification; End-stage renal disease; Cardiovascular disease; Computed tomography; Magnetic resonance imaging; Radial volumetric interpolated breath-hold examination (radial-VIBE) sequence

Background

Patients with chronic kidney disease (CKD) have a greater risk of cardiovascular disease (CVD) and all-cause mortality compared to age-matched controls within the general population[227]. This risk is greatest in patients with end-stage renal disease (ESRD) who require renal replacement therapy (RRT) in the form of dialysis or a kidney transplant[1]. Traditional cardiovascular risk factors (e.g., diabetes, hypertension, hyperlipidaemia), are prevalent amongst CKD populations. In addition, there are CKD-specific risk factors that contribute to the predisposition to CVD, such as excessive arterial calcification and vascular stiffening. In ESRD patients, aortic stiffness is higher compared to healthy controls[60], and arterial calcification may be partly responsible for this[228]. Clinically, both arterial stiffness and calcifications have been shown to be independent predictors of cardiovascular mortality in ESRD patients[229,230] and have been used as a surrogate end point for clinical trials in this population[231].

The thoracic aorta can be imaged in both cardiac computed tomography (CT) and cardiovascular magnetic resonance (CMR) and quantifying thoracic aortic calcification (TAC) may have some utility in improving risk prediction. In primary prevention cohort studies, TAC was shown to be an independent predictor for all-cause mortality[232,233], but not for cardiovascular events[234–237]. While in patients with stable angina, TAC was associated with increased risk of death and CVD[238]. Although data in ESRD patients are lacking, other arterial calcifications, such as coronary artery calcification (CAC) and abdominal aortic calcifications, are associated with higher risk of all-cause and cardiovascular mortality in advanced CKD (stages 4-5) and haemodialysis patients[239,240]. Therefore, it is plausible that TAC might also be a risk factor for cardiovascular events in ESRD patients.

CT is a well-established imaging modality for detecting vascular calcification in clinical practice. Calcification can be quantified on CT using the Agatston score[241], which takes into account the area and density of calcified lesions, or the volume score, which does not depend on calcium density[242]. Traditionally, calcification is hard to discern with conventional spin-echo sequence in magnetic resonance imaging (MRI) because it appears with various signal intensities[243]. Moreover, calcification is

hypointense due to low proton density and often lies adjacent to the dark arterial lumen[244].

Recent work has shown that a prototype proton density-weighted in-phase stack-of-stars MRI using a small flip angle gradient-echo readout can accurately quantify aorto-iliac and ilio-femoral vascular calcifications[245,246]. A similarly configured and commercially-available gradient-echo MRI sequence called radial volumetric interpolated breath-hold examination (radial-VIBE) could therefore serve as a potential alternative to CT in detecting and quantifying vascular calcification without ionising radiation[247]. However, whether this could be applied to detecting TAC is unknown.

The aim of this study was to compare radial-VIBE to CT for the detection and quantification of TAC, specifically in the descending thoracic aorta, in patients with ESRD using a semi-automated approach. In addition, the association between descending TAC and CAC was investigated.

Methods

Sources of images & other clinical data

Imaging data from adult patients with ESRD participating in 2 prospective research studies was used: 1) Vitamin K in kidney transplant organ recipients: Investigating vEssel Stiffness (ViKTORIES) trial (Current Controlled Trials number, ISRCTN22012044) and 2) The Interrogation of the Cardiomyopathy of Chronic Kidney Disease With advancEd caRdiac Imaging (TICKER) study (ClinicalTrials.gov number, NCT03704701). All subjects gave written informed consent to the respective studies, which were reviewed and approved by the local Research Ethics Committee. The ViKTORIES trial[248] is a phase II, double-blinded, parallel-group, randomised, placebo-controlled trial comparing vitamin K supplementation to placebo on vascular stiffness in renal transplant patients. The TICKER study is an ongoing observational study that is assessing the effects of dialysis on the myocardium using CMR. Both studies collected imaging data, of which the paired cardiac CT and CMR (acquired within 24 hours of each other) were used in the current study. For both VIKTORIES

and TICKER studies, the assessment of calcification was one of several prospectively defined research questions being addressed. The paired scans were performed at the Clinical Research Imaging Facility based at the Queen Elizabeth University Hospital in Glasgow.

CT image acquisition

Electrocardiogram-gated non-contrast scans of the heart were acquired at 120 kVp in a single heartbeat scan using an Aquilion ONE Vision Edition CT scanner (Canon Medical Systems Ltd., Crawley, UK). Radiation dose was reduced by using the Adaptive Iterative Dose Reduction 3D reconstruction algorithm.

CMR image acquisition

Non-contrast CMR images were obtained using a Siemens Prisma 3 Tesla scanner (Siemens Healthineers, Erlangen, Germany) with an 18-channel surface coil placed anteriorly, and a 32-channel spine coil placed posteriorly. Radial-VIBE images were acquired in coronal plane using Siemens StarVIBE product (Siemens Healthineers, Erlangen, Germany), which is a free-breathing, 3D, proton density-weighted, stack-of-stars, gradient echo sequence. The imaging parameters used were: field-of-view (FOV) 462 x 462 mm, slice thickness 3mm, repetition time (TR) 4.18 ms, echo time (TE) 2.46 ms, flip angle 2.5 degrees, acquired voxel size 1.2 x 1.2 x 1.2 mm, sampling bandwidth 720 Hz/pixel, scan time 4.30 minutes. No cardiac or respiratory gating was utilised.

Quantitative image analysis

One investigator analysed all of the images to measure calcification volume. A second investigator, who was added post-hoc, re-analysed a random sample of scans representing 10% of the cohort to assess the inter-observer reproducibility of our quantitative analysis protocols. To promote blinding, randomly ordered CT images were batch analysed before radial-VIBE images. The latter were analysed in a random order over a week later, without reference to CT results. Horos is a free and open source code software (FOSS) program that is distributed free of charge under the

Lesser General Public License at Horosproject.org and sponsored by Nimble Co LLC d/b/a Purview in Annapolis, MD USA. On sagittal views on both CT and radial-VIBE images, Horos was used to select a 9 cm segment of the descending thoracic aorta, starting from the level of the top of the vertebra closest to the diaphragmatic surface of the heart and then progressing superiorly as shown in Figure 5.1. If the vertebra was out of the FOV, then the area of analysis would begin from the inferior surface of the heart. The descending aorta was chosen as the region of thoracic aorta most reliably visualised on CT within a field of view allowing simultaneous imaging of CAC. The CT and radial-VIBE images containing only the selected portion of aorta were exported and ImageJ (version 1.52q, National Institutes of Health, USA)[249] was then used to detect and quantify the volume of calcification present within the descending thoracic aorta. Volume of calcification is the product of the area of the lesions detected and the slice thickness:

$$\text{Volume}_{(\text{in mm}^3)} = \sum(Area\ in\ mm^2 * slice\ thickness\ in\ mm)$$

Figure 5.1 - Sagittal (A) radial-VIBE and (B) computed-tomography (CT) images of descending thoracic aorta.

A 9 cm segment of thoracic aorta from the same patient is chosen on both CT and radial-VIBE images. Red horizontal lines mark the level of the top of the vertebra that is closest to the inferior surface of the heart. Yellow vertical lines correspond to 9 cm of thoracic aorta.

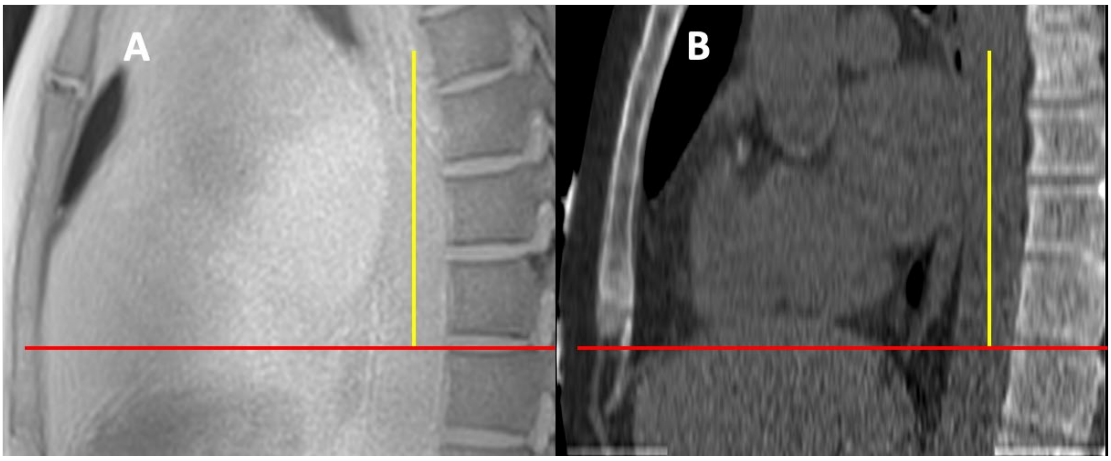

CT image analysis

CT images were reconstructed with 3 mm slice thickness and 3 mm slice interval to be used for analysis. Calcification was defined as voxels with attenuation values of 130 Hounsfield units (HU) or greater and appearing bright on CT (Figure 5.2), this corresponds to approximately 2 standard deviations (SD) higher than the attenuation of unenhanced blood. Although arbitrary, this is accepted as the conventional threshold for CT assessment of arterial calcification[241]. A median filter of 3 mm radius was used to reduce 'salt and pepper' noise while preserving sharp edges. Once a threshold had been set to segment calcifications, a region-of-interest (ROI) was manually drawn around the wall of the descending thoracic aorta if calcified lesion(s) was present. Lastly, the area of calcification within the aorta was measured using automated thresholding. The patient's total volume of calcification was then calculated offline. CAC Agatston scores were reported by a consultant radiologist in line with clinically approved protocols, blinded to treatment allocations and clinical variables using dedicated analysis software (Vitrea Advanced, Vital Images, Minnetonka, USA).

Figure 5.2 - Representative images of calcifications on computed tomography (CT) (A, C) and radial-VIBE (B, D).

Images A and B are axial slices; Images C and D are sagittal slices. Calcifications are indicated by the red arrows. For this participant, volume of calcification detected by CT = 834.81 mm^3, radial-VIBE volume = 634.02 mm^3.

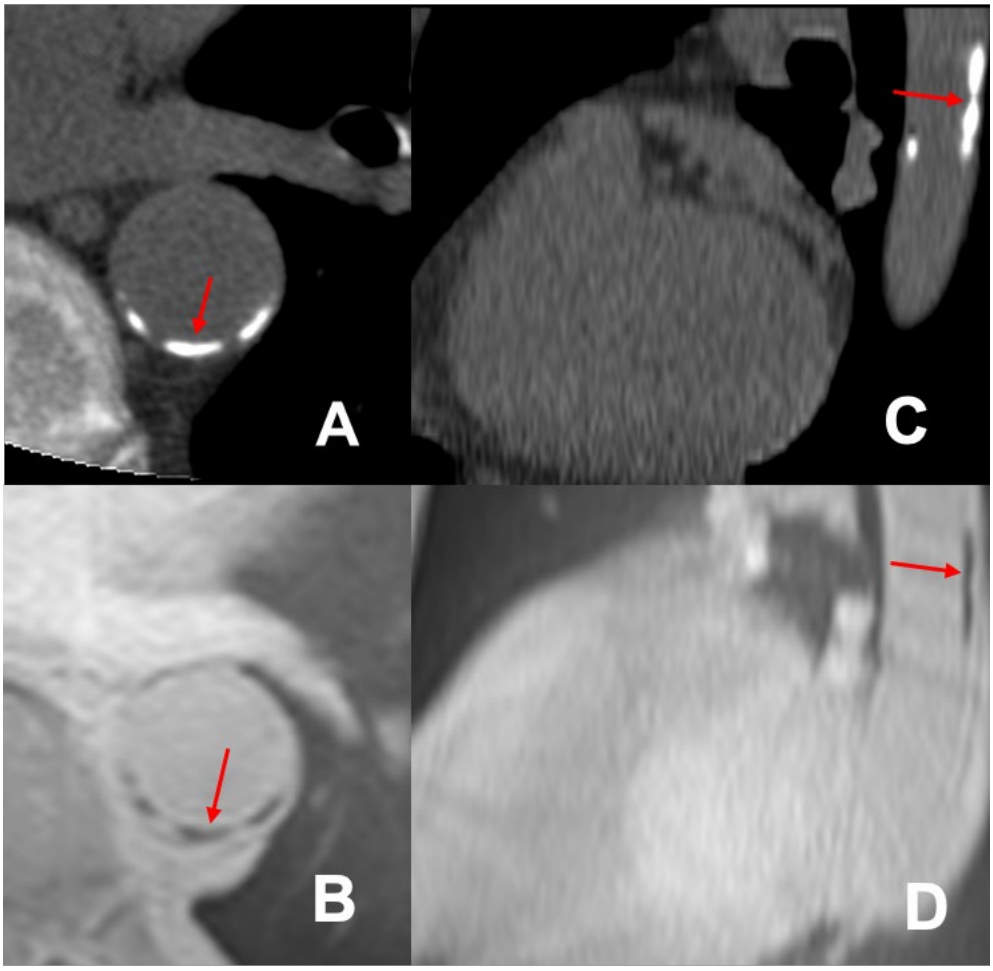

Radial-VIBE image analysis

Reconstructed radial-VIBE images with 3 mm slice thickness and 3 mm slice interval were used for analysis. On the transverse plane, ROIs were manually delineated around the aortic wall in every consecutive slice. Next, a bespoke segmentation algorithm was used to segment calcifications (based on signal intensity) and measure their area. Aortic calcification appears hypointense (i.e. dark) on radial-VIBE images (Figure 5.2) and was defined as a voxel with signal intensity of at least 2.5 SD below the mean signal intensity of voxels within the ROI (i.e. aorta) of each slice. A previous study, which utilised similar techniques, has defined calcification on MRI as between 2 and 3 SD below the mean signal intensity of the ROI[246]. In our cohort, 2.5 SD was chosen as it was quickly evident during the algorithm development that 2 SD insufficiently distinguished calcification from noise, while 3 SD excluded obvious calcification.

Qualitative image analysis

Two observers (E.E. and A.R., with one and four years experience of researching vascular calcification, respectively) subjectively compared all (n = 96) radial-VIBE scans to CT. A 5-point Likert scale (1 – very poor, 2 – poor, 3 – fair, 4 – good, 5 – excellent) was used to assess the confidence with which the radial-VIBE matched the CT with regards to calcification presence, location, size and shape[250]. Where scores disagreed, scans were reviewed to reach consensus.

Statistical analysis

Data were analysed with Minitab® Statistical Software (Version 19.2.0.0) and SPSS software package (IBM SPSS Statistics for Macintosh, Version 26.0. Armonk, NY: IBM Corp.). Normality of variables was assessed with P-P plot, Kolmogorov-Smirnov, and Shapiro-Wilk tests. Correlation between volume of calcifications in CT and radial-VIBE was assessed with Spearman's rank correlation coefficient (ρ), and linear regression. This is an exploratory, hypothesis-generating, study. The research question was prospectively defined and was considered in the design of the source studies. However, the sample size of the source studies was determined in relation to

primary end points unrelated to the methods described in this report. A post-hoc power calculation was not performed.

Spearman's rank correlation coefficient was also used to investigate the association between volume of aortic calcifications (detected by CT and radial-VIBE separately) and CAC Agatston score assessed by CT[251].

Bland-Altman plots were constructed, and mean bias (radial-VIBE volume minus CT volume) and 95% limits of agreement (LOA) were calculated between CT and radial-VIBE volume. However, as the assumptions of constant mean bias and standard deviation of differences were violated, linear regression was used to model the relationship between mean bias and the mean of calcium volume[252]. The standard deviation of the residuals from regression were then used to estimate 95% LOA.

To assess the degree of consistency and absolute agreement between CT and radial-VIBE volume, intra-class correlation coefficient (ICC) estimates and their 95% confidence interval (CI) based on a single-rating and 2-way mixed model were calculated. ICC was also used to measure intra- and inter-observer reliability of quantitative analysis by randomly sampling and reanalysing 10 paired CT and radial-VIBE scans after blinding of original volume scores. Weighted Cohen's kappa (κ) coefficient was used to assess inter-observer reliability of qualitative scores.

Sensitivity analyses

As a pre-specified sensitivity analysis, where there was a large discrepancy in the detected calcium volume between radial-VIBE and CT, the area of analysis was reassessed to check for any difference in ROI selection. A re-analysis of the volume of calcification would be done as part of sensitivity analysis if there was a clear discrepancy in area of analysis. This would remove blinding and therefore would be purely exploratory. Data points with standard residuals of 3 or more detected by linear regression were considered as outliers and a sensitivity analysis excluding them was performed.

Results

Baseline characteristics

A total of 96 participants was included in the analysis (24 from TICKER, 72 from ViKTORIES). Twelve were excluded from analysis (1 from TICKER, 11 from ViKTORIES) due to various reasons (See supplementary material S5.1).

Supplementary material S5.1: Flowchart of cardiovascular magnetic resonance (CMR) and computed tomography (CT) scans available for analysis.

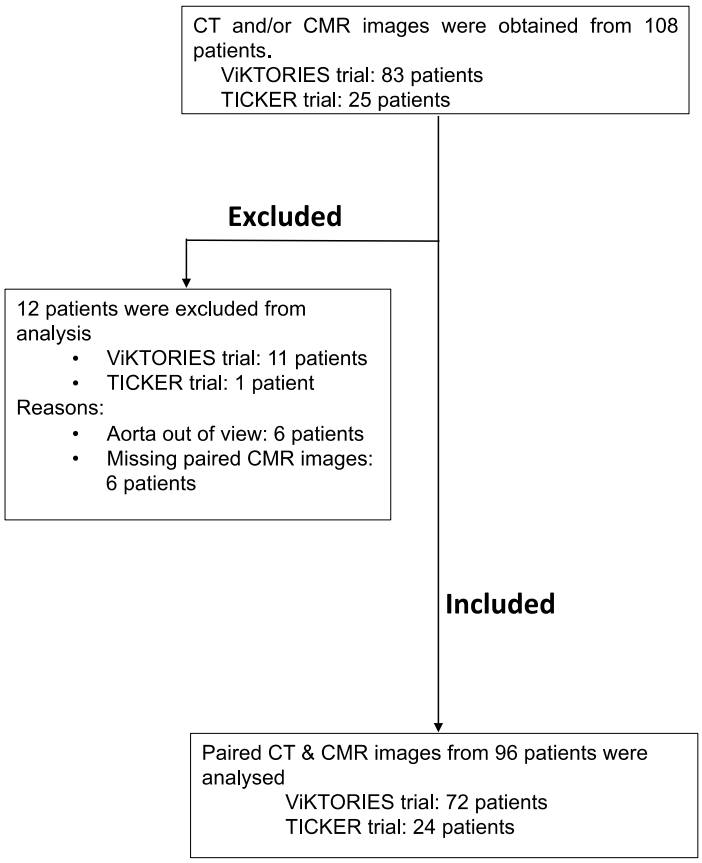

The relevant demographic and disease characteristics of the ViKTORIES and TICKER participants are shown in Table 5.1. The mean age of study participants was 59.6 years, a third were female and a third were current or ex-smokers (Table 5.1). Due to the selection criteria chosen for their respective studies, all the TICKER participants were receiving hospital-based intermittent haemodialysis, while ViKTORIES trial participants had a functioning kidney transplant. The median RRT vintage was 2 years for TICKER participants and 7 years for ViKTORIES participants (Table 5.1). The mean estimated glomerular filtration rate (eGFR) for patients with a functioning kidney transplant (i.e. ViKTORIES participants) was 52.5 ml/min/1.73m^2 (SD: 21.8 ml/min/1.73m^2).

Table 5.1 - Characteristics of TICKER and ViKTORIES participants at baseline.

Characteristics	**ViKTORIES N = 72**	**TICKER N = 24**	**Combined N = 96**
Mean age ± SD* (year)	57.9 ± 8.9	64.7 ± 1.86	59.6 (9.3)
Male sex (%)	45 (62.8)	15 (62.5)	60 (66.7)
White race (%)	70 (97.2)	21 (87.5)	91 (94.8)
Diabetes (%)	18 (25)	11 (45.8)	29 (30.2)
Smoking status (%)			
Non-smoker	47 (65.3)	18 (75.0)	65 (67.7)
Ex-smoker	19 (26.4)	5 (20.8)	24 (7.3)
Current smoker	6 (8.3)	1 (4.2)	7 (25.0)
Previous cardiovascular disease †	17 (23.6)	11 (45.8)	28 (29.2)
Mean eGFR ± SD (ml/min/1.73m^2) ‡	52.5 ± 21.8	-	-
Renal replacement therapy (RRT) vintage (years)			
Median	7.10	1.96	-
Interquartile range	10.48	2.69	-

*SD denotes standard deviation.

† Participants were considered to have previous cardiovascular disease if they had one or more of the following: history of ischaemic heart disease, heart failure, coronary revascularisation (including percutaneous coronary intervention and/or coronary artery bypass graft), stroke and/or transient ischaemic attack, and/or peripheral arterial disease.

‡ eGFR denotes estimated glomerular filtration rate.

Radial-VIBE vs CT volume

The median volume of calcification quantified was 191 mm^3 (range 0 to 1572; IQR 189 mm^3) by radial-VIBE and 11 mm^3 (range 0 to 4982; IQR 274 mm^3) by CT. Figure 5.3 illustrates the scatterplot of volume of TAC measured by radial-VIBE and

CT. CT did not detect calcification in a proportion of participants (41.7%), while radial-VIBE detected signal which the algorithm incorrectly reported as calcification in all of those individuals (ranging from 65 to 482 mm^3). There was only one case when calcification was detected in CT (2.2 mm^3) and none in radial-VIBE.

Figure 5.3 - Scatterplot of thoracic aortic calcification volume measured by radial-VIBE against computed-tomography (CT).

Red solid line is the line of best fit and green dashed lines represent its 95% confidence intervals (CI); black dashed line is the line of unity. The linear regression equation and R-squared value are on the bottom right; Spearman's rank correlation coefficient (ρ), with its 95% CI and p-value, are on the top left.

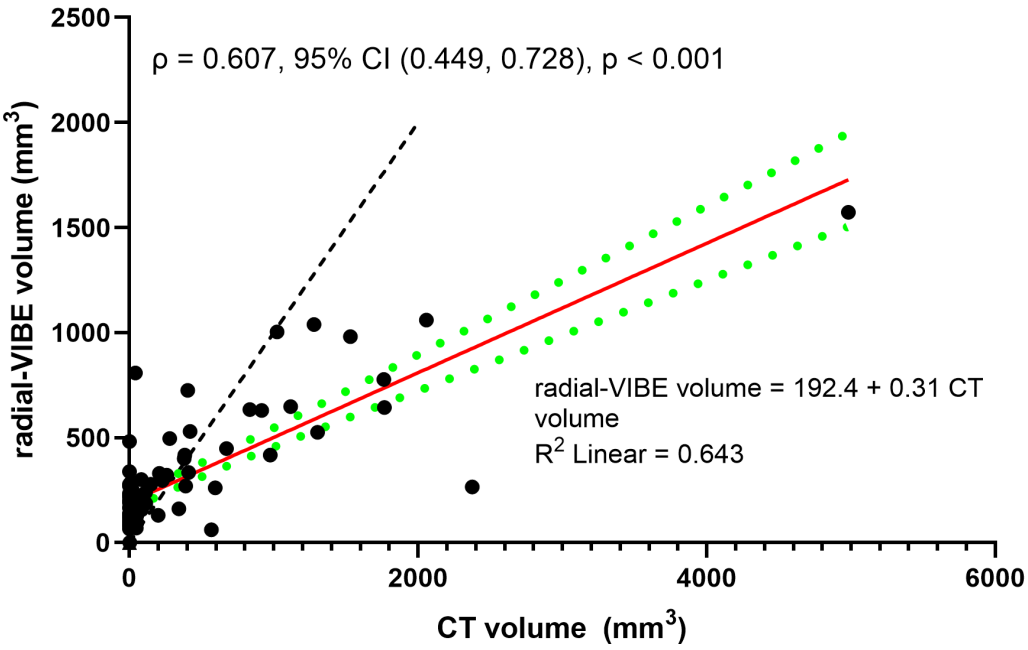

Spearman's rank correlation coefficient was assessed as variables were not normally distributed. There was a positive monotonic correlation between radial-VIBE and CT calcification volume (ρ = 0.607, 95% CI (0.449, 0.728), p <0.001). Linear regression equation for radial-VIBE volume was 192.4 + 0.31 CT volume.

The ICC estimates based on single-measure and 2-way mixed effects model for consistency and absolute agreement were similar (ICC for consistency: 0.537, 95% CI (0.378, 0.665); ICC for absolute agreement: 0.539, 95% CI (0.380, 0.667)).

According to the Bland-Altman plot (Figure 5.4), the bias (radial-VIBE volume minus CT volume) and standard deviations of the differences were proportional to the magnitude of mean volume (i.e. proportional bias was present). However, the direction of the bias inverted with increasing volume: at lower calcification volume, the differences tended to be positive (i.e. radial-VIBE values were higher than CT), while as the mean volume of calcification detected by CT and radial-VIBE increased, radial-VIBE values decreased proportionally relative to CT values and the bias became increasingly negative.

Figure 5.4 - Bland-Altman plot of difference in calcification volume against mean calcification volume.

Difference in calcification volume = radial volumetric interpolated breath-hold examination (radial-VIBE) minus computed tomography (CT) volume. The linear regression equations for bias and its estimated regression based 95% limits of agreement (LOA) are on the top right. Blue solid line represents bias; green-dashed lines are the estimated regression based 95% LOA; black-dashed lines are the crude 95% LOA.

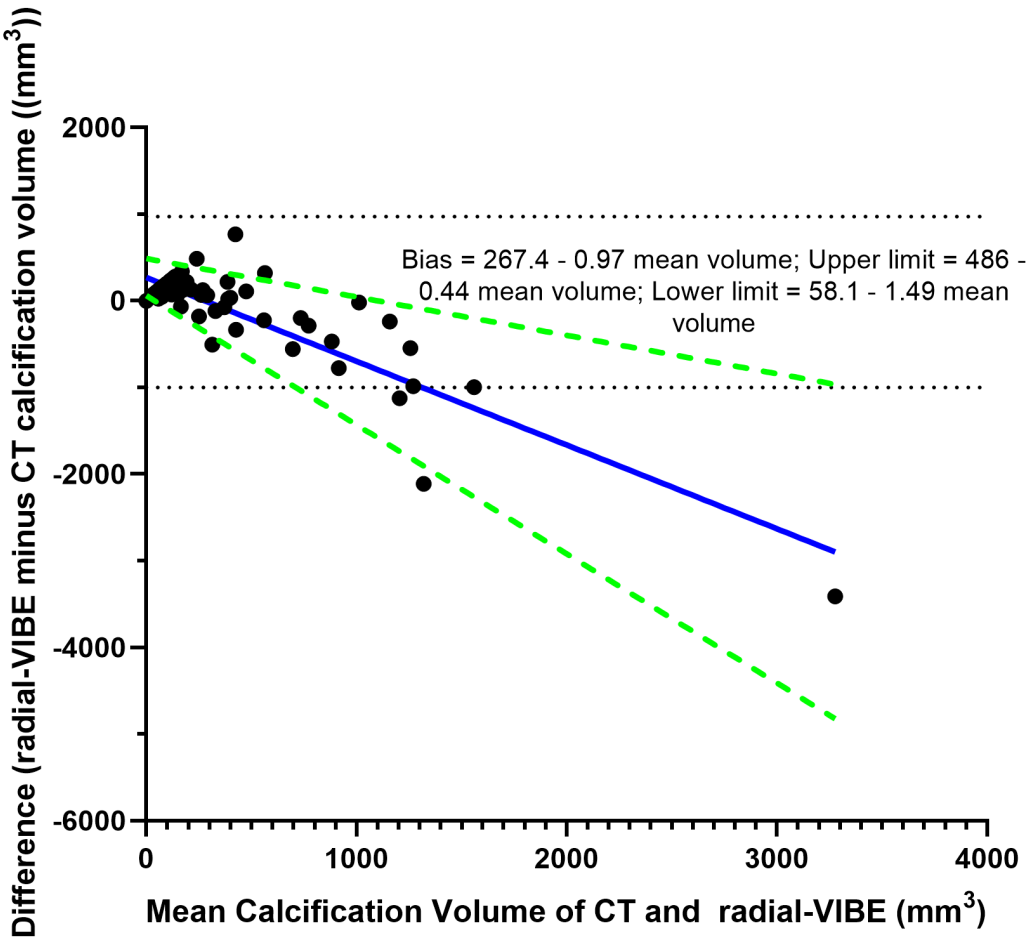

The relationship between bias and mean calcium volume modelled with linear regression was: Bias = 267.4 – 0.97 mean volume. P-value of the slope (-0.967) was <0.001, thus confirming that the difference in volume is related to the magnitude of volume (i.e. mean volume). The 95% LOA could be visualised in Figure 5.4, which illustrates that the standard deviations of the differences between radial-VIBE and CT results were also related to the mean volume.

Intra- and inter-observer reliability

The intra-observer reliability based on absolute agreement and 2-way mixed effects model was 1.00 for CT and 0.993 (95% CI (0.957, 0.998), $p < 0.001$) for radial-VIBE measurements. The inter-observer reliability using the same measures was 1.00 for CT and 0.990 (95% CI (0.959, 0.997), $p<0.001$) for radial-VIBE.

Comparison with Coronary Artery Agatston Score

There was a positive association between TAC volume detected by CT and CAC Agatston score ($\rho = 0.404$, 95% CI (0.214, 0.565), $p<0.001$). Meanwhile, there was also a positive, but weaker, association between TAC measured by radial-VIBE and CAC Agatston score ($\rho = 0.211$, 95% CI (0.008, 0.396), $p = 0.039$).

Outliers & Sensitivity Analyses

Three participants were identified as outliers as their standard residuals were larger than 3. The sections of aorta that were analysed on the CT and radial-VIBE in these patients were reviewed and deemed to be similar. Radial-VIBE images from 2 of the patients were of poor quality and had obvious artefact, which was likely to have influenced the results. No obvious explanation was found for the other outlier. Sensitivity analyses were performed with exclusion of these 3 outliers and the results remained relatively unchanged (results, scatter plot and Bland-Altman plot included in supplementary material S5.2 and S5.3).

Supplementary material S5.2: Sensitivity Analysis (with 3 outliers excluded) Results and Scatterplot.

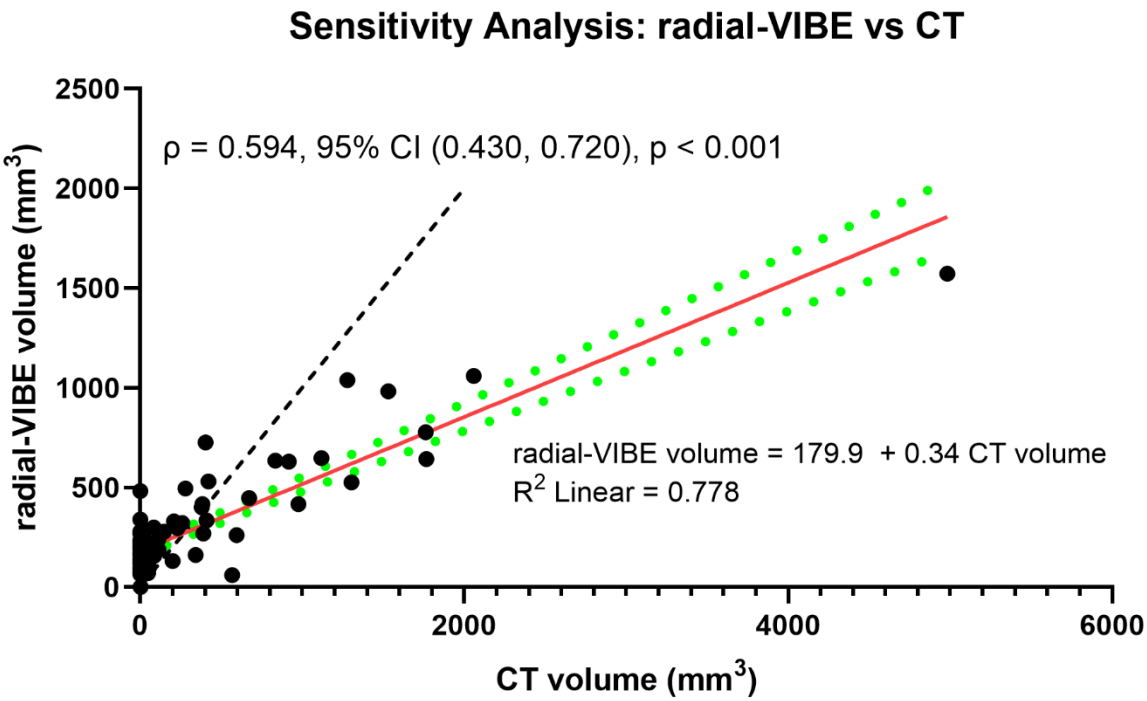

Supplementary material S5.3: Sensitivity Analysis Bland-Altman plot.

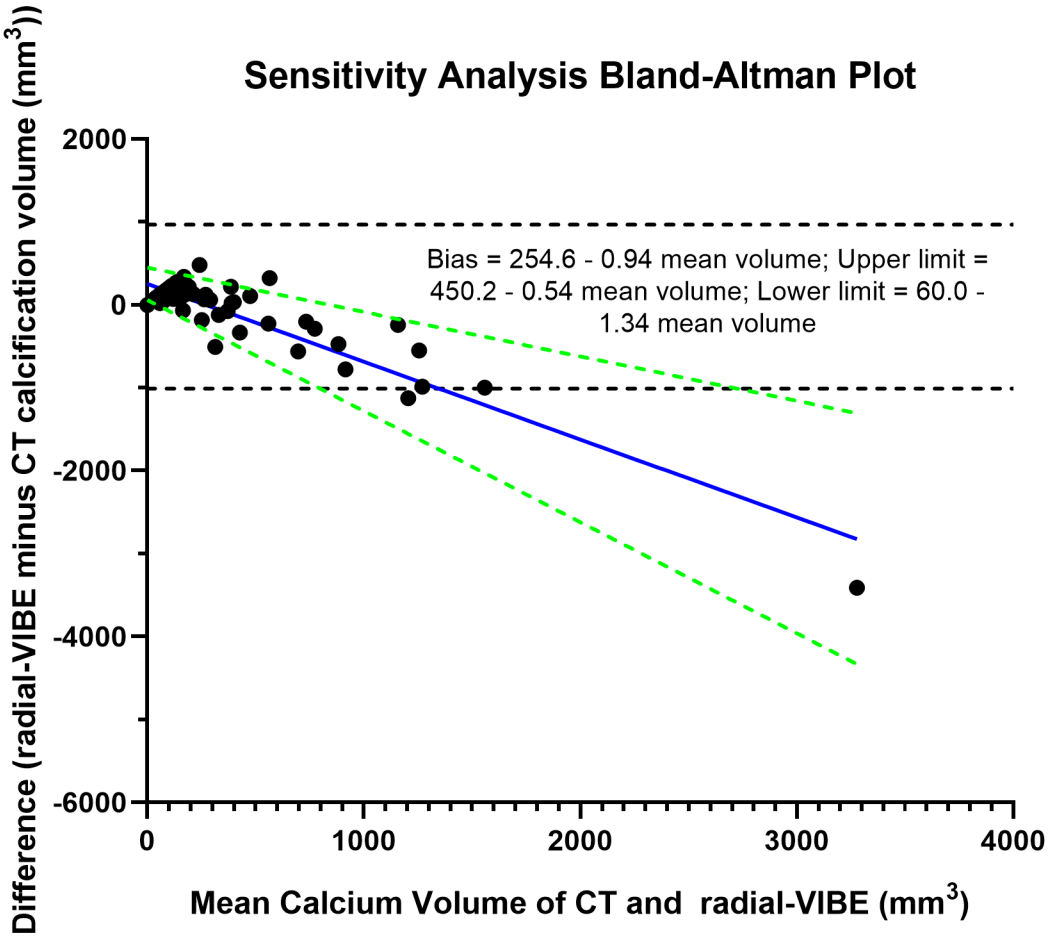

Qualitative assessment

The mean Likert score for the subjective, qualitative assessment of radial-VIBE compared to CT was 4.6 (SD 0.8). There was good agreement between the individual scores from the 2 observers ($\kappa = 0.822$, 95% CI (0.717, 0.927), $p < 0.001$). For the subgroup of 40 participants in whom quantitative analysis showed falsely detected 'calcification' on radial-VIBE that was not present on CT, the mean Likert score was 4.6 (SD 0.9). A total of 31 (78%) of these scored excellent agreement for no calcification being present, while 8 were downgraded for small volume false-positive findings on radial-VIBE, with one also having a small volume of false negative. In one participant, radial-VIBE correctly identified a small area of calcification that was

present on the CT, but which was subsequently removed from the CT images when the median filter was applied for quantitative analysis. Figure 5.5 shows case examples of when the subjective assessment of the paired scans yielded excellent agreement but the semi-automated, quantitative algorithm resulted in both over-detection and under-detection of calcification.

Figure 5.5 - Representative images of under-detection (A, B) and over-detection (D, E) on radial-VIBE compared to CT.

Images A and B are axial slices of radial-VIBE and image C is an axial slice of CT from the same patient. Red arrows on images A and B indicate calcifications, which appear as hypointense voxels. Red areas on image B illustrate the voxels that are considered as calcifications by the segmentation algorithm. Images D and E are identical axial slices of radial-VIBE belonging to another patient, and image F is the corresponding CT slice. Red areas on image E are the voxels considered as calcifications by the segmentation algorithm, which are likely to be noise and not genuine calcifications. For these 2 patients, the subjective analysis was deemed excellent agreement between radial-VIBE and CT, despite the quantitative analysis differing significantly.

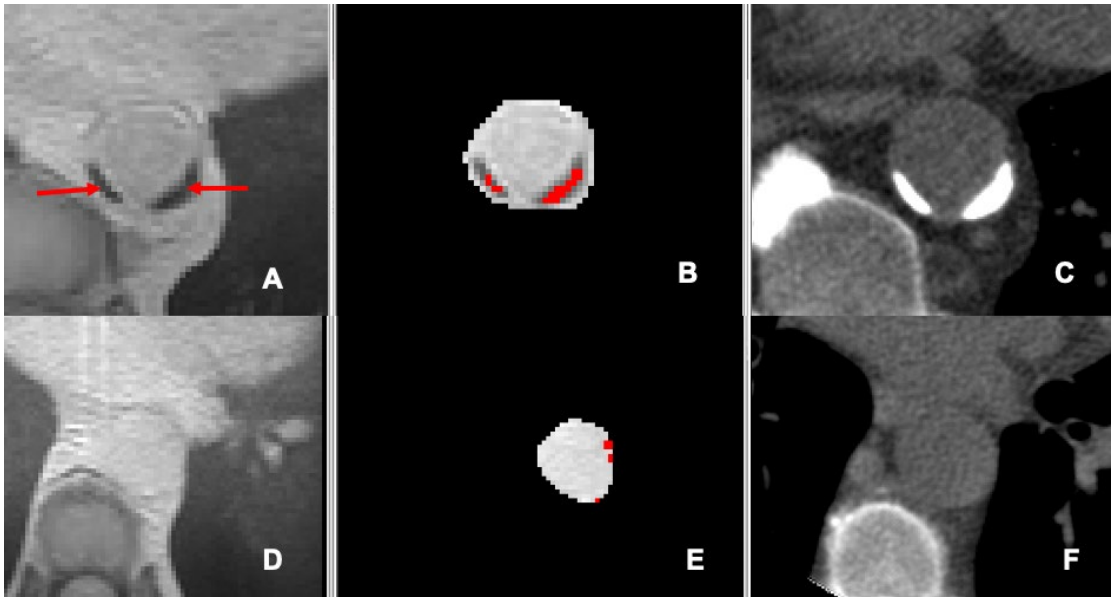

Discussion

This study confirms that radial-VIBE can be used to detect and quantify TAC with a positive association when compared to the gold standard CT. On subjective assessment radial-VIBE performs well when compared to CT, but when quantifying volume using a semi-automated method, the association is imperfect and proportional bias is observed. Compared to CT, radial-VIBE over-estimates the volume of

calcification when minimal calcification is present and under-estimates it when extensive calcification is present.

At lower mean volume of calcium, radial-VIBE had systematically higher volume of calcified lesions than CT. Several reasons might be responsible for this discrepancy. Firstly, it might be due to the presence of noise on radial-VIBE images, which had been falsely detected as calcification (Figure 5.5). The application of a median filter to reduce noise on radial-VIBE images was attempted but it affected the detection of obvious calcium lesions as well. On the other hand, a median filter was applied on the CT images, which could have contributed to the difference. Smaller calcified lesions were possibly removed by the filter, and hence explain the over-estimation of calcification volume when low levels of calcification were present, with one definite instance of this discovered on qualitative assessment. As an exploratory post-hoc analysis, we re-analysed the 40 participants who had calcification detected on radial-VIBE but not on CT. Removing the CT filter for these participants did not produce a meaningful improvement in results (data not shown). It is also possible that radial-VIBE images were affected by the presence of other compounds (e.g. haemosiderin) undetected by CT, which resulted in the presence of susceptibility artefacts. Due to the use of a proton density-weighted in-phase acquisition providing a bland image contrast, the boundaries of the aortic wall were visually obscured on most radial-VIBE scans. This made accurate delineation of the aorta challenging. It was likely that non-aortic voxels were included as ROI, which could introduce more noise and affect the segmentation algorithm's calculation of the threshold. Lastly, this study used a substantially larger voxel size than reported in a prior study of aorto-iliac and ilio-femoral calcifications[246], so that partial volume averaging of the low-signal calcifications with surrounding tissues may have been a more significant issue than in the prior study. Until improvements in radial-VIBE image quality are realised, a stepped analysis approach in which a subjective assessment is performed prior to algorithmic quantification of calcium deposits may negate some issues surrounding the false positive rate observed in the present study.

At higher mean volumes of calcium, radial-VIBE volumes were smaller than CT volumes. The reason for this could be due to blooming artefact of calcifications on CT, inappropriately magnifying dense lesions resulting in overestimation of their

volume[253]. However, this assumes vascular calcification is more susceptible to blooming artefact on CT than MRI, which may not be true. Another factor could be the presence of noise within the aorta of some radial-VIBE images that could cause uneven signal intensity and inflate the standard deviation (Figure 5.5). Consequently, the threshold for calcification would be extremely high and thus, diminish the segmentation algorithm's ability to detect calcification. This was found to be the case for one of the outliers that was identified, and another one in which radial-VIBE did not pick up any calcification but the paired CT did. The same effect could also occur when very large, dense areas of calcification are present, such that the calcium signal impacts on the mean intensity of the vessel lumen and subsequently, the threshold for calcification.

This study has several strengths. Firstly, the scanning protocols were standardised to limit variability. Secondly, CT and radial-VIBE images analysed in this study were obtained within 24 hours of each other, so the amount of calcification present in the patient's thoracic aorta would be identical during the acquisition of both scans. Thirdly, by studying patients with ESRD, who have a higher vascular calcium burden than their age- and sex-matched controls[254], we could compare calcium quantification across a range of severity (as evident by the present results showing CT calcium volume ranging from 0 to 4982 mm^3). The present findings would be applicable to other patient groups with a propensity towards vascular calcification including those with diabetes[255], cardiovascular disease[254] and elderly patients[256].

One of the limitations of this project was the manual delineation of aorta in the analysis of radial-VIBE images, whereas CT images were analysed with a more automated approach. Besides the poor definition of aortic wall in radial-VIBE images impairing the accuracy of manual segmentation as previously mentioned, manually drawing ROI was time-consuming and was less reproducible than CT analysis. However, several reasons led to that decision. Unlike CT, where the Hounsfield unit is calibrated with reference to water and its values are comparable among patients, the absolute signal intensity in MRI is not. The signal intensity is affected by various factors, which include proton density, pulse sequence, types and strength of magnet used for scanning[257]. Thus, the magnitude of signal intensity of the same tissue (e.g. heart) may vary across individuals. Consequently, it meant that calcium has no

'absolute' value which we could use for thresholding and segmentation. Instead, thresholding calcification in MRI images was dependent on its relative signal intensity compared to surrounding voxels – hence we used signal intensity greater than 2.5 SD below the mean signal intensity of ROI. This approach for thresholding calcifications in MRI images was used by Serhal *et al*. in their study, where 2 and 3 SD below the mean were classified as calcifications in the aorto-iliac and femoral arteries, respectively[246]. Due to the poor image quality of some scans in this study (often due to loss of signal from the large field of view/participant body habitus), 2 SD was not used as it could not sufficiently distinguish calcifications from noise, while 3 SD would significantly impair the detection of calcium with relatively low signal intensity. Furthermore, the thoracic aorta is near the air-filled lungs which are also hypointense. Segmenting the aorta while avoiding the lungs was crucial in order to prevent the mistake of identifying voxels in the lungs as calcification. Initially, the creation of a mask of the aorta from HASTE (Half-Fourier-Acquired Single-shot Turbo spin-Echo) images to segment the aorta was explored. Unlike radial-VIBE images, HASTE images have good aortic definition and manual segmentation is easier. Unfortunately, it was not possible to use the HASTE mask to subtract surrounding tissues from the radial-VIBE images due to different image parameters on the acquired scans (e.g. slice thickness and resolution).

Another limitation was that the typical CT scans for CAC do not cover the aortic arch and proximal descending thoracic aorta, which made it more challenging to find a common anatomical landmark in CT and radial-VIBE images to ensure that similar segments of the aorta were analysed. Additionally, the aortic arch and proximal descending thoracic aorta have been shown to be the areas of the aorta most prone to calcification[258] and it would have been useful to compare the detection of calcification by radial-VIBE and CT in those aortic segments.

The discrepancy in TAC volume between radial-VIBE and CT suggests that CT should remain the primary modality for assessing vascular calcification in clinical practice. Furthermore, CT has the advantages of wider availability, lower cost, and faster acquisition time compared to radial-VIBE. However, there is no doubt that radial-VIBE can detect vascular calcification and, if improvements in image quality are realised, it may be a plausible alternative to CT in the future, particularly where

patients are undergoing magnetic resonance angiography studies where additional information on calcified plaque can be valuable. The near-future role of radial-VIBE is perhaps best suited to realm of research, where its lack of ionising radiation can allow serial imaging, either as part of longitudinal study trying to monitor the progression of vascular calcification, or to assess the impact of therapeutics in clinical trials. Radial-VIBE has the additional benefit of allowing other CMR sequences to be acquired, thus providing information on the possible effects of therapies on cardiac structure and function, as well as aortic distensibility. However, ensuring adequate image quality would be essential to allow accurate quantification of TAC using radial-VIBE sequence.

Conclusions

In conclusion, this study supports the hypothesis that radial-VIBE can detect thoracic aortic calcification. However, there is proportional bias in the measurement of calcium volume by radial-VIBE compared to CT. Quantification of vascular calcification by radial-VIBE remains a promising area for future research, but improvements in image quality (e.g. through the use of optimised protocols, smaller voxels and motion correction) are necessary.

Declarations

Ethics approval and consent to participate

The West of Scotland Research Ethics Committee granted ethical approval for the acquisition and analysis of the images obtained from the TICKER and ViKTORIES trials. REC reference number for the TICKER study: 18/WS/0138. REC reference number for the ViKTORIES trial: 17/WS/0101. Written informed consent was provided by all participants.

Consent for publication

Written informed consent was provided for all representative images.

Availability of data and materials

Source data will be provided upon reasonable request.

Competing interests

The authors declare no competing interests in relation to the present study.

Funding

Dr Alastair Rankin is personally funded by a Clinical Academic Training Fellowship from The Chief Scientist Office (Scotland) (CAF/18/02). Dr Jennifer Lees was personally funded by a Kidney Research UK Training Fellowship (TF_013_20161125) for the ViKTORIES study and was supported by a British Heart Foundation Centre of Excellence Award (RE/13/5/30177) and Chief Scientist Office (Scotland) Lectureship (PCL/20/10). The investigators decided the study design, data collection, analysis, interpretation and presentation of results with no input from the study funders.

Authors' contributions

All authors have reviewed and contributed to this manuscript. AJR, JSL, SS, PHB, GHR and PBM conceived the study idea and study design. AJR and JSL recruited participants. RW led image acquisition. EE performed image analysis and statistical analysis. EE and AJR wrote the manuscript. IK wrote an initial version of software used for MRI calcium segmentation. IK, AR, RE and GHR advised on image analysis and critically reviewed the manuscript. SS and PBM critically reviewed the manuscript.

Acknowledgements

We wish to thank the participants for their contribution to this research. We wish to thank the radiographers at the Clinical Research Facility, Queen Elizabeth University Hospital, Glasgow, UK, for their expertise in image acquisition.

Authors' information (optional)

None.

Chapter 6 - Myocardial extracellular volume by contrast-enhanced computed tomography compared to native T1 mapping in patients on regular haemodialysis *(prepared ahead of submission)*

6.1 Manuscript

Alastair J Rankin[1], Elbert Edy[1], Stephen Rankin[2], Kenneth Mangion[1], Evonne McLennan[3], Thomas A Treibel[4], James C Moon[4], Colin Berry[1], Giles Roditi[1,5], Patrick B Mark[1].

1. Institute of Cardiovascular and Medical Sciences, University of Glasgow, Glasgow, UK
2. Department of Cardiology, NHS Greater Glasgow and Clyde, Glasgow UK
3. Clinical Research Imaging, NHS Greater Glasgow and Clyde, Glasgow, UK
4. Institute for Cardiovascular Sciences, University College London, London, UK
5. Department of Radiology, NHS Greater Glasgow and Clyde, Glasgow, UK

Abstract

Background: Myocardial fibrosis is prevalent in patients with kidney failure. Extracellular volume fraction (ECV) measured on cardiovascular magnetic resonance (CMR) imaging is the gold standard non-invasive method for quantifying myocardial fibrosis but is not routinely used in patients with kidney failure due to the concerns regarding gadolinium-based contrast agent exposure. We compared an alternative technique using ECV measured by contrast-enhanced cardiac computed tomography (ECV_{CT}) with myocardial native T1 time on MRI in patients on haemodialysis.

Methods: Prospective, single centre, observational study, in which patients on regular hospital haemodialysis underwent CMR with native T1 mapping and ECV_{CT} prior to dialysis. For the CT analysis, pre-contrast, post-contrast and delayed post-contrast (5 minutes) scans were acquired. Measurements from manually drawn regions of interest were combined with a venous haemotcrit to calculate ECV_{CT}).

Results: Twenty-three participants (15 male, mean age 65.8 +/- 9.1 years) with a median duration of renal replacement therapy of 2.9 (1.4, 4.1) years. There was no correlation between ECV_{CT} and native T1 time (global, septal or mid-ventricular anteroseptal) across 3 independent observers. The intraclass correlation coefficient for the inter-observer reproducibility of ECV_{CT} was 0.34.

Conclusion: There was no correlation between ECV-CT and native T1 in this small cohort of patients requiring dialysis. The study was limited by small sample size and the lack of a gold standard comparator without administering gadolinium-based contrast agent. It is possible that factors specific to kidney failure, for instance altered contrast pharmacokinetics, may impair the utility of ECV-CT in this population.

Keywords: Cardiovascular CT. Cardiovascular MRI. Myocardial fibrosis. Chronic kidney disease. Dialysis.

Introduction

Patients with chronic kidney disease (CKD) are at a greatly increased risk of cardiovascular disease.[41] This risk is most pronounced in patients with established kidney failure requiring dialysis, for whom cardiovascular disease is the single most common cause of death and accounts for between 25-40% of all deaths [45–47]. Myocardial fibrosis is believed to be the pathophysiological mechanism driving this increased cardiovascular risk [54–56] and accounts for the unique cardiovascular phenotype observed in patients with CKD: with relatively fewer deaths due to atherosclerotic events but more deaths due to sudden cardiac death and heart failure [44–47,53]. Previous successes using gadolinium-enhanced magnetic resonance imaging (MRI) to examine diffuse myocardial fibrosis in CKD [116,117] have been hindered by the subsequent discovery of an association between linear chelate gadolinium-based contrast agents and the very rare disease nephrogenic systemic fibrosis [259]. Accordingly, there is clinical need for novel non-invasive biomarkers to improve the diagnosis and management of myocardial fibrosis in patients with CKD.

Myocardial extracellular-volume (ECV) measured on gadolinium-based contrast agent (GBCA) enhanced MRI (ECV-MRI), is the gold-standard non-invasive technique for quantifying diffuse myocardial fibrosis and is a validated clinical biomarker that predicts mortality in patients with diabetes and heart failure [131,134,215,217,260]. However, this requires GBCA administration, for which there are residual clinical concerns in patients requiring dialysis. Previous studies have suggested that it is possible to calculate ECV using contrast-enhanced CT (ECV-CT), rather than GBCA-enhanced MRI. This involves comparing the relative change in CT signal intensity pre- and post-contrast for the myocardium compared to the blood pool, with results standardised to the individual's haematocrit. ECV-CT has advantages over ECV-MRI in that is potentially more widely available, has significantly faster acquisition time, is readily comparable between scanners and has fewer contraindications. In addition, ECV-CT is calculated from the direct impact of the iodinate-based contrast on the measured signal, as opposed to ECV-MRI which relies on the assumptions that the relaxivity of muscle and blood are equal and that water freely passes between compartments [134]. In patients with cardiac amyloid and aortic stenosis ECV-CT highly correlated with ECV-MRI ($r^2 = 0.85$) [133], and it has

been shown to predict adverse clinical outcomes in patients with aortic stenosis [261]. ECV-CT is a particularly appealing biomarker in patients requiring dialysis due to their propensity toward myocardial fibrosis, and one study has found ECV-CT values to be significantly higher in dialysis patients compared to controls [262]. Although iodine-based contrast has historically been linked with acute kidney injury, recent data suggests this risk is much smaller than previously thought [263,264], and the available clinical data in patients on regular dialysis is very reassuring [265–268]. In the absence of administering GBCAs, myocardial native T1 time is the most promising MRI biomarker to-date for CKD, and as such is the best alternative surrogate for ECV-MRI [115,206]. In this study, we compared ECV-CT with myocardial native T1 time on MRI in patients undergoing regular maintenance haemodialysis.

Methods

Participants

Individuals aged greater than 40 years who were established on regular, day-time hospital-based haemodialysis for at least 6 months were eligible for inclusion. Exclusion criteria included allergy to iodine-based contrast media, standard contra-indications to MRI and overt heart failure (defined as no previous clinical diagnosis of heart failure or with preserved left ventricular ejection fraction (>50%) on their most-recent transthoracic echocardiogram). Participants had to be able to comply with study procedures and provide informed consent. Participants were required to have a history of recurrent fluid overload (defined as ultrafiltration volumes of at least 1.5 litres mean fluid removal over the preceding 3 dialysis sessions) to facilitate a sub-study comparing CMR changes in response to fluid removal on dialysis https://clinicaltrials.gov/ct2/show/NCT03704701). Favourable ethical opinion was granted by the West of Scotland Research Ethics Committee 1 (Ref: 18/WS/0138). All study procedures were carried out in accordance with local guidelines and regulations and with respect to the declaration of Helsinki.

Sample Size

A total of 25 participants are required to identify a correlation coefficient of 0.6 between ECV-CT and native T1 time on CMR with power 0.90 and alpha 0.05.[252]

Study Protocol

This is a single centre observational study. Participants attended for CMR and contrast-enhanced CT within 24 hours prior to their scheduled dialysis session. Bio-impedance body composition monitoring (Fresenius Body Composition Monitor, Fresenius Medical Care, Hong Kong), and venepuncture for routine samples were also performed. All imaging was conducted at The Clinical Research Imaging Facility of the Queen Elizabeth University Hospital in Glasgow.

CT image acquisition

Electrocardiogram-gated scans of the heart were acquired in a single heartbeat using an Aquilion ONE Vision Edition CT scanner (Canon Medical Systems Ltd., Crawley, UK) with the following parameters typical: up to 320 detector rows with z-axis coverage 12-16 cm, 120 kVp, tube current time product 160 mAs, prospective ECG gating 65-75% of R-R interval and dose modulation algorithms switched off. Iomeron 400 (Iomeprol) contrast was administered at a dose of 0.8 ml/kg at a maximum rate of 7 ml/sec with a 50 ml saline chaser, as per clinical CT coronary angiogram protocols [269]. No additional rate control was administered due to risks of fluid overload, hyperkalaemia and intradialytic hypotension. Images were acquired pre-contrast, post-contrast (bolus-tracked for arterial phase with contrast monitoring in left ventricle) and delayed post-contrast (5 minutes after contrast administration). Images were reconstructed to 3mm/3mm thick axial sections with a FC03 kernel.

CT image analysis

A manual ROI method of ECV-CT measurement was performed using Horos software (Annapolis, USA). Horos is a free and open-source code software (FOSS) program that is distributed free of charge under the Lesser General Public License at Horosproject.org and sponsored by Nimble Co LLC d/b/a Purview in Annapolis, MD

USA. Pre-, post-, and delayed-contrast images were loaded into the viewer. A polygonal ROI was manually drawn in a central area of mid left ventricular (LV) septum on the post-contrast image. An additional blood pool ROI was drawn in the LV cavity, with care taken to avoid papillary muscles and artefact. The ROIs were first copied onto adjacent slices on the contrast images as quality control to ensure only myocardium and blood pool were included as appropriate. The ROIs were then pasted into the corresponding pre- and delayed-contrast images (Figure 6.1). Pre- and delayed-contrast ROIs were only manipulated if definite artefact avoidance or repositioning were required. Mean ROI signal intensity in hounsfield units (HU) was then transcribed and ECV-CT calculated using the following formula [133]:

ECV-CT = (1 – haematocrit) x (change in HU_{tissue}/change in HU_{blood})

The primary observer (AJR) batch analysed all CTs and CMR in a random order with anonymised CMRs relabelled to enable blinding. In addition, 2 independent blinded observers (EE and SR) analysed all CTs to assess inter-observer variability.

Figure 6.1 - Representative images of 4 chamber long axis views of the heart acquired using electrocardiograph-gated computed tomography pre-contrast (A), arterial phase post-contrast (B) and delayed post-contrast (5 minutes after contrast administration) (C).

ROIs were drawn on the contrast-enhanced image and then copied onto the corresponding pre-contrast and delayed post-contrast images to allow offline calculation of extracellular volume.

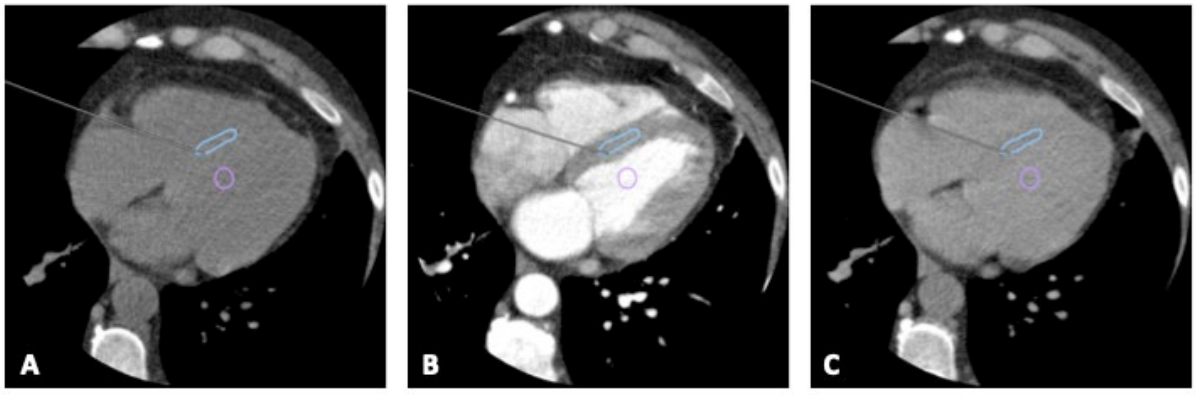

CMR Native T1 Image Acquisition

CMR images were acquired using a 3T MRI scanner (Prisma, Siemens Erlangen, Germany) with an 18-channel surface coil placed anteriorly and a 32-channel spine coil placed posteriorly. For native T1 mapping, basal, mid and apical short axis views were acquired using Siemens MyoMaps. Non-contrast, motion-corrected, optimized, modified Look-Locker inversion recovery sequences were used with the following typical parameters: FOV 340 x 272 mm, slice thickness 6.0 mm, voxel size: 1.9 x 1.9 x 6.0 mm, TR 272 ms, TE 1.12 ms, flip angle 35 degrees, minimum T1 100 ms, inversion-time increment 80 ms, bandwidth 1085 Hertz/pixel.

CMR Image Analysis

CMR analysis was performed utilizing dedicated CMR software (cvi42 software (version 5.10, Circle Cardiovascular, Canada)). Myocardial mass and volumes were measured in accordance with current guidelines [185] and have been described in detail previously [270]. Scanner derived T1 maps were used. Epi- and endocardial borders were manually drawn on the basal, mid and apical maps. Areas of obvious artefact were excluded from regions of interest (ROI). A 10% epi- and endocardial offset was applied to ensure only myocardial tissue was included. Blood pool ROI were drawn in the LV cavity on each slice, with care taken to avoid artefact and papillary muscles. Left and right ventricular insertion points were added to allow automatic division of segments according to the American Heart Association's 16 segment model [124]. Global values were derived by averaging results from all three short axis slices. Septal values were reported as the mean of segments 2, 3, 8, 9 and 14. The mid-ventricular anteroseptal (segment 8) value was reported as the segment least likely to be affected by motion artefact or infarct (due to collateralisation) and most akin to the manual ROIs drawn on long-axis views of the CT. A second independent observer (KM) analysed a random sample of CMRs representing >30% of the cohort to assess inter-observer variability.

Statistical Analysis

Continuous data with a normal distribution are presented as mean ± standard deviation (SD), and median and interquartile range (IQR) for skewed data, with normality defined according to Shapiro-Wilk test. Pearson Correlation Coefficient was used to compare the relationship between continuous variables. Intra- and interobserver variability was assessed by the intra-class correlation (ICC) coefficient (two-way mixed effect, absolute agreement, single measures). Statistical analysis was performed, and data plots created, using SPSS (version 27, IBM Corp, New York).

Results

Participant characteristics

Twenty-eight participants were recruited between 19th October 2018 and 9th March 2020. Recruitment was stopped early (target n=30) due to the COVID-19 pandemic. 2 participants withdrew consent prior to any study procedures and 3 did not receive contrast (2 due to inability to achieve intravenous access, 1 due to a contrast allergy which was identified on a clinical scan between recruitment and visit 1). Twenty-three participants were included in the analysis, of whom 15 were male and mean age was 65.8 +/- 9.1 years. Median duration of renal replacement therapy at time of recruitment was 2.9 (1.4, 4.1) years. All participants had a history of recurrent fluid overload with mean ultrafiltration volume of 2.11 (+/- 0.4) from the preceding 3 dialysis sessions prior to recruitment. CMR and CT were acquired within 1 hour of each other for all participants. Additional baseline characteristics are included in Table 6.1.

Table 6.1 - Baseline characteristics. Values are displayed as count (percentage), mean ± standard deviation or median (interquartile range), as appropriate.

N=23	
Age, years	65.8 ± 9.1
Male	15 (65%)
Primary renal diagnosis Diabetes Glomerulonephritis Polycystic Tubulo-interstitial nephritis Unknown Other	 7 (30%) 5 (22%) 1 (4%) 2 (9%) 3 (13%) 5 (22%)
Duration of renal replacement therapy (years)	2.9 (1.4, 4.1)
Dialysis access Catheter Arterial venous fistula Arterio-venous graft	 8 (35%) 11 (48%) 4 (17%)
Body mass index (kg/m2)	30.7 (26.7, 37.5)
Volume of fluid overload as measured on bioimpedance (l)	0.22 l (-0.85, 2.45),
Smoking Previous Current	 8 (35%) 1 (4%)
Hypertension	21 (91%)
Previous myocardial infarction	3 (13%)
Angina	5 (22%)
Stroke	6 (26%)
CMR parameters Left ventricular mass index, g/m^2 Left ventricular end-diastolic volume index, ml/m^2 Left ventricular end-systolic volume index, ml/m^2 Left ventricular ejection fraction, %	 55.8 +/- 23.5 100.8 +/- 34.6 49.8 +/- 32.3

	52.6 +/- 10.9
Myocardial native T1, ms	
Global	
Septal	1283 +/- 51
Mid-ventricular anteroseptal	1313 +/- 52
	1306 +/- 59
Myocardial native T2, ms	
Global	
Septal	42.6 +/- 3.4
Mid-ventricular anteroseptal	43.8 +/- 3.9
	42.7 +/- 3.3

ECV-CT and native T1 time

There was no correlation between ECV-CT and native T1 time (global, septal or mid-ventricular anteroseptal (segment 8)) across any of the 3 observers (Table 6.2; Figure 6.2). The intra-observer reproducibility (ICC) for ECV-CT for the primary observer (AJR) was 0.62. The inter-observer reproducibility (ICC) for ECV-CT was 0.34 overall (0.35, 0.59 and 0.42 for each pair). Supplementary material S6.1 includes the individual ECV-CT results for each observer. The reproducibility of native T1 was very good (intra-observer reproducibility (ICC) for global, septal and mid-ventricular anteroseptal native T1 were 0.98, 0.93, 0.81 with corresponding values for inter-observer reproducibility of 0.95, 0.94, and 0.77, respectively). Post-hoc subjective review of cases where ECV-CT values differed between observers did not find fault in the different ROIs chosen, as demonstrated in supplementary material S6.2, which includes a case example highlighting the slice-by-slice differences that can occur in ECV-CT measurements.

Table 6.2 - Correlation between extracellular volume measured by contrast-enhanced computed tomography (ECV-CT) and myocardial native T1 time on cardiovascular magnetic resonance imaging across 3 independent observers.

	ECV-CT (%) observer 1	ECV-CT (%) observer 2	ECV-CT (%) observer 3
Global T1 (ms)	0.23 (p = 0.30)	-0.26 (p=0.23)	-0.28 (p=0.19)
Septal T1 (ms)	0.22 (p=0.30)	-0.81 (p=0.71)	-0.11 (p=0.63)
Mid-ventricular anteroseptal (segment 8) T1 (ms)	0.27 (p=0.22)	-0.53 (p=0.81)	-0.008 (p=0.97)

Figure 6.2 - Scatter plots of ECV-CT (%) compared to myocardial native global (A), septal (B) and mid-ventricular anteroseptal (C) T1 (ms). Data shown from observer 1.

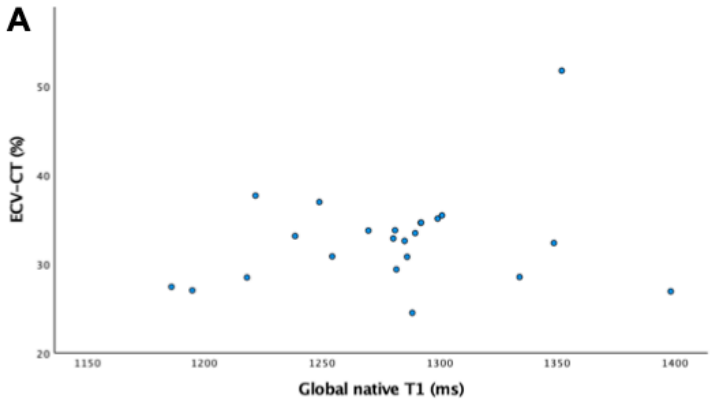

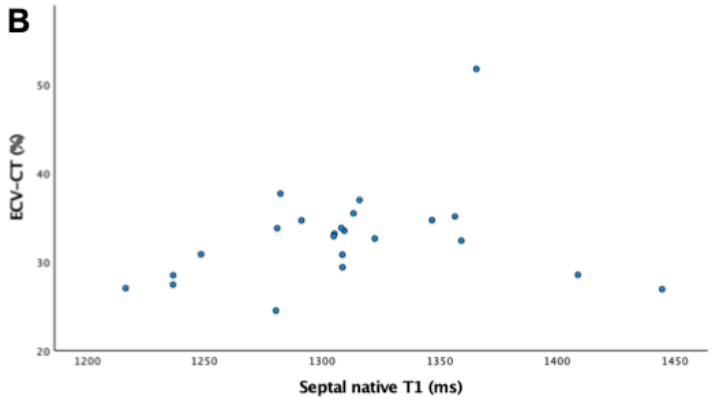

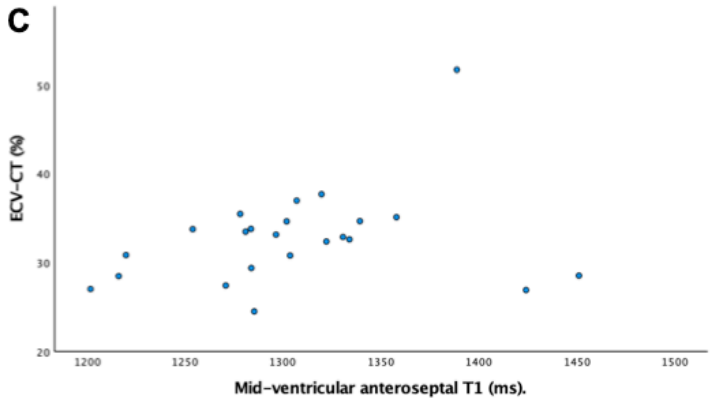

Supplementary material S6.1. Table showing the results for extracellular volume measured on CT (ECV-CT; %) for each of the 3 observers.

	Observer 1	Observer 2	Observer 3
1	32.4	31.6	32.8
2	27.4	37.5	32.5
3	30.8	35.6	29.8
4	32.6	33.0	35.1
5	33.8	36.3	33.7
6	28.5	31.6	32.7
7	30.8	31.2	29.3
8	33.5	30.7	31.7
9	24.5	28.2	24.5
10	29.4	37.5	30.8
11	27.0	32.5	45.4
12	34.6	31.1	32.3
13	51.7	37.1	30.8
14	33.8	37.9	29.4
15	37.7	38.2	36.3
16	33.2	33.7	35.0
17	35.1	51.8	44.8
18	32.9	32.9	42.4
19	35.5	32.7	40.8
20	37.0	48.9	33.1
21	34.7	57.8	43.3
22	26.9	18.6	21.6
23	28.5	26.0	40.2

Supplementary material S6.2. Images from a representative case of adequate quality highlighting the slice-by-slice differences in ECV-CT measurements, which we believe accounts for the lack of correlation with CMR parameters and the poor reproducibility within our data set. A, B, and C repeat the exemplary images displayed in Figure 6.1, but with region of interest (ROI) data displayed. Panels D, E and F are the same case, with the same ROIs drawn 1 slice apart (i.e. 3mm difference in slice location). The table underneath includes the mean ROI signal intensity in hounsfield units (HU) and haematocrit data that was used to calculate ECV-CT, and shows the large discrepancy in calculated ECV-CT from slices 3mm apart, despite absence of obvious artefact, scar or significant mal-alignment or mis-registration.

Slice location 1595.88 mm, ECV = 35.11%

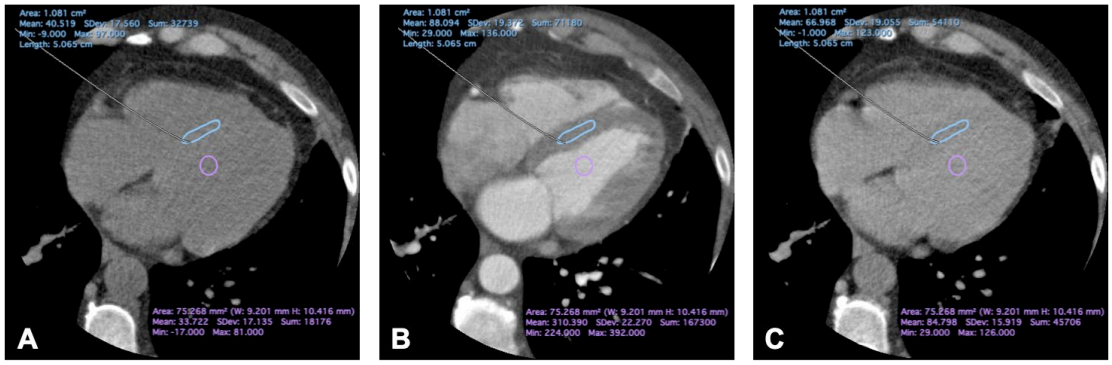

Slice location 1592.88 mm, ECV = 49.17%

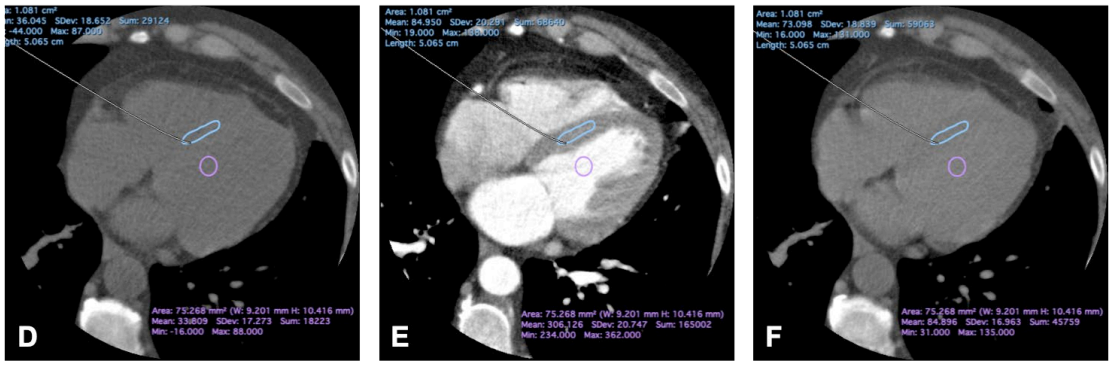

Slice location (mm)	Haematocrit (%)	HU tissue pre	HU blood pre	HU tissue post	HU blood post	ECV-CT
1595.88	32.2	40.519	33.722	66.968	84.798	35.109
1592.88	32.2	36.045	33.809	73.098	84.896	49.174

ECV-CT and other parameters of interest

ECV-CT did not correlate with global T2, septal T2, or mid-ventricular antero-septal T2 times across any of the 3 observers (supplementary material S6.3). Similarly, there was no correlation between ECV-CT and left ventricular mass, left ventricular mass index, left ventricular ejection fraction or fluid overload (measured by bioimpedance body composition monitoring) (supplementary material S6.3).

Supplementary material S6.3. Correlation between extracellular volume measured by contrast-enhanced computed tomography (ECV-CT) with cardiovascular MRI and clinical parameters of interest across 3 observers. There were no significant correlations detected.

	ECV-CT observer 1	ECV-CT observer 2	ECV-CT observer 3
Global T2 (ms)	0.14 (p =0.51)	0.06 (p=0.77)	0.06 (p=0.80)
Septal T2 (ms)	0.09 (p=0.68)	0.01 (p=0.98)	0.01 (p=0.97)
Mid-ventricular anteroseptal (segment 8) T2 (ms)	0.06 (p=0.79)	0.06 (p=0.80)	0.10 (p=0.66)
Left ventricular mass (g)	0.09 (p=0.68)	0.01 (p=0.98)	0.01 (p=0.97)
Left ventricular mass index (g/m^2)	0.26 (p=0.23)	-0.05 (p=0.83)	-0.12 (p=0.59)
Left ventricular ejection fraction (%)	0.08 (p=0.72)	-0.18 (p=0.40)	0.17 (p=0.45)
Over-hydration measured by bioimpedance (l)	0.19 (p=0.40)	0.08 (p=0.73)	0.04 (p=0.85)

Discussion

In this small prospective study in a cohort of patients undergoing regular haemodialysis there was no association between ECV-CT and any CMR parameter of interest, including myocardial native T1. There are numerous methodological reasons that could account for the lack of association that are discussed below. However, given the strength of the association between ECV-CT and ECV-MRI in previous studies in different patient cohorts [133,271], the lack of any association in the present data raises some concerns that biological reasons relating to kidney failure, rather than purely methodological limitations, may hinder the application of ECV-CT in patients requiring dialysis.

The major limitation of the present study is the lack of a gold standard comparator: myocardial native T1 was used instead of ECV-MRI. This was deliberate and unavoidable. The risk of nephrogenic systemic fibrosis with modern macrocyclic gadolinium contrast agents is sufficiently small that gadolinium administration is often justifiable on clinical grounds in patients with kidney failure requiring dialysis [272]. However, in an exploratory research setting where the individual participant stands nothing to gain, we believed that this risk, although extremely small, was not justifiable and a recent paper was retracted on these grounds [273]. Although native T1 is the most promising cardiovascular imaging biomarker in CKD at present, recent studies have shown that native T1 is acutely modifiable with dialysis, suggesting that the abnormal native T1 signal in patients with CKD is not entirely due to fibrosis [127,270]. The present study was small and under-powered: 23 participants were included whereas it was calculated that 25 were required to detect a correlation of 0.6 between ECV-CT and myocardial native T1. On one hand, it could be argued that a correlation of 0.6 is an over-estimation of the reasonably predicted magnitude of an association between these 2 indirectly related variables and as such a larger sample size would be necessary. On the other hand, any weaker association would have been of questionable clinical relevance. Regardless, the scatter plots (Figure 6.2), poor inter-observer reproducibility (ICC = 0.34) and wide intra-subject variability (supplementary material S6.2) make it clear that the application of ECV-CT as performed here in patients on dialysis faces significant barriers irrespective of the sample size studied. It may be that the intra-subject variability (supplementary

material S6.2) can be improved with technical modifications. Additional heart rate control was not utilised in the present protocol due to the risk of causing intra-dialytic hypotension, exacerbating pulmonary oedema, and increasing vulnerability to hyperkalaemia-induced bradycardia in patients who were due dialysis imminently. However, these risks would be reduced if scanning was performed the day after dialysis which may allow additional heart rate control, which in turn may improve image resolution, reduce motion artifact, and aid registration between pre-contrast and delayed contrast images. Additionally, the use of dual-energy CT [274] or spectral CT would obviate the need for a separate pre-contrast scan, thus removing the risk of mis-registration between pre-contrast and contrast scans and reducing the time that the patient has to lie still for while awaiting the delayed contrast sequence. Finally, post-acquisition software may be able to further improve registration and therefore reduce the risk that tiny changes in anatomical location can majorly affect the integrity of an ROI copied from one scan to the next.

It is possible that biological reasons relating to kidney failure account for the lack of association between ECV-CT and CMR parameters. Fluid overload and hypo-albuminaemia, which are prevalent in the dialysis population, are likely to affect the volume of distribution and pharmacokinetics of iodine-based contrast. Furthermore, it is not clear if the absence of glomerular filtration of the contrast (as would be expected in patients established on maintenance haemodialysis) will affect the steady-state concentration of contrast in the blood volume and consequently require a different time point for acquisition of the delayed images compared to protocols used in patients with normal kidney function (albeit data on the renal clearance of iodine-based contrast suggests that negligible renal clearance is likely to occur in 5 minutes [275]). Finally, it is possible that the myocardial fibrosis and left ventricular hypertrophy that occur in kidney failure may cause a proportional increase in intracellular and extracellular volume, unlike amyloid deposition which has been studied previously [133,271] such that ECV may be the wrong parameter to measure in this population.

Conclusions

In this small prospective study in patients undergoing regular haemodialysis there was no correlation between ECV-CT and myocardial native T1. ECV-CT remains an

appealing imaging biomarker both generally, due to its rapid acquisition time, widespread availability and the direct effect of iodine-based contrast on the measured signal (unlike gadolinium effects in CMR), and also specifically in dialysis patients, due to the prevalence of myocardial fibrosis combined with the persistent concerns regarding GBCA use in this population. However, using the present ECV-CT protocol in patients on dialysis has displayed poor intra-observer reproducibility and wide intra-subject variability. Future studies of ECV-CT in patients undergoing haemodialysis are warranted but would benefit from imaging on non-dialysis days, with additional heart rate control and using dual-energy or spectral CT with specific post-acquisition software to improve registration. Additionally, studies comparing ECV-CT and ECV-MRI in patients with less advanced CKD who can safely receive GBCAs are indicated.

Declarations

Ethics approval and consent to participate

All participants gave written consent prior to participation. Favourable ethical opinion was granted by the West of Scotland Research Ethics Committee 1 (Ref: 18/WS/0138, 13th August 2018).

Consent for publication

All participants gave written consent for their data and/or images to be published as part of a scientific report.

Availability of data and materials

Available via the corresponding author upon reasonable request.

Competing interests

The authors declare no competing interests relevant to the present study. Outside the present study: Patrick Mark reports speaker honoraria from Vifor-Fresenius, Astra Zeneca, Janssen, Napp, Novartis and Bristol Myers-Squibb, research grants from Boehringer Ingelheim and non-financial support from Pharmacosmos. Colin Berry is employed by the University of Glasgow which holds consultancy and research agreements with Abbott Vascular, AstraZeneca, Boehringer Ingelheim, Causeway Therapeutics, Coroventis, Genentech, GSK, HeartFlow, Menarini, and Siemens Healthcare.

Funding

Dr Alastair Rankin is personally funded by a Clinical Academic Training Fellowship from The Chief Scientist Office (Scotland) (CAF/18/02). Thomas Treibel is supported

by a BHF Intermediate fellowship (FS/19/35/34374). Colin Berry is funded by a British Heart Foundation Centre of Excellence Award (RE/18/6/34217).

Authors' contributions

All authors have reviewed and contributed to this manuscript. PBM, GR, AJR, JM and KM conceived the idea and analysis plan for this study. AJR recruited participants, performed study visits, analysed the CTs and CMRs, analysed the data and wrote the manuscript. EE and SR independently analysed the CTs. KM, GR, TT and CB advised on image analysis and critically reviewed the manuscript. KM also analysed a sample of CMRs for inter-observer reproducibility. EM led image acquisition. PBM and JM critically reviewed the manuscript (in addition to conceiving the idea).

Acknowledgements

We wish to thank all participants who kindly volunteered their time for this study.

Chapter 7 - Comparing the interobserver reproducibility of different regions of interest on multi-parametric renal magnetic resonance imaging in healthy volunteers, patients with heart failure and renal transplant recipients. MAGMA (2019).

7.1 Manuscript

Alastair J. Rankin[1], Sarah Allwood-Spiers[2], Matthew M.Y. Lee[1], Luke Zhu[1], Rosemary Woodward[3], Bernd Kuehn[4], Aleksandra Radjenovic[1], Naveed Sattar[1], Giles Roditi[5], Patrick B. Mark[1], Keith A. Gillis. Comparing the inter-observer reproducibility of different regions of interest on multi-parametric renal magnetic resonance imaging in healthy volunteers, patients with heart failure and renal transplant recipients. *Magn Reson Mater Phy.* 33, 103-112 (2020). https://doi.org/10.1007/s10334-019-00809-4

Abstract

Objective: To assess inter-observer reproducibility of different regions of interest (ROIs) on multi-parametric renal MRI using commercially available software.

Materials and Methods: Healthy volunteers (HV), patients with heart failure (HF) and renal transplant recipients (Tx) were recruited. Localiser scans, T1 mapping and pseudo-continuous arterial spin labelling (pCASL) were performed. HV and Tx also underwent diffusion-weighted imaging to allow calculation of apparent diffusion coefficient (ADC). For T1, pCASL and ADC, ROIs were drawn for whole kidney (WK), cortex (Cx), user-defined representative cortex (rep-Cx) and medulla. Intraclass correlation coefficient (ICC) and coefficient of variation (CoV) were assessed.

Results: 40 participants were included (10 HV, 10 HF and 20 Tx). The ICC for renal volume was 0.97 and CoV 6.5%. For T1 and ADC, WK, Cx, and rep-Cx were highly reproducible with ICC ≥0.76 and CoV <5%. However, cortical pCASL results were more variable (ICC >0.86 but CoV up to 14.2%). While reproducible, WK values were derived from a wide spread of data (ROI standard deviation 17% to 55% of the mean value for ADC and pCASL, respectively). Renal volume differed between groups ($p<0.001$), while mean cortical T1 values were greater in Tx compared to HV ($p=0.009$) and HF ($p=0.02$). Medullary T1 values were also higher in Tx than HV ($p=0.03$), while medullary pCASL values were significantly lower in Tx compared to HV and HF ($p=0.03$ for both).

Discussion: Kidney volume calculated by manually contouring a localiser scan was highly reproducible between observers and detected significant differences across patient groups. For T1, pCASL and ADC, Cx and rep-Cx ROIs are generally reproducible with advantages over WK values.

Introduction

Functional renal imaging is a burgeoning field of research that has the potential to translate into meaningful clinical applications for patients with kidney disease[276]. Multi-parametric magnetic resonance imaging (MRI) allows acquisition of multiple sequences with potential to inform regarding structure, tissue composition, perfusion and physiology of renal function in a single scan[277]. However, the clinical utility of each sequence, and indeed the potential additive benefit of their use together, are yet to be proven. The immediate research priority in renal MRI is focusing on the standardisation and harmonisation of image acquisition across research sites and MRI vendors. This 'ground-up' approach is driven by international, independently-funded working groups including PARENCHIMA[277], a subsidiary of the European Cooperation in Science and Technology (COST) Action group, and the UK Renal Imaging Network (UKRIN), amongst others. As image acquisition is standardised, scientific scrutiny must also be applied to the methods of analysis. Many of the MRI sequences employed produce quantitative results from modelling dependent on measurements using other sequences[278], and for which the resultant values will vary depending on whether whole kidney, renal cortex or renal medulla is selected[137]. Numerous analytic approaches have been reported to date, and the optimal technique in terms of time and clinical relevance, is not yet known. In addition, the absence of commercially available analysis software that is specifically designed for unique interests of renal MRI leads to use of in-house bespoke software which renders external validation of results challenging.

Our centre has an active renal MRI research group, with current projects exploring the clinical implications of multi-parametric renal MRI across healthy volunteers[166], as well as patients with heart failure, chronic kidney disease (CKD)[152] and renal transplants. We aim to compare different regions of interest (ROIs) and their inter-observer reproducibility using commercially available analysis software in healthy and patient populations, including native and transplant kidneys, across a selection of MRI sequences.

Methods

Study population and clinical parameters

Patients were recruited from nephrology and cardiology clinics, and from general advertisement, for the renal transplant (Tx), heart failure (HF) and healthy volunteer (HV) cohorts, respectively. For Tx and HF patients, the scans were acquired as baseline imaging for 2 separate ongoing clinical studies (ClinicalTrials.gov: NCT03705091 and NCT03485092). Basic biometric parameters were measured, and serum creatinine was measured in accredited clinical biochemical laboratories. Estimated glomerular filtration rate (eGFR) was derived using the Chronic Kidney Disease Epidemiology Collaboration (CKD-EPI) equation[2]. All participants gave written informed consent and regional ethics committee approval was granted; the study was conducted in agreement with the Declaration of Helsinki.

MRI acquisition

MRI was performed on a Siemens MAGNETOM Prisma 3T scanner (Siemens Healthcare, Erlangen, Germany) using an 18-channel phased array coil anteriorly and a 32-channel spine coil posteriorly. Scans for renal volume, perfusion and T1 were acquired on all patients (Figure 7.1), with the transplant kidney scanned for the Tx group. Diffusion-weighted imaging (DWI) was performed on the Tx and HV cohorts. Patients were imaged supine.

Figure 7.1 - Representative image of each MRI sequence for each participant group.

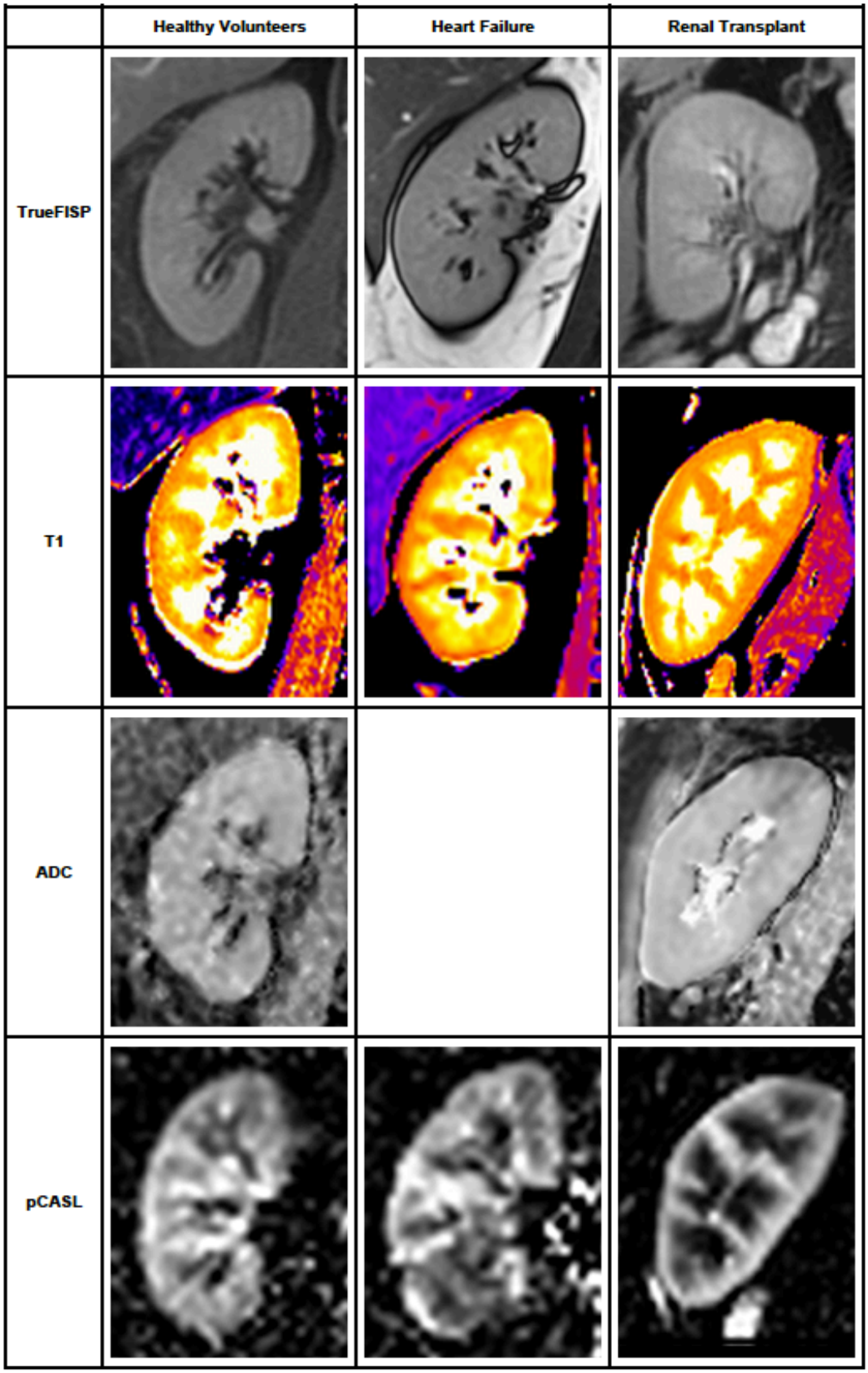

Volume: Coronal images were acquired during a breath-hold at expiration using a steady state free precession sequence (true fast imaging with steady state precession (TrueFISP)). The imaging parameters used are listed in supplementary material table S7.1 (HV and Tx cohorts) and supplementary material table S7.2 (HF cohort).

T1: T1 maps were acquired for a single coronal oblique slice through the centre of the kidney using a modified look-locker inversion recovery (MOLLI)[131,279] sequence with single shot TrueFISP readout[280]. For Tx and HV cohorts, images were acquired at 14 different inversion times (TI) (acquisition scheme 11(3)3) with an initial delay of 180 ms after the first inversion pulse and a delay of 260 ms after the second inversion pulse. The interval between subsequent measurements was 550 ms, resulting in TIs of 180, 260, 730, 810, 1280, 1360, 1830, 2380, 2930, 3480, 4030 4580, 5130, 5680 ms) and echo spacing of 3.04 ms. The acquisition time was 10 seconds. Images were acquired during free breathing.
For the HF cohort, images were acquired at 8 different inversion times (acquisition scheme 5(3)3) with a start TI of 100 ms, a TI increment of 80 ms (inversion times dependent on captured cardiac cycle) a reported TR of 280-340 ms and echo spacing of 2.44 ms. Images were acquired during a breath hold. Other imaging parameters are given in supplementary materials tables S7.1 and S7.2.
Motion correction and fitting of the T1 map was performed using a phase sensitive inversion recovery reconstruction implemented in the vendor software (Siemens, VE11C, MyoMaps)[281].

$$\Delta M = f\frac{2M_0}{\lambda}T_{1'}\alpha \exp\left(\frac{-\Delta t}{T_{1blood}}\right)\exp\left(\frac{-(t-\tau-\Delta t)}{T_{1'}}\right)\left(1-\exp\left(\frac{-\tau}{T_{1'}}\right)\right)$$

Supplementary material table S7.1. Imaging acquisition parameters for renal transplant and healthy volunteer cohorts

	Volume	T1 map	pCASL	DWI
Orientation	Coronal	Coronal oblique	Coronal oblique	Coronal oblique
Sequence	TrueFISP*	MOLLI	pCASL with 3D TGSE readout	2D SE-EPI
TR (ms)	417	Reported TR 550, echo spacing 3.04	6870	2300
TE (ms)	1.31	1.24	30.2	45
Flip angle (°)	37	35	28 (pCASL labelling) 180 (TGSE readout)	90
Field of view (mm*mm)	340×340	360*215	300*150	400*400
Matrix	169*256	320*252	96*48	134*134
Slice thickness (mm)	4.5	5	4	5
Slice gap (mm)	-1.125	-	-	1
Voxel size (mm^3)	1.3*1.3*4.5	1.1*1.1*5	3.3*3.3*4	1.5*1.5*5
Number of slices	70	1	16	17
Acceleration	GRAPPA R=2	GRAPPA R=2, phase partial Fourier 7/8	-	GRAPPA R=3
Acquisition time (min:sec)	00:35	00:10	03:33 (15 measurements)	01:40
Bandwidth (Hz/px)	850	1116	2265	2488

*For TrueFISP acquisition, a Fat-Sat method, where fat appears nulled rather than bright, was applied to improve localisation of transplant kidneys. This protocol was applied to healthy volunteers.

Supplementary material table S7.2. Imaging acquisition parameters for heart failure cohort

	Volume	T1 map	pCASL
Orientation	Coronal	Coronal oblique	Coronal oblique
Sequence	TrueFISP	MOLLI	pCASL with 3D TGSE readout
TR (ms)	553	Reported TR 295, echo spacing 2.44	6870
TE (ms)	1.68	1.12	31.22
Flip angle (°)	50	35	28 (pCASL labelling) 180 (TGSE readout)
Field of view (mm*mm)	340*380	360*307	150*300
Matrix	460*512	256*169	48*96
Slice thickness (mm)	5	8	4
Slice gap (mm)	0	-	-
Voxel size (mm^3)	0.7*0.7*5.0	1.4*1.4*8	3.1*3.1*4
Number of slices	39	1	16
Acceleration	GRAPPA R=2	GRAPPA R=2, phase partial Fourier 7/8	-
Acquisition time (min:sec)	00:51	00:10	2:24 (10 measurements)
Bandwidth (Hz/px)	1500	1085	2265

Arterial spin labelling: A pseudo-continuous arterial spin labelling (pCASL) scan[282] with a 3D turbo gradient spin echo (TGSE) readout was acquired during free breathing[283]. The prototype sequence comprises a slice-selective presaturation pulse to suppress the signal from preceding excitations and a frequency-offset-corrected inversion (FOCI) pulse positioned over the imaging region. This is followed by the pCASL slice-selective labelling pulse. For background saturation, 4 non-selective hyperbolic secant pulses are applied, interspersed with 3 slice selective saturation pulses, positioned superior to the labelling plane. The pCASL labelling plane was positioned in a transverse oblique slice of thickness 10mm perpendicular to the aorta and superior to the kidneys to label the blood in the descending aorta (Supplementary Material Figure S7.1). The start time of the pCASL labelling was 3000 ms and the pCASL duration was 1500 ms with a flip angle of 28°. The presaturation pulses and FOCI pulse were positioned in a transverse slab covering the kidneys. The pulses to suppress inflowing arterial blood were applied in a slab superior to the labelling plane to suppress inflowing arterial blood. Images were obtained in a coronal oblique orientation covering the whole kidney volume. A low-resolution pCASL scan with one measurement was acquired to confirm that the positioning of the labelling plane was appropriate to produce signal in the perfusion-weighted image. This was followed by a higher resolution scan with parameters as given in supplementary material tables S7.1 and S7.2. The sequence acquires label and control images and a reference proton density-weighted (M0) image. Perfusion maps were produced using inline software. In-plane 2D motion correction is applied retrospectively to proton density-weighted (M0), label and control images. Label and control images are subtracted to create perfusion-weighted images. Maps of perfusion rate (*f*) are calculated pixel by pixel using the motion-corrected proton density-weighted (*M0*) and perfusion-weighted (*ΔM*) images according to:

$$\Delta M = f\frac{2M_0}{\lambda}T_{1'}\alpha \exp\left(\frac{-\Delta t}{T_{1blood}}\right)\exp\left(\frac{-(t-\tau-\Delta t)}{T_{1'}}\right)\left(1-\exp\left(\frac{-\tau}{T_{1'}}\right)\right)$$

where f is the perfusion rate in ml/100mg/min; t is the time between labelling and imaging (3000 ms); τ is the duration of labelling pulse (1500 ms); Δt is the arterial transit time, assumed to be 750 ms; α is the labelling efficiency, assumed to be 0.98; λ is the blood-tissue water partition coefficient, assumed to be 0.9 ml/ 100g; T_{1blood} is the longitudinal relaxation time of arterial blood; $T_{1'}$ is the apparent longitudinal relaxation time of tissue. A fixed $T_{1blood} = T_{1'} = 1250$ ms was assumed in calculating the perfusion maps.

Supplementary Material Figure S7.1: Coronal, transverse and sagittal views showing the positioning of the ASL labelling plane (yellow) and the imaging volume (green) on a patient in the heart failure cohort.

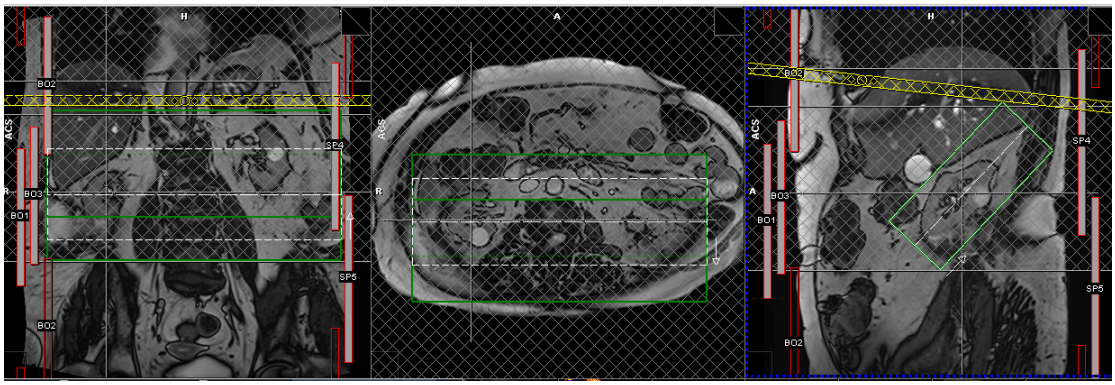

DWI: For the Tx and HV cohorts, DWI was performed using a single-shot spin-echo echo-planar imaging sequence with 17 slices positioned in a coronal oblique plane. Images were acquired at 10 b-values (0, 50, 100, 150, 200, 250, 300, 500, 750, 1000 s/mm^2) for 4 diffusion directions, averaged to give a 4-scan trace. SPectral attenuated inversion recovery (SPAIR) fat suppression was used and images were acquired during free breathing, with an acquisition time of 1min46s. Apparent diffusion coefficient (ADC) maps were created using the vendor software, performing a mono-exponential fit to the 10 b-values[284].

MRI analysis

Interobserver variability was compared across different methods of image analysis. For kidney volume, the renal contours were drawn around the whole kidney (excluding the renal pelvis) on the first and last slices containing renal tissue. Contours were then added to every alternate slice in between. This initial total kidney volume (linear interpolation for non-contoured slices) was then recorded ('alternate slices') prior to drawing contours to the remaining slices and noting the resultant volume ('every slice'). For pCASL and DWI, a single slice was chosen for analysis. ROIs were drawn manually around the whole kidney (WK), cortex (Cx), an area of user-defined representative cortex (rep-Cx), within the cortex at the superior and inferior poles (sup-Cx and inf-Cx, respectively) and in a representative area of medulla (Med) (Figure 7.2). Corticomedullary differentiation was assessed by ratio of Cx to Med. Each cohort was analysed by a pair of independent observers from a pool of 4 clinicians and 1 physicist, all with local training in renal MRI

analysis (SAS and LZ analysed HV, SAS and MMYL analysed HF and KAG and AJR analysed Tx). Image analysis was performed using the commercially available software cvi42 version 5.9.4 (Circle Cardiovascular Imaging, Calgary, Canada).

Figure 7.2 - Representative image (T1) displaying the regions of interest drawn for whole kidney (WK), cortex (Cx), representative cortex (rep-Cx), superior cortex (sup-Cx), inferior cortex (inf-Cx) and medulla (Med).

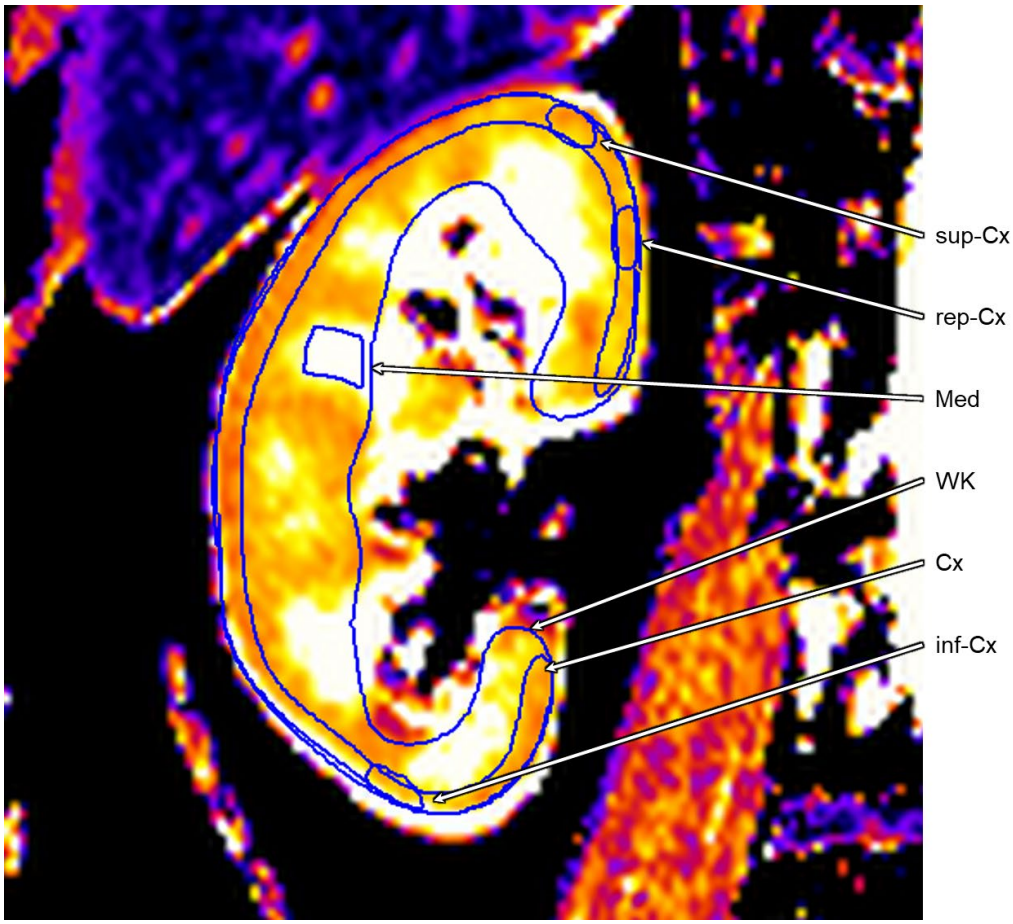

Statistical analysis

Descriptive statistics are reported as mean and standard deviation or median and range/inter-quartile range (IQR) for normally distributed and skewed data, respectively. Paired t-tests were used to compare kidney volume techniques and results were displayed graphically using a Bland-Altman plot[252]. Pearson correlation coefficient was used to quantify linear relationships between continuous variables. A total of 12 participants are required to detect a correlation coefficient of 0.8 with 90% power and alpha 0.05. Our

decision to include 40 participants yields a power >99.9% to detect a correlation coefficient of 0.8 at alpha 0.05. Inter-observer reproducibility was measured using coefficient of variation (CoV) (calculated by the standard deviation divided by the mean), and intraclass correlation coefficient (ICC) (two-way random, average measures). One-way ANOVA was used to compare mean results across the 3 participant groups, with t-tests to interrogate pairs where groups differed. The mean value of the 2 observers is reported unless otherwise stated. All analyses were performed using SPSS Statistics Version 25.0 (Armonk, NY: IBM Corp.) and a conventional significance level of <0.05 was used. Figures were generated using SPSS Statistics Version 25.0 (Armonk, NY: IBM Corp.) and Microsoft PowerPoint® 2019.

Results

Participant demographics

A total of 40 participants were included: 10 healthy volunteers, 10 patients with heart failure (with reduced ejection fraction of ≤40%) and 20 renal transplant recipients. Clinical characteristics are shown in Table 7.1.

Table 7.1 - Patient demographics and clinical characteristics

	All (n=40)	**HV (n=10)**	**HF (n=10)**	**Tx (n=20)**
Age (years), median (IQR)	56 (39-63)	43 (30-58)	62 (54-70)	51 (38-61)
Male (n, %)	28 (70%)	4 (40%)	7 (70%)	17 (85%)
eGFR (ml/min/1.73m2), median (IQR)	60.0 (37.7-76.7)	NA	77.1 (65.8-86.9)	48.4 (36.1-64.3)

Abbreviations: HV = healthy volunteers, HF = heart failure, Tx = renal transplant, eGFR = estimated glomerular filtration rate, IQR, interquartile range.

Renal volume

Calculation of renal volume was possible in 39 patients (98%) (1 patient did not have appropriate TrueFISP images). Mean difference in renal volume was 1.6 ml lower when contours were drawn on alternate slices as opposed to every slice ($p<0.001$) (Figure 7.3). There was no inter-observer difference in renal volume with either approach ($p=0.56$ for alternate slice, and $p=0.89$ for every slice). Tables 7.2 and 7.3 show the results and inter-observer reproducibility for renal volume, respectively.

Figure 7.3 - Bland-Altman plot comparing kidney volume as measured by contouring alternate slice versus every slice.

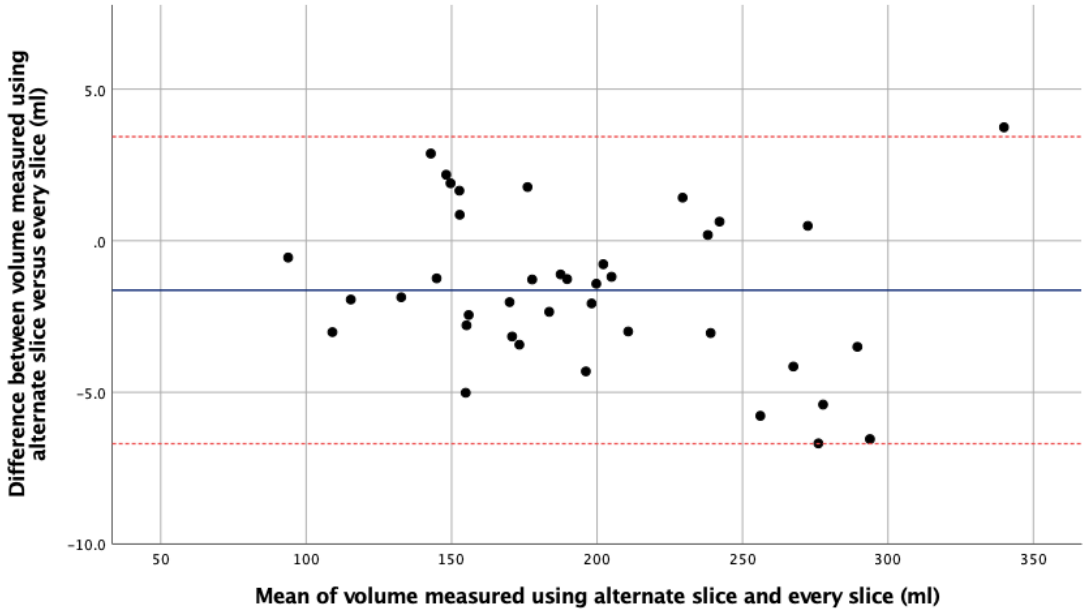

T1, pCASL, ADC: Comparison of different ROIs

T1, pCASL and ADC sequences were acquired in 39, 39 and 28 patients, respectively. Image quality was acceptable in all but 2 pCASL acquisitions in the Tx group who were excluded from further analysis. Table 7.2 shows the mean results for each sequence depending on whether ROIs were drawn for WK, Cx, rep-Cx, sup-Cx, inf-Cx and Med. The standard deviation in Table 7.2 represents the spread of mean values obtained. Table 7.3 shows the inter-observer reproducibility for each ROI by sequence and participant

group. For T1 and ADC, WK, Cx and rep-Cx were highly reproducible (ICC ≥ 0.76; CoV <5%). For pCASL, Cx and rep-Cx were less readily reproducible (ICC >0.86 but CoV up to 14.2%). The reproducibility of Med ROI was excellent for T1 but less good for pCASL and ADC (Table 7.3). Table 7.4 shows the spread of data within each ROI by reporting the mean ROI standard deviation as a proportion of the mean value. The spread of data from WK ROIs was higher than cortex-specific ROIs, even when the mean value for each was similar (Table 7.2).

Table 7.2 - Comparison of results depending on region of interest, MRI sequence and participant group.

The standard deviation presented represents the spread of mean values. Volume measured by contouring alternate slices was similar to contouring every slice in all groups. Within each group, the values for whole kidney, cortical and medullary regions of interest were different for T1 and pCASL. In contrast, ADC values were similar for whole kidney, cortical and medullary regions of interest.

	All (n=40)		HV (n=20)		HF (n=10)		Tx (n=10)	
	Mean	**S.D.**	**Mean**	**S.D.**	**Mean**	**S.D.**	**Mean**	**S.D.**
Volume (ml) (n=39)								
Alternate slice	195.8	56.8	147.8	30.9	170.6	45.3	230.1	49.2
Every slice	197.5	57.4	149.0	31.3	170.8	44.9	232.6	49.3
T1 (ms) (n=39)								
Whole kidney	1772.8	131.4	1702.4	76.7	1696.5	85.7	1842.6	134.4
Cortex	1630.2	102.0	1557.7	104.1	1595.5	80.1	1680.1	86.3
rep-Cx	1606.1	114.4	1545.4	113.2	1543.8	71.1	1664.6	105.0
sup-Cx	1655.6	119.5	1606.8	149.8	1600.0	93.4	1705.3	98.1
inf-Cx	1639.0	103.7	1587.0	94.3	1590.0	113.3	1687.0	82.0
Med	1975.8	74.9	1899.0	80.5	1940.2	71.3	2028.1	74.2
Cortex: Med	0.83		0.82		0.82		0.83	
pCASL (ml/min/100g) (n=37)								
Whole kidney	181.7	56.6	187.5	58.4	161.6	47.1	190.2	60.7
Cortex	221.0	80.0	235.1	79.3	175.7	59.5	239.3	84.3
rep-Cx	260.8	91.4	271.8	93.5	228.4	92.3	273.3	90.4
sup-Cx	196.4	75.9	230.5	77.9	160.4	54.2	197.4	79.6
inf-Cx	225.2	105.2	213.8	91.1	161.8	84.4	269.2	107.5
Med	95.8	41.8	108.8	45.1	121.5	31.5	73.0	45.9
Cortex: Med	2.3		2.2		1.4		3.3	

ADC ($x10^{-6}$ mm^2/s) (n=28)								
Whole kidney	1687.6	115.6	1687.2	97.4	-	-	1687.7	125.8
Cortex	1678.1	111.4	1704.0	96.8	-	-	1665.8	118.1
rep-Cx	1696.9	117.7	1719.9	158.6	-	-	1686.0	96.1
sup-Cx	1686.3	144.2	1720.4	120.6	-	-	1670.1	154.5
inf-Cx	1696.4	115.2	1700.5	111.8	-	-	1694.4	119.7
Med	1671.9	82.5	1726.3	93.9	-	-	1646.1	77.2
Cortex: Med	1.0		1.0				1.0	

Abbreviations: HV = healthy volunteers, HF = heart failure, Tx = renal transplant, S.D. = standard deviation, rep-Cx = area of representative cortex, sup-Cx = area of representative cortex at superior pole, inf-Cx = area of cortex at inferior pole, Med = medulla, pCASL = pseudo-continuous arterial spin labelling, ADC = apparent diffusion coefficient.

Table 7.3 - Inter-observer reproducibility by MRI sequence and analysis approach. Whole kidney and cortical ROIs were highly reproducible in all sequences.

	CoV (%)	ICC
Volume (ml) (n=39)		
Alternate slice	6.5	0.97
Every slice	6.7	0.96
T1 (ms) (n=39)		
Whole kidney	1.0	0.97
Cortex	1.2	0.97
rep-Cx	2.0	0.95
sup-Cx	3.2	0.96
inf-Cx	2.5	0.86
Med	2.6	0.87
pCASL (ml/min/100g) (n=37)		
Whole kidney	7.0	0.90
Cortex	10.3	0.93
rep-Cx	14.2	0.86
sup-Cx	19.1	0.69
inf-Cx	14.6	0.92
Med	29.6	0.73
ADC ($x10^{-6}mm^2/s$) (n=28)		
Whole kidney	2.0	0.90
Cortex	2.6	0.85
rep-Cx	3.7	0.76
sup-Cx	5.0	0.64
inf-Cx	3.8	0.62
Med	5.5	0.50

Abbreviations: CoV = coefficient of variation, ICC = intraclass correlation coefficient, rep-Cx = area of representative cortex, sup-Cx = area of representative cortex at superior pole, inf-Cx = area of cortex at inferior pole, Med = medulla, pCASL = pseudo-continuous arterial spin labelling, ADC = apparent diffusion coefficient.

Table 7.4 - Table representing the spread of data from which the mean is calculated depending on region of interest and MRI sequence.

The ROI standard deviation is generated by the analysis software to represent the spread of values within each ROI. This table reports the mean ROI standard deviation for each sequence and displays it as a proportion of the mean value. The spread of data is larger for whole-kidney values, which includes cortical and medullary values, as well as potential confounding data from vessels and renal pelvis. Conversely, the spread of data from the smaller ROIs of representative cortex may be uncharacteristically low if too small a ROI is drawn to be truly representative.

	ROI S. D. (mean)	**ROI S.D. as proportion of mean value**
T1 (ms) (n=39)		
Whole kidney	354.1	20.0%
Cortex	125.7	7.7%
rep-Cx	49.6	3.1%
sup-Cx	71.4	4.3%
inf-Cx	69.8	4.3%
Med	74.9	3.8%
pCASL (ml/100g/min) (n=37)		
Whole kidney	100.7	55.4%
Cortex	85.1	38.5%
rep-Cx	41.2	15.8%
sup-Cx	48.0	24.5%
inf-Cx	53.2	23.6%
Med	41.8	43.6%
ADC ($x10^{-6}$ mm^2/s) (n=28)		
Whole kidney	289.5	17.2%
Cortex	169.6	10.1%
rep-Cx	71.5	4.2%
sup-Cx	105.8	6.3%
inf-Cx	85.9	5.1%
Med	84.7	5.1%

Abbreviations: ROI = region of interest, S.D. = standard deviation, rep-Cx = area of representative cortex, sup-Cx = area of representative cortex at superior pole, inf-Cx = area of cortex at inferior pole, Med = medulla, pCASL = pseudo-continuous arterial spin labelling, ADC = apparent diffusion coefficient.

Correlation between different ROIs

For T1, the correlation coefficient for Cx compared to WK, rep-Cx, sup-Cx, inf-Cx and Med was 0.76, 0.93, 0.86, 0.85 and 0.62 respectively. The corresponding values for pCASL were 0.92, 0.91, 0.84, 0.81 and 0.26; and for ADC 0.87, 0.79, 0.75, 0.85 and 0.78 ($p<0.001$ for all, except pCASL Med which was not significant ($p=0.13$)).

Comparison between participant groups.

There was a significant difference in kidney volume between groups ($F=13.2$, $p<0.001$) with the greatest renal volume in Tx, then HF and then HV (Table 7.2). Mean T1 values also differed between participant groups (WK: $F=7.9$, $p=0.001$, Cx: $F=6.9$, $p=0.003$, rep-Cx: $F=7.1$, $p=0.003$). However, on paired comparisons there was no difference in T1 results between HV, and HF cohorts, while mean cortical T1 values were 122.4 ms ($p=0.009$) and 84.7 ms ($p=0.02$) greater in the Tx group compared to HV and HF groups, respectively. Medullary T1 values were also higher in Tx than HV (mean difference 129.1 ms, $p=0.03$). There were no differences between groups on any cortical ROI for pCASL or ADC. Medullary pCASL values were significantly lower in Tx group compared to HV (mean difference -35.7 ml/min/100g, $p=0.03$) and HF (mean difference -48.4 ml/min/100g, $p=0.03$).

Correlation between renal MRI and kidney function.

eGFR data was available for the 30 participants with heart failure or a renal transplant. There was no correlation between eGFR and renal volume, T1 or pCASL. There was a positive correlation between eGFR and ADC (Tx group only), with coefficients of: WK 0.47 ($p=0.04$), Cx 0.61 ($p=0.006$), rep-Cx 0.72 ($p=0.001$), sup-Cx 0.45 ($p=0.05$), inf-Cx 0.67 ($p=0.002$) and Med 0.48 ($p=0.04$).

Discussion

This study provides evidence to support the reproducibility of certain analysis techniques for renal MRI using commercially available analysis software. This is an essential step to allow studies exploring the clinical significance of functional renal MRI to report in

confidence. Our data show that measurement of renal volume by contouring a localiser image is highly reproducible between observers. Contouring alternate slices, as opposed to every slice, results in a small reduction in measured volume with the advantage of improved efficiency. We believe the 1.6 ml (0.8%) mean difference in volume by contouring alternate slices is clinically insignificant, but nevertheless we would advise consistency with whichever approach is chosen. Whilst automated contouring and volume calculation is being utilised by some centres[285] and is likely to improve time efficiency, this approach is still to be externally validated and widely available. For T1, pCASL and ADC, WK ROIs are highly reproducible and commonly reported, but the mean value is derived from an unduly wide range of values, as evidenced by the fact on average the ROI St dev represented between 17 and 55% of the mean value in our cohort. We would argue this summary statistic is a crude representation of the physiological tissue which we hope to describe, and that cortical values may have more biological relevance, without unacceptable reduction in reproducibility. Indeed, for ADC the correlation with renal function of cortical ROIs was stronger than for WK. When drawing a small ROI of representative cortex, pre-specifying its location to be at either the superior (sup-Cx) or inferior (inf-Cx) pole did not improve reproducibility compared to a user-defined location and reduced the correlation with total cortex (Cx) for T1 and pCASL. Furthermore, sup-Cx and inf-Cx are theoretically more susceptible to artefact from respiratory movement in native kidneys compared to regions of lateral/medial cortex that would move in plane. We therefore advise that either Cx or rep-Cx be used preferentially whenever cortical values are reported. Drawing an ROI for rep-Cx is likely to reduce analysis time compared to whole cortex, and in this small sample, the correlation between eGFR and ADC was greatest when rep-Cx was used. However, this is balanced against the lower ICC for rep-CX than Cx. Further studies are required to distinguish their benefits and we suggest that either Cx or rep-Cx can be used to report cortical values in the interim. Nevertheless, development of a harmonised approach across centres is vital to allow broader use of renal MRI in research and clinical settings[276].

While there was a significant correlation between ADC and eGFR, there was no association between renal volume, T1 and pCASL with renal function. Although this may generate scepticism with regards to the clinical relevance of these sequences, the development of MRI biomarkers is intended to provide physiologic and prognostic

information additional to existing clinical measures, but further studies are needed to clarify this.

We performed a limited comparison of medullary values. Future studies may wish to do analyse the medulla in more detail. Recent studies have reported measures of cortico-medullary differentiation (CMD) using T1 and ADC and their correlation with clinical parameters[148,286,287]. These studies were well-conducted, but there is a risk of over interpreting the significance of cortico-medullary findings. Loss of CMD is a well-established, non-specific finding in CKD that is detectable on ultrasound, computed tomography and MRI[288]. Any observed association between eGFR and CMD on T1 or ADC may underplay the utility of MRI as a functional measurement and may instead detect a crude structural change that is prevalent in CKD, and which can be measured in simpler ways.

The study is strengthened by its multi-parametric protocol across both healthy and diseased populations, including native and transplant kidneys, yielding clinically meaningful results. The study has a number of limitations. Whilst we have shown these analyses to be reproducible, the clinical significance of any approach is not yet established. We did not assess R2* (also known as blood-oxygen-level-dependent (BOLD) imaging). This parameter is recommended to be included in multi-parametric renal MRI protocols and its inclusion in this study would have been advantageous[276]. Only 2 observers reported each ROI for comparison of inter-observer reproducibility. Kidney volume measurements were not compared with established 3D contrast-enhanced techniques, and further studies are required to assess the clinical relevance of kidney volume as measured by this approach. The current pCASL sequences utilises a fixed T1 value. We accept there may be advantages to using a measured T1 and we are exploring this for future studies. Other centres have developed efficient and accurate analysis methods, often using in-house developed software, which we are unable to replicate. For instance, a technique that uses a histogram to numerically segregate cortical from medullary values has been reported[137]. These analysis strategies require bespoke software which generally rely upon precise harmonisation of acquisition parameters to allow use out-with the centre in which they are developed. Nevertheless, comparison of results generated using this technique with the approaches detailed here would be interesting. The use of commercially available software in this study is a strength. However, the license carries a cost and the software used is

designed for cardiovascular analysis, such that we have applied many of the modules out-with their intended use. There is an urgent need for widely available software that is specifically designed for multi-parametric renal MRI analysis, in order to advance the research and clinical application of renal MRI.

Conclusion

There are numerous strategies to analyse multi-parametric renal MRI with many centres using in-house bespoke software. The optimal approach is not yet known. These results provide justification for one approach using commercially available software. We suggest kidney volume can be calculated by contouring alternate slices, rather than every slice, of a localiser scan albeit validation with 3D volume techniques is still required. For T1, pCASL and ADC, we suggest whole kidney values, while highly reproducible, are used with caution given that the results represent a central value from an extremely wide range. Instead, manually delineated cortex or a small ROI of user-defined representative cortex can be used interchangeably in both native and transplant kidneys, with acceptable inter-observer reproducibility. Clinical correlation of the results generated from this approach is eagerly awaited.

Declarations

Acknowledgements

Yuehui Tao (Siemens Healthcare, Erlangen, Germany) and Peter Weale (Siemens Healthcare, Erlangen, Germany) for assisting with application of the pCASL prototype sequence.

Conflict of interest statement

The authors have a research agreement with Siemens for use of the renal pCASL work-in-progress sequence. Bernd Kuehn is an employee of Siemens Healthcare.

Authors' Contributions

All authors have contributed to this study. AJR, KAG, SAS and MMYL conceived the idea, designed the study and analysed the MRIs in conjunction with LZ. AJR, SAS and KAG wrote the manuscript, while LZ and MMYL prepared the figures. BK wrote the work-in-progress for pCASL. PBM, NS, GR, AR and RW, critically reviewed the manuscript.

Funding

A.J.R. is supported by a Clinical Academic Training Fellowship from The Chief Scientist Office (Scotland) (CAF/18/02). K.A.G., P.B.M., A.R. and G.R. are supported by a grant from Kidney Research UK (KS_IN_002_20180913) and P.B.M., N.S., A.R. acknowledge research support from Boehringer Ingelheim.

Chapter 8 - Multi-parametric renal MRI in comparison to histology in kidney transplant recipients with transplant dysfunction *(prepared ahead of submission)*

8.1 Manuscript

Alastair J Rankin[1], Keith A Gillis[2], Sarah Allwood-Spiers[3], , David Kipgen[5], Jana Crosby[5], Evonne McLennan[4], Giles Roditi[1,6], Patrick B Mark[1]

1. Institute of Cardiovascular and Medical Sciences, University of Glasgow, Glasgow, UK
2. Renal and Transplant Unit, NHS Greater Glasgow and Clyde, Glasgow UK
3. Department of Clinical Physics and Bioengineering, NHS Greater Glasgow & Clyde, Glasgow, UK
4. Clinical Research Imaging, NHS Greater Glasgow and Clyde, Glasgow, UK
5. Department of Pathology, NHS Greater Glasgow and Clyde, Glasgow, UK
6. Department of Radiology, NHS Greater Glasgow and Clyde, Glasgow, UK

Abstract

Background: Multi-parametric functional renal MRI may offer a non-invasive means to interrogate tissue characteristics in patients with transplant dysfunction. We aimed to assess the correlation between renal MRI and histology findings.

Methods: Adult patients referred for a clinically indicated biopsy of their transplant kidney were eligible for inclusion. A multi-parametric MRI protocol including anatomical images, T1 mapping, T2 mapping, T2* blood oxygenation level dependent images, diffusion weighted imaging (to calculate apparent diffusion coefficient), diffusion tensor imaging (to calculate fractional anistropy (FA)) and arterial spin labelling, was performed. MRI variables were compared to histological variables (percentage of cortex containing fibrosis and inflammation) and biochemical variables (serum creatinine and estimated glomerular filtration rate (eGFR)).

Results: Twenty-eight participants were recruited for whom 20 had complete MRI and histological data available. Recruitment was stopped early due to the COVID-19 pandemic. There was no correlation between any MRI variable and the percentage of cortex containing interstitial fibrosis. FA corticomedullary ratio correlated with the percentage of non-scarred cortex containing inflammation (ρ= 0.45 (-0.73, -0.02). T1 cortex inversely correlated with final eGFR (ρ =-0.45
(-0.72, -0.07) and there was a significant difference in T1-cortex between participants who developed graft failure versus those who did not ((median difference 209.1ms (p=0.005)). When MRI variables were compared between individuals with rejection on biopsy versus those who did not have rejection only BOLD T2*-cortex was significant (median increase 8.9 ms; p=0.04).

Conclusion In this small prospective study that was stopped early due to the COVID-19 pandemic, there was no correlation between any MRI variable and the percentage of renal cortex containing fibrosis. However, there were significant findings that merit further study, especially the prognostic role of T1-cortex which inversely correlated with final eGFR and differed between those who did and did not develop graft failure.

Introduction

Renal transplantation is the optimal treatment for people with renal failure and is associated with improvements in life expectancy and quality of life compared to dialysis.[289] Despite advances in our understanding of the immune system and development of drugs to prolong transplant function, the period of time for which a transplant functions remains finite, with 13% failing before 5 years and 26% failing before 10 years.[142] The most common reason for transplants to fail is the development of chronic immune-mediated rejection and other causes of irreversible fibrosis.[23–25]

Incident transplant dysfunction is most commonly detected due to a rise in serum creatinine with or without the emergence of proteinuria. These markers of acute transplant dysfunction are non-specific and usually herald further investigations into the individual causes, including donor-specific antibodies (DSA), calcineurin inhibitor drug levels (if relevant), renal transplant ultrasound, and viral titres for cytomegalovirus and BK virus. However, ultimately, a biopsy of the transplant kidney is often required for definitive diagnosis and to allow appropriate modification of treatment.[143,144] Biopsy of renal transplants include the risks of bleeding (ranging in severity from asymptomatic to fatal), infection (with seeding from urinary tract to bloodstream), loss of transplant function, non-diagnostic results and discomfort for patients.[145,146] Furthermore, a standard renal biopsy samples <1% of renal cortex tissue and is therefore prone to sampling error, which may mis-inform clinical practice (e.g. if an area of focal scarring is biopsied). If a treatment is instigated on the basis of a biopsy result, it can be necessary to repeat the biopsy to assess treatment response, thus doubling the risk exposure for patients. Accordingly, a non-invasive biomarker of renal transplant pathology is needed and could improve the management of renal transplant recipients by reducing risk exposure and increasing diagnostic accuracy.[151]

Functional multi-parametric magnetic resonance imaging (MRI) of the kidney is an exciting area of research where it is hoped that different MRI sequences can provide quantitative information regarding fibrosis, inflammation, perfusion, tissue oxygenation, and oedema, in addition to the standard anatomical and structural assessment that 3D imaging allows [141,276,290].

We aimed to compare functional MRI findings with the extent of cortical fibrosis and inflammation in kidney transplant recipients who had been referred for a clinically indicated biopsy of their transplant kidney.

Methods

Study protocol

This is a single centre observational study. Individuals were eligible for participation if they were 18 years or older with a kidney transplant and had been referred for a clinically indicated biopsy of their transplant kidney. They had to be able to provide informed consent and comply with study procedures. Exclusion criteria included contraindication to MRI, pregnancy, and suspected delayed graft function as the cause of their transplant dysfunction. Participants were recruited from the Glasgow Renal and Transplant Unit, which serves a population of 1.5 million and performs approximately 150 kidney transplant operations per year. Following informed consent, participants were invited to undergo an MRI of their transplant kidney within 1 week either side of their scheduled biopsy. Additional research bloods and urine samples were collected. If the participant was subsequently treated for acute rejection they were invited to attend for a repeat MRI scan within 2 weeks of completing acute treatment. Follow-up data was collated from routinely collected clinical data with participants' consent, with the most recent blood results censored at time of alternative renal replacement therapy, if applicable. Favourable ethical opinion was granted by the East Midlands – Leicester Central Research Ethics Committee (Ref: 18/EM/0305, 31st October 2018). All study procedures were carried out in accordance with local guidelines and regulations and with respect to the declaration of Helsinki. The study was prospectively registered at clinicaltrials.gov (NCT03780101).

Renal MRI acquisition

MRI acquisition was performed at the Clinical Research Imaging Facility of the Queen Elizabeth University Hospital in Glasgow using a 3T MRI scanner (PRISMA, Siemens Healthcare, Erlangen, Germany) with an 18-channel surface coil placed anteriorly and a 32-channel spine coil placed posteriorly. A multi-parametric protocol was used including the sequences outlined below (Figure 8.1). Typical parameters for each sequence are

included in supplementary material S8.1. We have previously described our protocols for T1 mapping, diffusion-weighted imaging and arterial spin labelling (ASL) in detail [291].

- **Renal volume**. Coronal images were acquired using a steady state free precession sequence (true fast imaging with steady state precession (TrueFISP)).
- **T1 mapping**. A single oblique coronal slice positioned through the centre of the transplant kidney was acquired. A modified look-locker inversion recovery (MOLLI) sequence with single shot true FISP readout was used. Images were acquired at 14 different inversion times (pattern 11(3)3) with a start TI of 180 ms and a TI increment of 80 ms. Motion correction and fitting of the T1 map was performed using a phase-sensitive inversion recovery reconstruction implemented in the vendor software (Siemens, VE11C, MyoMaps).
- **T2 mapping**. T2 maps were acquired in same plane as for T1 mapping, using a fast low angle shot (FLASH) inversion recovery gradient echo sequence, Images were acquired at T2 preparation times of 0ms, 30ms and 55ms. Motion correction and fitting of the T2 map was performed using the vendor software (Siemens, VE11C, MyoMaps)
- **BOLD T2***. T2* maps were in the same plane as for T1 mapping, using a spoiled gradient echo sequence. Images were acquired at 12 different echo times, and a T2* map was calculated from an exponential fit to these using the vendor software (Siemens, VE 11C, MyoMaps). Images were acquired during breath hold at expiration with an acquisition time of 11 seconds.
- **Apparent diffusion coefficient (ADC).** Diffusion-weighted imaging was performed using a single-shot spin-echo echo-planar imaging sequence with 17 slices positioned in a coronal oblique plane. Images were acquired at 10 b-values (0, 50, 100, 150, 200, 250, 300, 500, 750, 1000 s/mm^2) for 4 diffusion directions, averaged to give a 4-scan trace. SPectral attenuated inversion recovery (SPAIR) fat suppression was used and images were acquired during free breathing, with an acquisition time of 1min46s. Apparent diffusion coefficient (ADC) maps were created using the vendor software, performing a mono-exponential fit to the 10 b-values [291].
- **Fractional Anistropy (FA).** Diffusion tensor imaging was performed with 3 b-values (50, 200, 400 s/mm^2) and 20 diffusion directions. Images were acquired

during free breathing. Fractional Anisotropy maps were calculated using the vendor software (Siemens, VE11C, DTI Evaluation).

- **Arterial spin labelling:** A pseudo-continuous arterial spin labelling (pCASL) scan with a 3D turbo gradient spin echo (TGSE) readout was acquired during free breathing. Perfusion maps were produced using inline software.[291]

Figure 8.1 - Representative images from a multi-parametric 3T renal MRI protocol showing an anatomical image, T1 mapping, T2 mapping, T2* blood oxygenation level dependent imaging, diffusion weighted imaging for calculation of apparent diffusion coefficient (ADC), diffusion tensor imaging for fractional anisotropy, and arterial spin labelling (ASL).

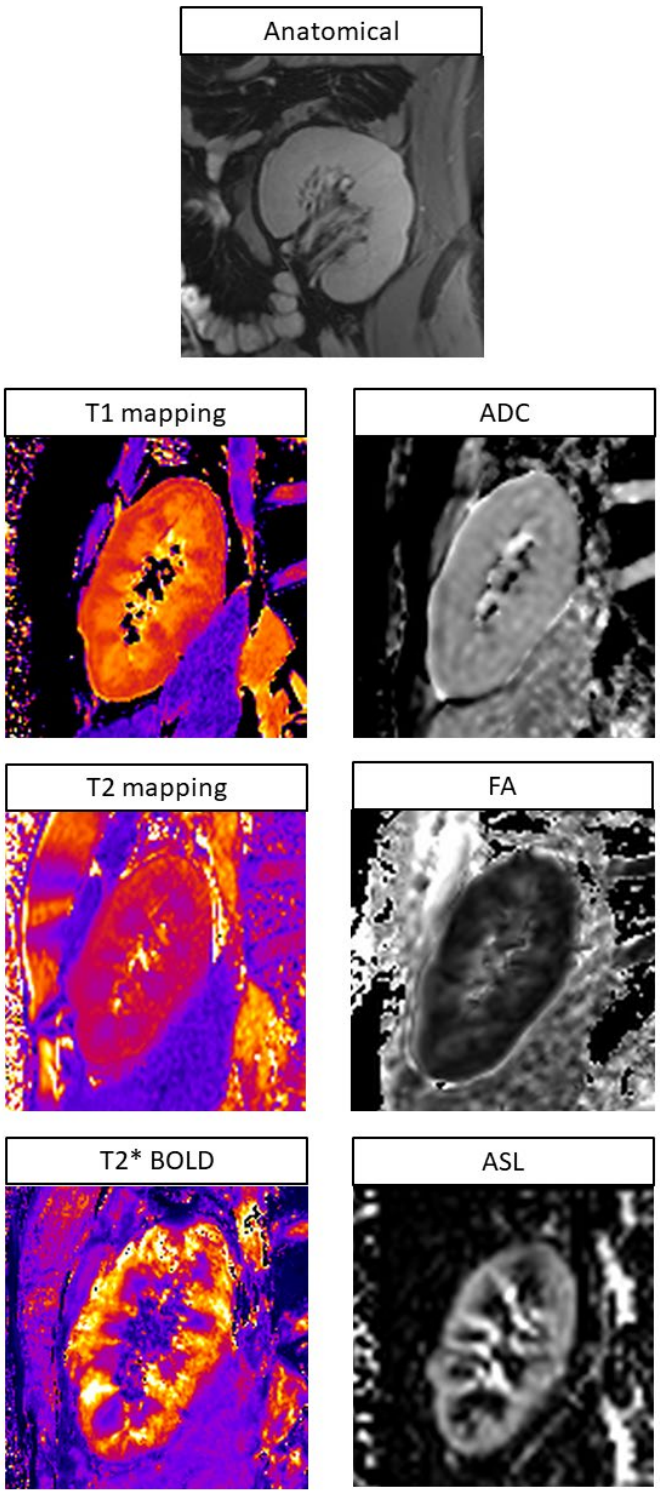

Supplementary material S8.1. Typical parameters for each MRI sequence

	Volume	T1	T2	BOLD T2*	ADC	FA	ASL
Orientation	Coronal	Coronal oblique	Coronal oblique	Coronal oblique	Coronal oblique	Coronal oblique	Coronal oblique
Sequence	TrueFISP with fat saturation.	MOLLI	T2 preparation module with FLASH readout	SPGR	2D SE-EPI, 4 diffusion directions, b-values 0, 50,100,150, 200, 250, 300, 500, 750, 1000 s/mm^2 , SPAIR fat suppression.	2D SE-EPI, 20 diffusion directions, b-values 50, 200, 400s/mm^2, with SPAIR fat supression	pCASL with 3D TGSE readout
TR (ms)	417	Reported TR 550, echo spacing 3.04	339	150	2300	2100	6870
TE (ms)	1.31	1.24	1.46 (T2 prep durations: 0, 30, 55)	1.64, 4.13, 6.78, 9.43, 12.08, 14.73, 17.38, 20.03, 22.68, 25.33, 27.98, 30.63.	45 Echo spacing 0.49ms.	46	30.2
Flip angle (°)	37	35	12	25	90	90	28 (pCASL labelling) 180 (TGSE readout)

Field of view (mm*mm)	340×340	360*215	360*215	400*400	400*400	405*400	300*150
Matrix	169*256	320*252	256*117	256*205	134*134	272*268	96*48
Slice thickness (mm)	4.5	5	8	5	5	5	4
Slice gap (mm)	-1.125	-	-	-	1	1	-
Voxel size (mm^3)	1.3*1.3*4.5	1.1*1.1*5	1.4*1.4*8	1.6*1.6*5	1.5*1.5*5	1.5*1.5*5	3.3*3.3*4
Number of slices	70	1	1	1	17	17	16
Acceleration	GRAPPA R=2	GRAPPA R=2, phase partial Fourier 7/8	GRAPPA R=2	GRAPPA R=2, phase partial Fourier 6/8	GRAPPA R=3	GRAPPA R=2, phase partial fourier 6/8	
Acquisition time (min:sec)	00:35	00:10	00:26	00:12	01:40	02:19	03:33
Bandwidth (Hz/px)	850	1116	1150	399	2490	2490	2264

*For TrueFISP acquisition, a Fat-Sat method, where fat appears nulled rather than bright, was applied to improve localisation of transplant kidneys. This protocol was applied to healthy volunteers.

Renal MRI analysis

MRI data were analysed by a single blinded observer using cvi42 software (version 5.10, Circle Cardiovascular, Canada)). For kidney volume, the renal contours were drawn around the whole kidney (excluding the renal pelvis) on each slice containing kidney tissue. For T1, T2, BOLD T2*, ADC, FA and ASL, manually drawn regions of interest (ROI) were placed in representative areas of renal cortex and medulla. Where necessary T1 images were used for anatomical reference. Cortico-medullary differentiation (CMD) was calculated by dividing values for cortex by medulla. We have previously published further details supporting our analysis methodology including inter-observer reproducibility [291].

Renal histology

Kidney biopsies were processed as per local clinical guidelines, with hematoxylin and eosin, periodic acid–Schiff, Masson trichrome, and Jones methenamine silver stains used for light microscopy. Additional sections were routinely examined using immunofluorescence and electron microscopy. The clinical histopathology reports were generated with reference to the Banff classification as per clinical standard [292]. The clinical report was used to collate the primary histological diagnosis, the percentage of cortex with interstitial fibrosis, the percentage of total cortex containing interstitial inflammation and the percentage of non-scarred cortex containing inflammation. A second pathologist independently reviewed all biopsies and reported the percentage of cortex containing fibrosis and inflammation to allow assessment of inter-observer reproducibility.

Statistical Analysis

Continuous data with a normal distribution are presented as mean ± standard deviation (SD), and median and interquartile range (IQR) for skewed data. Correlation was assessed by Spearman Rank Correlation coefficient (ρ) and 95% confidence intervals. Results were deemed statistically significant where confidence intervals did not cross 0. Inter-observer variability was assessed by the intra-class correlation (ICC) coefficient (two-way mixed effect, average measures). Mann-Whitney U test was used to compare differences in MRI variables depending on presence of graft failure and rejection respectively, with the conventional significance threshold of <0.05. Linear regression was performed as a post-hoc analysis to compare the association between T1 cortex and graft failure while accounting for

baseline eGFR. Statistical analysis was performed using SPSS (version 27, IBM Corp, New York).

Sample size calculation

A prospective sample size calculation determined that a total of 60 participants was necessary to identify a correlation of r=0.4 between MRI variables and interstitial fibrosis with 90% power and a type 1 error rate of 0.05. This was based on a previous study that reported a positive association between ADC and fibrosis (R^2=0.27) [148]. A recruitment target of 70 participants was set to allow for 15% drop out for participants with incomplete data sets.

Results

Participants

Twenty-eight participants were recruited between 15th February 2019 and 12th March 2020. Recruitment was stopped early (target 70 participants) due to the COVID-19 pandemic. Two participants did not undergo MRI (1 withdrew consent; 1 was unable to tolerate) and a further 2 participants did not undergo biopsy (1 due to hydronephrosis identified on their research MRI; 1 due to a spontaneous fall in the serum creatinine on the day of their biopsy). Consequently, 26 participants were included in the comparisons of MRI with biochemical outcomes, while 24 were included in comparisons with histological data. Median time from biopsy to MRI was 0 days (range: -4 to 15 days).

The mean age was 43 +/- 15 years, 16 were male (62%), and the median time since their current transplant was 3.6 years (IQR 0.5 – 6.6). Table 8.1 outlines additional baseline characteristics.

Table 8.1 - Baseline characteristics.

N = 26		
Age, years *Mean (s.d)*		43 (+/- 15)
Male *N (%)*		16 (62%)
Primary renal diagnosis *N (%)*	Diabetes	4 (15%)
	Glomerulonephritis	12 (46%)
	Renovascular disease	1 (3.8%)
	Hypertension	1 (4%)
	Polycystic kidney disease	2 (8%)
	Pyelonephritis	1 (4%)
	Unknown	3 (12%)
	Other	2 (8%)
Transplant type *N (%)*	Living related donor	6 (23%)
	Living unrelated donor	4 (15%)
	Donation after brain-stem death donor	13 (50%)
	Donation after cardiac death donor	3 (12%)
Time since current transplant, years *Median (IQR)*		3.6 years (IQR 0.5 – 6.6)
Immunosuppression *N (%)*	Tacrolimus	25 (96%)
	Ciclosporin	1 (4%)
	Belatacept	0 (0%)
	Mycophenolate	20 (77%)
	Azathioprine	3 (12%)
	Prednisolone	22 (85%)
Previous acute cellular rejection *N (%)*		6 (23%)
Previous acute antibody-mediated rejection *N (%)*		0
Previous BK virus nephropathy *N (%)*		2 (8%)
Previous Cytomegalovirus disease *N (%)*		2 (8%)
Indication for biopsy *N (%)*	Achieved function lower than expected	1 (4%)
	Acute kidney injury	4 (15%)
	Assess response to treatment	1 (4%)
	Chronically deteriorating kidney function with proteinuria	10 (38%)
	Chronically deteriorating kidney function without proteinuria	9 (35%)
	Nephrotic syndrome	1 (4%)
Creatinine at biopsy, umol/l		182 (161, 243)

Median (IQR)	
eGFR at biopsy, mmol/l/1.73m^2 *Median (IQR)*	34.2 (25.0, 40.3)

Abbreviations: s.d: standard deviation. IQR: inter-quartile range.

During a median follow-up of 2.0 (1.7 – 2.3) years, 7 required to start long-term haemodialysis and 3 participants died (1 COVID-19, 1 dialysis withdrawal, 1 sudden death). The median eGFR at follow-up was 31.9 (9.4 – 43.1) ml/min/1.73m^2 representing a median deterioration of 4.6 (-6.3, 20.5) ml/min/1.73m^2 (the corresponding values for serum creatinine are 203 (130-532) umol/l and 22 (-235, 27.0) umol/l). There was a wide range in primary diagnosis yielded from biopsy (Table 8.2). Additional outcome data is presented in Table 8.2.

Table 8.2 - Histological, biochemical and clinical outcome data

N = 24		
Primary histological diagnosis	Acute T-cell mediated rejection	4 (17%)
	Borderline T- cell mediated rejection	2 (8%)
	Acute antibody-mediated rejection	2 (8%)
	Chronic active antibody mediate rejection	1 (4%)
	Acute tubular necrosis	3 (13%)
	BK nephritis	1 (4%)
	Donor disease	1 (4%)
	Interstitial fibrosis and tubular atrophy	1 (4%)
	No significant histo-pathological abnormality	1 (4%)
	Recurrence of glomerulonephritis	2 (8%)
	Thrombotic microangiopathy	2 (8%)
	Other*	4 (17%)
Treated for rejection		7 (29%)
Interstitial fibrosis, % *Median (IQR)*		10 (4, 28)
Interstitial inflammation (total cortex), % *Median (IQR)*		20 (10, 50)
Interstitial inflammation (non-scarred cortex), % *Median (IQR)*		5 (1, 20)
N = 26		
Final serum creatinine, umol/l		203 (130, 532)

Median (IQR)	
Final eGFR, mmol/l/1.73m^2 *Median (IQR)*	31.9 (9.4, 43.1)
Graft failure *N (%)*	7 (27%)
Death *N (%)*	3 (12%)

*1 = moderate arteriolosclerosis with focal embolus and subsequently diagnosed with transplant artery stenosis; 1 diabetic nephropathy; 1 chronic transplant glomerulopathy; 1 de novo secondary focal segmental glomerulosclerosis

Abbreviations: IQR: inter-quartile range. eGFR: estimated glomerular filtration rate

Renal MRI in comparison to histology

There was no correlation between any MRI variable and the percentage of cortex containing interstitial fibrosis (Table 8.3). FA-CMD correlated with the percentage of non-scarred cortex containing inflammation (ρ=-0.45 (-0.73, -0.02). No other MRI variable (cortex, medulla or cortico-medullary ratio) correlated with the percentage of total cortex or non-scarred cortex containing interstitial inflammation (Table 8.3). Supplementary material S8.2 shows the mean results for MRI variables divided by histological diagnosis. The ICCs for the comparison of the 2 histologists' scores were: 0.89 for interstitial fibrosis, 0.94 for total interstitial inflammation and 0.78 for intestinal inflammation in non-scarred cortex.

Table 8.3 - Correlation between MRI variables and histological parameters, with statistically significant results highlighted in bold.

		Histology		
MRI variables		Interstitial fibrosis	Interstitial inflammation	Interstitial inflammation in non-scarred cortex
Volume		-0.06 (-0.46, 0.36)	-0.01 (-0.42, 0.41)	0.23 (-0.20, 0.59)
T1 (ms) N= 24	Cortex	0.14 (-0.29, 0.53)	0.28 (-0.16, 0.62)	0.26 (-0.17, 0.61)
	Medulla	-0.06 (-0.47, 0.36)	0.05 (-0.37, 0.46)	0.14 (-0.29, 0.53)
	Cortex: medulla	0.11 (-0.32, 0.50)	0.16 (-0.27, 0.54)	-0.02 (-0.43, 0.40)
T2 (ms) N= 24	Cortex	0.05 (-0.37, 0.46)	0.20 (-0.24, 0.56)	0.25 (-0.18, 0.60)
	Medulla	0.32 (-0.11, 0.65)	0.33 (-0.10, 0.65)	0.11 (-0.32, 0.50)
	Cortex: medulla	-0.34 (-0.66, 0.083)	-0.22 (-0.58, 0.21)	0.04 (-0.38, 0.45)
BOLD T2* (ms) N= 24	Cortex	0.08 (-0.35, 0.48)	0.11 (-0.32, 0.50)	0.17 (-0.27, 0.54)
	Medulla	-0.07 (-0.47, 0.36)	0.09 (-0.34, 0.49)	0.14 (-0.29, 0.52)
	Cortex: medulla	0.15 (-0.28, 0.53)	0.04 (-0.38, 0.44)	0.04 (-0.38, 0.44)
ADC ($x10^{-6}$ mm^2/s) N=20	Cortex	0.21 (-0.27, 0.60)	0.22 (-0.26, 0.61)	0.01 (-0.45, 0.46)
	Medulla	0.28 (-0.20, 0.65)	0.29 (-0.19, 0.66)	-0.01 (-0.46, 0.44)
	Cortex: medulla	-0.01 (-0.46, 0.45)	0.04 (-0.42, 0.49)	0.13 (-0.34, 0.55)
FA (0-1) N=23	Cortex	-0.24 (-0.60, 0.21)	-0.29 (-0.64, 0.15)	-0.39 (-0.70, 0.04)
	Medulla	-0.15 (-0.54, 0.29)	-0.08 (-0.49, 0.35)	0.13 (-0.31, 0.52)
	Cortex: medulla	-0.13 (-0.52, 0.31)	-0.19 (-0.57, 0.25)	**-0.44 (-0.73, -0.02)**
ASL (ml/100g/min) N=21	Cortex	-0.15 (-0.55, 0.32)	-0.12 (-0.54, 0.34)	0.04 (-0.41, 0.47)
	Medulla	0.07 (-0.38, 0.50)	-0.06 (-0.49, 0.40)	-0.21 (-0.60, 0.26)
	Cortex: medulla	-0.02 (-0.46, 0.43)	0.12 (-0.35, 0.53)	0.23 (-0.23, 0.61)

Abbreviations: BOLD = blood oxygenation level dependent; ADC = apparent diffusion coefficient; FA = fractional anisotropy; ASL = arterial spin labelling

Supplementary material S8.2. Table of mean values for each MRI variable by primary histological diagnosis

		T1-cortex	T1-medulla	T2-cortex	T2-medulla	T2*-cortex	T2*cortex	ADC-cortex	ADC-medulla	FA-cortex	FA-medulla	ASL-cortex	ASL-medulla
	N												
TCMR IA	N=2	1676.2	1950.6	50.7	52.8	60.9	49.1	1617.3	1590.7	110.0	206.7	108.1	10.7
TCMR IB	N=2	1816.3	2053.8	53.8	50.7	75.9	62.3	1624.7	1684.2	96.9	210.6	289.2	61.0
Borderline TCMR	N=2	1731.1	2162.5	50.3	54.2	61.6	39.8	1441.7	1633.9	83.2	205.1	152.7	37.2
Active ABMR	N=2	1590.4	1866.0	45.5	41.6	61.9	39.8	1464.3	1610.2	136.4	263.8	221.3	11.7
Chronic ABMR	N=1	1938.3	2269.4	54.2	48.0	77.9	37.9	1571.8	1679.1	95.2	151.3	138.0	12.3
TMA	N=2	1672.7	1797.3	47.0	46.8	60.1	53.4	1463.2	1546.6	127.6	247.2	205.1	83.3
ATN	N=3	1777.7	1922.0	51.7	47.1	53.3	52.7	1568.2	1667.2	111.3	60.1	114.3	17.5
BK nephritis	N=1	1777.9	2046.9	52.7	47.1	50.6	67.0	1395.3	1688.8	82.0	275.1	216.5	33.2
Recurrent GN	N=2	1760.2	2036.9	49.5	41.1	43.4	44.5	1596.4	1663.3	117.0	260.5	238.9	41.1
Donor disease	N=1	1626.8	2027.0	46.4	44.6	46.5	54.0	1485.1	1571.0	108.7	173.2	159.5	51.5
IFTA	N=1	2081.8	2066.1	47.6	47.4	58.5	36.1	1697.3	1867.5	155.4	216.4	.-	.-
No abnormality	N=1	1808.2	2180.6	53.4	48.6	68.1	37.9	.-	.-	159.4	214.7	130.9	20.7
Other *	N=4	1632.5	1922.2	49.7	46.2	63.1	47.3	1651.3	1616.7	135.3	242.9	146.5	44.2
1 = moderate arteriolosclerosis with focal embolus and subsequently diagnosed with transplant artery stenosis; 1 diabetic nephropathy; 1 chronic transplant glomerulopathy; 1 de novo secondary focal segmental glomerulosclerosis													

		T1-CMD	T2-CMD	T2*-CMD	ADC-CMD	FA-CMD	ASL-CMD
Primary histological diagnosis							
	N						
TCMR IA	N=2	.87	.96	1.28	1.02	.54	11.20
TCMR IB	N=2	.88	1.07	1.22	.96	.59	4.74
Borderline TCMR	N=2	.80	.93	1.57	.88	.43	4.53
Active ABMR	N=2	.85	1.09	1.61	.91	.51	19.67
Chronic ABMR	N=1	.85	1.13	2.06	.94	.63	11.22
TMA	N=2	.93	1.00	1.22	.95	.52	3.52
ATN	N=3	.92	1.10	1.01	.94	3.44	6.38
BK nephritis	N=1	.82	1.12	.76	.83	.30	6.52
Recurrent GN	N=2	.87	1.20	1.02	.96	.44	5.86
Donor disease N=1	.80	1.04	.86	.95	.63	3.10	
IFTA	N=1	1.01	1.00	1.62	.91	.72	.
No abnormality	N=1	.83	1.10	1.80	.-	.74	6.32
Other *	N=4	.86	1.09	1.41	1.02	.55	10.37
1 = moderate arteriolosclerosis with focal embolus and subsequently diagnosed with transplant artery stenosis; 1 diabetic nephropathy; 1 chronic transplant glomerulopathy; 1 de novo secondary focal segmental glomeruloscleros							

Units: T1 = ms. T2 = ms. BOLD T2* = ms. ADC = $x10^{-6}$ mm^2/s. FA = scalar 0-1. ASL = ml/100g/min

Abbreviations: TCMR 1A: T-cell mediated rejection Banff category 1A. TCMR 1B: T-cell mediated rejection Banff category 1B. TCMR: T-cell mediated rejection. ABMR: antibody mediated rejection. TMA: thrombotic microangiopathy. ATN: acute tubular necrosis. BK: BK polyomavirus.

GN: glomerulonephritis. IFTA: interstitial fibrosis and tubular atrophy. ADC: apparent diffusion coefficient. FA: fractional anisotropsy. ASL: arterial spin labelling. CMD: cortico-medullary differentiation

Renal MRI in comparison to biochemical data

T1 mapping variably correlated with serum creatinine and eGFR, with 5 of the 18 comparisons between T1 (cortex, medulla, and CMD) yielding significant results when compared to creatinine and eGFR (baseline, follow-up, change in value) (Table 8.4). FA-medulla and FA-CMD significantly correlated with baseline creatinine and baseline eGFR, with FA-medulla also correlating with follow-up creatinine and eGFR. Across 72 comparisons for the remaining 4 MRI variables (T2, BOLD T2*, ADC, ASL), the only significant correlation was ASL-CMD and baseline creatinine (Table 8.4). When comparing MRI findings for those who developed graft failure versus those whose transplant continued to function there were significant differences detected in T1-cortex (median 209.1ms (p=0.005)), FA-medulla (median -73.7 (p=0.04) and FA-CMD (median 0.21 (p=0.008)). In a post-hoc logistic regression analysis, T1-cortex remained statistically significant when baseline eGFR was added (T1-cortex: HR 1.02 (95% CI 1.00-1.03); eGFR HR 0.95 (0.83-1.09)).

Table 8.4 - Correlation between MRI variables and biochemical variables at baseline and follow-up, with statistically significant results highlighted in bold.

		Biochemistry					
		Baseline		Follow-up			
MRI variables		Baseline serum creatinine	Baseline eGFR	Final serum creatinine	Final eGFR	Delta creatinine	Delta eGFR
Volume		0.06 (-0.34, 0.45)	0.33 (-0.08, 0.64)	0.33 (-0.08, 0.64)	-0.12 (-0.49, 0.3)	-0.38 (-0.67, 0.02)	0.39 (-0.01, 0.68)
T1 (ms) N= 26	Cortex	0.16 (-0.25, 0.52)	-0.06 (-0.45, 0.35)	**0.45 (0.07, 0.72)**	**-0.45 (-0.72, -0.07)**	-0.46 (-0.72, -0.07)	0.35 (-0.06, 0.65)
	Medulla	-0.32 (-0.64, 0.08)	0.21 (-0.2, 0.56)	0.25 (-0.17, 0.59)	-0.34 (-0.65, 0.07)	-0.4 (-0.69, -0.01)	**0.54 (0.18, 0.77)**
	Cortex: medulla	**0.55 (0.2, 0.78)**	**-0.42 (-0.7, -0.02)**	0.1 (-0.31, 0.48)	-0.05 (-0.44, 0.36)	0.12 (-0.29, 0.49)	-0.33 (-0.64, 0.07)
T2 (ms) N= 26	Cortex	-0.05 (-0.44, 0.36)	0.15 (-0.26, 0.52)	0.35 (-0.06, 0.66)	-0.32 (-0.64, 0.09)	**-0.41 (-0.7, -0.02)**	**0.39 (0.00, 0.68)**
	Medulla	0.07 (-0.34, 0.45)	-0.29 (-0.62, 0.12)	0.03 (-0.37, 0.42)	-0.2 (-0.55, 0.22)	-0.02 (-0.41, 0.38)	0.05 (-0.35, 0.44)
	Cortex: medulla	-0.08 (-0.46, 0.33)	0.35 (-0.05, 0.66)	0.24 (-0.17, 0.58)	-0.06 (-0.45, 0.34)	-0.26 (-0.59, 0.16)	0.22 (-0.2, 0.56)
BOLD T2* (ms) N= 26	Cortex	0.11 (-0.3, 0.49)	0.03 (-0.37, 0.42)	0.31 (-0.1, 0.63)	-0.21 (-0.56, 0.2)	-0.21 (-0.56, 0.2)	0.15 (-0.26, 0.52)
	Medulla	0.13 (-0.29, 0.5)	-0.19 (-0.55, 0.22)	-0.21 (-0.56, 0.2)	0.27 (-0.14, 0.61)	0.34 (-0.07, 0.65)	-0.38 (-0.67, 0.03)

	Cortex: medulla	0.03 (-0.37, 0.42)	0.14 (-0.27, 0.51)	0.32 (-0.09, 0.63)	-0.31 (-0.63, 0.1)	-0.35 (-0.66, 0.05)	0.35 (-0.06, 0.66)
ADC ($x10^{-6}$ mm^2/s) N=22	Cortex	-0.09 (-0.5, 0.36)	0.04 (-0.4, 0.47)	0.11 (-0.33, 0.52)	-0.07 (-0.49, 0.38)	-0.08 (-0.49, 0.37)	0.08 (-0.37, 0.49)
	Medulla	-0.3 (-0.65, 0.15)	0.17 (-0.29, 0.56)	0.16 (-0.3, 0.55)	-0.14 (-0.54, 0.32)	-0.15 (-0.54, 0.31)	0.2 (-0.25, 0.59)
	Cortex: medulla	-0.16 (-0.56, 0.29)	0.14 (-0.31, 0.54)	-0.13 (-0.53, 0.32)	0.2 (-0.25, 0.58)	0.14 (-0.31, 0.54)	-0.13 (-0.53, 0.32)
FA (0-1) N=25	Cortex	0.08 (-0.33, 0.47)	-0.13 (-0.51, 0.29)	-0.04 (-0.44, 0.37)	-0.01 (-0.41, 0.4)	0.02 (-0.39, 0.42)	0.07 (-0.34, 0.46)
	Medulla	**-0.46 (-0.73, -0.07)**	**0.45 (0.05, 0.72)**	**-0.42 (-0.7, -0.01)**	**0.51 (0.13, 0.76)**	0.21 (-0.21, 0.57)	-0.06 (-0.46, 0.35)
	Cortex: medulla	**0.43 (0.03, 0.71)**	**-0.49 (-0.75, -0.1)**	0.28 (-0.14, 0.61)	-0.37 (-0.67, 0.04)	-0.13 (-0.51, 0.29)	0.08 (-0.34, 0.47)
ASL (ml/100g/min) N=23	Cortex	-0.32 (-0.66, 0.12)	0.21 (-0.23, 0.58)	-0.22 (-0.59, 0.22)	0.23 (-0.22, 0.59)	0.12 (-0.32, 0.51)	-0.06 (-0.47, 0.37)
	Medulla	0.1 (-0.34, 0.5)	-0.13 (-0.53, 0.31)	0.09 (-0.35, 0.49)	-0.07 (-0.48, 0.36)	0.07 (-0.36, 0.48)	-0.1 (-0.5, 0.34)
	Cortex: medulla	**-0.43 (-0.72, 0)**	0.41 (-0.02, 0.71)	-0.09 (-0.49, 0.35)	0.06 (-0.37, 0.47)	-0.17 (-0.55, 0.28)	0.22 (-0.22, 0.59)

Abbreviations: eGFR = estimated glomerular filtration rate; BOLD = blood oxygenation level dependent; ADC = apparent diffusion coefficient; FA = fractional anisotropy; ASL = arterial spin labelling

Acute rejection and repeat MRI

Twelve participants had at least borderline rejection reported on their biopsy, of whom 7 were treated for acute rejection. When MRI findings were compared between those who had rejection versus those who did not have rejection only BOLD T2*-cortex was significant (median increase 8.9 ms; p=0.04). Of the 7 patients who were treated for acute rejection, 4 attended for a repeat MRI (2 cancelled due to COVID and 1 did not attend), of whom 2 had progressive deterioration in renal function and 2 had stabilisation of renal function. There was no convincing trend in any MRI parameter with the differing clinical responses between the participants. For instance, cortical T1 increased in one of the participants with a good outcome by a similar amount as it did in a participant with a bad outcome (full data available in supplementary material S8.3).

Supplementary material S8.3: Biochemical and MRI data for the 4 participants who underwent repeat MRI following treatment for acute rejection. Of these participants 2 had poor outcome with progressive decline in kidney function while 2 had a good outcome with stabilisation of their kidney function. There was no apparent trend in MRI parameters between those participants with a good and poor outcome.

	Participant 1 Poor outcome	Participant 2 Poor outcome	Participant 3 Good outcome	Participant 4 Good outcome
Baseline serum creatinine	315	184	123	160
Creatinine at repeat MRI	515	265	128	145
Final creatinine at follow-up	550	607	130	183
Time between MRIs	18	12	21	14
ΔVolume	17.24	25.88	5.64	15.5
ΔT1-cortex	-0.9	-50.6	76.9	-95.3
ΔT1-medulla	-175.8	-115.1	471.9	-13.8
ΔT2-cortex	11.8	8.7	2.4	-6.3
ΔT2-medulla	9	-3.9	5.8	0.6
ΔBOLD T2*-cortex	26.1	9.9	6.7	2.7
ΔBOLD T2*-medulla	4.4	11	-18.7	6.7
ΔADC-cortex	-0.5	-115.9	26.7	-23.7
ΔADC-medulla	11.8	-220.5	-10.7	108.3
ΔFA-cortex	31.7	33.4	-5.1	-94.6
ΔFA-medulla	-9.9	-99.9	20.8	8.7
ΔASL-cortex	-	6	28.1	55.7
ΔASL-medulla	-	-11.9	3.7	26.9

Discussion

In this small prospective study that was stopped early due to the COVID-19 pandemic, there was no correlation between any MRI variable and the percentage of renal cortex containing fibrosis. T1-cortex and T1-CMD weakly correlated with final eGFR and baseline eGFR respectively. More convincingly, there was a significant difference in T1 cortex in those who required dialysis compared to those who did not, and this association remained significant when baseline eGFR was accounted for. From the 4 participants who were treated for acute rejection and underwent repeat MRI, there was no consistent trend in any MRI variable to differentiate good versus poor outcome. Similarly, there was no signal that any MRI variable could differentiate the different aetiologies of transplant dysfunction with wide.

In contrast to the present results, several previous studies have shown that functional MRI can detect fibrosis in renal allografts. Friedli *et al*. report MRI findings in 33 renal transplant recipients undergoing clinically indicated transplant kidney biopsy. They found that ADC corticomedullary difference negatively correlated with histological fibrosis ($r^2 = 0.64$, $p<0.001$), such that a negative it yielded 100% sensitivity and 71% specificity to discriminate fibrosis of 40% or more. Wang *et al* found that ADC negatively correlated with interstitial fibrosis ($\rho = 0.77$, $p<0.001$) in 103 renal transplant recipients who were undergoing clinically indicated biopsies. They also found that ASL and BOLD significantly associated with fibrosis ($r=0.77$, $p<0.001$ and $\rho = 0.61$, $p <0.001$, respectively) and all 3 variables was able to independently discriminate patients with and without 50% fibrosis with an area under the curve of ≥0.85. [149]. Bane *et al*. performed MRI in 27 renal transplant recipients in whom 15 had stable allograft function and 12 had chronic dysfunction (eGFR <30 ml/min/1.73 m^2). ADC and T1-CMD differentiated the functioning allografts from fibrotic ones, with excellent cross-validated diagnostic performance when used in combination. They also found that cortical ADC and T1 had good performance at predicting an eGFR decline of ≥4 ml/min/1.73 m^2 per year at 18 months [150]. Finally, Berchtold *et al.* examined multiparametric renal MRI in 164 patients with CKD, of whom 118 had a renal transplant, and found that ADC corticomedullary difference and T1 corticomedullary difference correlated with interstitial fibrosis, and when combined with eGFR in a multivariable model it could predict <10% fibrosis and >50% fibrosis with area under the curves of 0.88 and 0.91, respectively [147]. The most plausible explanation for the lack of association observed in the present study is reduced sample size (n=20 for ADC). The MRI scanners used in the studies were similar, with the exception of Bane et al who used a 1.5T scanner [150]. Analysis approaches varied across all the studies, but with previous studies using the mean results from a greater number of ROIs compared to a single representative ROI that was used here, albeit with some justification for the current approach [291].

The study has strengths, most notably it's comprehensive multi-parametric MRI protocol using state-of-the-art hardware and the very close time scale between MRI and biopsy. This study has limitations, the most notable of which is that it is underpowered. Complete datasets were available for 20 participants whereas 60 were required based on the pre-specified sample size calculation. There was a wide variety of histological diagnoses suggesting a heterogenous cohort, of whom 12 participants had some histological evidence of acute rejection reported, but only 7 were clinically treated as such, suggesting discrepancy in the clinical and histological impressions. Overall, the degree of fibrosis present in the cohort was low, with a

median of 10%. It unlikely that being able to differentiate 5 and 15% fibrosis would result in a change in management and therefore MRI's inability to differentiate here is of doubtful clinical significance. The multi-parametric MRI protocol combined with the comprehensive clinico-histopathological outcome data necessitated that multiple statistical comparisons were performed. While adjusting statistical thresholds for multiple comparisons is not recommended,[293,294] we acknowledge the increased likelihood of type 1 errors and, consequently, isolated significant results should be interpreted with caution (e.g. FA-CMD correlated with the percentage of non-scarred cortex containing inflammation, but the results for FA-cortex and FA-medulla were negative, as was FA-CMD when compared to total cortex containing inflammation).

Conclusion

This study was stopped prematurely and, consequently, was underpowered. However, in the setting of transplant dysfunction there is a clinical necessity to secure the correct diagnosis and thus the correct deployment of potentially toxic treatments. Accordingly margins for error in diagnosis are narrow. Even in this small cohort, it was evident that a wide variety of MRI results corresponded with the same findings on histology. As such, while larger studies may confirm moderate correlations between MRI variables and histology, on an individual patient level, it is unlikely that multi-parametric renal MRI will ever replace, or arguably compliment, kidney biopsy in the assessment of transplant dysfunction. The finding that T1-cortex differentiated those with future graft failure independent of baseline eGFR warrants further study to assess its role in prognostication irrespective of its lack in diagnostic differentiation.

Declarations

Acknowledgements

We are grateful to the participants for their contribution to this research. We are very grateful to the assistance of the clinical research nurses who assisted with study visits, including Deborah McGlynn, Nicola Thomson, and Kirsty Forsyth.

Funding

This study was funded by a grant from Kidney Research UK (KS_IN_002_20180913)

Conflicts of Interest

P.B.M. reports personal fees and/or non-financial support from Vifor, Napp, Pharmacosmos, Astra Zeneca, Astellas, Novartis and grants from Boehringer Ingelheim. K.A.G reports personal fees from Napp, Astrazeneca and Vifor.

Author contributions

AJR, PBM and KAG conceived the idea for the study. AJR lead recruitment, performed study visits, analysed the MRI, performed statistical analyses and wrote the manuscript. KAG assisted with study visits and critically appraised the manuscript. SAS write the MRI protocol and critically appraised the manuscript. DK and JC reported the histological results. EM led the MRI acquisition. GR issued clinical reports for the MRIs and critically appraised the manuscript. PBM oversaw study procedures and critically appraised the manuscript.

Chapter 9 – Final Discussion

9.1 Summary of findings

The key findings from this thesis are summarised below (by chapter)

9.1.1 Global longitudinal strain associates with mortality in kidney failure

- In a retrospective study of 215 participants with kidney failure, left ventricular global longitudinal strain (LV-GLS) on cardiovascular MRI associated with all-cause mortality, independent of baseline clinical variables and future renal transplantation. This effect was present even when >90% of the cohort had normal LVEF.
- The survival benefit of renal transplantation was evident even in the quartile of participants with the most severely impaired LV-GLS.
- Using LV-GLS, instead of LVEF, to diagnose cardiac dysfunction in patients with kidney failure could result in a major advance in our understanding of cardiovascular disease and prognosis in kidney failure, but LV-GLS in isolation is unlikely to be helpful when assessing an individual's suitability for renal transplantation.

9.1.2 Myocardial native T1 is modifiable by haemodialysis with fluid removal

- In a prospective study of 26 patients undergoing regular haemodialysis, acute changes in cardiac volumes and myocardial composition were detectable on 3T cardiovascular MRI following haemodialysis with fluid removal.
- Small, but significant, reductions in global myocardial T1 and T2 relaxation times were observed after dialysis suggesting that the abnormal native T1 signal in patients undergoing haemodialysis is not entirely due to fibrosis.
- The timing of cardiovascular MRI scanning in relation to a patient's dialysis schedule is crucial, particularly if serial scanning is required for clinical or research purposes

9.1.3 Radial-VIBE MRI can detect vascular calcification in patients with kidney failure

- In a prospective study of 96 individuals with kidney failure (24 haemodialysis, 72 transplant), a radial-VIBE sequence on MRI was able to detect thoracic aortic calcification. Subjective, qualitative, blinded, visual comparison between radial-VIBE and gold-standard CT yielded to a high degree of agreement (median Likert score 4.6 / 5.0 (SD 0.8)). However, on semi-automated quantitative analysis, there was proportional bias in the measurement of calcium volume by radial-VIBE compared to CT, with radial-VIBE over-estimating the volume of calcification when minimal calcification was present and under-estimating it when extensive calcification was present.

9.1.4 ECV-CT does not correlate with non-contrast cardiovascular MRI findings in patients on haemodialysis

- In a prospective study of 23 participants on regular haemodialysis there was no correlation between extracellular volume on CT (ECV-CT) and myocardial native T1. ECV-CT merits further study as a potential cardiovascular imaging biomarker, especially in dialysis populations who have a high prevalence of myocardial fibrosis but in whom current diagnostic strategies involving gadolinium-based contrast agents are relatively contraindicated. However, using the present ECV-CT protocol in patients on dialysis has displayed poor intra-observer reproducibility and wide intra-subject variability.

9.1.5 In multiparametric renal MRI analysis manually drawn regions of interest for the cortex or a representative area of cortex can be used interchangeably

- In a prospective study of 40 participants (10 healthy volunteers, 10 patients with left ventricular systolic dysfunction and 20 renal transplant recipients) comparing different regions of interest (ROI) for the analysis of renal MRI, it was found that manually

drawn ROIs delineating the cortex or in a representative area of cortex could be used interchangeably, with acceptable inter-observer reproducibility.

- Whole kidney ROIs for T1 mapping, arterial spin labelling and diffusion-weighted imaging were highly reproducible but should be used with caution given that the results represent a central value from an extremely wide range.
- Clinical correlation of the results using regions of interest from manually delineated cortex or an area of representative cortex are awaited from ongoing and future research studies
- For kidney volume, contouring alternate slices, rather than every slice, of a localiser scan produced similar results with improved time-efficiency, although validation of the measured volumes using 3D techniques is still required.

9.1.6 No meaningful correlation between multi-parametric renal MRI findings and renal histology in patients with transplant dysfunction

- In a small study of 28 participants (20 with complete data) that was stopped prematurely due to the COVID-19 pandemic, there was no correlation between any renal MRI variable and the percentage of renal cortex containing fibrosis. The study was underpowered to detect correlations of a moderate magnitude. However, in the setting of transplant dysfunction there is a clinical necessity to secure the correct diagnosis and thus the correct deployment of potentially toxic treatments. Accordingly, margins for error in diagnosis are narrow. Even in this small cohort, it was evident that a wide variety of MRI results corresponded with the same findings on histology. As such, while larger studies may confirm moderate correlations between MRI variables and histology, on an individual patient level, it is unlikely that multi-parametric renal MRI will ever replace, or arguably compliment, kidney biopsy in the assessment of transplant dysfunction. The finding that T1-cortex differentiated those with future graft failure independent of baseline eGFR warrants further study to assess its role in prognostication irrespective of its lack in diagnostic differentiation.

9.2 Strengths, limitations, and challenges

The specific strengths and limitations of the 6 manuscripts included in this thesis are described in the discussion section of each manuscript. As a complete body of work, this thesis has strengths and limitations. The multi-modal, multi-organ approach to imaging in this patient group is a strength of this thesis. There is no cure for established kidney failure. As a result, once a patient develops kidney failure, they will often undertake multiple forms of renal replacement therapy, dealing with the specific complications of each. When on haemodialysis, they will be subjected to a drastically increased cardiovascular risk. If they receive a kidney transplant, their cardiovascular risk is reduced significantly, however their worries often switch to concern for their transplant function. This thesis therefore follows a common path taken by many patients as it moves from dialysis to transplantation. The unifying theme joining these 6 distinct studies is the patient group for which they are relevant, and this patient/population specific focus is a strength. The design of the prospective studies was careful to maximise research potential, while minimising burden to participants, by allowing 3 distinct research questions to be answered by 2 patient visits (2 MRI, 1 CT) within 24 hours. Similarly, the renal MRI studies utilised clinical hospital visits to minimise burden to participants and ensure minimum time between biopsy and MRI. The breadth of imaging modalities examined in this thesis is also a weakness, as each in turn is afforded less detail. Furthermore, the patient group, although joined by the commonality of kidney failure, is heterogeneous, with notable differences between dialysis and transplant populations in terms of risk profile and care priorities. For all the studies, the sample size was small, and the studies were observational, allowing no causation or intervention to be assessed.

9.3 Future work

Based on the findings of the present thesis the following studies are warranted (by chapter):

9.3.1 Left ventricular global longitudinal strain

- Studies confirming the prognostic capabilities in an independent cohort, especially in a cohort more representative of the maintenance haemodialysis population with regards age and co-morbidities
- Longitudinal studies assessing if a change in LV-GLS associates with a change in prognosis

- Studies that can reliably assess the relationship between LV-GLS and cardiovascular outcomes in patients with kidney failure
- Studies exploring the potential differential prognostic capabilities of LV-GLS in men with kidney failure compared to women with kidney failure
- Studies exploring cardiovascular therapeutics in patients with kidney failure who have impaired LV-GLS

9.3.2 Native T1 mapping as a biomarker of cardiovascular risk in kidney failure

- Comparison of native T1 mapping before and after dialysis in patients that underwent dialysis but without fluid removal.
- Studies examining the prognostic capabilities of native T1 mapping in patients with kidney failure (with careful standardisation of imaging schedules and awareness of the potential confounding effect of fluid status and the dialysis process).

9.3.3 Radial-VIBE MRI for the detection of vascular calcification

- Further work is required on image optimisation of radial-VIBE and could benefit from utilising smaller voxel size, improved motion correction and optimised protocols allowing anatomical sequences to be utilised for creating a mask that can be applied to identical radial-VIBE images.

9.3.4 ECV-CT for detecting myocardial fibrosis in patients with kidney failure

- Studies examining ECV-CT in patients undergoing haemodialysis with imaging on non-dialysis days, with additional heart rate control and using dual-energy or spectral CT with specific post-acquisition software to improve registration.
- Studies comparing ECV-CT and ECV-MRI in patients with less advanced CKD who can safely receive gadolinium-based contrast agents.

9.3.5 Comparing regions of interest for the analysis of renal MRI

- Studies comparing ROIs of manually delineated cortex from a single slice versus a mean result from multiple adjacent slices
- Studies comparing ROIs of representative cortex from a single slice versus a mean result from multiple ROIs drawn on multiple adjacent slices

9.3.6 Renal MRI to investigate renal transplant dysfunction

- Larger studies (comprising at least 60 participants) comparing renal MRI to histology
- Retrospective analysis of previous studies to assess if T1-cortex associates with graft failure in other cohorts

9.4 Conclusion

There is a clear role for the development and validation of reliable biomarkers for patients with kidney failure. Initial application would be to clinical research, either as surrogate outcome measures in clinical trials exploring novel therapeutics or as participant enrichment tools to improve trial efficiency by identifying participants who are most likely to benefit. Beyond this, it is plausible that biomarkers could be applied in clinical practice to improve the management of patients with kidney failure.

The pathological basis for the excess cardiovascular mortality observed in patients with kidney failure is driven by myocardial fibrosis and vascular calcification. In clinical practice, diffuse myocardial fibrosis can be diagnosed and quantified using contrast-enhanced MRI. However, gadolinium-based contrast agents are relatively contraindicated in patients with kidney failure. Therefore, non-contrast methods that reliably identify myocardial fibrosis in kidney failure would allow better understanding, prognostication and potentially intervention in this high-risk patient population. Similarly, there are drawbacks to existing methods of identifying vascular calcification, in that although it can be reliably detected on CT, this requires exposure to ionising radiation, which limits the use of serial scanning in research settings. In the present thesis I aimed to interrogate some emerging imaging biomarkers for cardiovascular disease in kidney failure by studying: LV-GLS for prognostication in patients with kidney failure, exploring the changes in native T1 mapping in response to dialysis,

calculating myocardial ECV-CT in a cohort of patients undergoing regular dialysis and exploring a novel method for identifying vascular calcification on MRI.

LV-GLS on MRI appears to be superior to other imaging parameters for prognosticating all-cause mortality in people with kidney failure, but it remains to be proven if LV-GLS is modifiable and if any change associates with a proportional change in prognosis. As awareness of LV-GLS increases, it is likely that LV-GLS will be reported increasingly in clinical echocardiograms and cardiac imaging studies as an alternative index of cardiac function. However, for it to lead to a reduction in cardiovascular risk in patients with kidney failure it will require large, outcome-driven clinical trials proving that LV-GLS can be used to select patients who would benefit from a particular therapy. From the data presented in this thesis, is it not likely that LV-GLS in isolation offers any merit in assessing patients for transplant suitability.

Native T1 mapping may yet be proven to identify myocardial fibrosis in kidney failure but the fact it reduces in response to a single dialysis session with fluid removal means its role as a surrogate outcome measure in future clinical trials is doubtful. Any future studies exploring the role of native T1 mapping in kidney failure will need to carefully consider the confounding impact of fluid status on results. On the other hand, it is plausible that myocardial oedema, independent of myocardial fibrosis, portends a worse prognosis, and so a reduction in myocardial native T1 signal may be prognostically relevant, regardless of the cellular changes underlying it. Furthermore, the difference in native T1 signal observed in the present thesis was of a small magnitude. If an intervention were shown to reduce native T1 signal by a much larger amount, then the variability observed post-dialysis may be negligible in comparison.

Given the variability in myocardial native T1 observed in patients on dialysis, identifying an alternative method of quantifying myocardial fibrosis is appealing. ECV-CT would be readily available, avoid exposure to gadolinium and is supported by encouraging results in patients with cardiac amyloid and aortic stenosis. Unfortunately, in the present study, ECV-CT showed no correlation with any CMR parameter but, more concerningly, showed an unacceptably wide inter-observer reproducibility. Further analysis found significant changes in ECV-CT estimation even when the same observer examined adjacent slices in the same participant, without obvious artefact or biological explanation for the discrepancy. Whether this variability can be overcome by heart rate control and improved software registration remains to be seen.

Radial-VIBE MRI has advantages over CT for the identification of vascular calcification, but the fact that current radial-VIBE imaging does not allow reliable quantification of calcification volume dramatically reduces its utility in both research and clinical settings. The suggested strategies for improving radial-VIBE image quality are achievable and could translate to improvements in quantification accuracy. However, due to the accessibility and accuracy of CT, combined with the limited therapeutic interventions for vascular calcification, even if improvements are realised, the clinical utility of radial-VIBE is likely to be limited to patients who are already undergoing cardiovascular MRI or MRI-angiography for an alternative reason.

With regards renal MRI, it is possible that a multiparametric approach can allow interrogation of the kidney parenchyma with regards inflammation, fibrosis, perfusion and oedema. However, in the setting of acute kidney transplant dysfunction, a high level of diagnostic accuracy is required to justify potentially toxic treatments. Even from this small, under-powered study, it is clear that renal MRI (in its current form) cannot reliably differentiate varying aetiologies of transplant dysfunction. Renal MRI may still have clinical utility for the diagnosis of fibrosis in kidney transplants. Previous studies have shown functional renal MRI can reliably differentiate extensive from minimal fibrosis. If so, then this would be sufficient to avoid a patient with extensive fibrosis undergoing an invasive kidney biopsy and allow earlier focus on future renal replacement therapy planning. The lack of correlation between MRI findings and fibrosis in the present thesis is explained by the low levels of fibrosis in the sample (median 10%) and discriminating between low levels of fibrosis is not clinically relevant. Further studies exploring renal MRI for the detection of fibrosis are warranted.

Individuals living with kidney failure continue to have huge unmet care needs. Reliable imaging biomarkers would allow therapeutics to be trialled more readily to address these needs. However, the results of the present thesis suggest that, in their present form, neither functional MRI for the identification of cardiovascular disease in patients undergoing dialysis, nor renal MRI in patients with transplant dysfunction, are ready for implementation into clinical trial research protocols or clinical practice.

Chapter 10 References

1. Kidney Disease Working Group. Kidney Disease: Improving Global Outcomes (KDIGO) 2012 clinical practice guideline for the evaluation and management of chronic kidney disease. *Kidney Int 3, 1–150 (2013)*. 2013;3(1):30-130. Accessed January 14, 2022. https://kdigo.org/wp-content/uploads/2017/02/KDIGO_2012_CKD_GL.pdf

2. Levey AS, Stevens LA, Schmid CH, et al. A new equation to estimate glomerular filtration rate. *Ann Intern Med*. 2009;150(9):604-612. Accessed November 30, 2018. http://www.ncbi.nlm.nih.gov/pubmed/19414839

3. Inker LA, Eneanya ND, Coresh J, et al. New Creatinine- and Cystatin C–Based Equations to Estimate GFR without Race. *N Engl J Med*. 2021;385(19):1737-1749. doi:10.1056/NEJMOA2102953/SUPPL_FILE/NEJMOA2102953_DISCLOSURES.PDF

4. Hsu C, Yang W, Parikh R V., et al. Race, Genetic Ancestry, and Estimating Kidney Function in CKD. *N Engl J Med*. 2021;385(19):1750-1760. doi:10.1056/NEJMOA2103753/SUPPL_FILE/NEJMOA2103753_DATA-SHARING.PDF

5. Delgado C, Baweja M, Crews DC, et al. A unifying approach for GFR Estimation: RECOMMENDATIONS of the NKF-ASN task force on reassessing the inclusion of race in diagnosing kidney disease. *J Am Soc Nephrol*. 2021;32(12):2994-3015. doi:10.1681/ASN.2021070988/-/DCSUPPLEMENTAL

6. Levey AS, Eckardt K-U, Dorman NM, et al. Nomenclature for kidney function and disease: report of a Kidney Disease: Improving Global Outcomes (KDIGO) Consensus Conference. *J Am Med Assoc*. 2020;29:1117-1129. doi:10.1016/j.kint.2020.02.010

7. Bikbov B, Purcell CA, Levey AS, et al. Global, regional, and national burden of chronic kidney disease, 1990–2017: a systematic analysis for the Global Burden of Disease Study 2017. *Lancet*. 2020;395(10225):709-733. doi:10.1016/S0140-6736(20)30045-3

8. Scottish Renal Registry - Figures from January to December 2020 - Scottish Renal Registry - Publications - Public Health Scotland.

https://publichealthscotland.scot/publications/scottish-renal-registry/scottish-renal-registry-figures-from-january-to-december-2020/. Accessed January 14, 2022. https://publichealthscotland.scot/publications/scottish-renal-registry/scottish-renal-registry-figures-from-january-to-december-2020/

9. Tandukar S, Palevsky PM. Continuous Renal Replacement Therapy: Who, When, Why, and How. *Chest*. 2019;155(3):626-638. doi:10.1016/J.CHEST.2018.09.004

10. National Institute for Health and Care Excellence. *Renal Replacement Therapy and Conservative Management NICE Guideline*. NICE; 2018. Accessed January 20, 2022. https://www.nice.org.uk/guidance/ng107/chapter/Recommendations#choosing-modalities-of-renal-replacement-therapy-or-conservative-management

11. Roumeliotis A, Roumeliotis S, Chan C, Pierratos A. Cardiovascular Benefits of Extended-Time Nocturnal Hemodialysis. *Curr Vasc Pharmacol*. 2021;19(1):21-33. doi:10.2174/1570161118666200401112106

12. Graham-Brown MPM, Churchward DR, Hull KL, et al. Cardiac Remodelling in Patients Undergoing in-Centre Nocturnal Haemodialysis: Results from the MIDNIGHT Study, a Non-Randomized Controlled Trial. *Blood Purif*. 2017;44(4):301-310. doi:10.1159/000481248

13. McCullough PA, Chan CT, Weinhandl ED, Burkart JM, Bakris GL. Intensive Hemodialysis, Left Ventricular Hypertrophy, and Cardiovascular Disease. *Am J Kidney Dis*. 2016;68(5S1):S5-S14. doi:10.1053/J.AJKD.2016.05.025

14. Lok CE, Huber TS, Lee T, et al. KDOQI Clinical Practice Guideline for Vascular Access: 2019 Update. *Am J Kidney Dis*. 2020;75(4):S1-S164. doi:10.1053/J.AJKD.2019.12.001/ATTACHMENT/31161DA0-0384-4B50-99B9-DAD4DDA7C16F/MMC4.PDF

15. Blankestijn PJ, Grooteman MP, Nube MJ, Bots ML. Clinical evidence on haemodiafiltration. *Nephrol Dial Transplant*. 2018;33(Suppl 3):iii53. doi:10.1093/NDT/GFY218

16. Mehrotra R, Devuyst O, Davies SJ, Johnson DW. The Current State of Peritoneal Dialysis. *J Am Soc Nephrol*. 2016;27(11):3238. doi:10.1681/ASN.2016010112

17. Wolfe RA, Ashby VB, Milford EL, et al. Comparison of mortality in all patients on dialysis, patients on dialysis awaiting transplantation, and recipients of a first cadaveric transplant. *N Engl J Med*. 1999;341(23):1725-1730. doi:10.1056/NEJM199912023412303

18. Thiruchelvam PTR, Willicombe M, Hakim N, Taube D, Papalois V. Renal transplantation. *BMJ*. 2011;343(7832):1055-1059. doi:10.1136/BMJ.D7300

19. Becker BN, Becker YT, Odorico JS, Pirsch JD, Sollinger HW. Simultaneous Pancreas-Kidney and Pancreas Transplantation. *J Am Soc Nephrol*. 2001;12(11):2517-2527. doi:10.1681/ASN.V12112517

20. van de Laar SC, Robb ML, Hogg R, Burnapp L, Papalois VE, Dor FJMF. The Impact of Cold Ischaemia Time on Outcomes of Living Donor Kidney Transplantation in the UK Living Kidney Sharing Scheme. *Ann Surg*. 2021;274(5):859-865. doi:10.1097/SLA.0000000000005123

21. Ojo AO. Expanded criteria donors: process and outcomes. *Semin Dial*. 2005;18(6):463-468. doi:10.1111/J.1525-139X.2005.00090.X

22. Poggio ED, Augustine JJ, Arrigain S, Brennan DC, Schold JD. Long-term kidney transplant graft survival-Making progress when most needed. *Am J Transplant*. 2021;21(8):2824-2832. doi:10.1111/AJT.16463

23. Sellarés J, de Freitas DG, Mengel M, et al. Understanding the Causes of Kidney Transplant Failure: The Dominant Role of Antibody-Mediated Rejection and Nonadherence. *Am J Transplant*. 2012;12(2):388-399. doi:10.1111/j.1600-6143.2011.03840.x

24. Gaston RS, Cecka JM, Kasiske BL, et al. Evidence for Antibody-Mediated Injury as a Major Determinant of Late Kidney Allograft Failure. *Transplantation*. 2010;90(1):68-74. doi:10.1097/TP.0b013e3181e065de

25. Naesens M, Kuypers DRJ, De Vusser K, et al. The Histology of Kidney Transplant Failure. *Transplantation*. 2014;98(4):427-435. doi:10.1097/TP.0000000000000183

26. Voorend CGN, Verberne WR, Van Oevelen M, Meuleman Y, Van Buren M, Bos WJW. Changing the choice from dialysis to conservative care or vice versa in older

patients with advanced chronic kidney disease. *Nephrol Dial Transplant*. 2021;36(10):1958-1961. doi:10.1093/NDT/GFAB162

27. Macfarlane AJ, Kearns RJ, Clancy MJ, et al. Anaesthesia Choice for Creation of Arteriovenous Fistula (ACCess) study protocol : a randomised controlled trial comparing primary unassisted patency at 1 year of primary arteriovenous fistulae created under regional compared to local anaesthesia. *BMJ Open*. 2021;11(12):e052188. doi:10.1136/BMJOPEN-2021-052188

28. Lok CE, Rajan DK, Clement J, et al. Endovascular Proximal Forearm Arteriovenous Fistula for Hemodialysis Access: Results of the Prospective, Multicenter Novel Endovascular Access Trial (NEAT). *Am J Kidney Dis*. 2017;70(4):486-497. doi:10.1053/J.AJKD.2017.03.026

29. Davies SJ, Caskey FJ, Coyle D, et al. Rationale and design of BISTRO: a randomized controlled trial to determine whether bioimpedance spectroscopy-guided fluid management maintains residual kidney function in incident haemodialysis patients. *BMC Nephrol*. 2017;18(1). doi:10.1186/S12882-017-0554-1

30. Wald R, Rabbat CG, Girard L, et al. Two phosphate taRGets in end-stage renal disease trial (TARGET): A randomized controlled trial. *Clin J Am Soc Nephrol*. 2017;12(6):965-973. doi:10.2215/CJN.10941016

31. Edmonston DL, Isakova T, Dember LM, et al. Design and Rationale of HiLo: A Pragmatic, Randomized Trial of Phosphate Management for Patients Receiving Maintenance Hemodialysis. *Am J Kidney Dis*. 2021;77(6):920-930.e1. doi:10.1053/J.AJKD.2020.10.008

32. Rossignol P, Frimat L, Zannad F. The safety of mineralocorticoid antagonists in maintenance hemodialysis patients: two steps forward. *Kidney Int*. 2019;95(4):747-749. doi:10.1016/J.KINT.2018.12.006

33. Himmelfarb J, Vanholder R, Mehrotra R, Tonelli M. The current and future landscape of dialysis. *Nat Rev Nephrol 2020 1610*. 2020;16(10):573-585. doi:10.1038/s41581-020-0315-4

34. Fleming GM. Renal replacement therapy review: Past, present and future. *Organogenesis*. 2011;7(1):2. doi:10.4161/ORG.7.1.13997

35. Hosgood SA, Van Heurn E, Nicholson ML. Normothermic machine perfusion of the kidney: better conditioning and repair? *Transpl Int*. 2015;28(6):657-664. doi:10.1111/TRI.12319

36. Goldberg DS, Abt PL, Blumberg EA, et al. Trial of Transplantation of HCV-Infected Kidneys into Uninfected Recipients. *N Engl J Med*. 2017;376(24):2394-2395. doi:10.1056/NEJMC1705221

37. Jordan SC, Lorant T, Choi J, et al. IgG Endopeptidase in Highly Sensitized Patients Undergoing Transplantation. *N Engl J Med*. 2017;377(5):442-453. doi:10.1056/NEJMOA1612567

38. Eikmans M, Gielis EM, Ledeganck KJ, Yang J, Abramowicz D, Claas FFJ. Non-invasive biomarkers of acute rejection in kidney transplantation: Novel targets and strategies. *Front Med*. 2019;6(JAN):358. doi:10.3389/fmed.2018.00358

39. Porrett PM, Orandi BJ, Kumar V, et al. First clinical-grade porcine kidney xenotransplant using a human decedent model. *Am J Transplant*. Published online January 20, 2022. doi:10.1111/AJT.16930

40. Bello AK, Alrukhaimi M, Ashuntantang GE, et al. Complications of chronic kidney disease: current state, knowledge gaps, and strategy for action. *Kidney Int Suppl*. 2017;7(2):122. doi:10.1016/J.KISU.2017.07.007

41. Baigent C, Burbury K, Wheeler D. Premature cardiovascular disease in chronic renal failure. *Lancet*. 2000;356(9224):147-152. doi:10.1016/S0140-6736(00)02456-9

42. Go AS, Chertow GM, Fan D, McCulloch CE, Hsu C. Chronic Kidney Disease and the Risks of Death, Cardiovascular Events, and Hospitalization. *N Engl J Med*. 2004;351(13):1296-1305. doi:10.1056/NEJMoa041031

43. Matsushita K, van der Velde M, Astor BC, et al. Association of estimated glomerular filtration rate and albuminuria with all-cause and cardiovascular mortality in general population cohorts: a collaborative meta-analysis. *Lancet*. 2010;375(9731):2073-2081. doi:10.1016/S0140-6736(10)60674-5

44. USRDS. 2016 USRDS Annual Data Report: Epidemiology of Kidney Disease in the United States. *Am J Kidney Dis*. 2017;69(3):S659-S688.

doi:10.1053/j.ajkd.2017.01.035

45. Foley RN. Chronic Kidney Disease and the Risk for Cardiovascular Disease, Renal Replacement, and Death in the United States Medicare Population, 1998 to 1999. *J Am Soc Nephrol*. 2005;16(2):489-495. doi:10.1681/ASN.2004030203

46. Methven S, Steenkamp R, Fraser S. UK Renal Registry 19th Annual Report: Chapter 5 Survival and Causes of Death in UK Adult Patients on Renal Replacement Therapy in 2015: National and Centre-specific Analyses. *Nephron*. 2017;137 Suppl 1(Suppl. 1):117-150. doi:10.1159/000481367

47. Saravanan P, Davidson NC. Risk assessment for sudden cardiac death in dialysis patients. *Circ Arrhythm Electrophysiol*. 2010;3(5):553-559. doi:10.1161/CIRCEP.110.937888

48. Muntner P, He J, Astor BC, Folsom AR, Coresh J. Traditional and Nontraditional Risk Factors Predict Coronary Heart Disease in Chronic Kidney Disease: Results from the Atherosclerosis Risk in Communities Study. *J Am Soc Nephrol*. 2005;16(2):529-538. doi:10.1681/ASN.2004080656

49. Chen SC, Su HM, Tsai YC, et al. Framingham risk score with cardiovascular events in chronic kidney disease. *PLoS One*. 2013;8(3). doi:10.1371/JOURNAL.PONE.0060008

50. Lees JS, Welsh CE, Celis-Morales CA, et al. Glomerular filtration rate by differing measures, albuminuria and prediction of cardiovascular disease, mortality and end-stage kidney disease. *Nat Med*. 2019;25(11):1753-1760. doi:10.1038/S41591-019-0627-8

51. Wanner C, Amann K, Shoji T. The heart and vascular system in dialysis. *Lancet (London, England)*. 2016;388(10041):276-284. doi:10.1016/S0140-6736(16)30508-6

52. Burton JO, Jefferies HJ, Selby NM, McIntyre CW. Hemodialysis-induced cardiac injury: determinants and associated outcomes. *Clin J Am Soc Nephrol*. 2009;4(5):914-920. doi:10.2215/CJN.03900808

53. Herzog CA. Cardiac arrest in dialysis patients: approaches to alter an abysmal outcome. *Kidney Int Suppl*. 2003;63(84):S197-200. doi:10.1046/j.1523-1755.63.s84.17.x

54. Edwards NC, Moody WE, Chue CD, Ferro CJ, Townend JN, Steeds RP. Defining the natural history of uremic cardiomyopathy in chronic kidney disease: The role of cardiovascular magnetic resonance. *JACC Cardiovasc Imaging*. 2014;7(7):703-714. doi:10.1016/j.jcmg.2013.09.025

55. Aoki J, Ikari Y, Nakajima H, et al. Clinical and pathologic characteristics of dilated cardiomyopathy in hemodialysis patients. *Kidney Int*. 2005;67(1):333-340. doi:10.1111/j.1523-1755.2005.00086.x

56. Mall G, Huther W, Schneider J, Lundin P, Ritz E. Diffuse intermyocardiocytic fibrosis in uraemic patients. *Nephrol Dial Transplant*. 1990;5(1):39-44. Accessed November 10, 2017. http://www.ncbi.nlm.nih.gov/pubmed/2109283

57. Raggi P, O'Neill WC. Imaging for Vascular Calcification. *Semin Dial*. 2017;30(4):347-352. doi:10.1111/sdi.12596

58. London GM, Guérin AP, Marchais SJ, Métivier F, Pannier B, Adda H. Arterial media calcification in end-stage renal disease: impact on all-cause and cardiovascular mortality. *Nephrol Dial Transplant*. 2003;18(9):1731-1740. Accessed March 5, 2017. http://www.ncbi.nlm.nih.gov/pubmed/12937218

59. Mark PB, Doyle A, Blyth KG, et al. Vascular function assessed with cardiovascular magnetic resonance predicts survival in patients with advanced chronic kidney disease. *J Cardiovasc Magn Reson*. 2008;10(1):39. doi:10.1186/1532-429X-10-39

60. Zimmerli LU, Mark PB, Steedman T, et al. Vascular function in patients with end-stage renal disease and/or coronary artery disease: a cardiac magnetic resonance imaging study. *Kidney Int*. 2007;71(1):68-73. doi:10.1038/sj.ki.5002024

61. Inoue H, Shimizu S, Watanabe K, et al. Impact of trajectories of abdominal aortic calcification over 2 years on subsequent mortality: a 10-year longitudinal study. *Nephrol Dial Transpl*. 2018;33:676-683. doi:10.1093/ndt/gfx253

62. Fraser SDS, Roderick PJ, McIntyre NJ, et al. Suboptimal blood pressure control in chronic kidney disease stage 3: baseline data from a cohort study in primary care. *BMC Fam Pract*. 2013;14. doi:10.1186/1471-2296-14-88

63. Coresh J, Wei GL, McQuillan G, et al. Prevalence of high blood pressure and elevated

serum creatinine level in the United States: findings from the third National Health and Nutrition Examination Survey (1988-1994). *Arch Intern Med*. 2001;161(9):1207-1216. doi:10.1001/ARCHINTE.161.9.1207

64. Agarwal R, Nissenson AR, Batlle D, Coyne DW, Trout JR, Warnock DG. Prevalence, treatment, and control of hypertension in chronic hemodialysis patients in the United States. *Am J Med*. 2003;115(4):291-297. doi:10.1016/S0002-9343(03)00366-8

65. Port FK, Hulbert-Shearon TE, Wolfe RA, et al. Predialysis blood pressure and mortality risk in a national sample of maintenance hemodialysis patients. *Am J Kidney Dis*. 1999;33(3). doi:10.1016/S0272-6386(99)70188-5

66. Cheung AK, Chang TI, Cushman WC, et al. KDIGO 2021 Clinical Practice Guideline for the Management of Blood Pressure in Chronic Kidney Disease. *Kidney Int*. 2021;99(3S):S1-S87. doi:10.1016/J.KINT.2020.11.003

67. McCallum W, Sarnak MJ. Blood Pressure Target for the Dialysis Patient. *Semin Dial*. 2019;32(1):35. doi:10.1111/SDI.12754

68. Georgianos PI, Vaios V, Zebekakis PE, Liakopoulos V. Blood pressure targets in patients with chronic kidney disease: A critical evaluation of clinical-trial evidence and guideline recommendations. *J Clin Hypertens*. 2020;22(5):924-928. doi:10.1111/JCH.13859

69. Thomas R, Kanso A, Sedor JR. Chronic Kidney Disease and Its Complications. *Prim Care*. 2008;35(2):329. doi:10.1016/J.POP.2008.01.008

70. Wanner C, Krane V, März W, et al. Atorvastatin in Patients with Type 2 Diabetes Mellitus Undergoing Hemodialysis. *N Engl J Med*. 2005;353(3):238-248. doi:10.1056/NEJMoa043545

71. Baber U, Toto RD, de Lemos JA. Statins and cardiovascular risk reduction in patients with chronic kidney disease and end-stage renal failure. *Am Heart J*. 2007;153(4):471-477. doi:10.1016/J.AHJ.2006.10.042

72. McClellan W, Aronoff SL, Bolton WK, et al. The prevalence of anemia in patients with chronic kidney disease. *Curr Med Res Opin*. 2004;20(9):1501-1510. doi:10.1185/030079904X2763

73. Geddes CC. Pathophysiology of renal anaemia. *Nephrol Dial Transplant*. 2019;34(6):921-922. doi:10.1093/NDT/GFY266

74. Drü TB, Parfrey PS. Summary of the KDIGO guideline on anemia and comment: reading between the (guide)line(s). *Kidney Int*. 2012;82:952-960. doi:10.1038/ki.2012.270

75. Macdougall IC, White C, Anker SD, et al. Intravenous Iron in Patients Undergoing Maintenance Hemodialysis. *N Engl J Med*. 2019;380(5):447-458. doi:10.1056/NEJMOA1810742/SUPPL_FILE/NEJMOA1810742_DATA-SHARING.PDF

76. Moranne O, Froissart M, Rossert J, et al. Timing of Onset of CKD-Related Metabolic Complications. *J Am Soc Nephrol*. 2009;20(1):164. doi:10.1681/ASN.2008020159

77. Goldsmith DJA, Covic A, Fouque D, et al. Endorsement of the Kidney Disease Improving Global Outcomes (KDIGO) Chronic Kidney Disease-Mineral and Bone Disorder (CKD-MBD) Guidelines: a European Renal Best Practice (ERBP) commentary statement. *Nephrol Dial Transplant*. 2010;25(12):3823-3831. doi:10.1093/NDT/GFQ513

78. Au E, Wong G, Chapman JR. Cancer in kidney transplant recipients. *Nat Rev Nephrol 2018 148*. 2018;14(8):508-520. doi:10.1038/s41581-018-0022-6

79. Stengel B. Chronic kidney disease and cancer: a troubling connection. *J Nephrol*. 2010;23(3):253. Accessed January 17, 2022. /pmc/articles/PMC4823382/

80. Wong G, Staplin N, Emberson J, et al. Chronic kidney disease and the risk of cancer: An individual patient data meta-analysis of 32,057 participants from six prospective studies. *BMC Cancer*. 2016;16(1):1-11. doi:10.1186/S12885-016-2532-6/FIGURES/3

81. Viggiano D, Wagner CA, Martino G, et al. Mechanisms of cognitive dysfunction in CKD. *Nat Rev Nephrol 2020 168*. 2020;16(8):452-469. doi:10.1038/s41581-020-0266-9

82. Findlay MD, Dawson J, Dickie DA, et al. Investigating the relationship between cerebral blood flow and cognitive function in hemodialysis patients. *J Am Soc Nephrol*. 2019;30(1):147-158. doi:10.1681/ASN.2018050462/-/DCSUPPLEMENTAL

83. Sullivan MK, Rankin AJ, Jani BD, Mair FS, Mark PB. Associations between multimorbidity and adverse clinical outcomes in patients with chronic kidney disease: a systematic review and meta-analysis. *BMJ Open*. 2020;10(6):e038401. doi:10.1136/BMJOPEN-2020-038401

84. Sullivan MK, Jani BD, McConnachie A, et al. Hospitalisation events in people with chronic kidney disease as a component of multimorbidity: parallel cohort studies in research and routine care settings. *BMC Med*. 2021;19(1). doi:10.1186/S12916-021-02147-6

85. Neovius M, Jacobson SH, Eriksson JK, Elinder CG, Hylander B. Mortality in chronic kidney disease and renal replacement therapy: a population-based cohort study. *BMJ Open*. 2014;4(2):e004251. doi:10.1136/BMJOPEN-2013-004251

86. Naylor KL, Kim SJ, McArthur E, Garg AX, McCallum MK, Knoll GA. Mortality in Incident Maintenance Dialysis Patients Versus Incident Solid Organ Cancer Patients: A Population-Based Cohort. *Am J Kidney Dis*. 2019;73(6):765-776. doi:10.1053/J.AJKD.2018.12.011

87. Murray E, Eid M, Traynor JP, et al. The first 365 days on haemodialysis: variation in the haemodialysis access journey and its associated burden. *Nephrol Dial Transplant*. 2018;33(7):1244-1250. doi:10.1093/NDT/GFX380

88. Garthwaite E, Reddy V, Douthwaite S, Lines S, Tyerman K, Eccles J. Clinical practice guideline management of blood borne viruses within the haemodialysis unit. *BMC Nephrol*. 2019;20(1):1-22. doi:10.1186/S12882-019-1529-1/TABLES/5

89. Sars B, Van Der Sande FM, Kooman JP. Intradialytic Hypotension: Mechanisms and Outcome. *Blood Purif*. 2020;49(1-2):158. doi:10.1159/000503776

90. MacEwen C, Sutherland S, Daly J, Pugh C, Tarassenko L. Relationship between hypotension and cerebral ischemia during hemodialysis. *J Am Soc Nephrol*. 2017;28(8):2511-2520. doi:10.1681/ASN.2016060704/-/DCSUPPLEMENTAL

91. Rangaswami J, Workgroup on behalf of the AS of TK-PC of P (AST-KCD, Mathew RO, et al. Cardiovascular disease in the kidney transplant recipient: epidemiology, diagnosis and management strategies. *Nephrol Dial Transplant*. 2019;34(5):760-773. doi:10.1093/NDT/GFZ053

92. Magee CC, Pascual M. Update in Renal Transplantation. *Arch Intern Med*. 2004;164(13):1373-1388. doi:10.1001/ARCHINTE.164.13.1373

93. Silver Spring (MD): Food and Drug Administration (US); Bethesda (MD): National Institutes of Health (US). BEST (Biomarkers, EndpointS, and other Tools) Resource. *BEST (Biomarkers , EndpointS , other Tools) Resour*. Published online 2016. Accessed September 8, 2022. https://www.ncbi.nlm.nih.gov/books/NBK326791/

94. Strippoli GFM, Craig JC, Schena FP. The number, quality, and coverage of randomized controlled trials in nephrology. *J Am Soc Nephrol*. 2004;15(2):411-419. doi:10.1097/01.ASN.0000100125.21491.46

95. Walsh M, Merkel PA, Peh C-A, et al. Plasma Exchange and Glucocorticoids in Severe ANCA-Associated Vasculitis. *N Engl J Med*. 2020;382(7):622-631. doi:10.1056/NEJMOA1803537/SUPPL_FILE/NEJMOA1803537_DATA-SHARING.PDF

96. Singh AK, Szczech L, Tang KL, et al. Correction of Anemia with Epoetin Alfa in Chronic Kidney Disease. *N Engl J Med*. 2006;355(20):2085-2098. doi:10.1056/NEJMOA065485/SUPPL_FILE/NEJM_SINGH_2085SA1.PDF

97. Torres VE, Meijer E, Bae KT, et al. Rationale and design of the TEMPO (Tolvaptan Efficacy and Safety in Management of Autosomal Dominant Polycystic Kidney Disease and its Outcomes) 3-4 Study. *Am J Kidney Dis*. 2011;57(5):692-699. doi:10.1053/J.AJKD.2010.11.029

98. Becker AE, Heijmans CD, Essed CE. Chronic non-ischaemic congestive heart disease and endomyocardial biopsies. Worth the extra? *Eur Heart J*. 1991;12(2):218-223. Accessed November 10, 2017. http://www.ncbi.nlm.nih.gov/pubmed/2044556

99. Flett AS, Hayward MP, Ashworth MT, et al. Equilibrium Contrast Cardiovascular Magnetic Resonance for the Measurement of Diffuse Myocardial Fibrosis: Preliminary Validation in Humans. *Circulation*. 2010;122(2):138-144. doi:10.1161/CIRCULATIONAHA.109.930636

100. Defilippi CR, Herzog CA. Interpreting Cardiac Biomarkers in the Setting of Chronic Kidney Disease. *Clin Chem*. 2017;63(1):59-65. doi:10.1373/CLINCHEM.2016.254748

101. Savoj J, Becerra B, Kim JK, et al. Utility of Cardiac Biomarkers in the Setting of Kidney Disease. *Nephron*. 2019;141(4):227-235. doi:10.1159/000495946

102. Bansal N, Zelnick L, Go A, et al. Cardiac Biomarkers and Risk of Incident Heart Failure in Chronic Kidney Disease: The CRIC (Chronic Renal Insufficiency Cohort) Study. *J Am Heart Assoc*. 2019;8(21). doi:10.1161/JAHA.119.012336

103. Wang K, Zelnick LR, Anderson A, et al. Cardiac Biomarkers and Risk of Mortality in CKD (the CRIC Study). *Kidney Int Reports*. 2020;5(11):2002-2012. doi:10.1016/J.EKIR.2020.08.028

104. DeFilippi C, van Kimmenade RRJ, Pinto YM. Amino-terminal pro-B-type natriuretic peptide testing in renal disease. *Am J Cardiol*. 2008;101(3A). doi:10.1016/J.AMJCARD.2007.11.029

105. Cheng YJ, Yao FJ, Liu LJ, et al. B-type natriuretic peptide and prognosis of end-stage renal disease: a meta-analysis. *PLoS One*. 2013;8(11). doi:10.1371/JOURNAL.PONE.0079302

106. Arcari L, Engel J, Freiwald T, et al. Cardiac biomarkers in chronic kidney disease are independently associated with myocardial edema and diffuse fibrosis by cardiovascular magnetic resonance. *J Cardiovasc Magn Reson*. 2021;23(1):1-14. doi:10.1186/s12968-021-00762-z

107. Braunisch MC, Gundel P, Werfel S, et al. Electrocardiographic parameters of left ventricular hypertrophy and prediction of mortality in hemodialysis patients. *J Nephrol*. 2022;35:233-244. doi:10.1007/s40620-021-01068-0

108. Astan R, Akpinar I, Karan A, et al. The Effect of Hemodialysis on Electrocardiographic Parameters. *Ann Noninvasive Electrocardiol*. 2015;20(3):253-257. doi:10.1111/anec.12209

109. Kestenbaum B, Rudser KD, Shlipak MG, et al. Kidney Function, Electrocardiographic Findings, and Cardiovascular Events among Older Adults. *Clin J Am Soc Nephrol*. 2007;2(3):501-508. doi:10.2215/CJN.04231206

110. Chiu DYY, Green D, Abidin N, Sinha S, Kalra PA. Echocardiography in Hemodialysis Patients: Uses and Challenges. *Am J Kidney Dis*. 2014;64(5):804-816.

doi:10.1053/J.AJKD.2014.01.450

111. Badve S V., Palmer SC, Strippoli GFM, et al. The Validity of Left Ventricular Mass as a Surrogate End Point for All-Cause and Cardiovascular Mortality Outcomes in People With CKD: A Systematic Review and Meta-analysis. *Am J Kidney Dis*. 2016;68(4):554-563. doi:10.1053/j.ajkd.2016.03.418

112. Gillebert TC, Leite-Moreira AF, De Hert SG. Relaxation–Systolic Pressure Relation. *Circulation*. 1997;95(3):745-752. doi:10.1161/01.CIR.95.3.745

113. Stewart GA, Foster J, Cowan M, et al. Echocardiography overestimates left ventricular mass in hemodialysis patients relative to magnetic resonance imaging. *Kidney Int*. 1999;56(6):2248-2253. doi:10.1046/j.1523-1755.1999.00786.x

114. Graham-Brown MPM, Patel AS, Stensel DJ, et al. Imaging of Myocardial Fibrosis in Patients with End-Stage Renal Disease: Current Limitations and Future Possibilities. *Biomed Res Int*. 2017;2017:1-14. doi:10.1155/2017/5453606

115. Mangion K, McDowell K, Mark PB, Rutherford E. Characterizing Cardiac Involvement in Chronic Kidney Disease Using CMR—a Systematic Review. *Curr Cardiovasc Imaging Rep*. 2018;11(1):1-10. doi:10.1007/s12410-018-9441-9

116. Mark PB, Johnston N, Groenning BA, et al. Redefinition of uremic cardiomyopathy by contrast-enhanced cardiac magnetic resonance imaging. *Kidney Int*. 2006;69(10):1839-1845. doi:10.1038/sj.ki.5000249

117. Schietinger BJ, Brammer GM, Wang H, et al. Patterns of late gadolinium enhancement in chronic hemodialysis patients. *JACC Cardiovasc Imaging*. 2008;1(4):450-456. doi:10.1016/j.jcmg.2008.03.011

118. Collidge TA, Thomson PC, Mark PB, et al. Gadolinium-enhanced MR Imaging and Nephrogenic Systemic Fibrosis: Retrospective Study of a Renal Replacement Therapy Cohort. *Radiology*. 2007;245(1):168-175. doi:10.1148/radiol.2451070353

119. Bruce R, Wentland AL, Haemel AK, et al. Incidence of Nephrogenic Systemic Fibrosis Using Gadobenate Dimeglumine in 1423 Patients With Renal Insufficiency Compared With Gadodiamide. *Invest Radiol*. 2016;51(11):701-705. doi:10.1097/RLI.0000000000000259

120. Pedrizzetti G, Claus P, Kilner PJ, Nagel E. Principles of cardiovascular magnetic resonance feature tracking and echocardiographic speckle tracking for informed clinical use. *J Cardiovasc Magn Reson*. 2016;18(1):51. doi:10.1186/s12968-016-0269-7

121. Hensen LCR, Goossens K, Delgado V, Rotmans JI, Jukema JW, Bax JJ. Prognostic Implications of Left Ventricular Global Longitudinal Strain in Predialysis and Dialysis Patients. *Am J Cardiol*. 2017;120(3):500-504. doi:10.1016/j.amjcard.2017.04.054

122. Kramann R, Erpenbeck J, Schneider RK, et al. Speckle tracking echocardiography detects uremic cardiomyopathy early and predicts cardiovascular mortality in ESRD. *J Am Soc Nephrol*. 2014;25(10):2351-2365. doi:10.1681/ASN.2013070734

123. Krishnasamy R, Hawley CM, Stanton T, et al. Left ventricular global longitudinal strain is associated with cardiovascular risk factors and arterial stiffness in chronic kidney disease. *BMC Nephrol*. 2015;16:106. doi:10.1186/s12882-015-0098-1

124. Cerqueira MD, Weissman NJ, Dilsizian V, et al. Standardized myocardial sementation and nomenclature for tomographic imaging of the heart: A Statement for Healthcare Professionals from the Cardiac Imaging Committee of the Council on Clinical Cardiology of the American Heart Association. *Circulation*. 2002;105(4):539-542. doi:10.1161/hc0402.102975

125. Bull S, White SK, Piechnik SK, et al. Human non-contrast T1 values and correlation with histology in diffuse fibrosis. *Heart*. 2013;99(13):932-937. doi:10.1136/heartjnl-2012-303052

126. de Meester de Ravenstein C, Bouzin C, Lazam S, et al. Histological Validation of measurement of diffuse interstitial myocardial fibrosis by myocardial extravascular volume fraction from Modified Look-Locker imaging (MOLLI) T1 mapping at 3 T. *J Cardiovasc Magn Reson*. 2015;17(1):48. doi:10.1186/s12968-015-0150-0

127. Kotecha T, Martinez-Naharro A, Yoowannakul S, et al. Acute changes in cardiac structural and tissue characterisation parameters following haemodialysis measured using cardiovascular magnetic resonance. *Sci Rep*. 2019;9(1):1-8. doi:10.1038/s41598-018-37845-4

128. Antlanger M, Aschauer S, Kammerlander AA, et al. Impact of Systemic Volume Status

on Cardiac Magnetic Resonance T1 Mapping. doi:10.1038/s41598-018-23868-4

129. Schlieper G, Schurgers L, Brandenburg V, Reutelingsperger C, Floege J. Vascular calcification in chronic kidney disease: an update. *Nephrol Dial Transplant*. 2016;31(1):31-39. doi:10.1093/NDT/GFV111

130. Xu C, Smith ER, Tiong MK, Ruderman I, Toussaint ND. Interventions To Attenuate Vascular Calcification Progression in Chronic Kidney Disease: A Systematic Review of Clinical Trials. *J Am Soc Nephrol*. Published online March 22, 2022. doi:10.1681/ASN.2021101327

131. Messroghli DR, Moon JC, Ferreira VM, et al. Clinical recommendations for cardiovascular magnetic resonance mapping of T1, T2, T2 and extracellular volume: A consensus statement by the Society for Cardiovascular Magnetic Resonance (SCMR) endorsed by the European Association for Cardiovascular Imagin. *J Cardiovasc Magn Reson*. 2017;19(1):1-24. doi:10.1186/s12968-017-0389-8

132. Haaf P, Garg P, Messroghli DR, Broadbent DA, Greenwood JP, Plein S. Cardiac T1 Mapping and Extracellular Volume (ECV) in clinical practice: A comprehensive review. *J Cardiovasc Magn Reson*. 2016;18(1):1-12. doi:10.1186/S12968-016-0308-4/FIGURES/6

133. Treibel TA, Bandula S, Fontana M, et al. Extracellular volume quantification by dynamic equilibrium cardiac computed tomography in cardiac amyloidosis. *J Cardiovasc Comput Tomogr*. 2015;9(6):585-592. doi:10.1016/j.jcct.2015.07.001

134. Scully PR, Bastarrika G, Moon JC, Treibel TA. Myocardial Extracellular Volume Quantification by Cardiovascular Magnetic Resonance and Computed Tomography. *Curr Cardiol Rep*. 2018;20(3). doi:10.1007/s11886-018-0961-3

135. Winsett M, Amparo E, Fawcett H, et al. Renal transplant dysfunction: MR evaluation. *Am J Roentgenol*. 1988;150(2):319-323. doi:10.2214/ajr.150.2.319

136. Liou JT, Lee JK, Heiken JP, Totty WG, Molina PL, Flye WM. Renal transplants: can acute rejection and acute tubular necrosis be differentiated with MR imaging? *Radiology*. 1991;179(1):61-65. doi:10.1148/radiology.179.1.2006305

137. Cox EF, Buchanan CE, Bradley CR, et al. Multiparametric renal magnetic resonance

imaging: Validation, interventions, and alterations in chronic kidney disease. *Front Physiol*. 2017;8(SEP):1-15. doi:10.3389/fphys.2017.00696

138. Leung G, Kirpalani A, Szeto SG, et al. Could MRI Be Used To Image Kidney Fibrosis? A Review of Recent Advances and Remaining Barriers. *Clin J Am Soc Nephrol*. 2017;12(6):1019-1028. doi:10.2215/CJN.07900716

139. Morrell GR, Zhang JL, Lee VS. Magnetic Resonance Imaging of the Fibrotic Kidney. *J Am Soc Nephrol*. 2017;28(9):2564-2570. doi:10.1681/ASN.2016101089

140. Grenier N, Merville P, Combe C. Radiologic imaging of the renal parenchyma structure and function. *Nat Rev Nephrol*. 2016;12(6):348-359. doi:10.1038/nrneph.2016.44

141. Rankin AJ, Mayne K, Allwood-Spiers S, et al. Will advances in functional renal magnetic resonance imaging translate to the nephrology clinic? *Nephrology*. Published online 2021. doi:10.1111/NEP.13985

142. The Scottish Renal Registry. Scottish Renal Registry Annual Report 2016. Published 2016. hhttp://www.srr.scot.nhs.uk/Publications/Main.html

143. Kidney Disease: Improving Global Outcomes (KDIGO) Transplant Work Group. Special Issue: KDIGO Clinical Practice Guideline for the Care of Kidney Transplant Recipients. *Am J Transplant*. 2009;9:S1-S155. doi:10.1111/j.1600-6143.2009.02834.x

144. Transplantation B, Guidelines S. Management of the failing kidney transplant. *Br Transplant Soc*. Published online 2014. Accessed June 6, 2018. www.evidence.nhs.uk

145. Lees JS, McQuarrie EP, Mordi N, Geddes CC, Fox JG, Mackinnon B. Risk factors for bleeding complications after nephrologist-performed native renal biopsy. *Clin Kidney J*. 2017;10(4):573-577. doi:10.1093/ckj/sfx012

146. Stratta P, Canavese C, Marengo M, et al. Risk management of renal biopsy: 1387 cases over 30 years in a single centre. *Eur J Clin Invest*. 2007;37(12):954-963. doi:10.1111/j.1365-2362.2007.01885.x

147. Berchtold L, Friedli I, Crowe LA, et al. Validation of the corticomedullary difference in magnetic resonance imaging-derived apparent diffusion coefficient for kidney fibrosis detection: A cross-sectional study. *Nephrol Dial Transplant*. 2020;35(6):937-

945. doi:10.1093/ndt/gfy389

148. Friedli I, Crowe LA, Berchtold L, et al. New Magnetic Resonance Imaging Index for Renal Fibrosis Assessment: A Comparison between Diffusion-Weighted Imaging and T1 Mapping with Histological Validation. *Sci Rep*. 2016;6(July):1-15. doi:10.1038/srep30088

149. Wang W, Yu Y, Wen J, et al. Combination of functional magnetic resonance imaging and histopathologic analysis to evaluate interstitial fibrosis in kidney allografts. *Clin J Am Soc Nephrol*. 2019;14(9):1372-1380. doi:10.2215/CJN.00020119

150. Bane O, Hectors SJ, Gordic S, et al. Multiparametric magnetic resonance imaging shows promising results to assess renal transplant dysfunction with fibrosis. *Kidney Int*. 2020;97(2):414-420. doi:10.1016/j.kint.2019.09.030

151. Cooper JE, Wiseman AC. Acute kidney injury in kidney transplantation. *Curr Opin Nephrol Hypertens*. 2013;22(6):698-703. doi:10.1097/MNH.0b013e328365b388

152. Gillis KA, McComb C, Patel RK, et al. Non-Contrast Renal Magnetic Resonance Imaging to Assess Perfusion and Corticomedullary Differentiation in Health and Chronic Kidney Disease. *Nephron*. 2016;133(3):183-192. doi:10.1159/000447601

153. Goyal A, Sharma R, Bhalla AS, Gamanagatti S, Seth A. Diffusion-weighted MRI in assessment of renal dysfunction. *Indian J Radiol Imaging*. 2012;22(3):155-159. doi:10.4103/0971-3026.107169

154. Thoeny HC, De Keyzer F, Oyen RH, Peeters RR. Diffusion-weighted MR Imaging of Kidneys in Healthy Volunteers and Patients with Parenchymal Diseases: Initial Experience. *Radiology*. 2005;235(3):911-917. doi:10.1148/radiol.2353040554

155. Thoeny HC, Zumstein D, Simon-Zoula S, et al. Functional Evaluation of Transplanted Kidneys with Diffusion-weighted and BOLD MR Imaging: Initial Experience. *Radiology*. 2006;241(3):812-821. doi:10.1148/radiol.2413060103

156. Liu G, Han F, Xiao W, Wang Q, Xu Y, Chen J. Detection of renal allograft rejection using blood oxygen level-dependent and diffusion weighted magnetic resonance imaging: A retrospective study. *BMC Nephrol*. 2014;15(1):158. doi:10.1186/1471-2369-15-158

157. Blondin D, Lanzman R, Mathys C, et al. Funktionelle MRT der Transplantatnieren: klinische Wertigkeit der Diffusionsbildgebung. *RöFo - Fortschritte auf dem Gebiet der Röntgenstrahlen und der Bildgeb Verfahren*. 2009;181(12):1162-1167. doi:10.1055/s-0028-1109511

158. Palmucci S, Cappello G, Attinà G, et al. Diffusion weighted imaging and diffusion tensor imaging in the evaluation of transplanted kidneys. *Eur J Radiol Open*. 2015;2:71-80. doi:10.1016/j.ejro.2015.05.001

159. Kaimori JY, Isaka Y, Hatanaka M, et al. Visualization of kidney fibrosis in diabetic nephropathy by long diffusion tensor imaging MRI with spin-echo sequence. *Sci Rep*. 2017;7(1):2-9. doi:10.1038/s41598-017-06111-4

160. Hueper K, Khalifa AA, Bräsen JH, et al. Diffusion-Weighted imaging and diffusion tensor imaging detect delayed graft function and correlate with allograft fibrosis in patients early after kidney transplantation. *J Magn Reson Imaging*. 2016;44(1):112-121. doi:10.1002/jmri.25158

161. Simon-Zoula SC, Hofmann L, Giger A, et al. Non-invasive monitoring of renal oxygenation using BOLD-MRI: a reproducibility study. *NMR Biomed*. 2006;19(1):84-89. doi:10.1002/nbm.1004

162. Vermathen P, Binser T, Boesch C, Eisenberger U, Thoeny HC. Three-year follow-up of human transplanted kidneys by diffusion-weighted MRI and blood oxygenation level-dependent imaging. *J Magn Reson Imaging*. 2012;35(5):1133-1138. doi:10.1002/jmri.23537

163. Sadowski EA, Fain SB, Alford SK, et al. Assessment of Acute Renal Transplant Rejection with Blood Oxygen Level–Dependent MR Imaging: Initial Experience. *Radiology*. 2005;236(3):911-919. doi:10.1148/radiol.2363041080

164. Han F, Xiao W, Xu Y, et al. The significance of BOLD MRI in differentiation between renal transplant rejection and acute tubular necrosis. *Nephrol Dial Transplant*. 2008;23(8):2666-2672. doi:10.1093/ndt/gfn064

165. Djamali A, Sadowski EA, Samaniego-Picota M, et al. Noninvasive Assessment of Early Kidney Allograft Dysfunction by Blood Oxygen Level-Dependent Magnetic Resonance Imaging. *Transplantation*. 2006;82(5):621-628.

doi:10.1097/01.tp.0000234815.23630.4a

166. Gillis KA, McComb C, Foster JE, et al. Inter-study reproducibility of arterial spin labelling magnetic resonance imaging for measurement of renal perfusion in healthy volunteers at 3 Tesla. *BMC Nephrol*. 2014;15(1):23. doi:10.1186/1471-2369-15-23

167. Cutajar M, Thomas DL, Hales PW, Banks T, Clark CA, Gordon I. Comparison of ASL and DCE MRI for the non-invasive measurement of renal blood flow: Quantification and reproducibility. *Eur Radiol*. 2014;24(6):1300-1308. doi:10.1007/s00330-014-3130-0

168. Cutajar M, Hilton R, Olsburgh J, et al. Renal blood flow using arterial spin labelling MRI and calculated filtration fraction in healthy adult kidney donors Pre-nephrectomy and post-nephrectomy. *Eur Radiol*. 2015;25(8):2390-2396. doi:10.1007/s00330-015-3594-6

169. Cutajar M, Thomas DL, Banks T, Clark CA, Golay X, Gordon I. Repeatability of renal arterial spin labelling MRI in healthy subjects. *Magn Reson Mater Physics, Biol Med*. 2012;25(2):145-153. doi:10.1007/s10334-011-0300-9

170. Liu YP, Song R, Liang CH, Chen X, Liu B. Arterial spin labeling blood flow magnetic resonance imaging for evaluation of renal injury. *Am J Physiol Renal Physiol*. 2012;303(4):F551-8. doi:10.1152/ajprenal.00288.2011

171. Artz NS, Sadowski EA, Wentland AL, et al. Arterial spin labeling MRI for assessment of perfusion in native and transplanted kidneys. *Magn Reson Imaging*. 2011;29(1):74-82. doi:10.1016/j.mri.2010.07.018

172. Heusch P, Wittsack HJ, Blondin D, et al. Functional evaluation of transplanted kidneys using arterial spin labeling MRI. *J Magn Reson Imaging*. 2014;40(1):84-89. doi:10.1002/jmri.24336

173. Heusch P, Wittsack H-J, Heusner T, et al. Correlation of biexponential diffusion parameters with arterial spin-labeling perfusion MRI: results in transplanted kidneys. *Invest Radiol*. 2013;48(3):140-144. doi:10.1097/RLI.0b013e318277bfe3

174. Lanzman RS, Wittsack H-J, Martirosian P, et al. Quantification of renal allograft perfusion using arterial spin labeling MRI: initial results. *Eur Radiol*. 2010;20(6):1485-

1491. doi:10.1007/s00330-009-1675-0

175. Tonelli M. Chronic Kidney Disease and Mortality Risk: A Systematic Review. *J Am Soc Nephrol*. 2006;17(7):2034-2047. doi:10.1681/ASN.2005101085

176. Moody WE, Ferro CJ, Edwards NC, et al. Cardiovascular Effects of Unilateral Nephrectomy in Living Kidney Donors. *Hypertension*. 2016;67(2):368-377. doi:10.1161/HYPERTENSIONAHA.115.06608

177. Claus P, Omar AMS, Pedrizzetti G, Sengupta PP, Nagel E. Tissue Tracking Technology for Assessing Cardiac Mechanics: Principles, Normal Values, and Clinical Applications. *JACC Cardiovasc Imaging*. 2015;8(12):1444-1460. doi:10.1016/j.jcmg.2015.11.001

178. Vo HQ, Marwick TH, Negishi K. MRI-Derived Myocardial Strain Measures in Normal Subjects. *JACC Cardiovasc Imaging*. 2018;11(2P1):196-205. doi:10.1016/j.jcmg.2016.12.025

179. Taylor RJ, Moody WE, Umar F, et al. Myocardial strain measurement with feature-tracking cardiovascular magnetic resonance: Normal values. *Eur Heart J Cardiovasc Imaging*. 2015;16(8):871-881. doi:10.1093/ehjci/jev006

180. Eitel I, Stiermaier T, Lange T, et al. Cardiac Magnetic Resonance Myocardial Feature Tracking for Optimized Prediction of Cardiovascular Events Following Myocardial Infarction. *JACC Cardiovasc Imaging*. 2018;11(10):1433-1444. doi:10.1016/j.jcmg.2017.11.034

181. Gong IY, Al-Amro B, Prasad GVR, et al. Cardiovascular magnetic resonance left ventricular strain in end-stage renal disease patients after kidney transplantation. *J Cardiovasc Magn Reson*. 2018;20(1):83. doi:10.1186/s12968-018-0504-5

182. Rutherford E, Talle MA, Mangion K, et al. Defining myocardial tissue abnormalities in end-stage renal failure with cardiac magnetic resonance imaging using native T1 mapping. *Kidney Int*. 2016;90(4):1-8. doi:10.1016/j.kint.2016.06.014

183. Patel RK, Jardine AGM, Mark PB, et al. Association of Left Atrial Volume With Mortality Among ESRD Patients With Left Ventricular Hypertrophy Referred for Kidney Transplantation. *Am J Kidney Dis*. 2010;55(6):1088-1096.

doi:10.1053/j.ajkd.2009.12.033

184. Hicks KA, Mahaffey KW, Mehran R, et al. 2017 cardiovascular and stroke endpoint definitions for clinical trials. *Circulation*. 2018;137(9):961-972. doi:10.1161/CIRCULATIONAHA.117.033502

185. Schulz-Menger J, Bluemke DA, Bremerich J, et al. Standardized image interpretation and post processing in cardiovascular magnetic resonance: Society for Cardiovascular Magnetic Resonance (SCMR) Board of Trustees Task Force on Standardized Post Processing. *J Cardiovasc Magn Reson*. 2013;15(1). doi:10.1186/1532-429X-15-35

186. Ponikowski P, Voors AA, Anker SD, et al. 2016 ESC Guidelines for the diagnosis and treatment of acute and chronic heart failure. *Eur Heart J*. 2016;37(27):2129-2200. doi:10.1093/eurheartj/ehw128

187. Petersen SE, Aung N, Sanghvi MM, et al. Reference ranges for cardiac structure and function using cardiovascular magnetic resonance (CMR) in Caucasians from the UK Biobank population cohort. *J Cardiovasc Magn Reson*. 2017;19(1). doi:10.1186/s12968-017-0327-9

188. Koo TK, Li MY. A Guideline of Selecting and Reporting Intraclass Correlation Coefficients for Reliability Research. *J Chiropr Med*. 2016;15(2):155-163. doi:10.1016/j.jcm.2016.02.012

189. Moody WE, Taylor RJ, Edwards NC, et al. Comparison of magnetic resonance feature tracking for systolic and diastolic strain and strain rate calculation with spatial modulation of magnetization imaging analysis. *J Magn Reson Imaging*. 2015;41(4):1000-1012. doi:10.1002/jmri.24623

190. Singh A, Steadman CD, Khan JN, et al. Intertechnique agreement and interstudy reproducibility of strain and diastolic strain rate at 1.5 and 3 tesla: A comparison of feature-tracking and tagging in patients with aortic stenosis. *J Magn Reson Imaging*. 2015;41(4):1129-1137. doi:10.1002/jmri.24625

191. Krishnasamy R, Isbel NM, Hawley CM, et al. Left ventricular global longitudinal strain (GLS) is a superior predictor of all-cause and cardiovascular mortality when compared to ejection fraction in advanced Chronic Kidney Disease. *PLoS One*. 2015;10(5). doi:10.1371/journal.pone.0127044

192. Foley RN, Parfrey PS, Harnett JD, et al. Clinical and echocardiographic disease in patients starting end-stage renal disease therapy. *Kidney Int*. 1995;47(1):186-192. Accessed November 13, 2017. http://www.ncbi.nlm.nih.gov/pubmed/7731145

193. London GM, Pannier B, Guerin AP, et al. Alterations of left ventricular hypertrophy in and survival of patients receiving hemodialysis: follow-up of an interventional study. *J Am Soc Nephrol*. 2001;12(12):2759-2767. Accessed November 13, 2017. http://www.ncbi.nlm.nih.gov/pubmed/11729246

194. Hammer F, Malzahn U, Donhauser J, et al. A randomized controlled trial of the effect of spironolactone on left ventricular mass in hemodialysis patients. *Kidney Int*. 2019;95(4):983-991. doi:10.1016/j.kint.2018.11.025

195. Charytan DM, Himmelfarb J, Ikizler TA, et al. Safety and cardiovascular efficacy of spironolactone in dialysis-dependent ESRD (SPin-D): a randomized, placebo-controlled, multiple dosage trial. *Kidney Int*. 2019;95(4):973-982. doi:10.1016/j.kint.2018.08.034

196. Andersen D, Jensen JS, Mogelvang R, Schnohr P, Biering-Sorensen T. The Left atrium emptying fraction as a predictor of cardiovascular morbidity and mortality I na low risk general population. *J Am Coll Cardiol*. 2017;69(11):1536. doi:10.1016/s0735-1097(17)34925-2

197. Leibowitz D, Koslowsky J, Gilon D, Jacobs JM, Stessman-Lande I, Stessman J. Left atrial function and mortality in the oldest old. *Clin Cardiol*. 2017;40(12):1323-1327. doi:10.1002/clc.22831

198. Kanagala P, Arnold JR, Cheng ASH, et al. Left atrial ejection fraction and outcomes in heart failure with preserved ejection fraction. *Int J Cardiovasc Imaging*. 2020;36(1):101-110. doi:10.1007/s10554-019-01684-9

199. Rijnierse MT, Sadeghian K, Stekhoven SS, et al. Usefulness of Left Atrial Emptying Fraction to Predict Ventricular Arrhythmias in Patients With Implantable Cardioverter Defibrillators. *Am J Cardiol*. 2017;120:243-250. doi:10.1016/j.amjcard.2017.04.015

200. Tripepi G, Benedetto FA, Mallamaci F, Tripepi R, Malatino L, Zoccali C. Left atrial volume in end-stage renal disease: A prospective cohort study. *J Hypertens*. 2006;24(6):1173-1180. doi:10.1097/01.hjh.0000226208.11184.bb

201. Simek CL, Feldman MD, Haber HL, Wu CC, Jayaweera AR, Kaul S. Relationship between left ventricular wall thickness and left atrial size: Comparison with other measures of diastolic function. *J Am Soc Echocardiogr*. 1995;8(1):37-47. doi:10.1016/S0894-7317(05)80356-6

202. Tsang TSM, Barnes ME, Gersh BJ, Bailey KR, Seward JB. Left atrial volume as a morphophysiologic expression of left ventricular diastolic dysfunction and relation to cardiovascular risk burden. *Am J Cardiol*. 2002;90(12):1284-1289. doi:10.1016/S0002-9149(02)02864-3

203. Tabriziani H, Baron P, Abudayyeh I, Lipkowitz M. Cardiac risk assessment for end-stage renal disease patients on the renal transplant waiting list. *Clin Kidney J*. 2019;12(4):576-585. doi:10.1093/ckj/sfz039

204. Sharif A. The Argument for Abolishing Cardiac Screening of Asymptomatic Kidney Transplant Candidates. *Am J Kidney Dis*. 2020;75(6):946-954. doi:10.1053/j.ajkd.2019.05.033

205. Contti MM, Fregonesi Barbosa M, Del Carmen A, et al. Kidney transplantation is associated with reduced myocardial fibrosis. A cardiovascular magnetic resonance study with native T1 mapping. doi:10.1186/s12968-019-0531-x

206. Taylor AJ, Salerno M, Dharmakumar R, Jerosch-Herold M. T1 Mapping Basic Techniques and Clinical Applications. *JACC Cardiovasc Imaging*. 2016;9(1):67-81. doi:10.1016/j.jcmg.2015.11.005

207. Graham-Brown MPM, March DS, Churchward DR, et al. Novel cardiac nuclear magnetic resonance method for noninvasive assessment of myocardial fibrosis in hemodialysis patients. *Kidney Int*. 2016;90(4):835-844. doi:10.1016/j.kint.2016.07.014

208. Graham-Brown MPM, Rutherford E, Levelt E, et al. Native T1 mapping: inter-study, inter-observer and inter-center reproducibility in hemodialysis patients. *J Cardiovasc Magn Reson*. 2017;19(1):21. doi:10.1186/s12968-017-0337-7

209. Graham-Brown MPM, March DS, Churchward DR, et al. Novel cardiac nuclear magnetic resonance method for noninvasive assessment of myocardial fibrosis in hemodialysis patients. *Kidney Int*. 2016;90(4):835-844. doi:10.1016/J.KINT.2016.07.014

210. Dill T. Contraindications to magnetic resonance imaging. *Heart*. 2008;94(7):943-948. doi:10.1136/hrt.2007.125039

211. Board of the faculty of Clinical Radiology. Standards for intravascular contrast agent administration to adult patients Second edition. *R Coll Clin Radiol*. Published online 2011:3-15. doi:2016 Mar 12

212. Captur G, Gatehouse P, Keenan KE, et al. A medical device-grade T1 and ECV phantom for global T1 mapping quality assurance—the T1 Mapping and ECV Standardization in cardiovascular magnetic resonance (T1MES) program. *J Cardiovasc Magn Reson*. 2016;18(1):58. doi:10.1186/s12968-016-0280-z

213. Charlson ME, Pompei P, Ales KL, MacKenzie CR. A new method of classifying prognostic comorbidity in longitudinal studies: Development and validation. *J Chronic Dis*. 1987;40(5):373-383. doi:10.1016/0021-9681(87)90171-8

214. Hemmelgarn BR, Manns BJ, Quan H, Ghali WA. Adapting the Charlson comorbidity index for use in patients with ESRD. *Am J Kidney Dis*. 2003;42(1 SUPPL. 2):125-132. doi:10.1016/S0272-6386(03)00415-3

215. Puntmann VO, Carr-White G, Jabbour A, et al. T1-Mapping and Outcome in Nonischemic Cardiomyopathy All-Cause Mortality and Heart Failure. *JACC Cardiovasc Imaging*. 2016;9(1):40-50. doi:10.1016/j.jcmg.2015.12.001

216. Puntmann VO, Valbuena S, Hinojar R, et al. Society for Cardiovascular Magnetic Resonance (SCMR) expert consensus for CMR imaging endpoints in clinical research: Part i - Analytical validation and clinical qualification. *J Cardiovasc Magn Reson*. 2018;20(1):67. doi:10.1186/s12968-018-0484-5

217. Haaf P, Garg P, Messroghli DR, Broadbent DA, Greenwood JP, Plein S. Cardiac T1 Mapping and Extracellular Volume (ECV) in clinical practice: a comprehensive review. *J Cardiovasc Magn Reson*. 2016;18(1):89. doi:10.1186/s12968-016-0308-4

218. Graham-Brown MPM, Gulsin GS, Poli F, Parke K, Burton JO, McCann GP. Differences in native T1 and native T2 mapping between patients on hemodialysis and control subjects. *Eur J Radiol*. 2021;140:109748. doi:10.1016/j.ejrad.2021.109748

219. Buchanan C, Mohammed A, Cox E, et al. Intradialytic Cardiac Magnetic Resonance

Imaging to Assess Cardiovascular Responses in a Short-Term Trial of Hemodiafiltration and Hemodialysis. *J Am Soc Nephrol*. 2017;28(4):1269-1277. doi:10.1681/ASN.2016060686

220. Hwang IC, Kim HK, Park JB, et al. Aortic valve replacement-induced changes in native T1 are related to prognosis in severe aortic stenosis: T1 mapping cardiac magnetic resonance imaging study. *Eur Heart J Cardiovasc Imaging*. 2020;21(6):653-663. doi:10.1093/ehjci/jez201

221. Nakamori S, Fahmy A, Jang J, et al. Changes in Myocardial Native T 1 and T 2 After Exercise Stress A Noncontrast CMR Pilot Study. Published online 2019. doi:10.1016/j.jcmg.2019.05.019

222. Puntmann VO, Carr-White G, Jabbour A, et al. T1-Mapping and Outcome in Nonischemic Cardiomyopathy All-Cause Mortality and Heart Failure. *JACC Cardiovasc Imaging*. 2016;9(1):40-50. doi:10.1016/j.jcmg.2015.12.001

223. Liu D, Borlotti A, Viliani D, et al. CMR Native T1 Mapping Allows Differentiation of Reversible Versus Irreversible Myocardial Damage in ST-Segment-Elevation Myocardial Infarction: An OxAMI Study (Oxford Acute Myocardial Infarction). *Circ Cardiovasc Imaging*. 2017;10(8). doi:10.1161/CIRCIMAGING.116.005986

224. Bloem JL, Reijnierse M, Huizinga TWJ, Van Der Helm-Van Mil AHM. MR signal intensity: Staying on the bright side in MR image interpretation. *RMD Open*. 2018;4(1):728. doi:10.1136/rmdopen-2018-000728

225. Rankin AJ, Zhu L, Mangion K, et al. Global longitudinal strain by feature-tracking cardiovascular magnetic resonance imaging predicts mortality in patients with end-stage kidney disease. *Clin Kidney J*. Published online February 2, 2021. doi:10.1093/ckj/sfab020

226. Rutherford E, Weir-McCall JR, Patel RK, et al. Research cardiac magnetic resonance imaging in end stage renal disease - incidence, significance and implications of unexpected incidental findings. *Eur Radiol*. 2017;27(1):315-324. doi:10.1007/s00330-016-4288-4

227. Gansevoort RT, Correa-Rotter R, Hemmelgarn BR, et al. Chronic kidney disease and cardiovascular risk: Epidemiology, mechanisms, and prevention. *Lancet*.

2013;382(9889):339-352. doi:10.1016/S0140-6736(13)60595-4

228. Guérin AP, London GM, Marchais SJ, Metivier F. Arterial stiffening and vascular calcifications in end-stage renal disease. *Nephrol Dial Transplant*. 2000;15(7):1014-1021. doi:10.1093/NDT/15.7.1014

229. Blacher J, Guerin AP, Pannier B, Marchais SJ, London GM. Arterial calcifications, arterial stiffness, and cardiovascular risk in end-stage renal disease. *Hypertens (Dallas, Tex 1979)*. 2001;38(4):938-942. doi:10.1161/HY1001.096358

230. Blacher J, Guerin AP, Pannier B, Marchais SJ, Safar ME, London GM. Impact of aortic stiffness on survival in end-stage renal disease. *Circulation*. 1999;99(18):2434-2439. doi:10.1161/01.CIR.99.18.2434

231. Raggi P, Bellasi A, Bushinsky D, et al. Slowing Progression of Cardiovascular Calcification With SNF472 in Patients on Hemodialysis: Results of a Randomized Phase 2b Study. *Circulation*. 2020;141(9):728-739. doi:10.1161/CIRCULATIONAHA.119.044195

232. Allison MA, Hsi S, Wassel CL, et al. Calcified atherosclerosis in different vascular beds and the risk of mortality. *Arterioscler Thromb Vasc Biol*. 2012;32(1):140-146. doi:10.1161/ATVBAHA.111.235234

233. Santos RD, Rumberger JA, Budoff MJ, et al. Thoracic aorta calcification detected by electron beam tomography predicts all-cause mortality. *Atherosclerosis*. 2010;209(1):131-135. doi:10.1016/J.ATHEROSCLEROSIS.2009.08.025

234. Budoff MJ, Nasir K, Katz R, et al. Thoracic aortic calcification and coronary heart disease events: the multi-ethnic study of atherosclerosis (MESA). *Atherosclerosis*. 2011;215(1):196-202. doi:10.1016/J.ATHEROSCLEROSIS.2010.11.017

235. Hoffmann U, Massaro JM, D'Agostino RB, Kathiresan S, Fox CS, O'Donnell CJ. Cardiovascular Event Prediction and Risk Reclassification by Coronary, Aortic, and Valvular Calcification in the Framingham Heart Study. *J Am Heart Assoc*. 2016;5(2). doi:10.1161/JAHA.115.003144

236. Mahabadi AA, Dykun I, Erbel R, et al. Noncoronary Measures Enhance the Predictive Value of Cardiac CT Above Traditional Risk Factors and CAC Score in the General

Population. *JACC Cardiovasc Imaging*. 2016;9(10):1177-1185. doi:10.1016/J.JCMG.2015.12.024

237. Wong ND, Gransar H, Shaw L, et al. Thoracic aortic calcium versus coronary artery calcium for the prediction of coronary heart disease and cardiovascular disease events. *JACC Cardiovasc Imaging*. 2009;2(3):319-326. doi:10.1016/J.JCMG.2008.12.010

238. Eisen A, Tenenbaum A, Koren-Morag N, et al. Calcification of the thoracic aorta as detected by spiral computed tomography among stable angina pectoris patients: association with cardiovascular events and death. *Circulation*. 2008;118(13):1328-1334. doi:10.1161/CIRCULATIONAHA.107.712141

239. Cano-Megías M, Guisado-Vasco P, Bouarich H, et al. Coronary calcification as a predictor of cardiovascular mortality in advanced chronic kidney disease: a prospective long-term follow-up study. *BMC Nephrol*. 2019;20(1). doi:10.1186/S12882-019-1367-1

240. Okuno S, Ishimura E, Kitatani K, et al. Presence of abdominal aortic calcification is significantly associated with all-cause and cardiovascular mortality in maintenance hemodialysis patients. *Am J Kidney Dis*. 2007;49(3):417-425. doi:10.1053/J.AJKD.2006.12.017

241. Agatston AS, Janowitz WR, Hildner FJ, Zusmer NR, Viamonte M, Detrano R. Quantification of coronary artery calcium using ultrafast computed tomography. *J Am Coll Cardiol*. 1990;15(4):827-832. doi:10.1016/0735-1097(90)90282-T

242. Blaha MJ, Mortensen MB, Kianoush S, Tota-Maharaj R, Cainzos-Achirica M. Coronary Artery Calcium Scoring: Is It Time for a Change in Methodology? *JACC Cardiovasc Imaging*. 2017;10(8):923-937. doi:10.1016/J.JCMG.2017.05.007

243. Tsuchiya K, Makita K, Furui S, Nitta K. MRI appearances of calcified regions within intracranial tumours. *Neuroradiology*. 1993;35(5):341-344. doi:10.1007/BF00588364

244. Koktzoglou I. Gray blood magnetic resonance for carotid wall imaging and visualization of deep-seated and superficial vascular calcifications. *Magn Reson Med*. 2013;70(1):75-85. doi:10.1002/MRM.24445

245. Ferreira Botelho MP, Koktzoglou I, Collins JD, et al. MR imaging of iliofemoral

peripheral vascular calcifications using proton density-weighted, in-phase three-dimensional stack-of-stars gradient echo. *Magn Reson Med*. 2017;77(6):2146-2152. doi:10.1002/MRM.26295

246. Serhal A, Koktzoglou I, Aouad P, et al. Cardiovascular magnetic resonance imaging of aorto-iliac and ilio-femoral vascular calcifications using proton density-weighted in-phase stack of stars. *J Cardiovasc Magn Reson*. 2018;20(1). doi:10.1186/S12968-018-0479-2

247. Stoumpos S, Hall Barrientos P, Black DH, et al. Ferumoxytol MR Angiography: A Novel Technique for Assessing Iliac Vasculature in Potential Kidney Transplant Recipients. *JACC Cardiovasc Imaging*. 2020;13(8):1847-1848. doi:10.1016/J.JCMG.2020.02.032

248. Lees JS, Mangion K, Rutherford E, et al. Vitamin K for kidney transplant organ recipients: investigating vessel stiffness (ViKTORIES): study rationale and protocol of a randomised controlled trial. *Open Hear*. 2020;7(2). doi:10.1136/OPENHRT-2019-001070

249. Schneider CA, Rasband WS, Eliceiri KW. NIH Image to ImageJ: 25 years of image analysis. *Nat Methods*. 2012;9(7):671-675. doi:10.1038/NMETH.2089

250. Rensis L. A technique for the measurement of attitudes. *New York Sci Press*. Published online 1932.

251. Cohen J. A power primer. *Psychol Bull*. 1992;112(1):155-159. doi:10.1037//0033-2909.112.1.155

252. Bland M. *An Introduction to Medical Statistics*. Third edit. Oxford University Press; 2000.

253. Hoffmann, Udo; Ferencik, Maros; Cury RCAJ. Coronary CT angiography. *J Nucl Med*. 2006;May;47(5):797-806.

254. Braun J, Oldendorf M, Moshage W, Heidler R, Zeitler E, Luft FC. Electron beam computed tomography in the evaluation of cardiac calcification in chronic dialysis patients. *Am J Kidney Dis*. 1996;27(3):394-401. doi:10.1016/S0272-6386(96)90363-7

255. Schurgin S, Rich S, Mazzone T. Increased prevalence of significant coronary artery

calcification in patients with diabetes. *Diabetes Care*. 2001;24(2):335-338. doi:10.2337/DIACARE.24.2.335

256. Allison MA, Criqui MH, Wright CM. Patterns and risk factors for systemic calcified atherosclerosis. *Arterioscler Thromb Vasc Biol*. 2004;24(2):331-336. doi:10.1161/01.ATV.0000110786.02097.0C

257. Bloem JL, Reijnierse M, Huizinga TWJ, Van Der Helm-Van Mil AHM. MR signal intensity: staying on the bright side in MR image interpretation. *RMD open*. 2018;4(1). doi:10.1136/RMDOPEN-2018-000728

258. Craiem D, Chironi G, Casciaro ME, Graf S, Simon A. Calcifications of the thoracic aorta on extended non-contrast-enhanced cardiac CT. *PLoS One*. 2014;9(10). doi:10.1371/JOURNAL.PONE.0109584

259. Attari H, Cao Y, Elmholdt TR, Zhao Y, Prince MR. A Systematic Review of 639 Patients with Biopsy-confirmed Nephrogenic Systemic Fibrosis. *Radiology*. 2019;292(2):376-386. doi:10.1148/radiol.2019182916

260. Wong TC, Piehler KM, Kang IA, et al. Myocardial extracellular volume fraction quantified by cardiovascular magnetic resonance is increased in diabetes and associated with mortality and incident heart failure admission. *Eur Heart J*. 2014;35(10):657-664. doi:10.1093/eurheartj/eht193

261. Scully P, Patel ;, Augusto ;, et al. *Myocardial Fibrosis Quantification by Cardiac CT Predicts Outcome in Severe Aortic Stenosis*. https://academic.oup.com/ehjcimaging/article/22/Supplement_1/jeaa356.230/6131074

262. Yamada A, Kitagawa K, Nakamura S, et al. Quantification of extracellular volume fraction by cardiac computed tomography for noninvasive assessment of myocardial fibrosis in hemodialysis patients. *Sci Reports 2020 101*. 2020;10(1):1-10. doi:10.1038/s41598-020-72417-5

263. Goulden R, Rowe BH, Abrahamowicz M, Strumpf E, Tamblyn R. Association of Intravenous Radiocontrast With Kidney Function: A Regression Discontinuity Analysis. *JAMA Intern Med*. 2021;181(6):767-774. doi:10.1001/JAMAINTERNMED.2021.0916

264. Aycock RD, Westafer LM, Boxen JL, Majlesi N, Schoenfeld EM, Bannuru RR. Acute Kidney Injury After Computed Tomography: A Meta-analysis. *Ann Emerg Med*. 2018;71(1):44-53.e4. doi:10.1016/j.annemergmed.2017.06.041

265. Moranne O, Willoteaux S, Pagniez D, Dequiedt P, Boulanger E. Effect of iodinated contrast agents on residual renal function in PD patients. *Nephrol Dial Transplant*. 2006;21(4):1040-1045. doi:10.1093/ndt/gfi327

266. Weisbord SD, Bernardini J, Mor MK, et al. The effect of coronary angiography on residual renal function in patients on peritoneal dialysis. *Clin Cardiol*. 2006;29(11):494-497. Accessed April 6, 2018. http://www.ncbi.nlm.nih.gov/pubmed/17133846

267. Dittrich E, Puttinger H, Schillinger M, et al. Effect of radio contrast media on residual renal function in peritoneal dialysis patients—a prospective study. *Nephrol Dial Transplant*. 2006;21(5):1334-1339. doi:10.1093/ndt/gfi023

268. Janousek R, Krajina A, Peregrin JH, et al. Effect of Intravascular Iodinated Contrast Media on Natural Course of End-Stage Renal Disease Progression in Hemodialysis Patients: A Prospective Study. *Cardiovasc Intervent Radiol*. 2010;33(1):61-66. doi:10.1007/s00270-009-9715-3

269. Cavanagh P, Goddard A, Harden S. Standards of practice of computed tomography coronary angiography (CTCA) in adult patients. *Clin Radiol*. Published online 2014. Accessed April 18, 2018. www.rcr.ac.uk

270. Rankin AJ, Mangion K, Lees JS, et al. Myocardial changes on 3T cardiovascular magnetic resonance imaging in response to haemodialysis with fluid removal. *J Cardiovasc Magn Reson*. 2021;23(1):125. doi:10.1186/S12968-021-00822-4

271. Scully PR, Patel KP, Saberwal B, et al. Identifying Cardiac Amyloid in Aortic Stenosis ECV Quantification by CT in TAVR Patients. Published online 2020. doi:10.1016/j.jcmg.2020.05.029

272. Weinreb JC, Rodby RA, Yee J, et al. Use of intravenous gadolinium-based contrast media in patients with kidney disease: Consensus statements from the American college of radiology and the national kidney foundation. *Radiology*. 2021;298(1):28-35. doi:10.1148/RADIOL.2020202903

273. Xu HY, Yang ZG, Zhang Y, et al. Prognostic value of heart failure in hemodialysis-dependent end-stage renal disease patients with myocardial fibrosis quantification by extracellular volume on cardiac magnetic resonance imaging. *BMC Cardiovasc Disord*. 2020;20(1). doi:10.1186/s12872-019-01313-2

274. McCollough CH, Leng S, Yu L, Fletcher JG. Dual- and multi-energy CT: Principles, technical approaches, and clinical applications. *Radiology*. 2015;276(3):637-653. doi:10.1148/RADIOL.2015142631/ASSET/IMAGES/LARGE/RADIOL.2015142631.FIG18D.JPEG

275. Erley CM, Bader BD, Berger ED, et al. Plasma clearance of iodine contrast media as a measure of glomerular filtration rate in critically ill patients. *Crit Care Med*. 2001;29(8):1544-1550. doi:10.1097/00003246-200108000-00008

276. Caroli A, Pruijm M, Burnier M, Selby NM. Functional magnetic resonance imaging of the kidneys: where do we stand? The perspective of the European COST Action PARENCHIMA. *Nephrol Dial Transplant*. 2018;33(suppl_2):ii1-ii3. doi:10.1093/ndt/gfy181

277. Selby NM, Blankestijn PJ, Boor P, et al. Magnetic resonance imaging biomarkers for chronic kidney disease: a position paper from the European Cooperation in Science and Technology Action PARENCHIMA. *Nephrol Dial Transplant*. 2018;33(suppl_2):ii4-ii14. doi:10.1093/ndt/gfy152

278. Martirosian P, Klose U, Mader I, Schick F. FAIR True-FISP Perfusion Imaging of the Kidneys. *Magn Reson Med*. 2004;51(2):353-361. doi:10.1002/mrm.10709

279. Look DC, Locker DR. Time Saving in Measurement of NMR and EPR Relaxation Times. *Rev Sci Instrum*. 2003;41(2):250. doi:10.1063/1.1684482

280. Wolf M, de Boer A, Sharma K, et al. Magnetic resonance imaging T1- and T2-mapping to assess renal structure and function: a systematic review and statement paper. *Nephrol Dial Transplant*. 2018;33(suppl_2):ii41-ii50. doi:10.1093/ndt/gfy198

281. Xue H, Greiser A, Zuehlsdorff S, et al. Phase-sensitive inversion recovery for myocardial T1 mapping with motion correction and parametric fitting. *Magn Reson Med*. 2013;69(5):1408-1420. doi:10.1002/mrm.24385

282. Silva AC, Kim S-G. Pseudo-Continuous Arterial Spin Labeling Technique for Measuring CBF Dynamics With High Temporal Resolution. *Magn Reson Med*. 1999;42:425-429. doi:10.1002/(SICI)1522-2594(199909)42:3

283. Odudu A, Nery F, Harteveld AA, et al. Arterial spin labelling MRI to measure renal perfusion: a systematic review and statement paper. *Nephrol Dial Transplant*. 2018;33(2):ii15-ii21. doi:10.1093/ndt/gfy180

284. Caroli A, Schneider M, Friedli I, et al. Diffusion-weighted magnetic resonance imaging to assess diffuse renal pathology: a systematic review and statement paper. *Nephrol Dial Transplant*. 2018;33(suppl_2):ii29-ii40. doi:10.1093/ndt/gfy163

285. Kim Y, Ge Y, Tao C, et al. Automated Segmentation of Kidneys from MR Images in Patients with Autosomal Dominant Polycystic Kidney Disease. *Clin J Am Soc Nephrol*. 2016;11(4):576-584. doi:10.2215/CJN.08300815

286. Buchanan CE, Mahmoud H, Cox EF, et al. Quantitative assessment of renal structural and functional changes in chronic kidney disease using multi-parametric magnetic resonance imaging. *Nephrol Dial Transplant*. Published online 2019:1-10. doi:10.1093/ndt/gfz129

287. Pruijm M, Milani B, Pivin E, et al. Reduced cortical oxygenation predicts a progressive decline of renal function in patients with chronic kidney disease. *Kidney Int*. 2018;93(4):932-940. doi:10.1016/j.kint.2017.10.020

288. Semelka RC, Corrigan K, Ascher SM, Brown JJ, Colindres RE. Renal corticomedullary differentiation: Observation patients with differing serum creatinine levels. *Radiology*. 1994;190(1):149-152. doi:10.1148/radiology.190.1.8259395

289. Suthanthiran M, Strom TB. Renal Transplantation. *N Engl J Med*. 1994;331(6):365-376. doi:10.1056/NEJM199408113310606

290. Leung G, Kirpalani A, Szeto SG, et al. Could MRI Be Used To Image Kidney Fibrosis? A Review of Recent Advances and Remaining Barriers. *Clin J Am Soc Nephrol*. 2017;12(6):1019-1028. doi:10.2215/CJN.07900716

291. Rankin AJ, Allwood-Spiers S, Lee MMY, et al. Comparing the interobserver reproducibility of different regions of interest on multi-parametric renal magnetic

resonance imaging in healthy volunteers, patients with heart failure and renal transplant recipients. *Magn Reson Mater Physics, Biol Med*. 2020;33(1). doi:10.1007/s10334-019-00809-4

292. Haas M, Loupy A, Lefaucheur C, et al. The Banff 2017 Kidney Meeting Report: Revised diagnostic criteria for chronic active T cell–mediated rejection, antibody-mediated rejection, and prospects for integrative endpoints for next-generation clinical trials. *Am J Transplant*. 2018;18(2):293-307. doi:10.1111/ajt.14625

293. Rothman KJ. No adjustments are needed for multiple comparisons. *Epidemiology*. 1990;1:43-46.

294. Althouse AD. Adjust for Multiple Comparisons? It's Not That Simple. *Ann Thorac Surg*. 2016;101(5):1644-1645. doi:10.1016/J.ATHORACSUR.2015.11.024